Author:
Zentuti, Nader

Title:
Probabilistic Methodologies in the Creep Regime

Probabilistic Methodologies in the Creep Regime

By

NADER A. ZENTUTI

Department of Mechanical Engineering
UNIVERSITY OF BRISTOL

A dissertation submitted to the University of Bristol in accordance with the requirements of the degree of DOCTOR OF PHILOSOPHY in the Faculty of Engineering.

APR 2019

c. 56 000 words

“I do not know what I may appear to the world, but to myself I seem to have been only like a boy playing on the seashore, and diverting myself in now and then finding a smoother pebble or a prettier shell than ordinary, whilst the great ocean of truth lay all undiscovered before me.”

— Sir Isaac Newton

To my beloved parents. Words alone cannot truly describe the love and support they have given me.
This thesis is dedicated to Professor David Smith without whom this work would have not existed.
David tragically departed in November 2015.

Abstract

Structural integrity practitioners can encounter countless, complex and often unknown uncertainties when dealing with myriad applications. The existence of such uncertainties can span the lifecycle of engineering assets: commissioning, design, prototyping, material testing, manufacturing, physical testing, in-service data, inspection data, fitness-for-service assessments and decommission. Traditionally, a deterministic mindset has prevailed amongst the engineering community at large. However, given the widening acceptance of data science and machine-learning across a plethora of industries, trends towards accepting more probabilistic and data-driven solutions have emerged in engineering. Structural integrity is facing a similar change, with the nuclear sector now slowly recognising that there are strong needs that can be fulfilled by probabilistic paradigms. Presently the use of probabilistic approaches in the nuclear sector has been limited, bespoke and mainly summoned when traditional deterministic approaches fail to deliver business targets due to over conservatism. This work formulates a complete methodology based on the Monte-Carlo approach for conducting probabilistic calculations, focusing on applications considering the R5 Volume 2/3 procedure for high-temperature Advanced Gas Reactor (AGR) components. The presented methodology is generic enough to be applicable to a host of structural integrity applications. A number of case-studies are presented in Chapter 3-6 which consider specific implementation issues including the probabilistic representation of input parameters, treatment of correlations, loading uncertainties, conducting post-assessment sensitivity analyses, the extrapolation of assessment location probabilities to component-level and, thereafter, to population-level estimates. With the presented methods having implications for structural integrity applications in general, one of the aims of this work is to bridge the gap between the knowledge of statistical and probabilistic methods on one side, and the general structural integrity community on the other end. Consequentially, this work is intended to promote further implementation and engagement, aiding further acceptance within a wide range of structural integrity fields, and ultimately encouraging the creation of a unified probabilistic framework for structural integrity.

Acknowledgements

The accomplishment of this work could not have been possible without the expertise and guidance of my exceptional supervisors Prof Julian Booker and Dr Rick Bradford. Their support, generosity and sheer patience were never lacking, and I am truly fortunate to have worked with them. I am also grateful for the sponsorship of his research by EDF Energy, and for the support of Dr Marc Chevalier and Dr Dave Dean.

I wish to express my appreciation for everyone I had the pleasure of meeting as part of the Solid Mechanics Research Group at the University of Bristol. I would like to extend my sincere thanks to Prof David Knowles, Dr Mahmoud Mustafavi, Prof Chris Truman and Dr Harry Coules. I could not have achieved this without the friendship of my fellow PhD comrades, especially Joshua Hoole, Dr Sam Oliver, Chris Maire, Ed Hares, Satyajit Dey, Andrew James, Molly Probert, Kostas Kouzoumis, Dr Martin McMillan, Dr Andreas Andriotis, Dr Paolo Orrock, Dr Derrek Van Gelderen and everyone else from Queens Building.

Life for the past few years has been made richer by the personal relationships I had with Dr Francesca Migliaccio, Alarna Samarasinghe, Dr Amber Phillips, Dr Flora Derounian, Conrad de Kerckhove and Pietro Carnelli, for which I am very thankful. I cannot forget the wonderful interactions I had with my Senior Resident friends: Aewis, Ji-Yong, Witek, Rory, Jordan, Alice, Vedian, Kam and Katie. I would like to acknowledge my housemates Dan, Owain, Vicky and Rachel for their kindness and amusing company during the past few months.

Last but truly not least, I wish to express my gratitude and love towards my parents (Adel & Salma) and siblings (Hussam & Shireen) for their selfless support throughout my life, especially since I moved to the UK. Thanks to Anas Abumaise, Mohammed Abusharida and Amro Jaber for their true friendship which has literally transcended continents.

— Nader A. Zentuti
April 2019

AUTHOR'S DECLARATION

I declare that the work in this dissertation was carried out in accordance with the requirements of the University's Regulations and Code of Practice for Research Degree Programmes and that it has not been submitted for any other academic award. Except where indicated by specific reference in the text, the work is the candidate's own work. Work done in collaboration with, or with the assistance of, others, is indicated as such. Any views expressed in the dissertation are those of the author.

SIGNED: ..... DATE: .....

PUBLICATIONS

Two journal papers have been published thus far:

- Zentuti, N, Booker, J, Bradford, R and Truman, C, 2018, '*Correlations between Creep Parameters and Application to Probabilistic Damage Assessments*'. International Journal of Pressure Vessels and Piping, vol 165., pp. 295-305.
- Zentuti, N, Booker, J, Bradford, R and Truman, C, 2017, '*A Review of Probabilistic Techniques: Towards Developing a Probabilistic Lifetime Methodology in the Creep Regime*'. Materials at High Temperatures, vol 34., pp. 333-341.

Three additional papers were presented at conferences and seminars:

- Zentuti, N, Booker, J, Bradford, R and Truman, C, July 2018, '*Management of Complex Loading Histories for use in Probabilistic Creep-Fatigue Damage Assessments*'. in: Proceedings of the ASME 2018 Pressure Vessels & Piping Conference. American Society of Mechanical Engineers (ASME), Prague, Czech Republic.
- Zentuti, N, Booker, J, Hoole, J, Bradford, R and Knowles, D, April 2018. '*Probabilistic Structural Integrity*'. in: TAGSI/FESI Symposium, TWI, Cambridge, UK.
- Zentuti, N, Booker, J, Truman, C and Bradford, R, May 2017, '*Developing Probabilistic Methodologies in the Creep Regime*'. in: Proc. International Conference on Life/Crack Assessment Failures in Industrial Structures (HIDA 7), Portsmouth, UK.

Two further publications are planned, with the first being based on the work presented in Chapters 5, whilst the other will be a summary of Chapters 6:

- Zentuti, N, Booker, J, Bradford, R and Truman, C, '*Plant Data Analysis for Incorporation of Loading Uncertainties in Probabilistic Creep-Fatigue Damage Assessments*', International Journal of Pressure Vessels and Piping, Jan 2019 (submitted).
- Zentuti, N, Booker, J, Bradford, R and Truman, C, '*Probabilistic Structural Integrity: Methodology and Case-Study in the Creep Regime*', Probabilistic Engineering Mechanics, Mar 2019 (in preparation).

TABLE OF CONTENTS

List of Tables

List of Figures

Figure **Page**

List of Abbreviations

AGR	Advanced Gas-cooled Reactor
BE, LB, UB	Best estimate, lower bound and upper bound
CDF	Cumulative distribution function
CF	Confidence factor
CI	Confidence interval
CL	Confidence limit
CoV	Coefficient of variation
FE	Finite element (analysis)
LHS	Latin-hypercube sampling
MCS	Monte-Carlo Simulation
PDF	Probability distribution function
PoF	Probability of failure
PoI	Probability of creep-fatigue crack initiation
RSM	Response Surface Method
RT	Reactor trip transient instance
SA	Sensitivity analysis
SC	Stress component
SD	Standard deviation
SO	Steady operation event
SU	Reactor start-up transient instance
TC	Thermocouple
TN	Tubehole number
TP	Tubeplate plant component
TR	Transient instance

CHAPTER 1

INTRODUCTION

Some of the first mathematical conceptions of probability are commonly attributed to Bayes (1763) and Laplace (1812), and are widely accepted to be the founders of *Bayes theorem* which sits at the heart of probability theory [1]. It was Laplace, however, who widely applied his theorem to a range of problems, most famously the inference of Saturn's mass given astronomical data on its orbit. Since then, the concept of probability has perplexed and confused most who come across it. Most of the confusion stems from a few deep rooted misconceptions surrounding the probabilistic thinking. The most notable of these misconceptions relates to the truth that probability is not a measure of a real quantity, but rather a reflection of our state of the knowledge collated in order to produce such probability estimates. As such, a probability does not exactly predict, but rather narrows down our belief in a given occurrence or reality. One could argue that the mass of Saturn is impossible to measure with the same level of certainty by which one could measure the mass of an apple. Laplace's genius was to combine knowledge of classical mechanics with observations (i.e. data). His estimate was uncertain, mirroring his state of knowledge rather than implying that Saturn's mass was a randomly occurring quantity. What he discovered was a tool for plausibly combining and reconciling independent pieces of logical reasoning to create new information that would have remained unknown without such aggregation.

"Probability theory is nothing but common sense reduced to calculation"

— Pierre-Simon Laplace, Theorie Analytique Des Probabilite, 1814.

1.1 Background and Motivations

Probabilistic approaches have been used for over 50 years to infer the states and performances of engineering components, products and systems through the incorporation of uncertainties. These provide established methods and techniques for propagating uncertainty through engineering models. However, probabilistic implementation has remained limited and a deterministic culture still dominates many engineering domains to date [2]. This lack of prevalence in engineering is often related to engineers not being traditionally experienced in statistical concepts by default [3, 4]. Furthermore, despite probabilistic methods having been available for a number of years and are widely used, there is still a great deal of confusion stemming from vague language, ill-defined and inconsistent terminology, and misinterpretation often present in published material on the topic [5, 6]. Design and fitness-for-purpose assessment are two key application areas that can benefit from the adoption of probabilistics, which are essentially applicable to any situation where variability is expected to have an impact on the performance or failure potential of components or systems. The implementation of probabilistic approaches is intended to provide more confidence in assessment procedures and results. This is achieved, firstly, by examining and accounting for numerous sources of uncertainty, but also making full use of available data and understanding of the physics of failure. Probabilistic approaches must not be considered an alternative to conventional deterministic calculations, but rather a completely different, and often liberating, mindset which embraces complexity and uncertainty rather than obscuring them in favour of conservatism. Accordingly, they can be considered an evolution of traditional deterministic approaches, which have emerged from the reconciliation of statistical methods and physics of failure modelling, aided by advances in computational tools and hardware.

The application of probabilistic techniques in the area of high-temperature structural integrity has been gaining support and popularity in recent years, as examining uncertainties associated with plant components has become timely for life assessment and extension applications. Conventional calculations adhering to well-established structural integrity codes and procedures are predominantly deterministic, which most commonly rely on conservatism to account for uncertainty. This is usually achieved by applying safety factors, which are conservative but do not provide quantitative nor consistent measures of probabilities of possible failures. Furthermore, because these factors are usually subjective and commonly based on historic president, there is a lack of understanding of the level of conservatism they incurred. They also do not ensure intrinsic reliability, as evidenced by the occurrence of failures in-service [7]. Moreover, conservatism is commonly aggregated at each stage of an assessment procedure, which leads the results being challenging to justify, interpret or gauge whether they give adequate representations. As a result, some of the key uncertainties in the underlying assessment procedures can be neglected when opting for over conservatism, including [8, 9]:

- The issue of insufficient data to characterise material properties for long-term conditions.
- The use of extrapolations beyond the short-term experimental testing ranges.
- The inherent large scatter in the material data, especially creep and creep-fatigue data.
- The existence of various approaches for calculating the same parameters.
- Difficulties associated with modelling complex, or in some cases unknown, loading histories.
- Lack of understanding of the underlying failure mechanisms and their interactions.

The need for formally taking the above mentioned issues into account becomes unavoidable as plant components progress through their life expectancy, and the focus shifts from not only estimating the residual life whilst ensuring the highest level of safety, but also arguing for life extension in some cases. Consequently, traditional deterministic calculations are not intended for quantifying probabilities of failure, while probabilistic methods are well equipped tools for such applications, thus providing an opportunity to incorporate uncertainty in favour of optimal design and assessment. Probabilistic approaches allow for the systematic aggregation of uncertainties by incorporating knowledge and data related to manufacturing, inspection, in-service and material testing data to augment a valid picture of the state of in-service plant components. This results in safety being ensured by demonstrating that a failure will not occur, given the current level of knowledge, within an adequate confidence limit. This also allows for assessing the severity of possible component level failures towards wider systems. For implementing such methodologies within structural integrity, there are various facets of knowledge required [10]:

1. Understanding of the underlying physics of failure. Modelling of failure mechanisms is a general area of ever evolving knowledge and research where probabilistic techniques can aid in building confidence in the implemented models. Though it must be acknowledged that probability of failure estimates heavily depend on the rigour of the underlying physics of failure models, which are considered a major uncertainty source.

2. A general appreciation of probabilistic approaches and statistical concepts and the ability to relate these to a physical issue of interest.

3. Useful data and records related to the components of interest e.g. material properties, manufacturing information, loading data, history of repairs as well as past failures.

4. Computational expertise to facilitate the deployment of efficient algorithms.

5. Predefined target reliabilities related to the levels of tolerable frequencies of failure for specific components of interest.

Limited work has been conducted in the area of probabilistic high-temperature structural integrity. There has been some work focusing on aspects of creep rupture and creep-fatigue crack growth [11–17]. Creep-fatigue crack initiation, however, has received limited attention still [13, 18–21], and is the interest of this PhD project which was conducted in parallel with the drafting and acceptance of Appendix 15 for the R5 Volume 2/3 assessment procedure developed by EDF Energy. Furthermore, most literature is concerned with specific problems and applications, while no substantial work has been done on formalising a general approach which details each stage of conducting a probabilistic structural integrity calculation. This research built on the current deterministic approaches for determining the lifetime of plant components as outlined in the R5 Volume 2/3 procedure. This specific procedure was chosen as a key focus for this project, but the proposed methodologies have been presented, wherever possible, as to be divorced from any specific code or standard. Therefore, they can be implemented within the context of other structural integrity areas and are not exclusive to high-temperature applications. Subsequently, this research project was motivated by the the following needs:

1. The examination of probabilistic approaches which have been used in various industries and a requirement for distilling them to the key ones relevant to probabilistic structural integrity. This was not intended to be an exhaustive review, but was rather meant to be the first stage in identifying the main approaches needed for constructing a complete probabilistic assessment.

2. Providing justifications for a prospective shift from the currently followed deterministic procedures toward a probabilistic and risk management mind-set.

3. Identifying the various sources of uncertainty and their characterisation through probabilistic analyses. Such need is not currently addressed by conventional deterministic approaches.

1.2 Research Objectives

A challenge hindering the implementation of probabilistic methods in structural integrity is related to their perceived complexity and nuanced nature, which constitutes a mental barrier. This is exacerbated by the fact that accounting for various sources of uncertainty usually translates to greater complexity in the models, which in turn necessitates for the various constituents of such a model to be clearly defined, understood and verified. Generally, three attributes are typical, and undesirable, of a questionable model, and should be kept in mind during implementation. These are lack of transparency, lack of perpetual improvement and unaccountably [22]. The latter aspect is usually accounted for by virtue of adhering to regulations, standards and rigorous independent verification. This in turn feeds back into perpetual improvement and updating of the models to include as much current knowledge and data as possible. The subject of this thesis

is predominately concerned with the transparency aspect. The ultimate aim of this work is to contribute towards demystifying and popularising probabilistic applications, thus promoting their acceptance and implementation in the wider structural integrity community (academic, industrial and regulatory stakeholders alike). It is also argued that this will have a secondary benefit of promoting scrutiny and periodical improvement through usage and, in time, paving the way towards a unified probabilistic approach for structural integrity. Accordingly, the research objectives have been identified as follows:

1. Undertake a critical literature review examining: the relevant available literature, assessment procedures for use in case-studies and a wide range of probabilistic techniques.

2. Investigate the effectiveness and utility of probabilistic methods and techniques over conventional deterministic approaches, especially for plant applications which are inherently complex.

3. Develop a complete methodology incorporating systematic methods for the management of uncertainties (from inputs to outputs), and demonstrate its implementation on an in-service plant component subject to creep-fatigue crack initiation.

4. Provide context through application to case-studies.

5. Disseminate widely the research, with the intention of contributing to the R5 approach, mirroring industry's change in attitude in this area and promoting wider acceptance.

This PhD project focused on implementing probabilistic approaches in conjunction with the R5 Volume 2/3 [23] high temperature assessment procedure for Advanced Gas Reactor (AGR) applications. The R5 procedure was developed by the UK power generation industry and has been the major methodology applied to AGR components. The methodologies and approaches discussed in this thesis have, however, broader implications for structural integrity in general. Given appropriate expertise of a specific structural integrity domain and understanding of the probabilistic methods, the concepts presented in this work can be translated to applications beyond AGR and R5 applications. Therefore, this work is not intended to present a methodology that is only relevant to AGR applications, but rather to demonstrate implementations of probabilistic approaches using R5 as the underlying structural integrity assessment framework. Consequently, the discussed concepts and methods must be understood to be in themselves divorced from any specific structural integrity procedure. Where possible, the proposed methodologies were presented in general terms as to be applicable to a host of other structural integrity areas, with the aim of promoting and popularising probabilistic approaches within the structural integrity community at large. The Monte-Carlo approach, for example, is a general method which can be applied in conjunction with any structural integrity framework in order to estimate probabilities of failure. Nevertheless, this work has a clear link to the R5 approach which was driven by the

industrial sponsor (EDF Energy) and key aspects of this research (specifically topics related to sensitivity analysis and correlations) have influenced the new probabilistic appendix (Appendix 15) for the R5 Volume 2/3 procedure.

1.3 Research Methodology

Research methodology (RM) refers to the manner in which a body of research work is conducted in order to satisfy predefined objectives. This project followed a classical and logical approach for conducting the research work in order to satisfy the research objectives outlined in Section 1.2. A RM structure, referred to as a *received scientific methodology*, is articulated in [24]:

1. *Conducting a preliminary study*: a review of literature concerning probabilistic high-temperature creep-fatigue applications (Chapters 2) was conducted. Furthermore, an understanding of the tools, techniques and approaches required to conduct a full probabilistic assessment was formulated and an overview was collated to provide focus, which is included in Chapter 3).

2. *Hypothesis formulation*: e.g. one of the chief objectives was to establish whether probabilistic methods are applicable to high temperature structural integrity applications and whether they provide benefits when compared with traditional deterministics. This was addressed in the first three sections of Chapter 3.

3. *Hypothesis evaluation and testing*: this was achieved by conducting the various case-studies discussed in this thesis. From a probabilistic standpoint, an underdeveloped area within high-temperature structural integrity has been identified, which was creep-fatigue crack initiation. Key packages of work that are linked to creep-fatigue crack initiation were identified, and various methodologies were formalised. Crack initiation was used as a point of demonstration only, as the methodologies developed are intended to be transferable to other structural integrity applications. The main packages included: characterisation of material property uncertainty, correlations between input parameters, probabilistic treatment of loading conditions and sensitivity analysis. Where possible, the developed methodologies were demonstrated and contextualised using case-studies looking at various aspects of creep-fatigue crack initiation assessments.

4. *Hypothesis acceptance or rejection*: the outcome of this project suggests the probabilistic implementation is indeed applicable to a wide range of structural integrity applications, but clear understanding of the challenges and limitations must be advised. Finally through reflection on the work conducted, formalising routes for probabilistic implementation has emerged as a key need for progressing this work moving forward.

This research project was driven by the need for pertinent and novel work and was iteratively informed by the involvement and experience of the industrial collaborator (EDF Energy) through: quarterly meetings, presentations and frequent contact (remote and through periodic on-site visits to EDF's Barnwood office in Gloucester, UK).

1.4 Thesis Structure

It is suggested that this thesis should be read sequentially, as it constantly refers back to subtle concepts and ideas that would have been introduced earlier. A glossary of frequently used terms in this thesis is included in Section 1.5. Each chapter starts with an abstract followed by an introductory overview, and is concluded with a summary which highlights the main ideas and conclusions from each chapter. The main probabilistic approaches and techniques are presented in Chapter 3. However, methodologies which build and expand on these concepts are presented in each chapter, preceding their application in relevant case-studies. Highlights of the main topics covered in this thesis are presented below.

Chapter 2 - Literature Review This chapter starts with an overview of the main failure mechanics at high-temperatures (relevant to AGR applications) and highlights some of the main codes and standards that have been used to assess such failures. Furthermore, a critical review of the available literature examining probabilistic applications within high-temperature structural integrity is also presented.

Chapter 3 - The Case for Probabilistic Structural Integrity A formal discussion on the merits, prospective advantages and important considerations concerning probabilistic implementation. Two case-studies discussing various topics including sensitivity analysis, model uncertainty and uncertainty in material properties are also presented.

Chapter 4 - Correlations Between Input Parameters An approach is formulated for assessing and incorporating important correlations between input parameters. An investigation was conducted into the correlation between creep deformation and ductility as part of a case-study, the aim of which was to demonstrate that such correlation can have a significant impact on probabilistic assessment results.

Chapter 5 - Loading Uncertainties This chapter explores methodologies and techniques for predicting characteristic loading conditions (typically stress states and metal temperatures) based on plant data. Methods such as linear regression, Response Surface Method and directly sampling histograms are used for the treatment of transient and steady-operating conditions as experienced by plant components prone to creep-fatigue damage. A tubeplate plant component is introduced as the object of a case-study which applies the methods discussed in this chapter.

Chapter 6 - Probabilistic Methodology for Plant Components This chapter incorporates all the concepts discussed in previous chapters, whilst introducing methods for estimating probabilities at component and population levels. A probabilistic assessment of the tubeplate component is presented to demonstrate the now complete methodology, which ultimately aggregates available knowledge and data to provide estimates for individual components as well as populations of components.

Chapter 7 - Conclusion A reflection on work, lessons learned, the role of this body of work and the future of probabilistic structural integrity. This chapter also summarises the thesis, highlighting research contributions and outcomes whilst providing some suggestions for further work.

1.5 Important Terminology

Terms that are frequently used throughout this thesis are explicitly defined below.

- *Probabilistic Approach*: any calculation that incorporates some degree of uncertainty in its input conditions.
- *Deterministic Approach*: any calculation that assumes fixed input conditions.
- *Performance function*: any process, procedure, calculation or numerical model that maps a set of input conditions onto a desired output. In this thesis the performance function usually refers to a set of calculations used to infer creep-fatigue damage, which is prescribed by the R5 Volume 2/3 assessment procedure.
- *Confidence Interval*: a range of values defined such that there is a specified probability that the value of a parameter lies within it. The range is defined by the area under a probability density function (PDF) e.g.a 95% confidence interval implies that its range encloses 95% of all possible values of a parameter.
- *Confidence Limits*: values at the extremities of a confidence interval range, and can also be termed *scatter bands*.
- *Methodology*: a compatible collection of goals, assumptions, underlying methods, results evaluation and interpretation [24].
- *Method*: an approach or technique that is used to perform a specific function or, more accurately within the context of this thesis, a calculation.
- *Uncertainty*: can be categorised in terms of either *aleatory* (arising due to chance or irreducible randomness) or *epistemic* (arising from a lack of knowledge and the inability to explain physical failure mechanisms) uncertainties [19]

- *Monte-Carlo simulation*: repeated runs (or *trials*) of a procedural calculation with combinations of input parameter values determined by their respective weighted probability.
- *A sample*: input parameter values obtained from either randomly sampling (i.e. based on random number generator) or based on all values having the same probability of occurrence (e.g. equal probability in latin-hypercube sampling).
- *Correlation*: a numerical value which defines the strength of a relationship (e.g. linear or monotonic) between two parameters, which is measured from experimental data-sets.
- *Probability of failure*: the probability of the performance function yielding an output value that exceeds a failure criterion. In this thesis, failure refers to the initiation of a shallow crack dude to the accumulation of creep-fatigue damage.

CHAPTER 2

LITERATURE REVIEW

Metallic components operating at high temperatures (typically larger than a third of their melting temperatures in °C [25]) are susceptible to a host of possible failure mechanisms. Typical examples include components in power generation plants (e.g. boiler parts) or gas turbine components (e.g. blades) in an aircraft engine. This work was originally driven by the need for formalising probabilistic approaches for high-temperature applications which are pertinent to AGR plant assessments. This chapter provides brief descriptions of the most common failure mechanisms for AGR plant components, focusing on creep and creep-fatigue which were of most interest. To demonstrate safety within design and fitness-for-purpose assessment applications, a number of codes, standards and procedures have emerged in different countries. Some of these documents are highlighted in this chapter whilst a greater emphasis on the R5 Volume 2/3 assessment procedure was given due to its relevance to AGR plants. Thereafter, an overview of available literature on previous probabilistic implementations within high-temperature structural integrity is presented, thus summarising the current state of this area of research.

2.1 High-Temperature Failure Mechanisms

2.1.1 Creep

Creep is a time-dependent plastic deformation of metallic materials operating at high-temperatures, under the influence of mechanical and/or thermal stresses. Prolonged exposure to creep inducing conditions leads to the accumulation of creep deformation and eventually rupture [25]. Deformation is often characterised by three stages as shown in Figure 2.1 [26, 27]:

1. Primary creep: during which the creep strain rate decreases as a result of work hardening.

2. Secondary creep: the creep strain rate reaches a steady state minimum value as a result of balancing between work hardening and recovery of ductility at high-temperatures.

3. Tertiary creep: which precedes creep rupture, and is caused by the accumulated creep damage reducing the load bearing cross-section which in turn leads to an accelerated creep strain rate.

Long term creep failure (at relatively low stresses and temperatures e.g. those typical of Advanced Gas-Cooled Reactor, AGR, boiler components) is usually characterised by brittle, intergranular crack propagation as a result of cavities forming and coalescing along grain boundaries [28]. Creep damage is driven by diffusion processes along grain boundaries and across dislocation lines, whilst the creep deformation may be a combination of dislocation movement and diffusion [26].

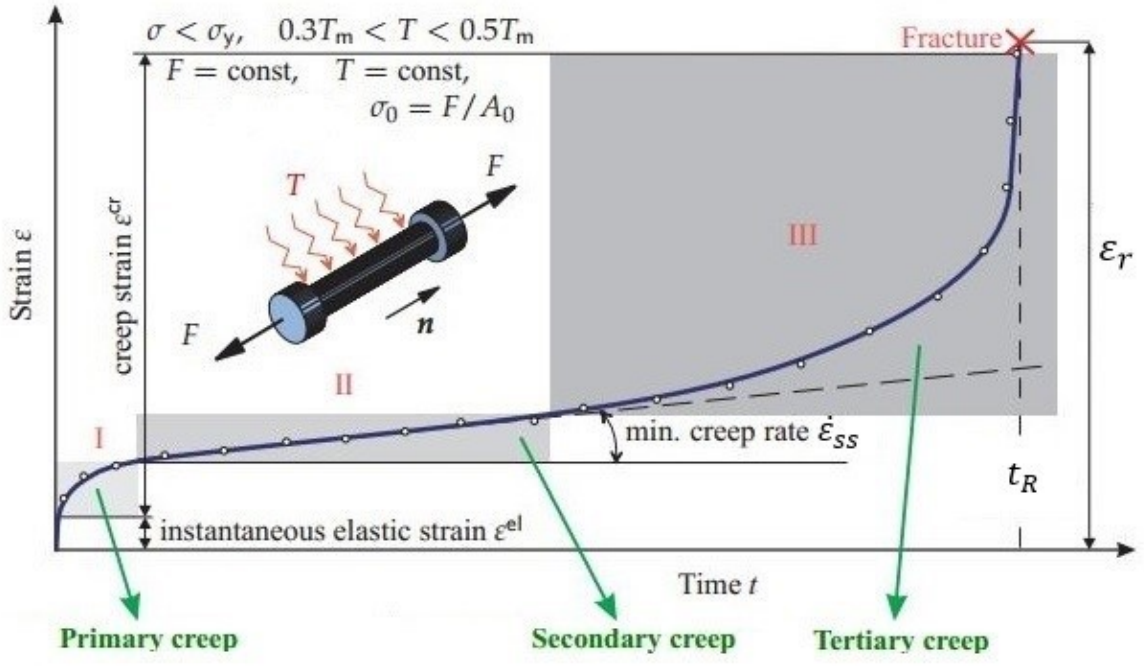

Figure 2.1: A typical creep curve showing the three stages of creep deformation for a uniaxial case [29, 30]. redThe applied temperature (T) is high enough relative to the melting temperature (T_m) as to induce creep deformation under the influence of the applied force (F). Some of the parameters which characterise creep behaviour include the time to creep rupture (t_R), ductility which is defined as the creep strain at failure (ε^{cr}) and the minimum creep rate $\dot{\varepsilon}_{SS}$.

2.1.2 Cyclic Loading and Creep-Fatigue

Creep-fatigue is a dominant failure mechanism caused by cyclic mechanical or thermal stresses, typically resulting from repeated heating and cooling cycles [28]. This is associated with the

interaction between low-cycle fatigue and the accumulation of creep deformation during hold periods (also referred to as creep dwells). Possible causes also include residual stresses in heavy section components resulting from internal thermal gradients. High stresses may also arise in thin section components if their cyclic deformation is constrained by surrounding assemblies [31]. Furthermore, structural responses under cyclic loading differ from monotonic loading, as components may fail at lower stresses then those typically needed for monotonic plastic collapse (i.e. the limit load). Depending on the magnitude of stresses, four possible behaviours can be observed under cyclic loading [32]:

(a) The loads remain within the elastic limits and no plastic deformation occurs as shown in Figure 2.2a.

(b) Plastic strain is incurred within the initial loading cycles, but the response soon becomes purely elastic. This is termed *strict shakedown* and is shown in Figure 2.2b.

(c) If a closed deformation loop is achieved (i.e. plastic deformation occurs on both ends of the cycle as shown in Figure 2.2c) then no net plastic strain is incurred and a stable cycle is attained, thus *global shakedown* is achieved.

(d) If net plastic strains are accumulated over subsequent loading cycles, then *ratcheting* (Figure 2.2d) occurs, which eventually leads to plastic collapse.

Additional to the cyclic responses shown in Figure 2.2, periods of exposure to creep inducing conditions (i.e. high temperatures and significantly severe loads) can result in the accumulation of creep strain which is additional to the plastic and ratchet strains described above. Assuming creep does occur, the first two conditions listed above are permissible, and in the presence of a creep dwell may only require a creep assessment. A global shakedown case would be examined through a creep-fatigue assessment which looks at the evolution of both the creep and fatigue damages over the component lifetime. Ratcheting must be generally avoided but maybe permissible if the ratchet strain is sufficiently small.

2.1.3 Reheat Cracking

Reheat cracking (also known as stress relief cracking) may effect in-service low alloy steel welds. This results from the relieving of weld residual stresses by creep deformation during high-temperature operation [33]. As the yield strength of a metallic material is reduced at elevated temperatures, if the relaxing residual stress exceeds the yield strength, then plastic deformation occurs. If this deformation is accommodated by dislocation movement (or displacement in a flexible system), then the residual stresses are relieved without any subsequent issues. However, if that does not occur, then the stresses will be relieved by creep deformation at grain boundaries. Furthermore, other factors (e.g the presence of impurities or the precipitation of carbides within the grains) may lead to a relative reduction in intergranular strength, which in turn promotes

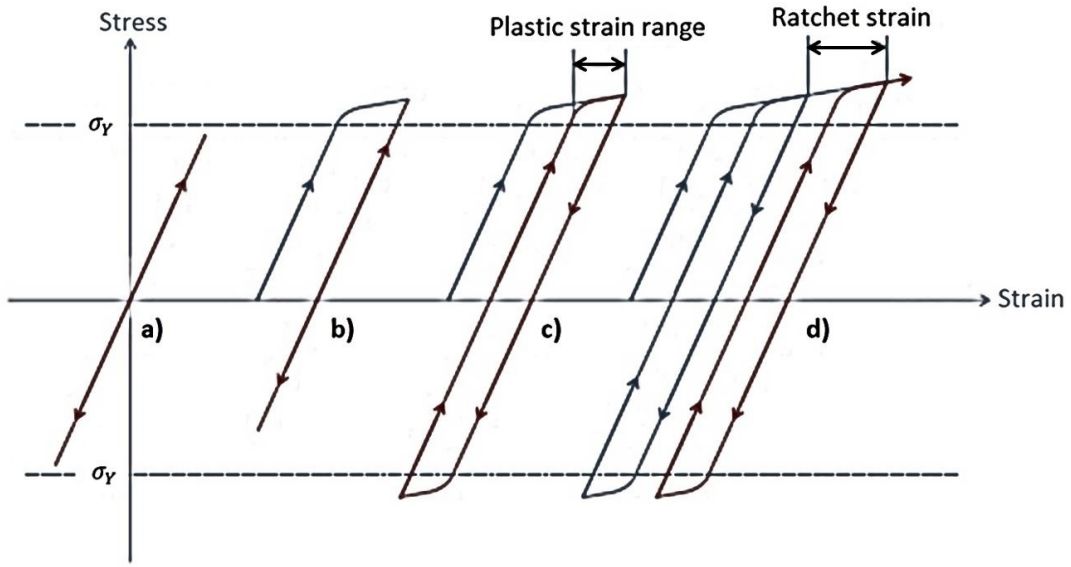

Figure 2.2: Possible structural responses to cyclic loading.

reheat cracking. It is also contingent on a number of other factors including grain sizes in the heat affected zone (where coarser grains are present) and the weld bead profile. Typically, reheat cracking is only expected in welded components and, to countermeasure it, post-weld heat treatment can be implemented.

2.1.4 Material Degradation

For austenitic stainless steels operating in carbon rich environments (e.g. CO_2 in AGRs) at high temperatures, carburisation may occur whereby the added carbon content combines with chromium to form various types of chromium carbides. This results in grain boundaries being depleted from chromium, which is the element that gives austenitic stainless steels their high-temperature corrosion resistant properties. This causes vulnerability to oxidation and intergranular fracture [31]. Furthermore, precipitation of these carbides along grain boundaries promotes the initiation of creep cavities [15]. A further example of material degradation is erosion due to fluid flow within pipes, which leads to metal loss over their operational lives [31].

2.2 High-Temperature Codes and Standards

Historically, numerous codes, standards and procedures have been developed to assess high-temperature components where the main modes of failure are creep or creep-fatigue [34]. Chief examples are the American ASME III Subsection NH [35] and the ASME III Division 5 [36] design codes, the French RCC-MRx design codes [37], the BS7910 assessment procedure by the British Standards Institution [38] and the R5 procedure [23] developed by the UK power genera-

tion industry, which has been the major methodology applied to AGR components. Currently, the use of probabilistic methods has been included in some structural integrity codes and procedures including the R6 [39] (the low-temperature counterpart to R5) structural integrity procedure for structures containing defects by EDF Energy and R5 Volume 4/5 Appendix A7 concerning creep-fatigue crack growth, though the extent of such guidance is quite limited [40]. BS7910 also provides some general advice on the application of reliability analysis methods in Appendix K, while the ASME codes mentioned above do not contain specific guidance on probabilistic implementations [5]. Presently no formal advice is available for R5 Volume 2/3, which has recently prompted the creation of Appendix 15 to provide some general, non-prescriptive advice on conducting probabilistic assessments. This new appendix was recently approved for inclusion by the R5 Panel [41], though it is not yet published within the current version of the R5 procedure.

From a regulatory prospective in the UK, there has limited interest for the use of probabilistic methods for nuclear structural integrity safety cases, with the implementation of probabilistics for the assessment of graphite cores in AGRs being an exception. Nevertheless, the UK regulator (the Office for Nuclear Regulation, ONR) has historically taken a non-prescriptive approach, which implies that probabilistic safety cases can still be presented to the ONR and will be judged on the merits argued within individual safety cases. As a result, the main proponents for probabilistic implementation have been from industry and academic stakeholders. This is in contrast with the Canadian Nuclear Standard CSA N285.8 for CANDU reactors which allows for the use of probabilistic methods for reactor core assessments [42]. Furthermore, proposals for including probabilistic acceptance criteria for pressure tubes have also been recently put forward [43]. The absence of explicit sanctions for the use of probabilistics in nuclear structural assessments is a curious inconsistency since nuclear safety cases, more broadly, are intrinsically reliant upon probabilistic concepts. For example, the PSA (probabilistic safety assessment), ALARP (as low as reasonably practicable) and the dose-frequency staircase which are probabilistic in nature [19, 44]. As a result, in the UK nuclear sector the main drivers for probabilistic implementation have been from industry (e.g. the creation of Appendix 15 by EDF Energy [41] and the formulation of probabilistic working principles by the working group led by Rolls-Royce [5]) and academia (e.g. this PhD project).

A detailed examination of the above mentioned codes and procedures is beyond the purposes of this work. However, given that the focus of this project has been on creep-fatigue, a high-level comparison between two major procedures which protect against such failures (the EDF R5 Volume 2/3 procedure and the ASME BPVC Section 3 Division 1 Subsection NH code) is presented below. Examples of idealised loading cycles (the construction of which is part of the discussed procedures) including creep dwells can be found in Figures 3.4 and 5.2. The following is a non-exhaustive comparison of the salient aspects between the two procedures [45]:

1. **Material data**: ASME NH includes some data on a limited selection of alloys, whilst that is beyond the purpose of R5 and data is obtained from other sources such as EDF Energy's R66 handbook [46].

2. **Elastic follow up for secondary stresses**: Both suggest approaches for estimating the elastic follow up factor, but in some cases ASME NH assumes, conservatively, that load control conditions apply for simplicity.

3. **Pre-creep assessment tests**: Both R5 and ASME NH compare primary stresses to yield properties to test for plastic collapse. Furthermore, both require the achievement of global shakedown and the avoidance of ratcheting. R5 also provides a test for the significance of creep, while such approach is not demanded in ASME NH.

4. **Estimation of stress states**: Both are based on simplified estimates of non-linear stress-strain responses using elastic stress as the starting point, as opposed to full non-linear analysis based on FE models. Complex stress analyses are typically only required when the standard procedure produces overly pessimistic results and, therefore, there is a need for more realistic estimations of the loading stresses. Both approaches give advice on the treatment of multi-axial stress states.

5. **Strain range and creep strain**: R5 uses a *Neuber transformation* to relate the elastic stresses and strains to their plastic equivalents, in conjunction with a cyclic stress-strain relationship such as *Ramberg-Osgood*. Creep strain, which can effect the strain range, is calculated in R5 using a forward creep expression with an appropriate follow up factor. A method included in ASME NH adds an extra strain (to account for creep relaxation) to the strain obtained from the isochronous stress-strain curves assuming (conservatively) a constant stress at the shakedown limit. Both methods provide similar advice on how to account for the effects of multi-axiality and volumetric strain on the stain range.

6. **Hysteresis cycle**: For R5, the start of dwell stress is found using a cyclic stress-strain relationship and then the whole cycle is repositioned relative to the shakedown limit, $K_s S_y$ (a process called *symmetrisation*). By contrast ASME NH uses isochronous stress-strain curves with the total strain range to estimate the stress at the beginning of the dwell.

7. **Creep stress relaxation**: To approximate the stress drop during the creep dwell, ASME NH includes a method based on isochronous stress-strain curves. For R5, by comparison, a common approach is to use the strain hardening version of RCC-MR's creep deformation model in conjunction with a forward creep relationship. R5 also provides advice as to the approximation of elastic-follow up, and provides guidance on whether *primary reset* (the creep strain resets after every loading cycle) or *continuous hardening* (the creep strain is continuously accumulated throughout the entire cyclic loading history) should be assumed.

8. **Estimation of creep damage**: a key distinction between ASME and R5 is that they evaluate creep damage differently, as the former uses a *time-fraction rule*, whilst the latter implements a *ductility exhaustion* approach.

9. **Fatigue damage**: Both R5 and ASME NH rely on experimental data to extrapolate the fatigue endurance using *Miner's rule*. However, the major difference is that ASME NH uses continuous cycling fatigue data, while R5 makes a distinction between crack initiation and crack growth. The effect of these differences on the results are only noticeable in certain circumstances, for example, if the creep strain is significant or if the strain range is affected by interacting cycles.

10. **Damage limits**: R5 assumes crack initiation if the total creep-fatigue damage reaches a value of unity (i.e. $D_T = 1$), thus it uses a linear interaction model between the creep and fatigue damages which is not material dependent. By comparison, ASME NH uses a bi-linear model which is material dependent.

11. **Degradation due to environmental and ageing effects**: such effects are acknowledged and are subject to current and further development work (e.g. on the effect of carburisation on creep ductility). Limited advice is available in the current version of R5, though some considerations for the effect of carburisation on creep ductility is to be included in future revisions. Though ASME NH incorporates some of these effects in terms of tensile properties through strength reduction, environmental and ageing effects have not been formally addressed.

Overall, both R5 and ASME NH aim to be conservative rather than accurate. However, ASME NH has more simplifications embedded in its analysis, and thus is generally more conservative. This stems from the fact that ASME NH is a code/standard, as opposed to a detailed assessment procedure like R5 [45]. For some cases where ASME would yield overly pessimistic results, R5 provides an alternative for reducing conservatism, especially when complex loading conditions are involved. For such situations, a more sophisticated representation of the stress-strain cycles (which R5 provides when compared with ASME NH) is desirable. In that respect, R5 provides more flexibility, though it is heavily reliant on the judgement of the practitioner for specifying the input material data as limited advice is provided for that aspect. Therefore, it must be acknowledged that ASME NH is a *prescriptive* code, whereas R5 aims to be more *descriptive* of the underlying high-temperature assessment methodology. Nevertheless, there is a significant degree of overlap between R5 and ASME NH.

2.3 Probabilistic High-Temperature Structural Integrity

This section examines some of the available literature on employing probabilistic techniques with creep and creep-fatigue assessments, which was found to be a rather limited area of work. Conventional deterministic assessments which use bounding values (i.e. pessimistic) for input parameters introduce various degrees of conservatism, as they fail to make full use of the statistical information that could be inferred from available data [9]. Most previous work in this area of research has concentrated on creep rupture (e.g. using simple time-fraction rules for creep damage) and creep-fatigue crack growth (e.g. R5 Volume 4/5) assessments [11–17, 47]. However, the subject of probabilistic creep-fatigue crack initiation assessments (the R5 Volume 2/3 type, which is the focus of this PhD project) seems to be under explored, with the exception of work by M. Chevalier [19] and R. Bradford [13, 18, 20, 21]. Regardless of the technical application (be that creep rupture, creep crack growth or crack crack initiation), most previous work focused on targeting specific problems or applications faced by practitioners, typically when deterministic calculations were found to be unsatisfactory. As such, there is a clear need for developing probabilistic frameworks that are methodology driven and provide descriptive advice for a range of possible structural integrity applications.

2.3.1 Applications to Creep Rupture and Crack Growth

The starting point for the most basic probabilistic approach is to treat input parameters as random variables, and then use a Monte-Carlo Simulation (see Section 3.4.1) based on a performance function in order to infer the variability of an output parameter of interest. A recurring approach in the literature has been the statistical treatment of creep rupture, strain and crack growth data to account for experimental data scatter before usage in creep assessments (e.g. [14, 16]). This was commonly done through the incorporation of statistical error terms in the various models used. For example, in [14] the the error terms for uniaxial time to creep rupture (t_R) and steady-state creep strain rate ($\dot{\varepsilon}_c$), were included as follows:

$$\dot{\varepsilon}_c = C' \sigma^{n+e_n} 10^{e_C} \tag{2.1a}$$

$$t_R = A' \sigma^{\nu+e_\nu} 10^{e_A} \tag{2.1b}$$

where σ is the uniaxially applied stress, while C', n, A' and ν are model parameters which are material specific. The 10^e terms account for the *standard error* on the respective intercepts (i.e. C' and A', which are assumed to be lognormally distributed), while e_n and e_ν are the *standard errors* on the slopes. Error terms are treated as random variables, commonly assumed to be normally distributed, while least squares linear regression can be used to characterise the error terms.

Bayesian regression has also been used to characterise variability in creep-fatigue rupture predictions using creep extrapolation models (e.g. the Larson-Miller model) [15]. Due acknowledgement was given for the issues of over-fitting and the inadequacy of these regression methods beyond available data ranges. Alternatively, the data (e.g. for t_R) can be fitted to an appropriate distribution, regardless of the underlying power law, using techniques such as those discussed in Section 3.4.2. Scatter in test data may be attributed to a number of sources including: test procedures and measuring equipment, data analysis methods and the physics of interacting failure modes (e.g. interactions between creep and fatigue damages) [11]. Interestingly, in [16] a distinction is made between scatter due to variations within a specific material cast (random variations attributed to the failure processes) and variations between different casts (e.g. due to differences in chemical compositions or manufacturing processes). These were quantified by dividing the available data into appropriate subsets from which statistical measures could be inferred.

Especially for creep models where power laws are used, lognormal distributions have been commonly adopted (e.g. in [11, 13, 14, 16, 18, 20, 21]) to statistically characterise various material data, most often the time to creep rupture. For operating loads and temperatures other distributions may be more appropriate, for which some advice can be found in [21]. Furthermore, in the BS-PD6605 procedure a range of models were fitted to creep rupture data using the *maximum likelihood* method. Two key characteristics of this procedure were the use of Weibull and log-logistic error distributions to model the stochastic nature of the data and the inclusion of unfailed test results using a survival function [48, 49]. Following the statistical data characterisation, some previous work [14] has adopted simple sensitivity analysis using deterministic calculations for which some advice is available for creep-fatigue crack growth analysis in the R5 Volume 4/5 assessment procedure. Similarly, in [11] sensitivity was assessed by correlating the output to the input parameters to establish the parameters of most importance (i.e. the ones which introduced the most variability in the output parameters).

The incorporation of further degrees of complexity in probabilistic models are also possible. For instance, complex time dependent geometric effects related to material loss can be included, an example of which is [47], which places emphasis on the effect of oxidation on geometries and temperature profiles in assessed components. Moreover, a challenging aspect in assessments which examine components with complex geometric features is the approximation of stress states. For instance, [12] and [17] adopted probabilistic methodologies to gas turbine components under creep-fatigue conditions. Crucially, the issue of incorporating computationally intensive FE analysis into the probabilistic framework was acknowledged, and the adoption of the Response Surface method (RSM) in conjunction with Design of Experiments (DOE) was suggested as a alternative for reducing computational efforts.

The subject of correlations between the various parameters involved in creep assessments is generally acknowledged for its importance, but not widely examined. For example, in [16] it is suggested that joint probability distributions can be used to sample correlated parameters, but this was expected to be challenging. The difficulty in quantifying correlations arises from the absence of rigorous statistical data treatment [11]. These correlations can be between [21]:

1. Material properties (e.g. average creep strain rate and creep ductility).
2. Operating conditions (e.g. between stress and temperature).
3. Material properties and operating conditions (stress and/or temperature).
4. Assessment locations within the same component.

2.3.2 Applications to Creep Crack Initiation

As previously stated, probabilistic creep-fatigue crack initiation assessments seems to be an underdeveloped area of research; limited amount of literature in the public domain examining this topic can be found. The most insightful literature on this topic include [13, 18–21], which were concerned with R5 Volume 2/3 creep-fatigue initiation assessments, and featured a number of issues which are of interest to this research work:

- Basic statistical concepts e.g. probability distributions.
- The different loading cycles involved including their sequence and interactions, as well as variations within a single cycle type.
- The challenges associated with modelling stresses and temperatures based on historic data.
- Implementation of the Latin-Hypercube Sampling (LHS) approach.
- Possible approaches for treating time dependent variables.
- Treatment of correlated parameters, but provide limited quantitative advice as to the degree of these correlations.
- Treatment of components which are part of large populations (e.g. boiler tubes).
- Discussion of the effect of the creep strain re-priming assumption on the assessment results.
- Statistical modelling of failure data using Binomial distributions.
- Characterisation of uncertainties in inspections techniques and using Bayesian statistics to take their effects on predicted probability of failure into account.

Pertinent to this research work, [21] includes a complete R5 Volume 2/3 assessment of an AGR plant component (tube bifurcations) for which the effects of tube flow restrictions (which can cause overheating) and environmental degradation (carburisation) were examined. A main achievement from this work was providing plausible explanations for failures related to tube restrictions, which was not previously achievable with deterministic assessments. Bounding deterministic calculations claimed that tube failures due to restrictions should have been of major concern. However, using a probabilistic approach, the work in [21] suggested that overheating due to tube restrictions only affected a small number of tubes and thus should have not been a recurring issue for the whole population of boiler tubes. This was revealed to be a more realistic conclusion than the deterministic expectation. However, even the probabilistic assessment results were not in agreement with the instances of failures observed in-service. In the same work, it was noted that conventional assessments were unable to predict the incidences of cracking found during inspections, and using probabilistic insight this was attributed to not accounting for an unknown failure mechanism (believed to be carburisation). A conclusion backed by the probabilistic results was that the increased incidences of cracking were unlikely to have been attributable to nominal degradation (i.e. creep-fatigue and tube restrictions) only. Instead, the additional degradation mechanism (carburisation) was likely to have contributed to the overall degradation. By matching probabilistic results with inspection results, a quantitative assessment of the degree of degradation introduced by carburisation was possible. The main conclusion was that carburisation led to reductions in creep ductility and fatigue endurance, which resulted in increased failure occurrences.

2.4 Summary

The most common high-temperature failure mechanisms were described as an introduction to future discussions in this thesis. A number of codes and procedures were discussed, while some of the important features of two relevant examples (ASME NH and the R5 Volume 2/3) were discussed to provide some background. The main discussion points that have emerged from this literature review are:

- Work relevant to probabilistic structural integrity has been limited to date and, in most cases, problem driven. This signals a clear need for a complete methodology for highlighting and incorporating a wide array of probabilistic methods and techniques.
- A good range of probabilistic topics and implementation issues have been considered in the available literature, which provided the starting points for this research.
- Creep-fatigue crack initiation has been identified as a key failure mechanism of interest within high-temperature structural integrity and, as a result, formed part of the focus of

this PhD project.

- In general, there is a significant appetite in the nuclear sector for incorporating probabilistic methods into structural integrity applications, which is evidenced by the increasing engagement of industry and academic stakeholders in recent years.

CHAPTER 3

THE CASE FOR PROBABILISTIC STRUCTURAL INTEGRITY

This chapter considers the benefits and importance of adopting probabilistic approaches within structural integrity. This is supported by a discussion on the common modes of application for probabilistic techniques, with a reflection on how they can translate to design and fitness-for-purpose assessment applications. The main challenges faced by probabilistic implementation are also acknowledged and some ideas for overcoming them are suggested. What follows is a brief introduction to the main probabilistic techniques repeatedly used in this work, which constitute the main building blocks for the proposed probabilistic methodology. A case-study assessing a simple uniaxial creep-fatigue test specimen for creep-fatigue damage using the R5 Volume 2/3 procedure is presented to demonstrate the implementation and utilities of the main probabilistic approaches. The results include discussions on quantitative sensitivity analysis and the examination of model uncertainty.

3.1 Why a Probabilistic Paradigm?

As previously alluded to, probabilistic thinking is nothing more than the aggregation of various forms of knowledge to infer a reality that is not possible to establish directly. Relative to deterministic thinking, it allows for the full incorporation of uncertainty (i.e. imperfect knowledge) in order to get probability measures. In that respect, it is a more holistic representation of the current state of knowledge with regards to a situation of interest and, as such, purely an evolution of the deterministic mindset. It also provides quantitative measures of performance, helping practitioners to distil information from complex analyses into meaningful conclusions. For an application where a measure of reliability is needed whilst driving for optimal performance, probabilistic methods comprise systematic frameworks which aid in building confidence [50, 51].

In recent years, the applicability of probabilistic methods have become viable, mainly due to advances in commercially available computational hardware, thus allowing for more complex and quicker analyses and simulations. Traditional deterministic mindsets prefer using factors of safety to achieve conservative design and assessments, without providing quantified measures of reliability nor conservatism. Table 3.1 provides a high-level comparison of important characteristics between deterministic and probabilistic paradigms [10]. Consequently, the key benefits of incorporating probabilistic methods include:

1. Allow for the full utilisation of available data sets (regardless of sample size), thus incorporating rather than obscuring uncertainties. Accordingly, lack of data should be viewed as a strong case for adopting probabilistics, as the greater the uncertainty, the more strongly motivated is a probabilistic approach. The commonly quoted opposite arguments, e.g. deterministic calculations are better because there is a lack of data, can be paradoxical.

2. Lack-of-knowledge is accepted and conservatism can be avoided or added depending on the application.

3. In more sophisticated applications, they allow for the integration of analysis and inspection data.

4. Models can be expanded to include larger data-sets or better knowledge at later stages, and improvements can be done systematically, thus mirroring the evolution of the state of knowledge.

5. They provide quantitative measures of risk which can support decision making processes for both design and assessment applications. This can aid in focusing attention towards areas which will yield optimal improvement of performance, whilst saving both effort and cost. Examples are targeting and prioritising inspection routines for plant assessment applications, and saving on prototyping for design applications.

3.2 Utilities of Probabilistic Approaches

Probabilistic analyses can serve a wide range of applications, which ultimately are dictated by the desired objectives. Some of the main modes of application are summarised in Table 3.2. Within structural integrity specifically, however, engineering calculations can usually be considered either *design* or *fitness-for-service assessment* problems. The latter, which was the main focus for this work, is more concerned with demonstrating safety given some sort of acceptance criterion, whilst a component progresses through its life-expectancy. This can benefit from having some in-service data and knowledge of past failures to inform the assessment formulation. A useful concept for visualising the utilities of probabilistic design and assessment is the Load–Strength

Interference problem, which is shown schematically in Figure 3.1a. The probability of failure is the area of the envelope defined by the $L > S$ condition. Now supposing that Figure 3.1a represents an unsatisfactory design, then Figures 3.1b shows two possible courses of action for reducing the probability of failure. Similarly, if Figure 3.1a is taken to represent the state of a component in-service, then examples of probabilistic implementations (shown schematically in Figure 3.1c) can include:

1. Accounting for the current state of the material under consideration. In-service conditions can result in the alteration of material behaviour over time through mechanisms such as ageing or degradation. These mechanisms can be positive or undesired, but typically introduce more uncertainty in the estimates as to reflect the uncertain understanding of these additional failure mechanisms.

2. Depending on the level of complexity included, improved assessments can include better statistical representations of in-service loads and material properties (e.g. by examining plant measurements) which can reduce conservatism. Inspection data can play important roles in such applications.

3. If an assessment yields an estimate that is not acceptable, then a course of action may be to reduce the operating loads to reduce the projected damage by the end of service, and a probabilistic assessment can measure the benefits, or lack thereof, of taking such intervention.

This design versus assessment example serves to show that probabilistic structural integrity can have many modes of applications which depend on predefined purposes. As a result, different strategies are applicable to different scenarios. For example, during the design stage changing the material is an option, whilst the same suggestion would not be possible whilst assessing an existing asset and, consequently, different strategies would be required to demonstrate reliability. It is suggested in this work that a general appreciation of the entire ecosystem of probabilistic approaches and methods (some introduced in this chapter and others discussed in later chapters) is needed in order to tackle a variety of structural integrity problems, which on the one hand may require general solutions (e.g. using the Monte-Carlo approach) whilst some applications may need specific tools (e.g. using a Response Surface method, RSM, when FE models are needed).

Table 3.1: Comparison between key aspects of deterministic versus probabilistic calculations.

	Deterministic	Probabilistic
Inputs	Single values e.g. mean, upper or lower bounds	Distributions, histograms, ranges or single values
Outputs	Single value and pass/fail results	Distributions (or histograms) and a probability of failure
Uncertainty incorporation	Using factors of safety to simply uncertainty	Explicitly and quantitatively accounted for using available data and competing models or assumptions
Correlations	Based on judgement	Measured from data
Sensitivity analysis	Local	Local and global
Run time	Single runs	Typically $> 10^5$ runs using Monte-Carlo and single runs for semi-probabilistic approaches (FORM and SORM)

Table 3.2: Main utilities of probabilistic approaches and techniques [52].

Application	Objective(s)
Reliability/risk assessment	Evaluate the probability of failure (or reliability).
Performance assessment	Given a design or state of a system, establishing the range of performances the can be expected, thus providing measures for improvement.
Optimisation	Reduce redundancies through more economic design. Optimise a design given multiple competing requirements.
Sensitivity analysis	Identifying the input conditions (e.g. parameters, assumptions and models) which contribute the most to the output uncertainty.
Characterisation of uncertainties	Increase confidence in processes and outputs.

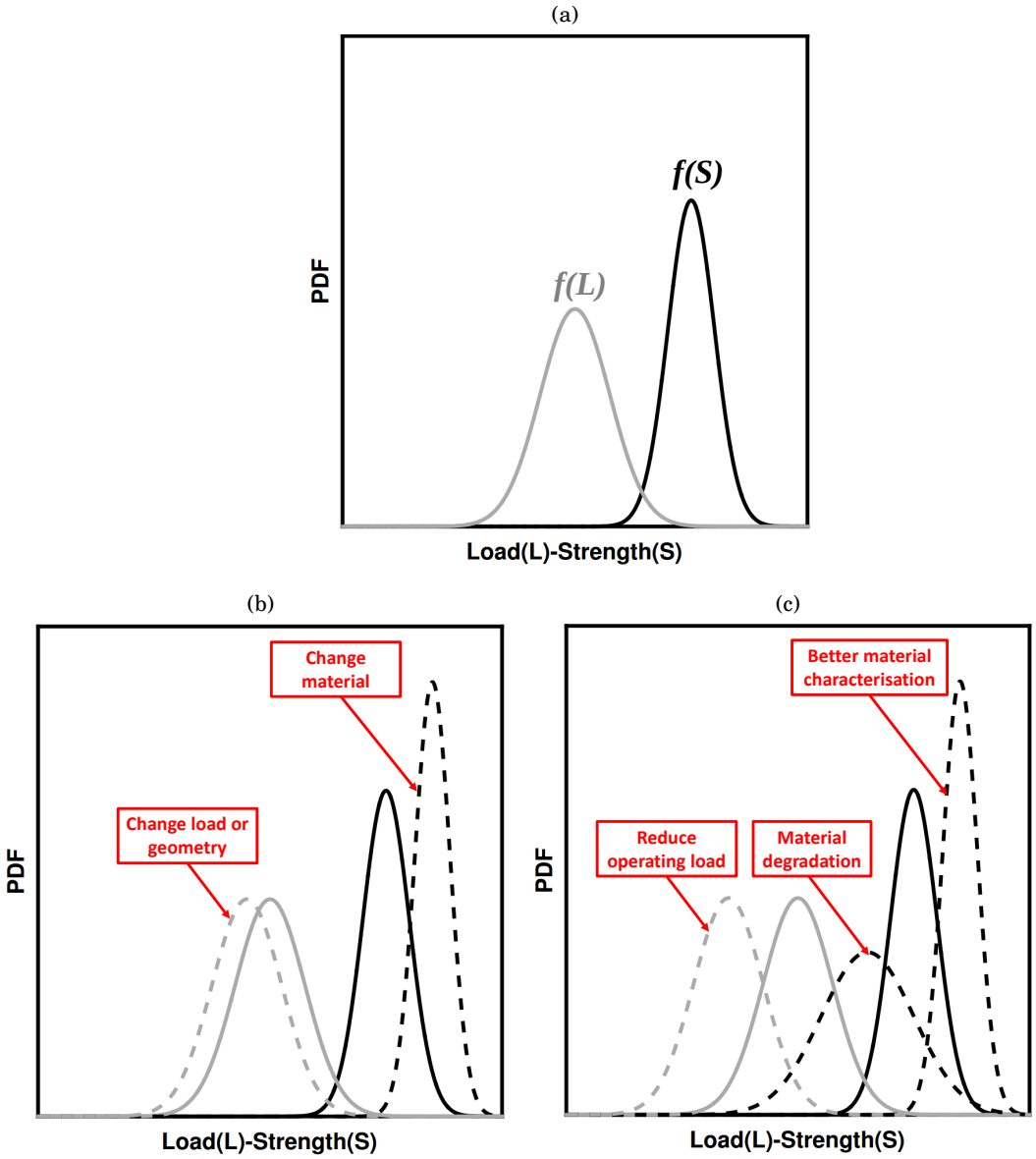

Figure 3.1: A baseline Load-Strength Interference problem is shown in (a). Also shown are possible effects that can be examined using (b) probabilistic design and (c) probabilistic fitness-for-service assessment for inferring and managing the probability of failure.

3.3 Challenges to Probabilistic Implementation

At the current stage, there are a number of hindrances to implementing the various probabilistic methods in structural integrity applications. The main issues are highlighted in Table 3.3 which also presents suggestions and possible benefits of addressing such limitations. Invariably, some of the highlighted challenges are not unique to probabilistic structural integrity (e.g. lack of physics of failure understanding or data), but are general problems faced by the structural integrity community that can be potentially tackled using probabilistic approaches.

3.4 Probabilistic Methods for Structural Integrity

3.4.1 The Probabilistic Approach

Various approaches exist for assessing the reliability of components given an input-output procedure (also called a *performance function*) and predefined performance criterion. These include semi-probabilistic (approximate) methods such as the First and Second Order Reliability Methods (FORM and SORM), while the Monte-Carlo Simulation (MCS) is a fully probabilistic method [4, 52, 53]. The former type of methods are more appropriate for problems where the performance can be expressed using closed-form solutions, typically involving inputs and outputs which are normally distributed and linear, e.g. during early stages of design applications. Some sources advise that non-normal parameters can still be used with FORM and SORM by virtue of transforming them to normal equivalents first [5]. However, from experience this is not applicable nor rigorous for highly non-normal parameters and those described by discreet distributions (e.g. arbitrarily distributed histograms for loading conditions), especially when the sought probability estimates are expected to be highly sensitive to distribution tails. This leaves the MCS as the only applicable method for complex problems, especially when the inclusion of non-normal input parameters is needed. Given that the calculations required as part of a creep-fatigue crack initiation assessment are typically complex, non-linear, multi-staged and may require numerical integration routines, the MCS is deemed to be the only viable option for estimating probabilities of creep-fatigue crack initiation (PoI). Essentially, a MCS approximates the probability distribution of an output parameter based on the repeated computations of the performance function using randomly generated combinations of the input variables, with the samples going into these randomly generated combinations being sampled from the associated PDFs or possibly discreet data. The performance function is defined by the underlying deterministic procedure, which for this work is prescribed by the R5 Volume 2/3 procedure. To produce appropriate representations of the creep-fatigue damage distribution, a suitably large number of Monte-Carlo *trials* (typically $10^5 - 10^7$) must be computed. This puts a limitation on the applicability of MCS for computationally intensive calculations. For such cases a sampling strategy such as *Latin-Hypercube Sampling* can aide in reducing the number of trials needed to produce a representative output PDF [54].

Table 3.3: Mapping of suggested solutions and rewards onto the main challenges faced by probabilistic implementation in structural integrity.

Challenges	Solutions	Rewards
Limited physics of failure understanding	Perpetual build up of understanding backed by well-established statistical tools.	Building confidence in the underlying physics of failure models.
Lack of observations/data	Targeting experimental work and data gathering.	Better quantitative data characterisation whilst reducing unnecessary costs.
Unfamiliarity with probabilistic and statistical concepts	Education and promotion towards prospective practitioners (training, seminars and case-studies).	Creating a common level of understanding, promoting verification and maturity of implementation routes.
Lack of synergy between analysis and inspection	Borrowing tools from other fields (e.g. Kalman Filters in Computer Science).	Channelling sources of information into an augmented state of knowledge (e.g. better understanding of plant material conditions).
The need for formalised implementation routes	Collaboration between industry, academic and regulatory stakeholders.	The shaping of a coherent and unified probabilistic methodology open for scrutiny and improvement.
Independent verification and self validation	Structured implementation will result in systematic troubleshooting and iterative improvement.	Better confidence in the probabilistic models and estimates.
Lack of coding expertise	Build on existing experience; most engineering degrees including coding aspects.	Wider acceptance of probabilistic approaches through implementation and building well-verified communal codes.
Computational intensity	Better use of hardware and numerically efficient algorithms.	Being able to tackle high reliability problems and saving on execution time and costs.

.

3.4.2 Probability Distributions

3.4.2.1 Distribution fitting

The main purpose of this is to firstly find the type of distribution that best fits a data set (e.g. normal, lognormal or Weibull), and then to optimise the distribution parameters as to provide the best agreement with the data. There are two key approaches for fitting appropriate distributions to data samples: the *linear regression method* [4, 55] and the *maximum likelihood method* [4, 56].

Linear regression method The steps required are summarised as follows [55]:

1. For data samples sized 30 or larger, a histogram is constructed, which firstly arranges the data into discrete bins (or data classes), and thus the frequency of each bin is found [4]. The number of bins (k) is selected based on the number of data points (N_D), and it should not be too large as to depict random fluctuations, nor too small as to miss important features of the data set. Common formulations for defining k include [55]:

   $$k = ||\sqrt{N_D}|| \tag{3.1}$$

   $$k = ||1 + 3.22\log_{10}(N_D)|| \tag{3.2}$$

   where the $||x||$ function yields the nearest integer value of x.

2. The cumulative density function (CDF) of the data (now in histogram form) is constructed using an appropriate *ranking equation*. Steps 2-4 still apply if the data set is too small to construct a histogram ($N_D \leq 30$), but ideally would still be larger than 15 [4]. There are a number of possible ranking equations and without any information as to what is the best underlying distribution, the approach is to trial a number of them and choose the one that produces the best results. Three examples of common ranking equations are:

   $$F_i = \frac{i - 0.5}{N_D} \tag{3.3a}$$

   $$F_i = \frac{i}{N_D + 1} \tag{3.3b}$$

   $$F_i = \frac{i - 0.3}{N_D + 0.4} \tag{3.3c}$$

   which are the *Hazen*, *Mean* and *Median* ranks respectively [55] and where F_i is the ranked value of the ith bin, i is the cumulative frequency of the bin and N is the total sample size.

3. A function of the data, $g_x(x_i)$, is plotted against a function of the ranked values, $g_y(F_i)$. The choice of both functions is dependent on the type of distribution to be fitted. The resulting slope (A_1) and intercept (A_0) of the regression line can then be used to approximate the distribution parameters according to the type of distribution desired. Since this step is contingent on the type of distribution and assuming no prior knowledge, it is often the case that multiple distribution types would be trialled. The following is an example for fitting a lognormal distribution (which has extensively been used in this project):

(3.4a) $$g_x(x_i) = ln(x_i)$$

(3.4b) $$g_y(F_i) = \Phi^{-1}_{SND}(F_i)$$

were Φ^{-1}_{SND} is the inverse function of the standard normal distribution. Thus the regression line is:

(3.5) $$g_y(F_i) = A_0 + A_1 g_x(x_i)$$

For a lognormal distribution the PDF is defined as:

(3.6) $$f(x) = \frac{1}{\alpha x\sqrt{2\pi}} \exp\Big[-\frac{(\ln(x)-\lambda)^2}{2\alpha^2}\Big]$$

where the mean (λ) and dispersion (α) parameters are given by:

(3.7a) $$\lambda = -\frac{A_0}{A_1}$$

(3.7b) $$\alpha = \frac{1}{A_1}$$

4. The final step is conducting a *goodness-of-fit test* using χ^2 and computing the squared regression coefficient, R^2. As there are multiple combinations of ranking equations and distributions that could be used, this step is needed to establish which option produces the best fit, thus also yielding associated distribution parameters that best fit the data. The χ^2 test does not assume any degree of normality and hence it can be used to compare any fitted PDF to the histogram of the original data to establish agreement. The test statistic is given by:

(3.8) $$\chi^2 = \sum_{i=1}^{k} \frac{(O_i - E_i)^2}{E_i}$$

were O_i refers to the observed frequencies (from the histogram), while E_i are the expected frequencies (from the fitted distribution). The R^2 metric is calculated as the squared value of the Pearson correlation coefficient (see Eq 4.1) between $g_x(x_i)$ and $g_y(F_i)$, with a value close to 1 indicating that a fitted distribution agrees well with the data.

Maximum likelihood method To apply this method, the same steps as those for the linear regression method apply apart from the third step. This method estimates the distribution parameters by maximising the *likelihood function* which is defined as [56]:

$$\mathscr{L}(x) = \prod_{i=1}^{N_D} f(x_i) \tag{3.9}$$

Given a distribution PDF, $f(x_i)$, is a function of the distribution parameters (e.g. λ and α for a lognormal distribution), the likelihood function is differentiated with respect to each parameter in turn. This yields as many equations as the number of required parameters (e.g. two equations in the case of a lognormal distribution) which can be solved to yield the best estimates for the parameters.

3.4.2.2 Statistical treatment of input parameters

Conventional deterministic calculations fail to make full use of the statistical information that could be inferred from available data. Scatter in test data may be attributed to a number of sources including: test procedures and equipment, data analysis methods and interactions between failure modes [11]. Lognormal distributions have been commonly adopted to statistically characterise various material data, especially for creep models where power laws are used (e.g. see Eq 2.1) [11, 13, 14, 16, 18, 20, 21]. For operating loads and temperatures, other distributions may be more appropriate, for which some advice can be found in [21]. Furthermore, sampling of discreet data (i.e. histograms) may also be appropriate. Regardless of the probabilistic application, for any given input parameter, it is encouraged that full use of the available data is made by choosing from the following options for input characterisation:

1. *Single value*: a parameter is fixed at a value believed to be appropriate (conservative perhaps), which is acceptable when very little data or understanding is available. This may be the only option when one or two data points are available.

2. *Range of values*: applies to parameters which are known to be variable but lack of data hinders fitting a distribution with confidence. An option is to implement the range of values probabilistically as a flat (uniform) PDF. The limits in this case would be based on experienced judgement and the range covered by whatever data is available.

3. *Probability distribution*: fitting one of many possible distribution types (e.g. normal, log-normal and Weibull) to the available data and using goodness-of-fit tests (e.g. χ^2, Kolmogorov–Smirnov or Anderson–Darling) to decide which type is best suited. Typically, sample sizes ≥ 15 would be appropriate for this option [4], while for smaller data sets means and standard deviations can be calculated.

4. *Histograms*: if no probability distribution is appropriate, then constructing a discreet representation of the distributed data, in the form of a histogram, may be more appropriate.

Sometimes the underlying data is not available, but a source may quote a mean and a standard deviation, or a 95% confidence limit value. These suffice to define a two parameter probability distribution (e.g. normal or lognormal). If a parameter is assumed to follow a lognormal distribution, then its logarithmic value follows a normal distribution. The mean and standard deviation of the latter normal distribution can be calculated based on the best estimate (BE) and lower-bound (LB) values which are commonly quoted in material property handbooks:

$$SD = \frac{1}{CF}\log_{10}\left(\frac{BE}{LB}\right) \tag{3.10a}$$

$$\mu = \log_{10}\left(BE\right) \tag{3.10b}$$

were CF refers to a confidence factor which depends on the confidence limit associated with the LB. For example, if the LB is assumed to coincide with the 95% confidence limit, then CF is 1.6445 which is obtained using the inverse of the normal CDF.

3.4.3 Latin-Hypercube Sampling

Latin-Hypercube Sampling (LHS) is based on the principle that for each input parameter the samples supplied to MCS must have equal probability. If an input parameter distribution is known then samples are determined by dividing the area under the PDF into portions of equal area, which in fact represent equal probabilities of occurrence. This concept is depicted in Figure 3.3 for an arbitrary normal distribution. This ensures that even though there may be a relatively small number of samples, these are truly representative of the underlying distribution. By realising that there may be a prohibitively large number of possible combinations of the various variables that could occur for each trial, it is necessary to sample a small subset of all possible combinations. However, care is required to ensure that this sampled subset is representative. For this purpose the LHS strategy may be used [18]:

1. Suppose there there are V distributed variables (these would include time varying as well as time independent ones) then the dimension of the hypercube is V.

2. Also suppose that each variable can have B different values. Then each side of the hypercube is divided into B ranges of distributed values (or *bins*).

3. As a result, the hypercube is divided into B^V cells, with each cell representing a possible combination of parameters (i.e. a trial).

4. Then exactly B cells are chosen such that no two chosen cells share a bin in any variable, thus giving B different combinations of the V parameters which together sample every

bin once for every parameter. This is illustrated in Figure 3.2, which compares LHS with random sampling.

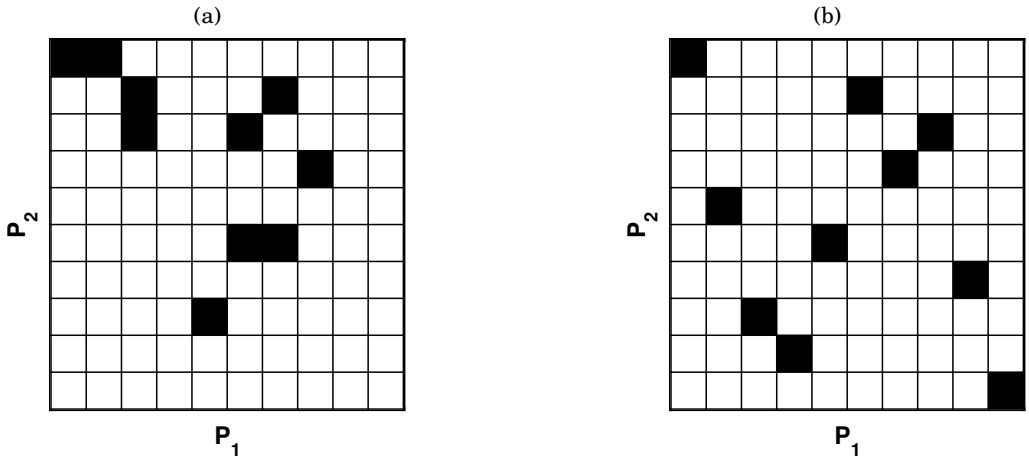

Figure 3.2: Examples showing two parameter spaces (P_1 and P_2) with 10 samples being obtained using (a) random sampling and (b) latin-hypercube sampling, with the latter showing that each parameter bin is chosen once only.

This sampling method relies upon all resulting B combinations (i.e. trails) having equal probability which is ensured by choosing the bins (i.e. the ranges of values) to have equal probability. Therefore, careful definition of the bins is crucial to the outcome of a MCS using LHS. Furthermore, the LHS methodology constrains all distributed variables to have the same number of bins, B. Consider the example of a random variable, x, that is normally distributed and characterised by a normal error parameter z and PDF:

$$f(z) = \frac{1}{\sqrt{2\pi}} exp\left(-\frac{z^2}{2}\right) \tag{3.11}$$

where x can take one of B possible values:

$$x_b = \mu_x + z_b \sigma_x \tag{3.12}$$

where z_b is one of B possible values ($b = 1,2,..,B$) of the error parameter z, while μ_x and σ_x are the mean and standard deviation of x. The bin definition is based on the pre-requisite that all bins have equal probabilities. Therefore, if the b^{th} bin is denfied by:

$$z_b \in [\zeta_{b-1}, \zeta_b] \tag{3.13}$$

then

$$\frac{1}{B} = F(\zeta_b) - F(\zeta_{b-1}) \tag{3.14}$$

where F is the cumulative density function (CDF) and the ζ values define the bin boundaries. Solving for ζ_b gives:

$$\zeta_b = F^{-1}\Big(F(\zeta_{b-1}) + \frac{1}{B}\Big) \tag{3.15}$$

Given that $\zeta_0 = -\infty$ and $\zeta_B = +\infty$ (and thus $F(\zeta_0) = 0$ and $F(\zeta_B) = 1$), and starting from $b = 1$, each bin can be defined based on equal probability. This must not be confused with the bins on the x (or z) axis being equally sized, which is not the case. Eq 3.15 poses a practical difficulty when distributions (including the normal distribution) which have no closed-form expression for CDF are used. In this case the bin boundaries must be found numerically. Thereafter, a representative value of z_b must be determined. This is taken to be the mean value of z within the bin boundaries:

$$z_b = \frac{\int_{\zeta_{b-1}}^{\zeta_b} z f(z) dz}{\int_{\zeta_{b-1}}^{\zeta_b} f(z) dz} \tag{3.16}$$

where the denominator is equal to $1/B$. For a normal distribution Eq 3.16 has a closed-form solution:

$$z_b = \frac{B}{\sqrt{2\pi}}\Big[exp\Big(-\frac{\zeta_{b-1}^2}{2}\Big) - exp\Big(-\frac{\zeta_b^2}{2}\Big)\Big] \tag{3.17}$$

As an example, the samples obtained using LHS for an arbitrary normally distributed parameter is shown in Figure 3.3. The samples are closer together towards the peak of the PDF and further apart towards the tails. The use of Eq 3.16 is particularly important for the first and last bins since it assigns a finite mean (z_b) to a bin of theoretically infinite width. The values z_0 and z_B define the extremes of the sample, i.e. the minimum and maximum values. Furthermore, the number of bins determines the number of standard deviations enclosed by the minimum and maximum values. The above algorithm can also be used for parameters following any distribution. A further refinement of LHS is *Orthogonal sampling* which stipulates that:

1. The total multivariate space is divided into sub-spaces.
2. Choosing the combinations of bins such that the entire multivariate sample space is a latin-hypercube sample.
3. Ensuring that all sub-spaces have the same number of samples.

3.4.4 Surrogate Modelling

In some applications there may be a stage where a time consuming calculation is needed. Consider the example of a component subject to some form of ever changing load. The considerable variability in the loading conditions makes the use of a single value overly conservative. This issue may also be exacerbated by the need for intermediary models to obtain the desired quantities (e.g. stresses from a finite-element (FE) model). An alternative is to formulate a *surrogate*

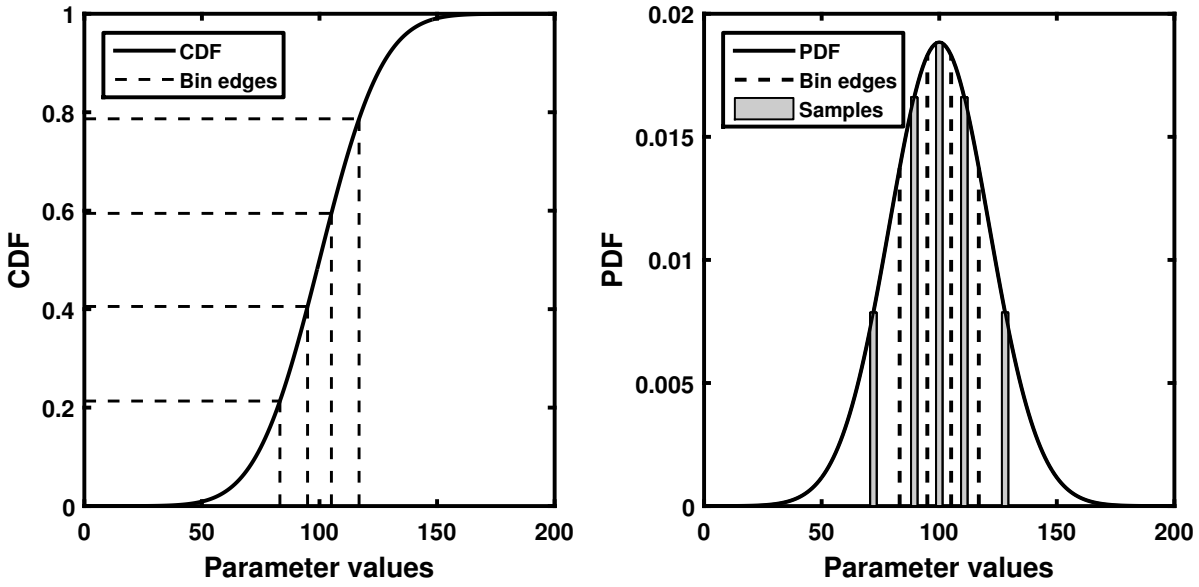

Figure 3.3: Example showing parameter samples having equal probabilities for an arbitrary normal distribution, with the samples being further apart (i.e. wider bins on the left figure) towards the tails of the distribution.

model, which in essence is a statistical model which uses some input parameter to predict the desired quantity using a closed-form formulation. This attempts to mimic the behaviour of the intermediary model (which may require a substantial amount of time to conduct a single run), based on examining input-output data spanning a wide range of possible conditions. For a probabilistic structural integrity calculation, the value of using a surrogate model is in providing a means for approximating stresses as simple functions of key input(s). This mitigates the resorting to running time consuming FE models multiple times within one probabilistic MCS trial (of which there typically may be more than 10^5 independent runs, if not orders of magnitude larger), which would be computationally prohibitive. Typical examples of surrogate modelling approaches include Least-Squares Regression (LSR), the Response Surface Method (RSM) [12, 54, 57] and Artificial Neural Networks (ANN) [58], which can all be viable depending on the application. This project has been predominately focused on using RSM (essentially a multi-variate regression method) which is described below. The intent behind using RSM is to run time consuming complex code, calculations, experiments or processes (e.g. a finite element models) for a limited number of cases, and then to generate surrogate statistical models fitted to the observed response. This simpler statistical model can then be implemented within a Monte-Carlo simulation, which makes the RSM applicable and sometimes essential for modelling real engineering problems [59].

For a linear model fit using RSM the following expression can be fitted to a system response

or dataset [12, 57]:

$$Y = X\beta + \epsilon \tag{3.18}$$

where Y and X are the output and input matrices respectively. If the dataset is of size N_D, then Y and X are sized $N_D \times 1$ and $N_D \times p$, where p is the number of fitted parameters (e.g. $p = 2$ if a first order fit is used). β is the vector of fitted parameters (sized $p \times 1$) and ϵ is vector of residual terms (sized $N_D \times 1$). An estimate for β can be found using:

$$\hat{\beta} = (X^T W X)^{-1} X^T W Y \tag{3.19}$$

where W is an $N_D \times N_D$ diagonal matrix of weights. In the balanced case, all diagonal elements in W are equal to 1. A discussion on setting the weights can be found in [60, 61]. As a result, a mean prediction can be obtained from $X\hat{\beta}$, while the error term is treated as a random quantity characterised by examining the residuals relative to the model fit (e.g. using Analysis of Variance, ANOVA) [62]. In summary, the key steps involved as part of RSM can be summarised as follows:

1. Selection of the independent input valuables that have major influence on the output using a screening strategy (either based on sensitivity analysis or design of experiments).

2. A Design-of-Experiments (DOE) approach is used to define the parameter designs which are used to conduct numerical experiments to gauge the output response. Four examples of established techniques for the definition of experimental designs are: the *full three-level factorial*, the *Box-Behnken*, the *central composite* and the *Doehlert* designs [57].

3. Finding the regression coefficients using Eq 3.19 and based on the N_D observations.

4. Conducting statistical characterisation of the error between observed and predicted responses using an analysis of variance (ANOVA) approach. This includes assessing the fitness of the fitted regression model through statistical tests (typically F and t-tests).

3.4.5 Statistical Testing

Statistical testing tools serve a multitude of purposes, some of which are summarised in Table 3.4. For example, hypothesis testing is often used to assess whether two data sets are statistically similar [62]. Commonly used test statistics are the *t-test* and the *F-test*. However, a key underlying assumption when using these tests is that the data sets should follow normal distributions. By comparison, the *Mann-Whitney* test [63] is a generalisation of the t-test (i.e. it is a non-parametric test) and does not impose any restrictions on the underlying distributions. A further use of hypothesis testing is assessing *goodness-of-fit* between a fitted distribution and a data set. The χ^2 test, which compares expected and observed frequencies, can be used for this purpose but it strictly does not apply for small samples ($N < 15$). The *Kolmogorov-Smirnov test*, which is based on comparing cumulative frequencies, can also be used for assessing goodness-of-fit and it does

not impose restrictions on sample size [55].

For finding the critical values associated with a test statistic, a distribution characterising it is required (e.g. the t-distribution when using the t-test with normally distributed variables). But these distributions are only available for tests applicable to parameters following the Normal, Lognormal or Exponential distributions. For other distributions, approaches such as the *likelihood ratio* statistic can be used to conduct hypothesis testing [56].

Table 3.4: Comparison of statistical testing tools for normally and non-normally distributed data.

Purpose	**Normally distributed data**	**Any distributed data**
Significance and hypothesis testing	t-test	Mann-Whitney test.
	F-test	Levene's (using the mean), Brown–Forsythe (using the median) and Welch tests.
Error analysis	ANOVA	Mood's median, Kruskal-Wallis and Friedman tests.
Goodness-of-fit	χ^2-test	Kolmogorov-Smirnov, Anderson–Darling and Likelihood-ratio tests.
Correlations	Pearson coefficient	Spearman Rank coefficient, Kendall coefficient

3.4.6 Sensitivity Analysis (SA)

Within the context of this work, sensitivity is a measure of the uncertainty in the probabilistic output (e.g. creep-fatigue damage) introduced by the various input conditions. Sensitivity analysis was subdivided into four types of analyses determined by the subject input conditions:

1. *Stochastic input parameters*: which involves using various approaches for quantitatively measuring the variability of the output results due to input parameters modelled using probability distributions [11, 55, 64, 65]. These are discussed in more detail below.

2. Input parameters which are believed to be important but are not treated as stochastic due to lack of either knowledge or data, and would be considered epistemic (or unknown) uncertainties. These input parameters could be incorporated using uniform probability distributions spanning the known (or assumed) range of possible values i.e. using ranges of values as described in Section 3.4.2.2. However, this is better preceded by a simple sensitivity study which essentially tries to assess whether investing the time to religiously model such parameters would yield a significant effect on the probabilistic assessment

results. This can be achieved by plotting the out uncertainty (e.g. the variability of the damage results) as a function of an input parameter and assess whether it has a significant effect, which can be quantified by changes in probability estimates.

3. *Model uncertainties*, which arise from the existence of competing phenomenological representations of the failure mechanisms involved, e.g. having various models to represent creep ductility, damage or deformation as functions of loading temperature and stress. These would be categorised as epistemic uncertainties, which arise from an initial lack of knowledge as to which models better represent the failure mechanisms. Assessing which model yields the better representation can only be done comparatively and with respect to experimental or inspection data. However, when constructing a probability assessment the knowledge of whether the output results are at all sensitive to which model used can be quite valuable. In which case a purely comparative analysis contrasting the results obtained from using different models is initially sufficient.

4. *Assumption uncertainties*, which relates to the use of specific assumptions at various stages of a procedure. An example which is explored in Chapter 6 considers that in a creep-fatigue assessment one could assume, conservatively, that creep strain resets at the start of every loading cycle, which is referred to as *primary-reset*, or that creep strain continuously accumulates from one cycle to the next, which is termed *continuous-hardening*. Using either of these assumptions would introduce an uncertainty in the assessment results, as a real cyclic creep behaviour is more likely fall somewhere in between the two assumptions depending on the nature of every loading cycle. These uncertainties are conceptually similar to model uncertainties, but are typically more subjective as their consideration can be based on technical experience and judgement.

The first category of input conditions typically considers uncertainties which are *aleatory* (i.e. random) in nature, whilst the latter three types examine the sensitivity toward epistemic uncertainties. To reiterate, aleatory uncertainties can be implemented in a MCS by using appropriate probability distributions, whilst accounting for epistemic uncertainties typically involves conducting multiple Monte-Carlo simulations examining all possibilities for each epistemic uncertainty source [19]. As a result, the general guidance is that sensitivity to epistemic uncertainties can be assessed through comparative analyses (e.g. comparing results using Model 1 against Model 2), whilst sensitivity to stochastic inputs (i.e. aleatory uncertainties) can be assessed using quantified metrics, which are discussed below.

When a large number of stochastic input parameters is considered, SA provides a quantitative tool for identifying which should be considered with the most care (e.g. requiring further data acquisition), and which could be omitted from the probabilistic procedure all together. This is done by calculating the *sensitivity indices*, which are measures of the contributions of each

input parameter toward the overall variability in the output. There are various approaches for calculating the sensitivities indices and four such approaches, which were explored in [9] and are summarised in Table 3.5, were used in the case-study presented in this chapter (see Section 3.7.4.2) to demonstrate their utility. The following are brief descriptions of each of the four SA approaches.

Finite-difference approach [55, 64, 66] Assuming the input parameters can be considered normally distributed and statistically independent, then the sensitivity indices (S_i) can be defined as the weighted percentage contributions of each distributed input variable to the variance (not the standard deviation) of the output variable:

$$S_i = \frac{\left(\frac{\partial \phi}{\partial x_i}\right)_k^2 \sigma_{x_i}^2}{\left[\sum_{i=1}^{I} \left(\frac{\partial \phi}{\partial x_i}\right)_k^2 \sigma_{x_i}^2\right]} \tag{3.20a}$$

where I is the total number of input parameters, σ_{x_i} is the standard deviation of the x_i input parameter, and ϕ is the output. The partial derivative can be estimated using finite differences:

$$\left(\frac{\partial \phi}{\partial x_i}\right)_k = \frac{(\phi_{k+1} - \phi_{k-1})}{2\Delta x_i} \tag{3.20b}$$

$$\Delta x_i = 2\sigma_{x_i} \tag{3.20c}$$

where ϕ_{k+1} and ϕ_{k-1} are evaluations of the output at the extremities of each input:

$$(x_i)_{k\pm1} = \mu_{x_i} \pm \Delta x_i \tag{3.20d}$$

where μ_{x_i} is the mean value of the x_i parameter. This approach is fairly simple and quick to implement as it only requires $2I$ model runs to evaluate the sensitivity indices (i.e. 2 model evaluations at the upper and lower bounding values per input parameter). For this approach to give sensible results, however, there are two assumptions that need to be satisfied. Firstly, each input parameter is assumed to independently contributed towards the variance of the output parameter. Secondly, the input distributions need to exhibit a degree of normality. The latter requirement follows from the usage of the variance as an indicator of output sensitivity. If the input parameters are not all normal, then the variance loses its value as a consistent measure of uncertainty across all inputs, and thus this type of SA could lead to misleading results. However, even if the input parameters are not normally disturbed, the finite-difference approach still provides a quick tool for screening the input parameters for least dominance. As a result, this provides a first screening stage before more computationally taxing SA approaches are adopted, for which the required number of model runs may increase substantially with the number of input parameters.

Variance based approach [64] Generally, variance based approaches operate on two key assumptions:

1. The variance of the output parameter is a measure of uncertainty.
2. The contribution of an input parameter towards the output variance is indicative of sensitivity.

A convenient way of quantifying the sensitivity of each input parameter is to examine the reduction in output variance introduced by fixing one parameter at a time, while treating the other inputs stochastically. The simplest expression for estimating the first-order sensitivity indices is:

$$S_i = \frac{V(\phi) - E[V(\phi|x_i)]}{V(\phi)} \tag{3.21}$$

where $V(\phi)$ is the variance of the output and $E[V(\phi|x_i)]$ is the conditional expected value of $V(\phi)$ given x_i has a fixed value (e.g. $x_i = \mu_{x_i}$). This type of approach is fairly simple to implement, even though it may still require a significant number of model runs to achieve good estimates of the sensitivity indices. However, its key drawback lies in the first of the above mentioned assumptions. For highly-skewed distributions (e.g. lognormal) the variance by itself does not provide a good measure of uncertainty. As a result, this poses a limitation on the types of distribution the inputs and output must have for this method to produce meaningful estimates of the sensitivity indices.

Correlation based SA [11] The relative importance of each parameter can be quantified by computing the correlation coefficients between each input and the out:

$$S_i = \frac{corr(x_i, \phi)}{\sum_{i=1}^{I} corr(x_i, \phi)} \tag{3.22}$$

where $corr$ refers to a correlation function (e.g. the Pearson or Spearman correlations). For this work the Spearman correlation was mainly used.

δ-sensitivity approach [64, 65] This is a global SA approach which quantifies the influence of each distributed input parameter on the output parameter PDF. This method was originally developed to provide a SA approach which is:

1. *Global*: the analysis must consider the full distributions of the input parameters.
2. *Quantitative*: produces a measure of the relative importance of each input parameter.
3. *Model-free*: the approach does not assume any a priori input-output relationship
4. *Moment independent*: the approach does not rely on a single measure (or statistic) of the input and output parameter distributions e.g. the mean or variance. Instead it considers the effect of the full input distributions on the output parameter distribution.

Table 3.5: Comparison of four sensitivity analysis approaches where R is the number of runs required, I is the number of input parameters and N is the number of trials in the probabilistic assessment.

Approach	**R**	**Advantages**	**Disadvantages**
Finite-difference approach [55, 64]	$2 \times I$	Simple and quick to implement.	Inputs are assumed to be normally distributed and have no interactions. Thus it examines local sensitivity only.
Variance-based approach [64]	$I \times N$	Conceptually simple to implement.	Not suitable for highly-skewed distributions (e.g. lognormal) as it assumes normal distributions.
Correlation-based approach [11]	N	Requires the same number of runs as the probabilistic assessment.	As the effect of each parameter is not isolated, it can overestimate the importance of the least influential parameters.
δ-sensitivity [64, 65]	$I \times N^N$	Measures global sensitivities.	Computationally taxing as it requires large numbers of runs.

A δ_i factor can be defined for each input parameter which uses the shift in area under the output PDF as a measure to quantify sensitivity. Suppose I input parameters are considered $(x_1, x_2, ...x_I)$ and that an output parameter PDF, $f_\phi(\phi)$, can be obtained through a MCS. By fixing one input parameter at a predefined value x_i^n $(n = 1, 2, ..N)$ the output PDF can be evaluated for N possible values of x_i. These are conditional output PDFs, $f_{\phi|x_i^n}(\phi)$. A simple formulation for calculating the δ factors can be defined if the N possible values of each input parameter all have equal probability (e.g. if LHS is used):

$$\delta_i = \frac{1}{2N} \sum_{n=1}^{N} \left[\int |f_\phi(\phi) - f_{\phi|x_i^n}(\phi)| d\phi \right] \tag{3.23a}$$

Thereafter, the associated sensitivity indices can be calculated as:

$$S_i = \frac{\delta_i}{\sum_{i=1}^{I} \delta_i} \tag{3.23b}$$

This approach does not require normality of the input and output PDFs, as Eq 3.23 can be used with any type of distribution or even a histogram, which is an appealing aspect. However, the main drawback of this approach is that it is computationally taxing, as it requires IN^N trails. But if an appropriate sampling approach is used for defining the N possible values, then decent results may still be obtained even for a relatively small N. Furthermore, if a less intensive SA approach, say the finite-difference method, is used first to screen for non-influential parameters, an argument can be made for the reduction of parameters considered, thus reducing the number of model runs needed.

3.5 Target Reliabilities

In the UK, for high integrity plant components the current practice for providing the necessary demonstration of safety in safety cases is to use the 'four legs' structure developed by the Technical Advisory Group on the Structural Integrity of High Integrity Plant (TAGSI) [67]. This framework is recognised by the Office for Nuclear Regulation (ONR) and is accepted to provide a suitable and useful framework for justifying high reliability claims [68]. Guidance on the tolerability of risk for nuclear plant operations (mainly concerned with any potential risks to staff and the wider public) is provided by the Health and Safety Executive (HSE) as detailed in [69–71]. The level of reliability that must be ensured for a given occurrence is generally determined by the severity of the possible consequences, with components being categorised in terms of the allowable failure frequency per annum, mirroring the perceived severity of the associated consequences. For example, for safety critical components (e.g. those under the 'Incredibility of Failure', IoF, category), a relatively low frequency of failure most be demonstrated. For AGR plants components in general, guidance on the respective categories and associated target reliabilities that must be demonstrated for individual components is provided in [72]. The tubeplate component examined in the case-studies in Chapters 5 and 6 of this thesis is categorised as an IoF component with an associated target reliability of $< 10^{-7}$ per year. Current procedures for ensuring that target reliabilities are met do not calculate the failure rates of individual components directly (i.e. using probabilistic analyses), but rather rely on the strength of a complete safety case which is based on the individual strength and general agreement between: deterministic structural integrity assessments, histories of observed failures or survivals and inspection results. This practice is in general agreement with the safety principles set by the ONR [73].

Moreover, nuclear safety cases in the UK are based on the ALARP principle (As Low as Reasonably Practicable) [44, 73], which is compatible with probabilistic assessments for ensuring the reliability of individual components and wider systems by providing quantifiable failure rates [67]. Furthermore, arguments for the safety of a given system also include Probabilistic Safety Assessments (PSA) which are based on postulated sequential failures of components, back-up systems and protective systems. Given that safety cases are not exclusively based on assessment, probabilistic paradigms can help with the integration between assessment, observed failure histories and inspection results, which presently is not done explicitly. It is worth noting that this PhD project considered aspects related to assessment only, whilst the probabilistic treatment of observed failures and inspection data (and indeed the integration of these three components of safety assurance) have been identified as areas of further work. The insurance of safety within any probabilistic structural integrity framework invariably involves:

- Calculating a failure probability (which is the subject of this thesis).
- The calculation (or otherwise external and independent imposition) of a target reliability.

- The comparison of the two values to demonstrate that the target reliability is satisfied.

Calculating target reliabilities is an area of work that requires further consideration. The current consensus is that component-level reliability targets can be reverse-engineered based on the plant safety requirements (e.g. those set by the HSE in [69–71] and the ONR in [73]) as the starting points and a PSA model as the vehicle to infer the desired target reliability for each component [74]. This general approach is proposed by the Reliability and Integrity Management working group as part of current development of the ASME Section XI code [5]. tools such as fault tree analysis have also been used and suggested as tools for ascertaining the target reliabilities of constituent components of wider systems [19]. Nevertheless, such target reliability calculations can be onerous and require a great deal of knowledge including [5]:

- Understanding of the overall system architecture. To infer the target reliability for a given component thus requires detailed knowledge of the whole plant, which in practice is supplied to the practitioner/analyst by the safety case or the PSA model.
- Knowledge of all failure possibilities (on the system and component levels) as well as any possible interactions between failure occurrences.
- The mechanisms by which failures aggregate from individual components to the wider system.
- The existence of protective systems or measures which introduce redundancy and therefore a higher tolerance for some failure occurrences.

For IoF components, the target reliability is translated from the Basic Safety Objective (part of the Safety Assessment Principles set by the ONR) for a large release of radioactivity which is set at $< 10^{-7}$ per year [67, 73]. Suggested values of target reliabilities for individual component failures based on the severity of the consequences of such failures can be found in some codes and standards including [75–77].

3.6 Assessment Implementation

Probabilistic assessments as described in this work are suited to implementation using general-purpose, high-level coding languages including Python, R and MATLAB, the latter of which was used. Various techniques that are common practice within these languages are suited for the application at hand. For example, *vectorisation* is a very efficient strategy in MATLAB which allows for the increase of number of trials without proportional increase in execution time. One drawback is that the number of trials must be specified in advance and therefore a convergence plot (e.g. tracking the output median, mean or standard deviation as a function of number of executed trials) may require extra computations. However, given that LHS has been suggested, the

number of trials must be chosen in advance in any case (as it affects the sampling of each input distribution), and therefore this is a minor issue. Using vectorisation, all trials are progressed through the simulated history simultaneously, which makes it a slightly time consuming because some trials are computationally quicker than others. This is regarded as a small sacrifice given the improved efficiently relative to sequential calculations, and could be resolved with complex algorithms.

Three further attributes make these languages ideal. Firstly, they have numerous statistical libraries which have been in the public domain for years, which implies that they have been thoroughly validated and verified. Secondly, they also provide a plethora of data visualisation tools, which are essential in conducting, reporting, presenting and independently verifying probabilistic assessments. Finally, they provide options for conducting parallel computations, which can be essential. This can be done using CPU or GPU hardware. The former was used in this work primarily for simplicity. However, when moving towards assessing multiple assessment points with large MCS trials each ($\geq 10^6$) in parallel, using a GPU, which is ideal for large array manipulations, would be more appropriate.

3.7 Case-Study: Probabilistic Assessments of Uniaxial Creep-Fatigue Tests

3.7.1 Case-study Definition

The subject of this case-study is the R5 V2/3 assessment procedure as applied to a uniaxial specimen under creep-fatigue conditions. The test was conducted using displacement control, with a hold period (i.e. creep dwell) at peak cycle strain, as shown in Figure 3.4. The material was 316H stainless steel tested at 550°C. Displacement controlled creep-fatigue tests are not commonly taken to gross specimen failure, thus a criterion as to what constitutes failure is usually required. Experimentally, failure (or in this case creep-fatigue crack initiation) of the specimen was defined by the peak cycle stress falling below a predefined level as defined by the ASTM E2714-13 standard [78] for conducting creep-fatigue tests. The test being considered was taken to a 5% drop in peak cycle stress, which defines the number of cycles to creep-fatigue initiation, which is common practice and in adherence with the ASTM E2714-13 testing guidelines. The probabilistic assessment considered six input parameters which were treated stochastically, and the assessment estimated the creep-fatigue damage at the end of the test. Firstly, the probabilistic assessment results were compared with their conventional deterministic equivalent. Furthermore, four sensitivity analysis approaches were applied with the aim of assessing which assessment input parameters were of most influence towards the output variability. Probabilistic results using competing creep deformation and ductility models were compared in order to assess sensitivity towards the models used. Finally, by making use of stress data that was recorded

during the test, the uncertainty introduced by the procedure itself through estimating stresses was also examined.

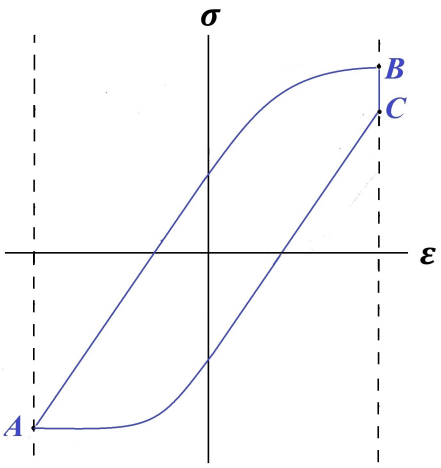

Figure 3.4: Stress-strain (σ-ε) hysteresis cycle for a displacement controlled creep-fatigue test with creep dwell at peak cycle. The elastic follow-up factor (the factor by which the creep strain increment exceeds the elastic strain decrease) is $Z = 1$ because the displacement is fixed during the test (i.e. displacement control).

3.7.2 Procedure Definition

This section provides a detailed account of the R5 assessment procedure [23, 79, 80] for a uniaxial test specimen subject to displacement controlled, creep-fatigue conditions. As shown in Figure 3.4, the hysteresis cycle is divided into two portions:

- Portion CA: half-cycle without creep dwell (monotonic unloading)
- Portion ABC: half-cycle with creep dwell. This is divided into AB (monotonic loading) followed by BC (the creep dwell).

Starting with portion CA, and noting that the creep-fatigue test was in displacement control, the total strain range is the elastic-plastic strain range ($\Delta\varepsilon_T = \Delta\varepsilon_{ep}^{CA}$). Thus the elastic-plastic stress range ($\Delta\sigma_{ep}^{CA}$) can be found using a *Ramberg-Osgood* expression:

$$\Delta\varepsilon_T = \Delta\varepsilon_{ep}^{CA} = \frac{\Delta\sigma_{ep}^{CA}}{\bar{E}} + \left(\frac{\Delta\sigma_{ep}^{CA}}{A}\right)^{1/\beta} \tag{3.24a}$$

where $\bar{E}$ is the modified Young's modulus:

$$\bar{E} = \frac{3E}{2(1+\nu)} \tag{3.24b}$$

while A and β are the Ramberg-Osgood parameters. By virtue of the *symmetrisation* process, and by assuming isothermal conditions, the *reverse stress datum* (σ_{RD}, which denotes the absolute location of point A in Figure 3.4) is given by:

$$\sigma_{RD} = \frac{\Delta\sigma_{ep}^{CA}}{2} \tag{3.25}$$

For portion AB a *modified* Ramberg-Osgood expression is used:

$$\Delta\varepsilon_T = \Delta\varepsilon_{ep}^{AB} = \frac{\sigma_B + \sigma_{RD}}{\bar{E}} + \left(\frac{2\sigma_B}{A}\right)^{1/\beta} \tag{3.26}$$

which gives the stress at the beginning of the creep dwell, σ_B. It follows that, under displacement control with $Z = 1$, $\sigma_B = \sigma_{RD}$, which comes as a result of the elastic-plastic strain ranges for portion CA and portion AB being identical. To estimate the stress relaxation during the creep dwell (portion BC), a time stepping scheme was used to calculate the stress drop and the creep damage for the first creep dwell. Thus using the following relaxation equation:

$$\frac{Z}{\bar{E}}\frac{d\sigma}{dt} = -\left[\dot{\varepsilon}_c(\varepsilon_c,\sigma) - \dot{\varepsilon}_c(\varepsilon_c,\sigma_{ref})\right] \tag{3.27}$$

where σ_{ref} (the reference stress) is set to zero because the creep-fatigue test was in displacement control (i.e. only secondary loads apply), Z is the elastic follow-up factor (the factor by which the creep strain increment exceeds the elastic strain decrease) and $\dot{\varepsilon}_c$ is calculated instantaneously as a function of current creep strain and the instantaneous relaxing stress using:

$$\dot{\varepsilon}_c = Max[\dot{\varepsilon}_p, \dot{\varepsilon}_s] \tag{3.28}$$

where $\dot{\varepsilon}_p$ and $\dot{\varepsilon}_s$ are the instantaneous primary and secondary creep strain rates respectively, which are given by the *strain hardening* version of the *RCC-MR* creep deformation model [81]:

$$\dot{\varepsilon}_p = K\varepsilon_c^X\sigma^Y \tag{3.29a}$$

$$\dot{\varepsilon}_s = C\sigma^n \tag{3.29b}$$

$$K = C_1^{1/C_2}C_2 \tag{3.29c}$$

$$X = \frac{C_2 - 1}{C_2} \tag{3.29d}$$

$$Y = \frac{n_1}{C_2} \tag{3.29e}$$

where C, C_1, C_2, n, n_1, K, X and Y are creep constants. Because Eq 3.29a is singular at $\varepsilon_c = 0$, and for the first time step only, the initial creep strain can be calculated using a *time hardening* expression:

$$\varepsilon_c = \varepsilon_p = C_1 t^{C_2}\sigma^{n_1} \tag{3.30}$$

An alternative creep deformation model was development as part of the High Temperature Behaviour of Austenitic Stainless Steels (HTBASS) [82], which is given by:

$$\dot{\varepsilon_c} = \exp\Big(-\frac{Q_p}{RT}\Big)(\varepsilon_c + D\varepsilon_p)^{(x_0+x_1T)}\sigma^{T^\beta} + C_0\exp\Big(-\frac{Q_s}{RT}\Big)\sigma^{(T/T_n)^\gamma} \tag{3.31}$$

where the terms on the left represent primary creep, while those on the right model secondary creep behaviour. Thus the rate of change in stress was calculated using a discretised form of Eq 6.20a:

$$(\sigma)_{i+1} = (\sigma)_i + (\Delta\sigma_c)_i = (\sigma)_i - \frac{E}{Z}(\dot{\varepsilon}_c\delta t)_i \tag{3.32}$$

from which the stress drop ($\Delta\sigma_c$) and creep strain ($\Delta\varepsilon_c$) per cycle were obtained. The creep strain for successive time increments is found using:

$$\varepsilon_{i+1} = \varepsilon_i + \dot{\varepsilon}_c\delta t \tag{3.33}$$

The creep damage per cycle (d_c) was determined using a ductility exhaustion model:

$$(d_c)_{i+1} = \frac{\varepsilon_{i+1}}{\varepsilon_f} \tag{3.34}$$

where ε_f is the uniaxial ductility, which in this case-study has been modelled using two competing approaches:

1. Using a creep-rate and stress *independent* ductility exhaustion approach (denoted by the abbreviation DE). This essentially assumes that ductility is a material property which has a natural variability than can be modelled statistically using a lognormal distribution.

2. Using a creep-rate and stress *dependent* ductility exhaustion approach in the form of the Stress Modified Ductility Exhaustion (SMDE) model [82, 83]:
   (3.35)
   $$\ln(\varepsilon_f) = \boldsymbol{Max}\Big[\ln(A_1) + \frac{G_1}{RT} + n_1\ln(\varepsilon_c) + m_1\ln(\sigma), \boldsymbol{Min}\Big[\ln(\varepsilon_L), \ln(A_2) + \frac{G_2}{RT} + m_2\ln(\sigma)\Big]\Big]$$
   where ε_L is the lower shelf ductility. It is worth noting that the upper shelf ductility was omitted from the SMDE model. This is because the failure mechanism typical of the upper shelf ductility is physically not possible under displacement control [82].

Consequently, the total strain range including the effect of the creep dwell for this half cycle is:

$$\Delta\varepsilon'_T = \Delta\varepsilon_T + \Big(\Delta\varepsilon_c - \frac{\Delta\sigma_c}{\bar{E}}\Big) \tag{3.36}$$

This increased strain range is the one used for calculating the fatigue endurance. However, it is worth noting that if $Z = 1$ then the total strain range is virtually unchanged as $\Delta\varepsilon_c = \frac{\Delta\sigma_c}{\bar{E}}$. By comparison, if $Z > 1$ then the total strain range is increased (i.e. $\Delta\varepsilon'_T > \Delta\varepsilon_T$).

The following stage of the assessment is to calculate the fatigue damage per cycle. Fatigue endurance data obtained from [46] was fitted to the following expression [9]:

$$\log_{10}\left(\frac{N_f}{15}\right) = C_f(\Delta\varepsilon)^{n_f} \tag{3.37}$$

where N_f is the number of cycles to fatigue failure, $\Delta\varepsilon$ is the strain range in percentages and C_f and n_f are the coefficient and exponent of the fitted power law respectively. The fatigue damage per cycle is found as follows:

$$N_i = N_f \exp\left(-8.06N_f^{-0.28}\right) \tag{3.38a}$$

$$N_g = N_f - N_i \tag{3.38b}$$

$$N'_g = NgM \tag{3.38c}$$

using $a_0 = 0.2mm$ as the initiated crack depth, the adjustment factor was found as $M = 0.187$ (see R5 Volume 2/3 [23] Appendix A10 for details). Thus the fatigue damage (d_f) is:

$$N_0 = N'_g + N_i \tag{3.38d}$$

$$d_f = \frac{1}{N_0} \tag{3.38e}$$

and the total damage (d) per cycle is:

$$d = d_c + d_f \tag{3.39}$$

Finally, multiplying d by the number of cycles to uniaxial creep-fatigue failure (which is determined experimentally) gives the expected damage at failure, D, which is the output of this analysis. This essentially assumes that all loading cycles incur the same total damage, as *primary-reset* was assumed, which is based on inserting only the creep strain accumulated since the start of a given dwell into the creep strain rate formula. This also does not account for effects of cyclic hardening or softening that may lead to a change in the peak cycle stress.

3.7.3 Input Parameters

Six input parameters were treated stochastically as part of the R5 probabilistic assessment. These are summarised in Table 6.1 below. Lognormal distributions were used for all parameters following the advice in the available literature [11, 13, 14, 16, 18, 20, 21], implying that the logarithms of the parameters are normally distributed with mean and standard deviations calculated using Eq 3.10. It was assumed that the range between the lower and upper bounds coincided with the the range between the 5% and 95% confidence limits (i.e. CF = 1.6445). The BE and LB values for the six parameters were obtained from [46, 79, 81]

Table 3.6: Summary of stochastic input parameters which were treated as probabilistic in the case-study examining the uniaxial creep-fatigue specimen.

Parameter	Description	Units
C_1	Primary creep coefficient in RCC-MR deformation model [81]	$MPa^{-n_1}hr^{-C_2}$
C	Secondary creep coefficient in RCC-MR deformation model [81]	$MPa^{-n}hr^{-1}$
ε_f	Uniaxial creep ductility (creep strain at failure) [46]	$\%$
A	Ramberg-Osgood coefficient [46]	MPa
C_f	Coefficient in fatigue endurance data fit [46]	–
E	Young's modulus [46]	MPa

3.7.4 Results and Discussion

3.7.4.1 Uncertainties in Assessment Results

An insightful analysis is to contrast deterministic and probabilistic results, thus giving a measure as to how conservative the former can be. The benefit of such analysis lies in the ability to examine the performance of the underlying structural integrity procedure (R5 Volume 2/3 in this case-study) against experimental results or results based on per-specified input conditions (i.e. assuming upper or lower bounds in a deterministic assessment). The object of this case-study is a uniaxial creep-fatigue specimen for which the number of cycles to failure was know, and hence can be compared with what is expected analytically through a probabilistic creep-fatigue assessment procedure. Therefore, in this case-study the proposed comparison serves as an assessment of how well the underlying procedure can predict failure of the specimen. Figure 3.5 shows such a comparison for the uniaxial creep-fatigue test being examined. This shows that a conventional deterministic assessment (in this case using best estimate deformation and lower bound ductility and fatigue endurance conditions) is significantly conservative, as it predicts a damage of about 10, when a damage of 1 would have been optimal. The probabilistic results also indicate that the deterministic estimate is quite improbable. The probabilistic results are still disproportionately conservative when compared with the failure criterion, which suggests that the overall probabilistic assessment (with all its aggregated complexities and assumptions) are not exactly accurate in predicting the expected damage at failure (i.e. $D = 1$). This suggests that there may be room for reducing conservatism, perhaps by better characterisation of the dominant material parameters (e.g. creep ductility) or by improving on the procedure itself (e.g. seeking a better modelling approach for cyclic loading and hysteresis cycle construction; see Section 3.7.4.3). Nevertheless, given the current level of complexity incorporated in the probabilistic assessment, the results are not completely conservative as there is a portion of the PDF which lies to the left of the failure criterion.

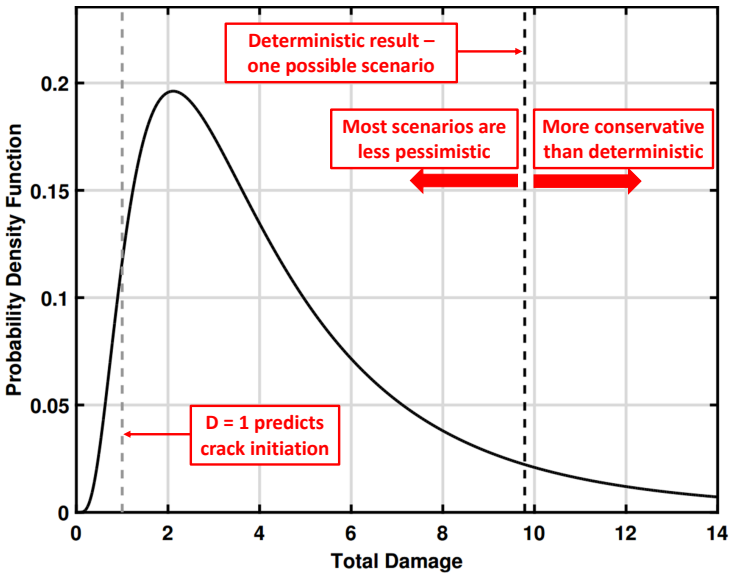

Figure 3.5: Results from a probabilistic assessment of a uniaxial creep-fatigue specimen. The assessment was taken to specimen failure and, therefore, results larger than unity are considered to be conservative predictions.

3.7.4.2 Quantitative sensitivity analysis

The results from applying the four SA approaches (see Section 3.4.6) are shown in Figure 3.6. Overall, the four approaches produced similar results as they agreed that ductility and the primary-creep constant in the RCC-MR deformation model (C_1) were most dominant. It is perhaps not surprising that the Young's modulus is the least influential parameter, as it exhibits small variability when compared with the other parameters, especially the creep related ones. The secondary creep constant (C) also seems to be non-influential, which can be explained by two factors. Firstly, the hardening assumption that was used was to re-prime at the start of each dwell, which implies that every cycle will start in the primary creep regime. Secondly, the creep-fatigue test under consideration had 1 hour dwells, which may well be too brief a period for secondary creep to substantially develop. The fatigue constant (C_f) and the Ramberg-Osgood constant (A) had modest degrees of influence. These observations were not surprising since the lifetime is partially influenced by fatigue (although creep dominates in this case) while A determines the stress at the beginning of the dwell, which has a direct influence on creep damage.

Importantly, all results presented in this section only apply to the situation at hand (i.e. a uniaxial creep-fatigue test with specific testing and material conditions) and for the level of complexity that was allowed in the probabilistic assessment (in this case only 6 parameters were treated stochastically). If more probabilistic input parameters were included in the assessment (e.g. variations in the temperature) the SA may have yielded completely different results, as

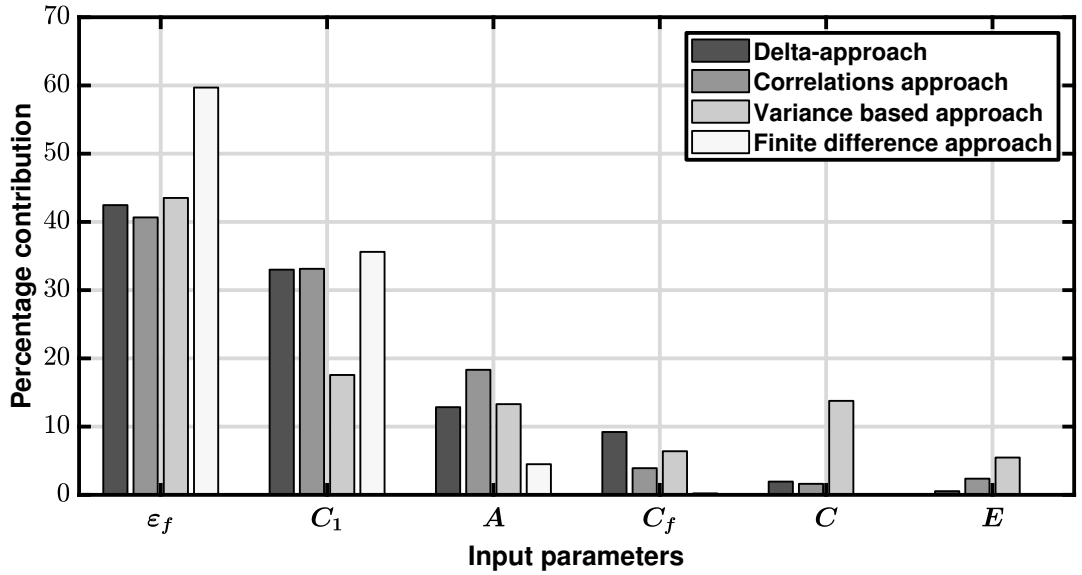

Figure 3.6: Comparison of SA results using four approaches as applied to the uniaxial creep-fatigue case-study.

the relative importance of each input parameter may have been affected by the inclusion of further, perhaps more important, input parameters. For example, in some creep applications (e.g. plant assessment applications) uncertainty in the elastic follow-up factor (Z) can have significant contributions towards the output creep damage results and, as a result, should be included in the SA. Though this parameter is not as important as it is an experimentally controlled parameter during the uniaxial creep test being considered. Furthermore, the failure of the specimen considered was dominated by creep (i.e. the calculated creep damage was far larger than its fatigue counterpart), which explains the modest influence of the fatigue parameter. However, the SA results would have been markedly different had the situation been fatigue dominated. Therefore, the results shown in Figure 3.6 must not be interpreted as general results, but rather examples demonstrating the utilities of the SA approaches considered in this work.

Out of the four SA approaches used, the one which is believed to provide the results with most confidence is the δ-approach, as it is a global, fully probabilistic technique which does not assume any a priori distributions for the input parameters. Therefore, the results produced by this approach will be used as the baseline for the following discussion. The correlations approach produced similar results to the δ-approach but only required a fraction of the model runs, which makes it an appealing choice. The finite-difference approach provided results in agreement with the δ-approach, however, it seemed to underestimate the influence of C_f and A. Similarly, the variance approach overestimated the importance of E and C. The main conclusion from comparing the four approaches was that a global approach should be implemented if the computational capability is available. This is believed to provide a more realistic estimate of the importance of

all input parameters. The finite-difference approach still provides a rapid assessment tool for identifying (and possibly excluding) the least dominant parameters. Consequentially, it provides the first screening stage before more computationally intense SA approaches can be feasibly adopted, for which the required number of model runs may increase substantially with the number of input parameters. The variance approach provided somewhat misleading results, even though it required a considerable number of model runs. It is advised, therefore, that this approach only be used with input parameters that are strictly accepted as normally distributed.

3.7.4.3 Examination of model uncertainty

With the calculation of creep damage being a vital part of a creep-fatigue life assessment, an examination of the uncertainty introduced by combinations of creep damage and deformation models is essential. For this purpose, deterministic calculations can provide a measure of accuracy, but not the degree of uncertainty. Two combinations were examined:

1. Constant (creep-rate and stress independent) ductility exhaustion with the RCC-MR creep deformation model (RCC-MR with DE).

2. Stress-Modified Ductility Exhaustion (creep-rate and stress dependent) with the HTBASS deformation model (SMDE with HTBASS).

A comparison contrasting the probabilistic results obtained from using the two options above is shown in Figure 3.7 for the uniaxial creep-fatigue test. This demonstrates that the latter combination of models outperformed the former both in terms of accuracy (by achieving a peak probability at a value of damage closer to unity) and variability (by producing a narrower distribution). Thus using the combination of SMDE and the HTBASS creep deformation model produced the best results. In this case, the examination of model uncertainty can be done comparatively by contrasting results using competing models and by gauging their performance with respect to the failure criterion (i.e. $D = 1$). Note that the latter examination is only possible because it is known, at least within experimental methodology definitions, that creep-fatigue crack initiation was incurred. However, for an in-service plant component the situation is more complex as the knowledge of whether a crack was initiated is uncertain, but can be informed by inspection data.

In this case-study, the variability in the probabilistic assessment results has been attributed to the variability in the input parameters detailed in Table 6.1. In physical terms, however, these parameters introduce variability because they are used to estimate key quantities including the stress at the beginning of the dwell (σ_B, see Eq 6.16) and the creep stress relaxation ($\Delta\sigma_c$, see Eq 6.20b). However, for a creep-fatigue test, one can have the benefit of knowing these quantities as they are usually recorded over the course of the experiment, which was the case for the test examined. Therefore, it is possible to assess the performance of the underlying procedure (i.e. the hysteresis cycle construction and creep relaxation calculation) in estimating

these quantities using a probabilistic framework. This was done by conducting a set of three probabilistic assessments:

1. One assuming no experimental knowledge of either σ_B nor $\Delta\sigma_c$ is used, which is a fully analytical assessment.
2. One using the cyclic σ_B data, thus skipping a large section of the R5 procedure, but still relying on the creep relaxation routine to estimate the stress drop, $\Delta\sigma_c$.
3. One final assessment that not only uses the σ_B data, but since the stress is continuously recorded during the creep relaxation, this stress can be used instead of using the creep relaxation calculation.

The results associated with these three assessments (which were all based on DE and RCC-MR models combinations) are shown in Figure 3.8. By comparing the fully analytical assessment results with the one using experimental σ_B and $\Delta\sigma_c$ (i.e. the solid line versus the dotted one), it can be concluded that the procedure for hysteresis cycle construction does generally tend to err on the side of conservatism. To reiterate, the analytical estimate of σ_B is based on a Ramberg-Osgood approach, while $\Delta\sigma_c$ is calculated through the integration of forward creep coupled with the RCC-MR model for creep deformation. It appears that approximating σ_B and $\Delta\sigma_c$ individually introduce similar degrees of uncertainty, which is indicated by the dashed line lying roughly midway between the other two lines. Notably, σ_B and $\Delta\sigma_c$ are correlated, as a large σ_B would in general lead to a larger stress drop, producing a larger creep strain, thus an increased strain range. This makes separating the effect of each parameter challenging using this kind of analysis. Interestingly, the assessment which used all experimental stress data available (the solid line) is still showing a considerable amount of uncertainty, which is attributed to analytical formulations being used for creep deformation and damage. These seem to still incur a rather substantial amount of uncertainty. This leads to the conclusion that even though the approximation of stresses does introduce significant uncertainty, scatter in the creep parameters still dominates the assessment results, which is corroborated by the SA presented in Figure 3.6. Nevertheless, the combined uncertainty introduced by approximating σ_B and $\Delta\sigma_c$ is quite substantial and focusing on improving the analytical methods for their estimation would yield markedly less conservative estimates. This approach allows for the examination of the uncertainty introduced by various key stages in the underlying assessment, which can be valuable for targeting further development work.

3.8 Case-Study: Uncertainty Sources in Material Properties

3.8.1 Case-Study Definition

A common wisdom in material data experimentation is the notion that scatter in a particular experimental quantity can be attributed to material variability specific to a given cast, and

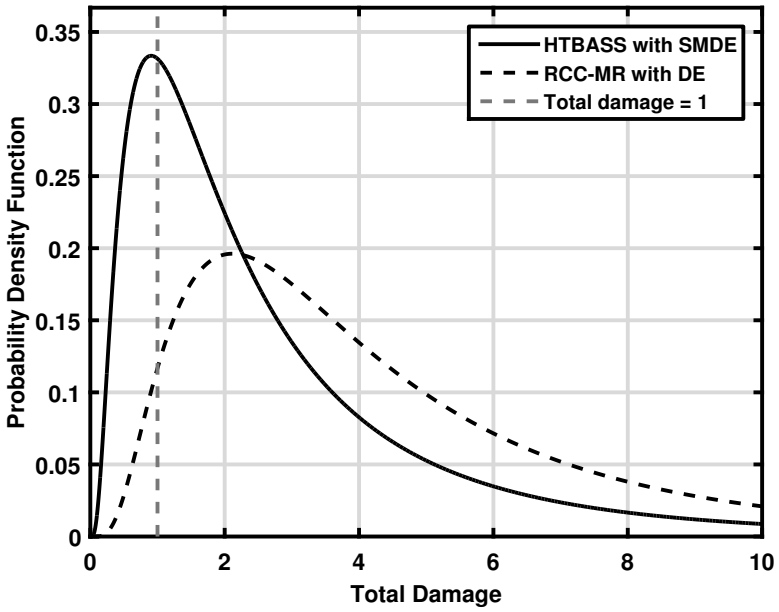

Figure 3.7: A comparison between results obtained using two competing combinations of models for creep deformation and ductility.

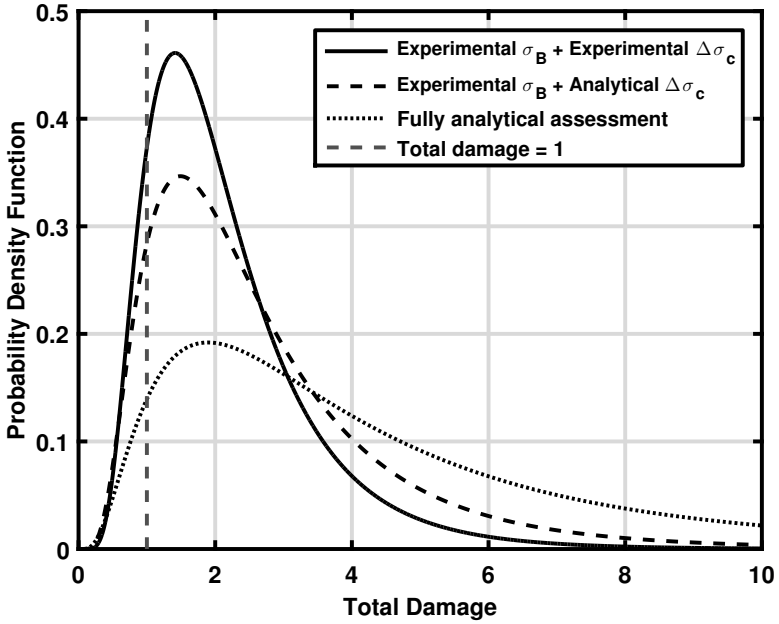

Figure 3.8: Probabilistic results from three assessments examining the effect of removing uncertainty associated with estimating key stress quantities (σ_B and $\Delta\sigma_C$).

to variability arising from different casts of the same material (i.e. cast-to-cast variability). To account for such observations, there is a need to develop statistical measures to quantify uncertainties in cast specific and cast-to-cast material properties. Firstly a clear categorisation of the uncertainties involved is needed. Uncertainty is commonly defined in terms of either *aleatory* (characterised by chance or irreducible randomness in the data) or *epistemic* (arising from a lack of knowledge and the inability to explain physical failure mechanisms) uncertainties [19]. For the current context, the overall uncertainty in a material property (creep time to rupture in this case-study) can be considered as comprising of two parts: an epistemic component due to cast-to-cast differences, and an aleatory component due to scatter within a given cast. An example looking at creep rupture data for an austenitic stainless steel was prepared to demonstrate this issue, which is shown in Figure 3.9. The available data-sets were rather small (some having less than 10 data points), however, by fitting normal distributions, this example served the purpose of demonstrating the basic concepts at hand.

3.8.2 Methods

Assuming a simple power law relationship between the time to creep rupture (t_R) and the uniaxially applied stress (σ) gives the following expressions:

$$t_R = A\sigma^n \tag{3.40a}$$

$$\log(t_R) = \log(A) + n\log(\sigma) \tag{3.40b}$$

In this example, cast specific data can be used to estimate the parameters A and n using least squares regression. An error parameter can be added to model the data scatter relative to the regression fit:

$$\log(t_R) = log(A') + (n')\log(\sigma) + \epsilon \tag{3.41a}$$

where A' and n' are estimates of A and n, and the error term ϵ can be represented by a normal distribution with zero mean:

$$\epsilon \sim N(0, SD_\epsilon) \tag{3.41b}$$

This error term represents the aleatory uncertainty in t_R which is associated with a specific cast. After evaluating A' and n', a normal distribution can be fitted to the ϵ data using the methods described in Section 3.4.2. By treating ϵ as independent of the input stress, it is assumed that the t_R has constant variance (i.e. it is *homoscedastic*). To account for cast-to-cast variations, it is suggested in [16] that an extra term can be added to Eq 3.41a to account for this epistemic uncertainty:

$$\log(t_R) = log(A') + (n')\log(\sigma) + \epsilon + \log(\Delta t_R) \tag{3.42}$$

were $\log(\Delta t_R)$ can be represented by a normal distribution. An approach for characterising this extra term is to examine the cast-to-cast variability in terms of *mean* time to creep rupture. This means that each cast will have a mean time to creep rupture at a particular stress, thus producing a new data-set of mean values. By finding the mean and standard deviation of this new data-set, the variability of $\log \Delta t_R$ can be inferred. Thereafter, the uncertainty in t_R can be incorporated in a probabilistic assessment using 3.42.

3.8.3 Results and Discussion

Some limited cast-specific creep rupture data was available for 316H stainless steel. This comprised of uniaxial creep rupture data for three casts, though some of the case-specific data sets were rather small with Casts 1-3 having 20, 7 and 4 data points respectively. For each cast, A' and n' were calculated using linear regression, and the error term ϵ was characterised using a normal distribution. Thereafter, using Eq 3.41a cast-specific t_R predictions were obtained for an arbitrary value of stress. These uncertain predictions are shown in Figure 3.9. A similar approach was followed which used all data (i.e. all casts were included), and its associated prediction is also included in Figure 3.9. From this example one major conclusion was that the uncertainty attributed to cast-to-cast variations dominated the overall variability. This can be inferred from Figure 3.9 where large disparities can be observed between casts. It is worth noting that this large discrepancy was, partially, due to the material tested being ex-service (thus aged material) and having operated at different plant conditions. The prediction based on all data (the solid line in Figure 3.9) is skewed towards lower t_R, which is attributed to the data-set for Cast 1 being substantially larger than those for the other two casts (20 versus 7 and 4 data points). Furthermore, based on the means of the three cast-specific distributions shown in Figure 3.9, the scatter in the $\log(\Delta t_R)$ (see Eq 3.42) could be inferred, but in this case this would be based on only three data points comprising of the means of each distribution. Given the data limitation, a characterisation of $\log(\Delta t_R)$ was not attempted, but the method discussed is still valid.

A further consideration is whether the assumption of homoscedasticity should be challenged i.e. whether the uncertainty can be a function of stress. Experimental experience with creep testing indicates that long-term data is usually more scattered because there are more chances of the test procedures and equipment to interfere with the data [11]. If this issue is to be addressed, then the material data scatter should be inferred from data-sets that are stress partitioned. Given the available data for Cast 1, there was a chance of examining this approach. Figure 3.10 shows a t_R prediction for Cast 1 (the same as the one discussed above), as contrasted with a prediction that is based on stress partitioned data. Essentially, a subset of the 20 data points associated with Cast 1 had the same stress, a distribution of which is shown in Figure 3.10, as compared with a prediction based on the data including all available stresses. It can be observed that although the uncertainty has slightly increased due to the use of a smaller subset, the mean prediction of t_R

has increased. This approach is analogous to seeking better material characterisation which was represented Figure 3.1(c). This case-study highlights important issues related to:

1. The identification of uncertainties in material data depending on their sources (i.e. those arising from cast-to-cast versus cast specific variations).

2. The importance of partitioning the available data (e.g. by applied stress) in order to obtain meaningful results with the best degree of confidence.

These issues are particularity relevant when considering populations of components which are manufactured from different casts. In such cases, taking into account these sources of uncertainty is vital in order to obtain probabilistic results that are representative of the populations of interest.

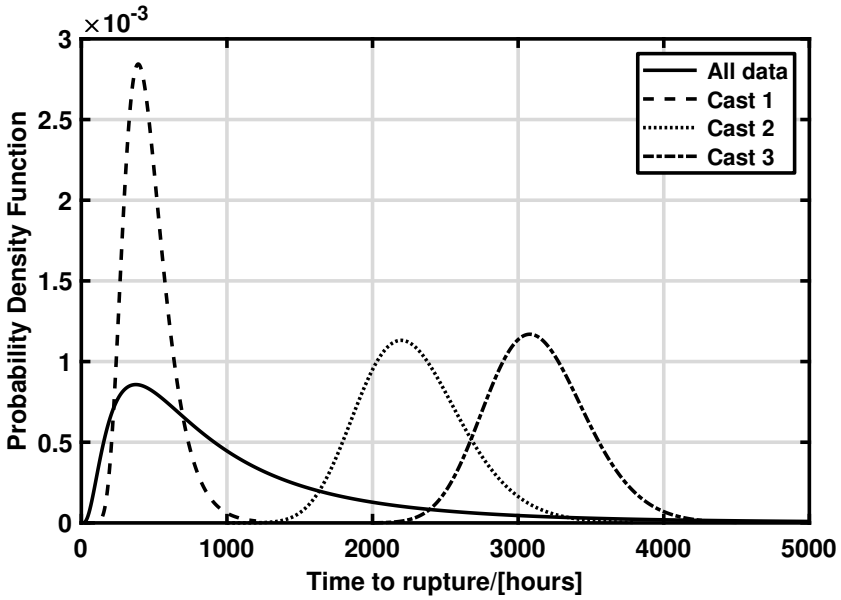

Figure 3.9: PDFs showing the variability of t_R at an arbitrary stress for three casts of an austenitic stainless steel.

3.9 Component Selection for Plant Component Case Study

Examining a plant component came as a natural progression from the knowledge and expertise built as part of the previous two case studies (cast-to-cast variations and uniaxial creep fatigue). This was intended to inform future probabilistic assessments as it will provide further advice on the statistical treatment of input data and the treatment of complex temperature and stress histories. Furthermore, this will also involve building a better understanding of uncertainties inherent to a real plant component e.g. cyclic histories, load types and variations, transient

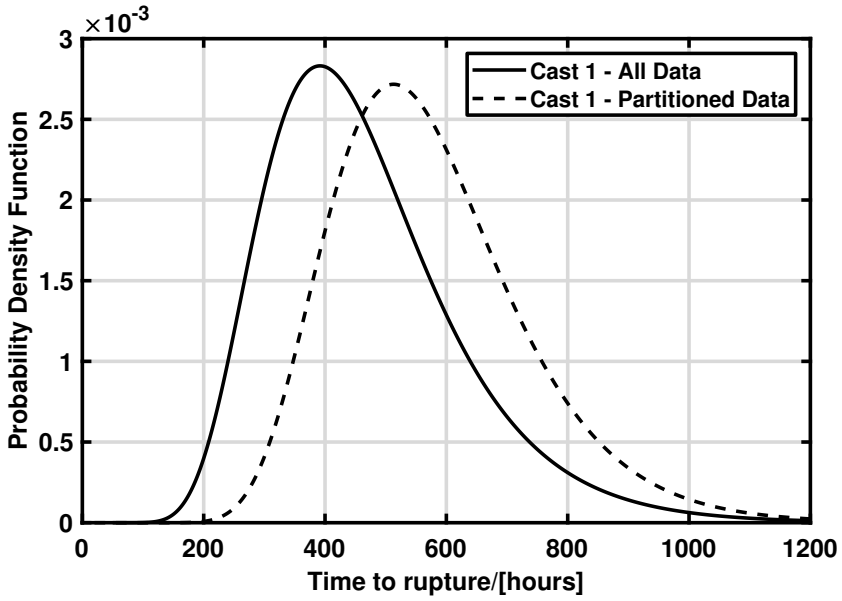

Figure 3.10: For a single cast, this figure shows a comparison of t_R predictions (all at the same stress) obtained from the linear regression analysis using all available Cast 1 data (Eq 3.41a) and a distribution fitted to cast and stress specific data.

thermal effects and the choice of assessment point. This section outlines the selection process that was carried out for choosing the subject component for the case-studies presented in Chapters 5 and 6.

The component selection was the outcome from a pre-job meeting and correspondences between EDF staff (M. Chevalier, J. Johns, G. Rayner and J. Tao) and UoB stakeholders (N. Zentuti, J. Booker and R. Bradford). Firstly, four components were short-listed, the details of which are highlighted in Table 3.7, and six possible failure mechanisms were postulated.

The tubeplate (TP) was chosen as the best candidate. This was based on the preference to avoid carburisation, weldments and reheat cracking. It was also agreed that the tube spacer may be considered as a future case-study to examine the interactions of failure mechanisms beyond creep-fatigue. This may be more appropriate and timely once other EDF projects investigating the effects of carburisation are finalised. A more detailed description of the TP is included in Section 5.2, for which failure mechanisms are driven by creep-fatigue, large thermal transients and over-heating due to tube restrictions. Furthermore, the TP is subjected to complex stress states which include large thermal stress gradients due to large temperature differences (called *tilts*) between the tubes being joined by the TP.

Table 3.7: Details of shortlisted components for the probabilistic R5 Volume 2/3 case-study. Possible failure mechanisms are creep-fatigue (CF), carburisation (CR), failures due to weldments (WF), thermal transients (TT), tube restrictions (TR) and reheat cracking (RC).

Component	**Possible failure mechanisms**						**Characteristics**
	CF	CR	WF	TT	TR	RC	
Tubeplate	Yes	No	No	Yes	Yes	No	Large thermal stress gradient due to temperature differences between tubes joint by the ligament. Potentially complex stress state. Superheated steam.
Tube spacer	Yes	Yes	Yes	Yes	No	No	Complex stress state (high transient stresses).
Bifurcation	Yes	Yes	Yes	No	No	No	Similar components have been considered in the past. Superheated steam.
Detuning straps	Yes	No	Yes	Yes	No	No	Station-specific and bespoke design. Originally introduced to dampen vibrations. Relatively simple stress state. It was assumed that carburisation is negligible in Dungeness components.

3.10 Summary

This chapter was devoted to formalising clear arguments for probabilistic structural integrity implementation, while providing a pragmatic view on the challenges and limitations involved. The following are the key ideas that have been covered in this chapter:

1. A high-level discussion on the chief modes of application for probabilistic methods has provided clear insight into the prospective benefits from shifting towards a probabilistic paradigm.

2. A review of the main methods and techniques required to conduct a complete probabilistic calculation was presented, thus providing the building blocks for the prospective methodology proposed by this PhD project. There are numerous probabilistic approaches and techniques that serve a variety of purposes. The choice of which approaches to use is predominantly dictate by the mode (e.g. design versus assessment) and purpose (e.g. reliability estimation versus sensitivity analysis) of the application at hand. As a result, it is suggested that in order to tackle a variety of structural integrity problems, a general knowledge of the various approaches in existence is needed in order to formulate probabilistic analyses tailored to such problems.

3. Deployment of some of these approaches was exemplified through a case-study assessing a simple uniaxial test specimen for creep-fatigue damage. Even for this relatively simple case, there are considerable sources of uncertainty, and a number of approaches were demonstrated, including quantitative sensitivity analysis of the input parameters and considerations of model uncertainty.

4. In conclusion, probabilistic paradigms lend themselves well to structural integrity applications which are inherently uncertain; the former can serve important and insightful functions which cannot be fulfilled using conventional deterministic calculations. This argument is especially true for applications concerning plant components, which involve levels of uncertainty considerably beyond the simple case-study discussed in this chapter.

CHAPTER 4

CORRELATIONS BETWEEN INPUT PARAMETERS

This chapter formalises an approach for identifying and incorporating correlations between input parameters in probabilistic creep crack initiation assessments. In order to measure the correlations from experimental data, the methodology is based on partitioning data obtained from uniaxial creep test results into subsets according to temperature and stress. The methodology can be implemented to identify correlations for any material and any combination of input parameters. An implementation method is also presented for sampling correlated parameters in Monte-Carlo simulations using the Spearman rank order correlation. This is followed by a discussion of the key effects that incorporating correlations might have on probabilistic results. A case-study is presented to demonstrate this correlations methodology by examining 316H stainless steel uniaxial data and identifying correlations between creep deformation, creep ductility and rupture life. While a degree of correlation between ductility and creep deformation exists, it was found to be uncertain. Conducting post-assessment sensitivity analyses based on uncorrelated parameters is suggested as part of the methodology, providing focus as to which correlations are most important and, therefore, should be considered.

4.1 Overview

A crucial aspect of any probabilistic assessment is the statistical characterisation of uncertainties in the input parameters. As discussed in Section 3.8, these uncertainties can be defined in terms of either *aleatory* uncertainties, characterised by chance or irreducible randomness in the data, or *epistemic* uncertainties which arises from a lack of knowledge of the underlying mechanisms [19]. The overall uncertainty in a material property can, therefore, be considered as comprising of two parts: an aleatory component due to scatter within a given cast, and an epistemic component due to cast-to-cast differences. The former are considered random variations, whilst the latter

are typically due to subtle differences in chemical compositions or manufacturing processes. Inter-parameter correlations can also contribute to the overall uncertainty in the output result of a probabilistic calculation. The subject of incorporating correlations between creep parameters (e.g. creep strain rate and creep ductility [21]) is generally acknowledged for its importance, but not widely identified and addressed. Difficulties with identifying important correlations arise from the absence of rigorous statistical data treatment [11]. In [16] it is proposed that uncertainties can be quantified by dividing the available data into appropriate subsets from which statistical measures can be inferred.

In Section 4.2 a methodology for firstly characterising and then incorporating correlations between input parameters in probabilistic assessments is presented. To demonstrate the implementation of this methodology, the probabilistic assessment for the uniaxial creep-fatigue test (see Section 3.7 for details) was examined with due focus on the effect of correlations between creep ductility and deformation. Material properties are key sources of uncertainty, especially the creep related ones due to large scatter. Consequentially, correlations between creep ductility and creep deformation were of most interest. The results and discussion in this Chapter are focused on 316H stainless steel, for which the required data was extracted from a materials testing database managed by EDF Energy. Correlations between creep ductility and creep deformation were calculated based on uniaxial creep test results which were firstly partitioned by applied temperature and stress. Following these calculations, an example driven discussion (Section 4.3.4) on how key correlations can affect probabilistic output results is presented. It was found that identifying and incorporating this correlation can have a considerable, and advantageous, effect on the predicted probability of initiation (PoI).

4.2 Methodology

4.2.1 Correlation Coefficients

The Pearson correlation coefficient [55, 62] is the ubiquitous correlation statistic. It measures the strength of the *linear* relationship between two parameters. It also has a weak, and very often ignored, requirement that the parameters should be normally distributed. This is a parametric coefficient, since its expression includes the means of both parameters:

$$r = \frac{\sum_{i=1}^{N_D}(X_i - \bar{X})(Y_i - \bar{Y})}{\left(\sqrt{\sum_{i=1}^{N_D}(X_i - \bar{X})^2}\right)\left(\sqrt{\sum_{i=1}^{N_D}(Y_i - \bar{Y})^2}\right)} \tag{4.1}$$

where X_i and Y_i represent a data point, $\bar{X}$ and $\bar{Y}$ are the means and N_D is the total number of data points. The Spearman correlation, which is a non-parametric equivalent to Pearson's, determines the strength and direction of the *monotonic* relationship between two parameters [4]. It is calculated as the Pearson correlation between the ranks of the two sets of data being

examined and is given by:

$$C_S = 1 - \frac{6\sum_{i=1}^{N_D} d_i^2}{N_D(N_D^2 - 1)} \tag{4.2}$$

where d_i is the difference between the ranks assigned to each X_i and Y_i data pair. The magnitudes of C_S and r range from 0 to 1 (0 indicating no correlation and 1 indicating a perfect correlation), while their signs indicate whether the parameters are correlated (if the correlation is positive) or anti-correlated (if the correlation is negative) [4, 55]. For most of the applications presented in thesis, the Spearman correlation was deemed to be more appropriate as it does not assume linearity (an assumption which may not apply for the parameters of interest) and is a non-parametric statistic which does not impose any *a priori* assumptions on the distributions of the input parameters. Therefore, parameters following different types of distributions can still be correlated using the Spearman correlation.

4.2.2 Sampling of Correlated Input Parameters

For normally distributed variables, the *Cholesky decomposition* can be used to sample multiple input parameters while taking their inter-correlations into account [18]. However, a more general approach is based on using *Gaussian copulas*. A detailed account of this method can be found in [84], whilst a practical example showing its implementation in MATLAB can be found in [85]. The aim is to generate multivariate samples having arbitrary PDFs and Spearman correlations. The method involves two key steps to transform normally distributed, correlated samples to ones which adhere to any arbitrary distribution. Furthermore, the random variables comprising the multivariate samples do not have to necessarily follow the same type of distribution, thus providing a desirable degree of flexibility to this method. In [84] this procedure is termed NORTA (**NOR**mal **t**o **A**nything), which in essence can be broken down into two steps:

1. Firstly, a multivariate normal parameter (Z) is transformed into a multivariate uniform parameter U, in which case the distribution of U is known as a *copula*.

2. Secondly, U is transformed into the desired multivariate parameter X, with its constituent variables having arbitrary cumulative distribution functions (CDFs). Thus the procedure is summarised in the following equation:

$$\mathbf{X} = \begin{bmatrix} F_{X_1}^{-1}[U_1] \\ F_{X_2}^{-1}[U_2] \\ \vdots \\ F_{X_V}^{-1}[U_V] \end{bmatrix} = \begin{bmatrix} F_{X_1}^{-1}[\Phi(Z_1)] \\ F_{X_2}^{-1}[\Phi(Z_2)] \\ \vdots \\ F_{X_V}^{-1}[\Phi(Z_V)] \end{bmatrix} \tag{4.3}$$

   where Φ is the standard normal CDF, F_{X_v} is the desired CDF for the v^{th} random variable and there are V number of variables being correlated.

4.2.3 Effect of Sample Size on Measured Correlations

A further important consideration is whether the sample size of a data-set has an effect on the calculated correlation, and in turn how the latter affects the results of a probabilistic assessment which uses correlations based on relatively small data sets. The approach used to examine this effect was to produce two large (10^5 samples) sets of correlated parameters. Thereafter progressively smaller sets were obtained by randomly sampling from the large population set, and the associated correlations were calculated and compared with the correlation for the large population. The two parameters produced for this analysis were normally distributed and the Spearman correlation was used. Figure 4.1 shows how reducing the sample size causes a drift away from the correlations based on large populations, suggesting that for smaller data sets the correlations are usually smaller than those for the larger populations. However, this effect is not noticeable for sets larger than 30 data points. This effect can be rather considerable, and must be noted when correlations based on small data sets are used in probabilistic analyses.

As to how this affects the probabilistic results, it solely depends on the nature of the probabilistic assessment and the degree of conservatism (or lack thereof) that comes with using a smaller correlation coefficient. As discussed in Section 4.2.4, for probabilistic creep damage assessments, a positive correlation between creep deformation and ductility yields a lower PoI. Thus a smaller positive correlation would increase the predicted PoI and, therefore, has a conservative effect. Furthermore, if the assessment results are rather sensitive to a particular correlation, then even a fairly modest change (Figure 4.1 suggests a drop of approximately 10% for very small sample sizes) may have a significant affect.

4.2.4 Implications for Probabilistic Results

Figure 4.2 shows a scatter plot for two creep parameters which are assumed to be statistically independent. Without a correlation between the scatters in the properties, two overly populated regions exist in the plot (referred to as regions of atypical behaviours in Figure 4.2a). In this context atypical means relatively infrequent, but without a correlation these samples are as frequent as the more typical samples. The effect of excluding correlations is to effectively increase the overall uncertainty in the probabilistic results, a measure of which is the width of the output parameter PDF (see Figure 4.13 as an example). Incorporating correlations has the effect of reducing the number of samples in these atypical regions as shown in Figure 4.2b.

Figure 4.3 shows a proposed procedure for firstly assessing the importance of incorporating a possible correlation between input parameters, then calculating this correlation based on partitioned data sets, and thereafter incorporating it at the sampling stage during a probabilistic assessment. The main output of a probabilistic assessment is assumed to be a probability of failure (PoF), or initiation in this case, at the end of life (EoL). The procedure does rely on

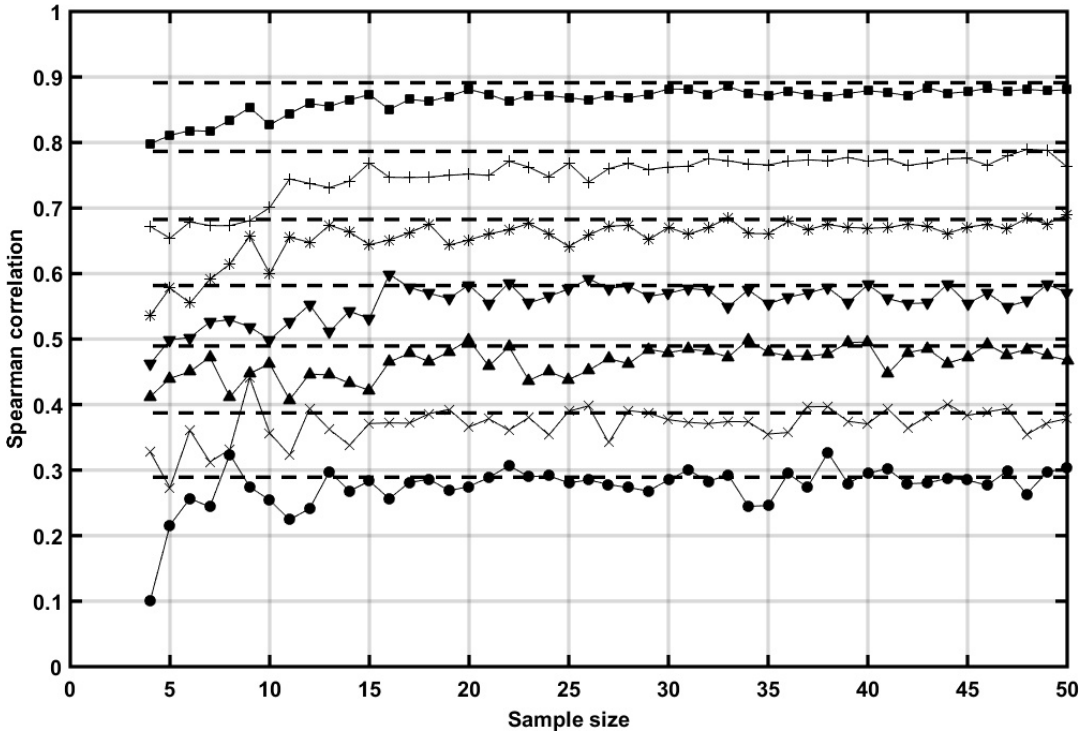

Figure 4.1: A comparison for seven degrees of correlation (from 0.3 to 0.9) between the Spearman correlation coefficient as a function of sample size against correlations based on large populations (10^5 samples), the latter of which are represented by dashed lines. This shows that for smaller sample sizes the calculated coefficient deviates from the population coefficient.

conducting a sensitivity analysis to establish which input parameters dominate the results of the probabilistic assessment. In the absence of adequate data-sets, a postulated range of correlations can still be trialled, and for a given probabilistic assessment a plot equivalent to the one shown in Figure 4.14 can be produced. Such a plot can assist in making a judgement as to what an adequate correlation could be in the absence of experimental evidence to characterise such correlation. Indeed even when some data is available, the sought correlation might still be uncertain (for example following a distribution like the one shown in Figure 4.10), in which case trialling a range of possible correlations to examine their effect on the PoF would aid judgement.

To quantify the effects that incorporating a correlation has on the results of a probabilistic assessment, a number of approaches are suggested:

1. The Mann-Whitney test [63] (also known as the Wilcoxon rank sum test) which tests the null hypothesis that the two sets of results are sampled from two continuous distributions with equal medians, against the alternative that they are not. By using the left-tailed hypothesis version, this establishes whether correlations cause a significant increase in predicted damage by comparing the medians of the PDFs.

2. The quotient test [86] which measures the probability of increasing the overall damage (i.e. shifting the PDF to the right) by introducing a correlation relative to the uncorrelated case. This is defined as:

$$P_{shift} = p\left(\frac{D_{Corr}}{D} \geq 1\right) \tag{4.4}$$

where D and D_{Corr} denote sets of random samples from the distributions of uncorrelated and correlated results respectively. If absolutely no effect exists, then P_{shift} should be close to 0.5. This would in essence mean that the probability of achieving a PDF shift to the right is equal to that of a left shift, and thus no clear effect can be deduced.

3. The F-test which compares two data sets in terms of their variances. This test only applies to data sets which are normally distributed and thus can be somewhat restrictive. However, noting that the PDFs in Figure 4.13 were lognormal, the logarithm of the results can be treated as normal, rendering the F-test applicable.

4. The Brown-Forsythe's test [87, 88] which is an equivalent to the F-test but remains robust for non-normally distributed data. This relies on firstly transforming the data sets using their respective medians, for example:

$$z = |D - \tilde{D}| \tag{4.5}$$

where D denotes the results obtained from a probabilistic assessment using uncorrelated parameters, and $\tilde{D}$ is the associated median. Thereafter an F-test is performed on the two transformed sets of results for the equivalence of their variances (i.e whether the two sets of results are *homoscedastic*).

5. The probability of failure defined as:

$$PoF = \int_{1}^{\inf} f(D)dD \tag{4.6}$$

where $f(D)$ represents the PDF of the total damage parameter D. Ultimately the effect of assuming a correlation on the estimated failure probability is what is truly of interest.

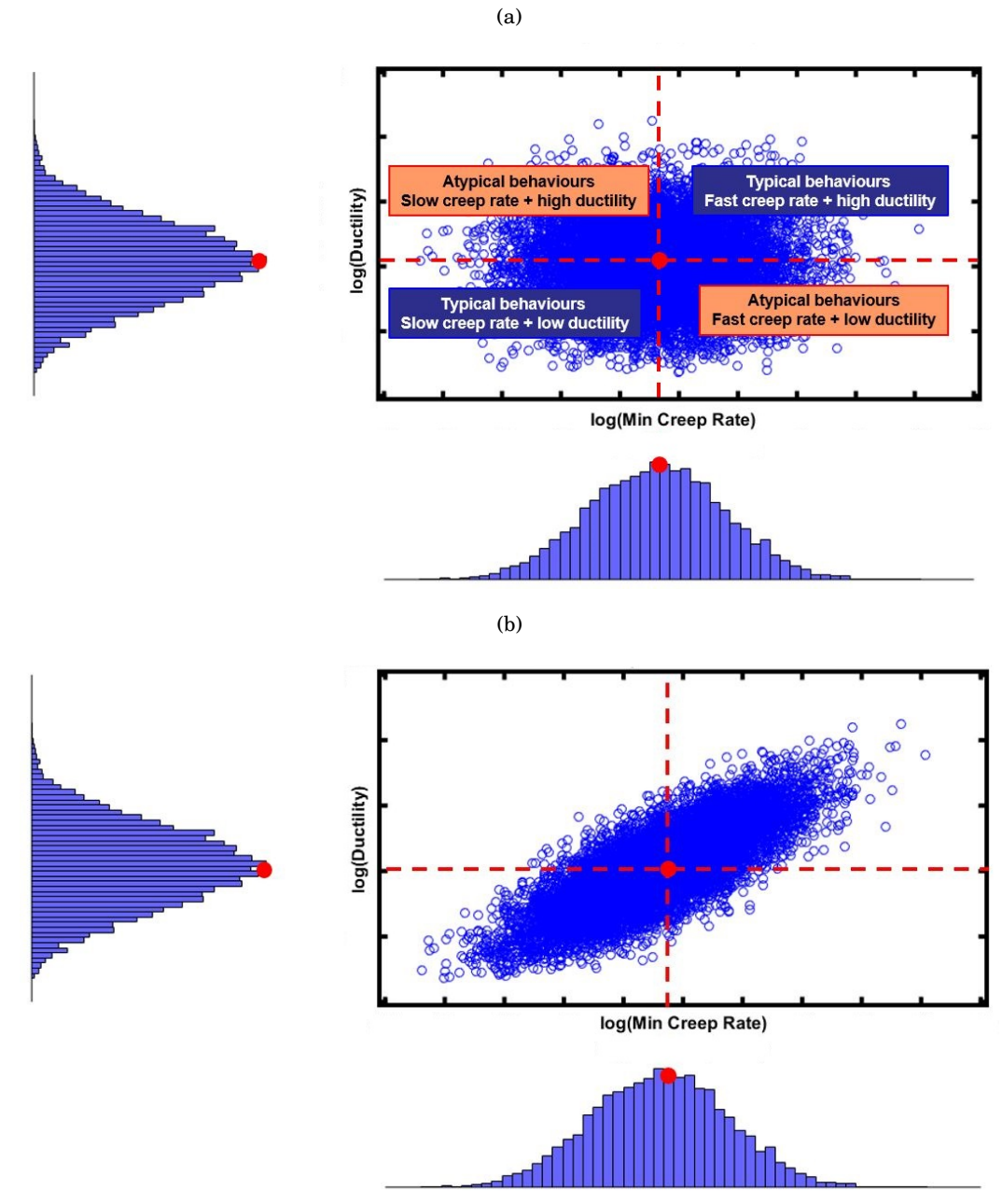

Figure 4.2: Scatter plots showing data samples of minimum creep rate (at an arbitrary stress) and ductility data with a) no correlation and b) a postulated 0.8 (i.e. 80%) correlation.

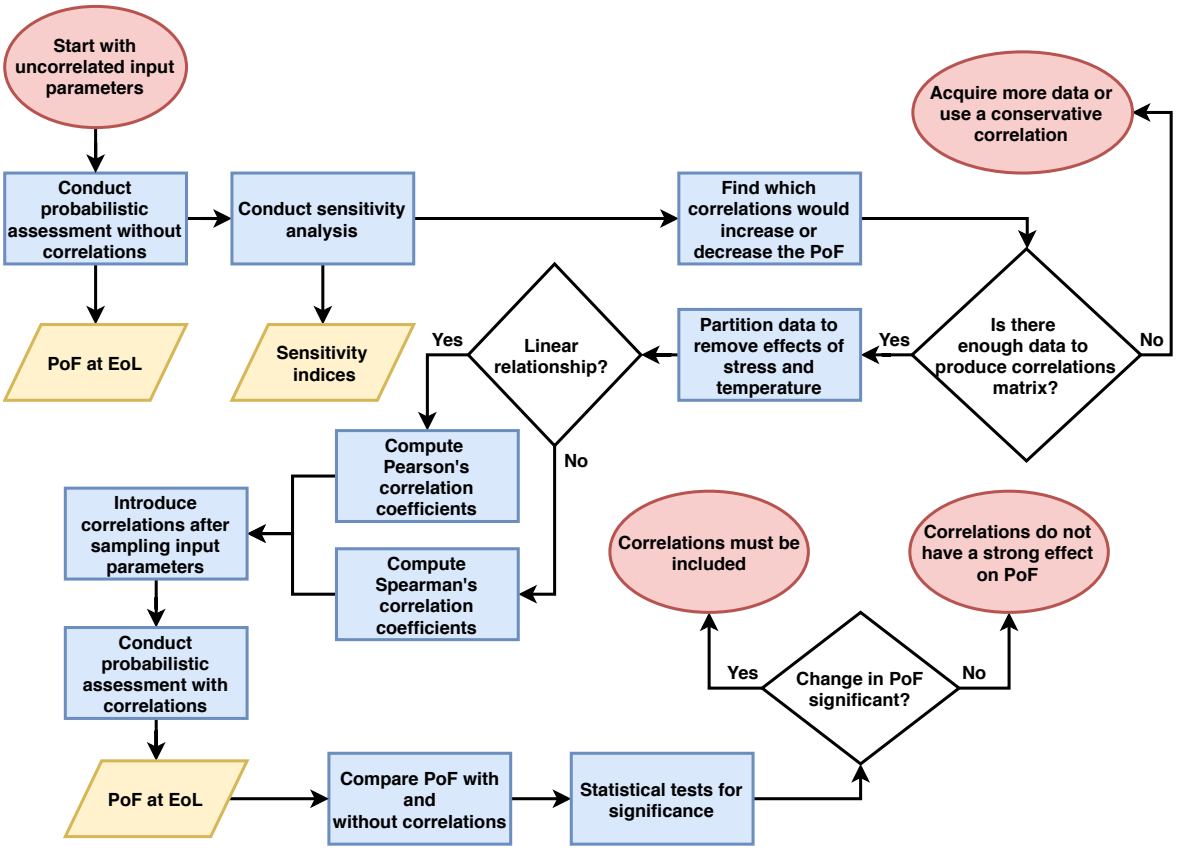

Figure 4.3: Proposed procedure for assessing the importance of input parameter correlations in probabilistic creep assessments.

4.3 Case-Study: Correlations Between Creep Ductility and Deformation

4.3.1 Uniaxial Creep Data

Most creep deformation and creep damage models are fitted to uniaxial creep rupture tests. It was therefore deemed appropriate to examine data sets from such tests to infer potential correlations between key creep parameters. Chosen due to their importance towards creep damage calculations, the parameters which were considered in this work are the following:

1. The uniaxial creep ductility, ε_f. Two measures of uniaxial ductility were available: the last recorded inelastic engineering strain (excluding any plastic strain introduced by the initial loading), ε_{LS}, and the percentage reduction of area at the necking point of the specimen (PRA).

2. The rupture time, t_R.

3. The average creep strain rate, $\dot{\varepsilon}_A$, which was calculated as ε_{LS} over t_R.

4. The minimum (secondary) creep strain rate, $\dot{\varepsilon}_S$. This was only available for 289 uniaxial creep tests within the database.

5. The primary creep strain rate coefficient, K. With the creep strain rate ($\dot{\varepsilon}_P$) being variable during the primary stage of a creep test, K was chosen as an intermediary measure to characterise the primary deformation. The coefficient was based on the strain hardening version of the RCC-MR [81] model, thus it was calculated by fitting the creep strain rate data in the primary stage to the following expression:

$$\log(\dot{\varepsilon}_P) = \log(K) + X\log(\varepsilon_C) + Y\log(\sigma) \tag{4.7}$$

   where ε_C is the instantaneous creep strain, and the creep constants X and Y were taken from [81]. It is worth noting that the data used in this work are based on engineering stress and strain measurements.

The last recorded inelastic strain was the closest experimental recorded data to the desired uniaxial ductility that was available for all tests. The only other similar quantity was the percentage reduction of area. The former can be dependent on the rate of data recording whilst the latter is typically calculated based on room temperature measurements. Therefore, the inaccuracies in both ε_{LS} and PRA are considered epistemic uncertainties introduced by the experimental approach. It must be pointed out that the database included a vast array of tests that had been conducted over decades of research and in many different laboratories, and therefore finding a consistent measure that can be extracted from all tests was not always possible. This is a common problem in creep testing as strict consistency in conducting the tests and reporting the results is

not always achievable across different laboratories at different times. Accordingly, the proposed approach for addressing this issue was to compare the correlations between $\dot{\varepsilon}_A$ and each of ε_{LS} and PRA. Effectively, together the two measures of ductility are used as surrogates in this work as ductility is not easily experimentally defined. As will be later discussed, this is especially compelling because last recorded inelastic strain and reduction of area are strongly correlated, which essentially implies that they are both proportional to the same quantity (i.e. ductility).

For primary creep, the aim was to find a single measure of creep rate per test. For some of the tests, stress and strain were recorded during the test rather than just recording the last strain. Therefore the power law expression in Eq 4.7 was fitted to the stress-strain data recorded during each test. This raw creep strain data was only available for a total of 289 uniaxial creep tests. For a single test it is not possible to fit three parameters at the same time. Thus by fixing two of the parameters at the values quoted in [7], for a single test a single value of K can be obtained. The purpose of this approach must not be confused with finding the optimal values of K, X and Y for 316H given all tests. Rather it attempts to encapsulate a measure of primary creep rate into a single value per test. This approach was driven by the limitation of the available data and the inherent uncertainty associated with characterising primary creep deformation.

The raw data for the creep parameters which was used in this work cannot be reproduced due to propriety issues. However, similar data plots for average creep rate, ductility and rupture time for 316H can be found in [89]. The data used in this case-study included test conditions ranging between 500-850°C and 30-470 MPa. However, due to the long-term nature of creep testing and the variety (and in some cases inconsistency) of purposes that these tests had historically, the test matrix was rather sparse and biased towards either high stresses, high temperatures or both. This sparsity is a key limitation of the available raw data. Nevertheless, the proposed methodology in this chapter is still valid and can be conducted again if better data-sets (i.e. larger sample sizes and spanning the complete range of test conditions of interest) are obtained.

4.3.2 Data Partitioning

Following the approach in [16], the available data was partitioned firstly by temperature only and then by both temperature and stress. Repeated tests using the same cast are rather rare and as a result it was not possible to correlate scatter in creep properties within specific casts. Repeats of the same test conditions, but for different casts were available, which are the focus of this work. Correlations between casts are believed to be more important as cast-to-cast variability typically dominates the uncertainty in creep test data. Cast-to-cast variabilities are typically attributed to marked or even subtle differences in chemical compositions, and in the case of Type 316 stainless steels these differences can produce large scatter in the creep properties [19]. Furthermore, when assessing populations of the same component for creep damage, it is often the case that these

populations would comprise of a multitude of casts. This provides a further justification for basing this current work on data-sets having multiple casts.

The main reason for partitioning the available data was to limit the effect of temperature and stress dependencies, thus isolating pure scatter in the data. Partitioning by either stress or temperature only would effectively introduce a misleading correlation that is driven by the stress or temperature dependencies of the input parameters. This would in turn bias the correlations measured from the stress or temperature partitioned data-sets. Therefore, it is advised that correlations obtained from data subsets partitioned by temperature alone must only be examined qualitatively. Furthermore, correlations from temperature and stress partitioned subsets are those advised to be used in probabilistic assessments. Whilst rigorous, a disadvantage of partitioning by both stress and temperature is the drastic reduction of the sample sizes from which meaningful correlations could be inferred.

4.3.3 Correlations Results and Discussion

Figures 4.4 and 4.5 show various correlations obtained for temperature partitioned data subsets. As previously discussed not partitioning by stress can have a marked effect on the calculated correlations, and thus these results are not directly applicable to probabilistic assessments. However, it is worth noting that these results showed a changeover in correlations around 600°C. It is unclear what is the cause of this phenomenon but it may be related to a temperature induced failure mechanism change. For 316H it was previously observed that there is a trough around 500-550°C in ductility when plotted as a function of temperature [90]. This might be linked with the effect in Figure 4.5 as a manifestation of the creep ductility variation with temperature for 316H.

An important outcome, however, was that scatter in average and minimum creep rates appear to be strongly correlated, which was expected. This observation can be useful in the absence of enough raw data to calculate the minimum creep rate. The average creep rate data can be used as a proxy for inferring - not in absolute but rather in monotonic terms - the severity of scatter in the creep deformation data. Indeed it is believed that average and minimum creep rates should be strongly correlated, as they are both indirect measures of the same phenomenon i.e. creep deformation. However, it is thought that some uncertainty was introduced by the data manipulations required for calculating these quantities from the raw test data.

The more important results are depicted in Figures 4.6 to 4.10, which are based on data subsets partitioned by both temperature and stress. These show that consistently positive correlations between ductility (taken as the ε_{LS}) and various measures of creep deformation exist, albeit the exact values of these positive correlations are uncertain. Results for correlations

between minimum creep rate versus ductility, and primary creep rate versus ductility were based on a small number of data subsets which had relatively small samples sizes (see Figure 4.6). This was a consequence of only a portion of the available data (286 tests out of >1400 tests) having the full creep curve recorded. Consequently, for the vast majority of the available data, minimum and primary creep rates were not calculated. Nevertheless, Figure 4.6 still shows that some significant correlations do exist between the various parameters, not least at 550°C which is the closest temperature to the range of most interest.

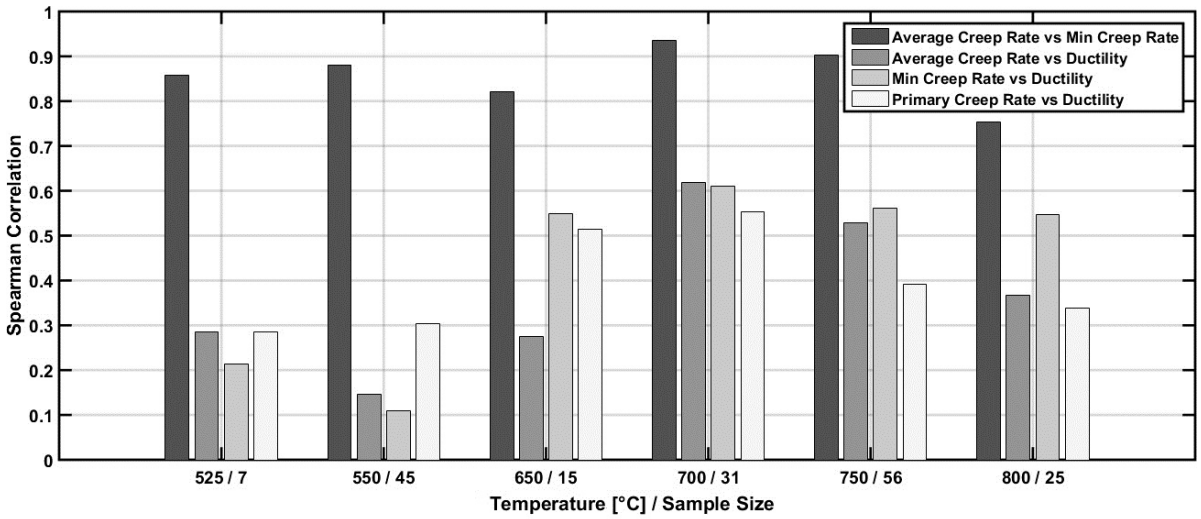

Figure 4.4: Correlations between three measures of creep deformation and ductility (taken as ε_{LS}) based on temperature partitioned subsets.

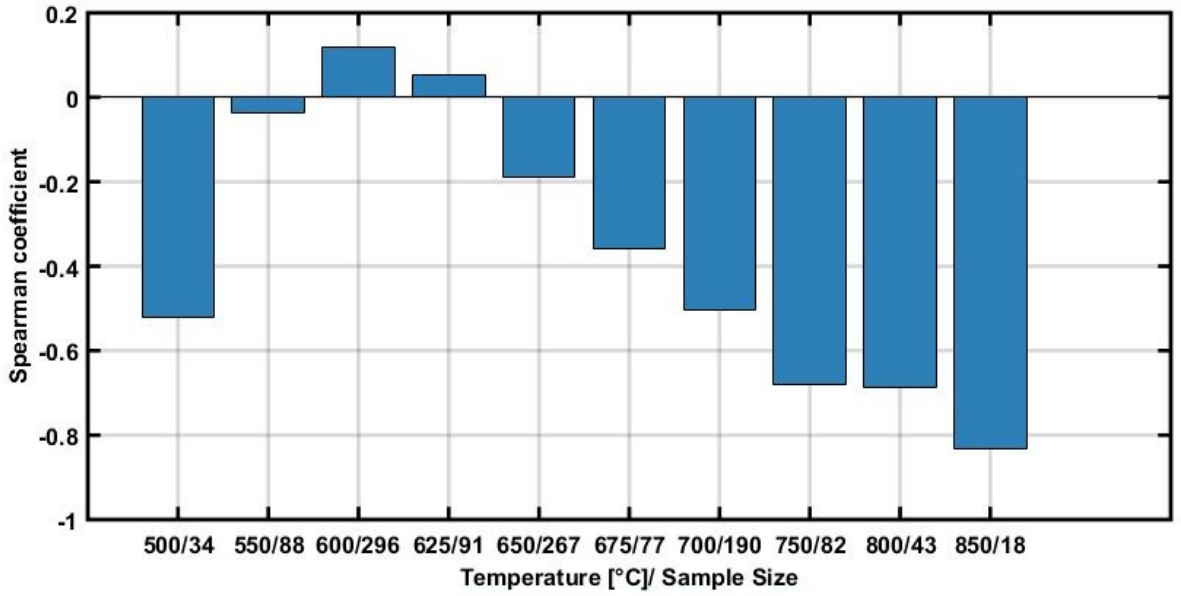

Figure 4.5: Correlations between creep rupture time and creep ductility (taken as ε_{LS}) based on temperature partitioned subsets.

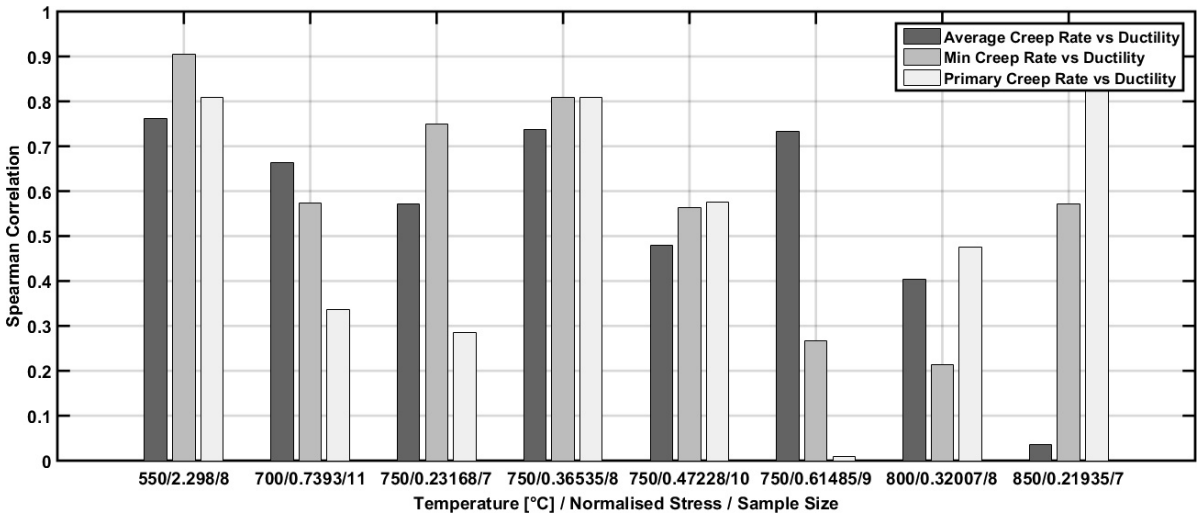

Figure 4.6: Correlations between three measures of creep deformation and creep ductility (taken as ε_{LS}) based on temperature and stress partitioned subsets. The normalised stress is the applied stress over the temperature specific proof stress [91].

Two measures of ductility were examined: the last recorded inelastic strain and the percentage reduction of area. Both are uncertain experimental results which attempt to measure uniaxial ductility. Figure 4.7 shows Pearson correlations results between these two measures based on 25 data subsets, each having a sample size of at least 10 data points. The Pearson correlation is used in this instance, as an exception, to prove that the two parameters are proportional (i.e. linearly correlated). The results show that ε_{LS} and PRA are in fact strongly correlated, which essentially implies that they are both proportional to the same quantity (i.e. ductility). For the closest temperature to plant operating temperatures (600°C) the correlations are consistently strong. Therefore, correlations between each of these two parameters and average creep rate can together provide enough quantitative evidence for the correlation of interest. The correlations results are shown in Figures 4.8 and 4.9, each was based on 25 data subsets, each having a sample size of at least 10 data points, for which enough information was available to calculate the average creep rate.

Note that the results at 550°C were not included because that subset had a sample size less than 10 data points. Furthermore, it is worth clarifying that the testing matrix is biased towards higher stresses and temperatures. This is due to the requirement for accelerated creep testing, which is a limitation of current creep testing efforts. To compromise between practicality and cost on the one hand and producing results at conditions closer to the those of interest, higher stresses and temperatures are commonly used in experiments. Using accelerated creep testing results for predicting plant material behaviour is considered an epistemic uncertainty, which is a major area of research. However, the results shown in Figure 4.6 indicate that correlations at the same temperature but different stresses (see the results for 750°C) do not show a clear

stress dependency. This was also the case for the results shown in Figures 4.8 and 4.9. Stress or temperature dependencies were not, therefore, identified as they may have been effectively masked by the significant variability in the correlation results.

Nevertheless, the results in Figures 4.8 and 4.9 indicate that a significant positive correlation does exist. Figure 4.10 shows histograms of these results, along with the normal and the Minimum Extreme Value Type I distributions, which were found to best represent the histograms. The normal distribution is described by the following PDF:

$$f(C_S) = \frac{1}{\sigma_{SD}\sqrt{2\pi}} \exp\Big[-\frac{(C_S-\mu)^2}{2\sigma_{SD}^2}\Big] \tag{4.8}$$

where C_S is the Spearman correlation, μ is the mean and σ_{SD} is the standard deviation. By contrast, the PDF for the Minimum Extreme Value distribution is:

$$f(C_S) = \frac{1}{\theta} \exp\Big[\frac{C_S-\nu}{\theta} - \exp\Big(\frac{C_S-\nu}{\theta}\Big)\Big] \tag{4.9}$$

where θ and ν are the scale and location parameters respectively. A summary of the parameters calculated from fitting these two distribution types to the histograms is presented in Table 4.1.

For a creep damage assessment based on creep rupture time (e.g. using a time fraction rule) instead of ductility, the required correlation is between scatter in creep rupture time and creep deformation. Figure 4.11 shows correlations between average creep rate and creep rupture time. The two parameters are negatively correlated and a stress dependency can be observed, as lower stresses seems to exhibit lower correlation values. As this work is more focused on ductility based creep damage assessments, the effects that this correlation might have on the probabilistic results of a rupture time based assessment were not explored and these results were only included for completeness.

Finally, Figure 4.12 shows results for correlations between scatter in the creep rupture time and ductility. Some degree of stress dependency is observed with somewhat weak positive correlations at lower stresses and even weaker (often negative) correlations for higher stresses. However, due to the nature of creep damage assessments, creep rupture and creep damage caused by deformation are decoupled, which is the case in the R5 Volume 2/3 [23, 92] assessment procedure. Therefore, although insightful, these correlations are not directly applicable to such creep crack initiation assessments. These results may be relevant for probabilistic assessments which assess creep crack initiation and creep rupture in parallel, in which case a correlation between ductility and rupture time is applicable. Furthermore, a probabilistic assessment based on time-fraction damage (i.e. creep rupture) but including relaxation of secondary stresses, would also require the correlation between deformation and rupture.

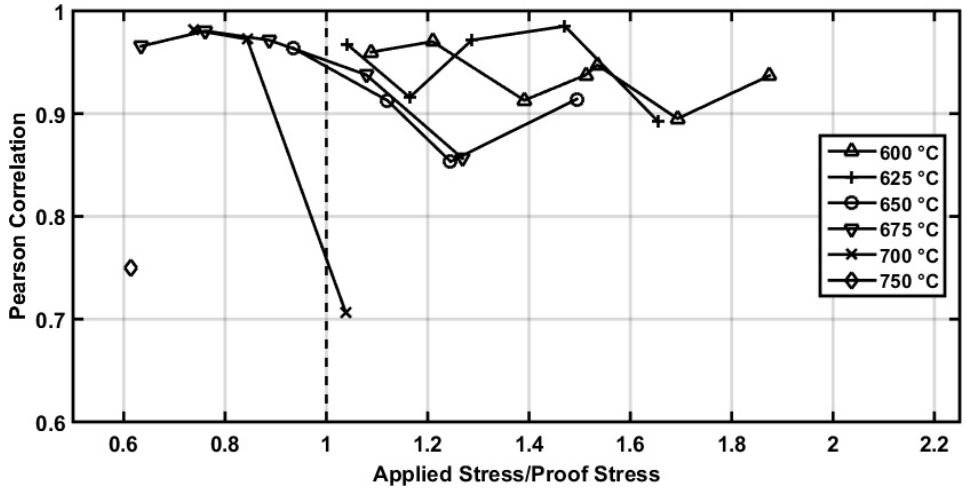

Figure 4.7: Correlations between ε_{LS} and PRA based on temperature and stress partitioned subsets. Each subset has a minimum of 10 data points, and the proof stress is temperature specific and was obtained from [91].

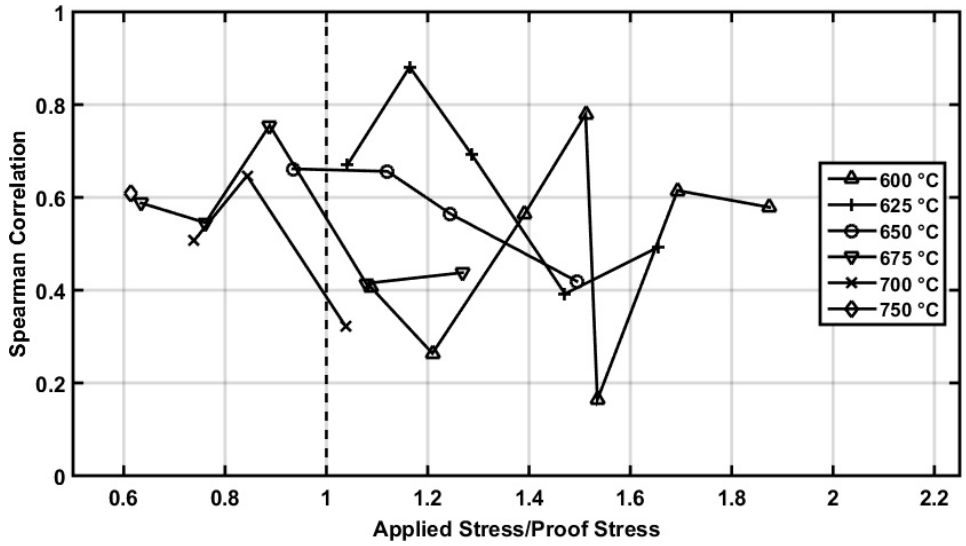

Figure 4.8: Correlations between $\dot{\varepsilon}_A$ and ε_{LS} based on temperature and stress partitioned subsets. Each subset has a minimum of 10 data points, and the proof stress is temperature specific and was obtained from [91].

Table 4.1: Fitted parameters for the distributions shown in Figure 4.10

Correlation	**Distribution parameters**			
	Normal		**Minimum Extreme Value**	
	μ	σ_{SD}	ν	θ
$\dot{\varepsilon}_A$ - ε_{LS}	0.545	0.168	0.618	0.138
$\dot{\varepsilon}_A$ - PRA	0.363	0.238	0.465	0.193

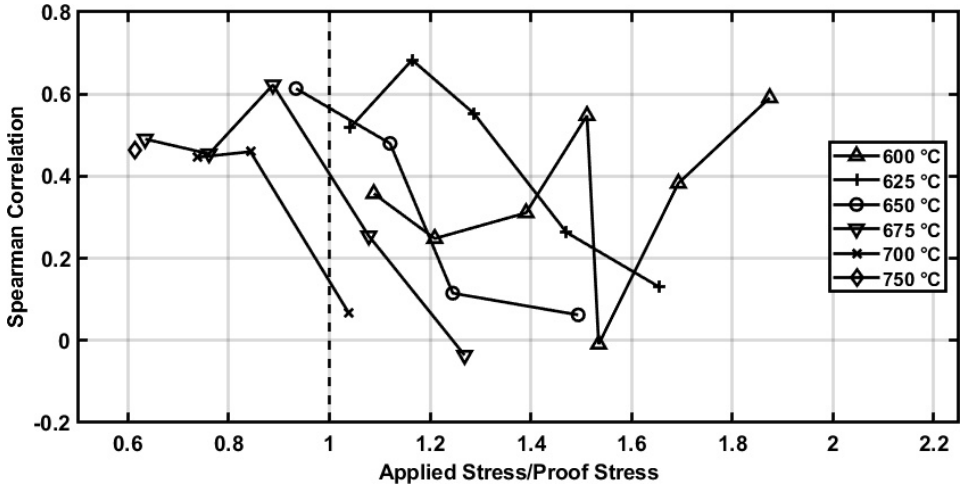

Figure 4.9: Correlations between $\dot{\varepsilon}_A$ and PRA based on temperature and stress partitioned subsets. Each subset has a minimum of 10 data points, and the proof stress is temperature specific and was obtained from [91].

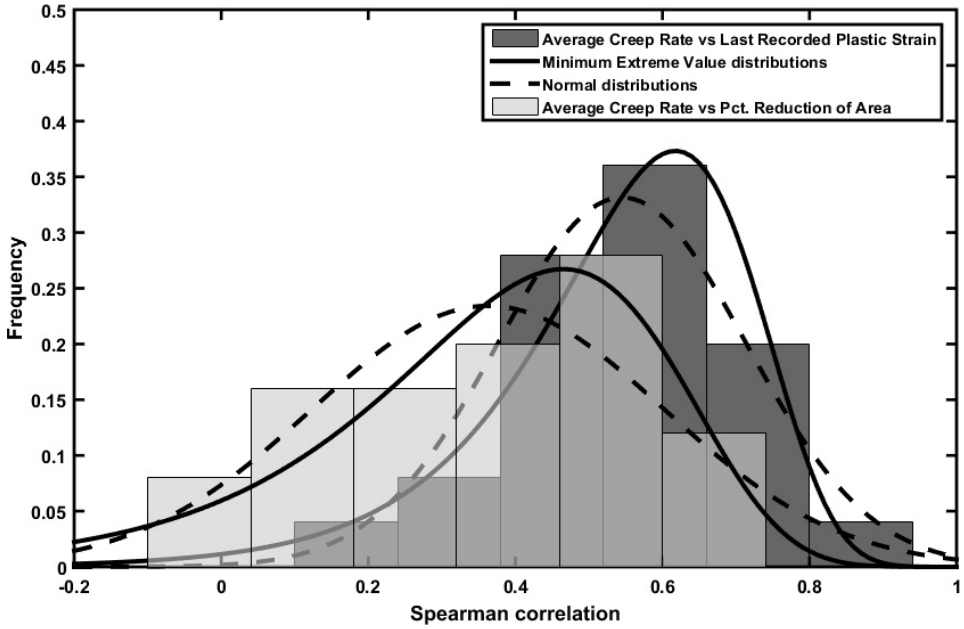

Figure 4.10: Distribution fits to average creep rate versus ductility correlation results presented in Figures 4.8 and 4.9.

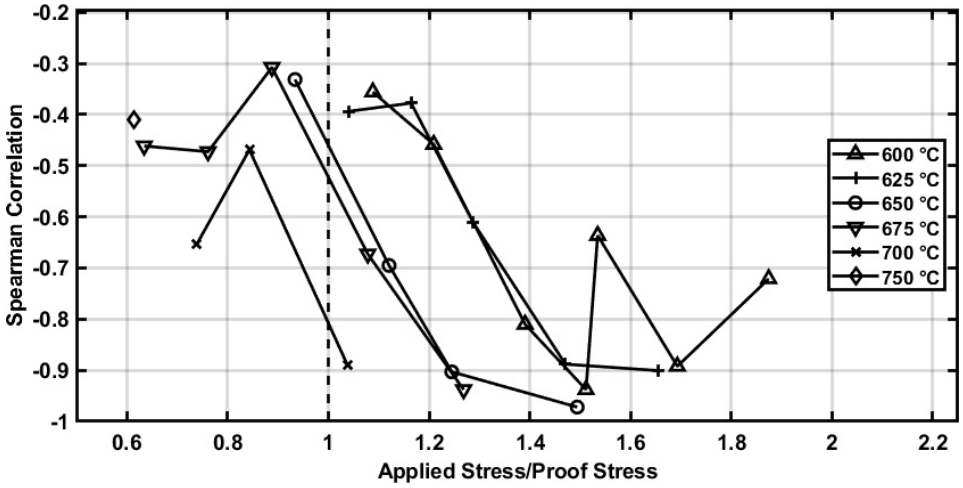

Figure 4.11: Correlations between average creep rate ($\dot{\varepsilon}_A$) and and rupture time (t_R) based on temperature and stress partitioned subsets. Each subset has a minimum of 10 data points, and the proof stress is temperature specific and was obtained from [91].

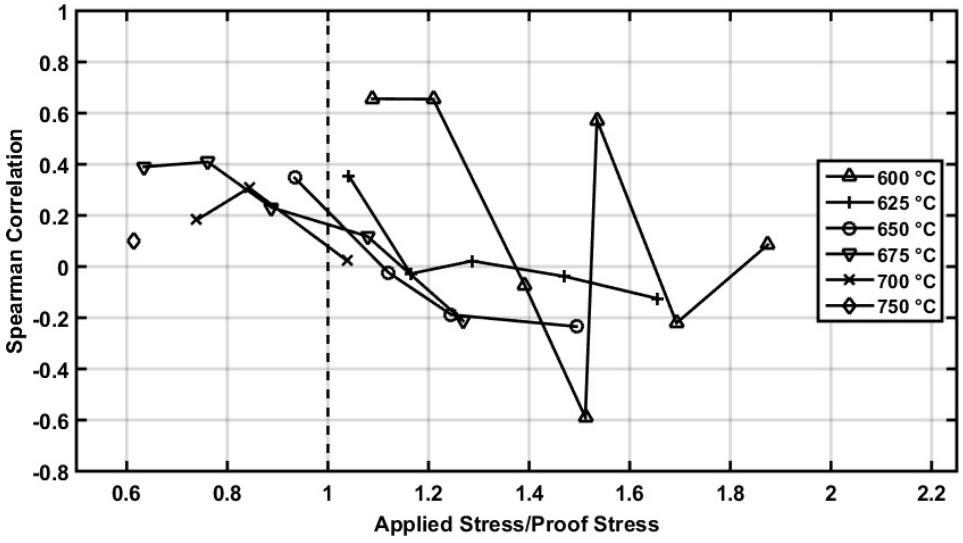

Figure 4.12: Correlations between creep rupture time (t_R) and uniaxial creep ductility (ε_{LS}) based on temperature and stress partitioned subsets. Each subset has a minimum of 10 data points, and the proof stress is temperature specific and was obtained from [91].

4.3.4 Application to Uniaxial Creep-Fatigue Case-Study

Figure 4.13 shows probabilistic results for a creep-fatigue initiation assessment of a uniaxial specimen. This probabilistic creep-fatigue assessment used the RCC-MR creep deformation model and stress independent ductility exhaustion for the calculation of creep damage. The details of this probabilistic assessment can be found in Section 3.7. Incorporating a positive correlation between uniaxial ductility and the primary creep rate had a significant effect by reducing the overall uncertainty in the results. On the other hand, the postulated 0.8 correlation between ductility and secondary creep rate had virtually no effect. This can be explained in light of previous work in which this probabilistic assessment was subject to four types of sensitivity analysis techniques (see Figure 3.6). All four analyses indicated that the secondary creep rate had a marginal effect on the probabilistic results, whilst the primary creep rate and ductility dominated. As a result, the effects shown in Figure 4.13 indicate that correlations have a significant effect on the assessment results only if both parameters have a strong degree of influence.

The five measures outlined in Section 4.2.4 were calculated for the results shown in Figure 4.13 to examine the effects of a postulated 80% positive correlation between primary creep rate and ductility. The results are summarised in Table 4.2. These results indicate that no significant shift of the PDF was observed as the Mann-Whitney test showed that the median was not significantly affected, whilst the quotient test yielded a result very close to 50%. Effects on predicted damages notwithstanding, the F-test and Brown-Forsythe's test indicated that this correlation had a significant effect on the variance, which in effect is a measure of uncertainty or dispersion in the results. More importantly, the correlation had a significant effect on the predicted PoF, which is often the most crucial outcome of a probabilistic assessment. Therefore, the key benefit of incorporating a positive correlation is reducing the area between the right hand tail of the distribution and the line demarking the failure criterion (in this case a damage equal to unity), thus reducing the predicted PoF. This effect is further highlighted in Figure 4.14 which shows that for the probabilistic assessment being considered, there is a linear relation between the predicted PoF and the postulated correlation coefficient.

Table 4.2: Summary of statistical measures for comparing the correlated and uncorrelated results in Figure 4.13.

Test statistic	**Result**
Mann-Whitney test	Null hypothesis upheld (medians are equivalent)
Quotient test	48.5%
F-test	Variances of logarithms are not equivalent
Brown Forsythe's test	Variances are not equivalent
Probability of failure	Uncorrelated: 9.6% & Correlated: 1.4%

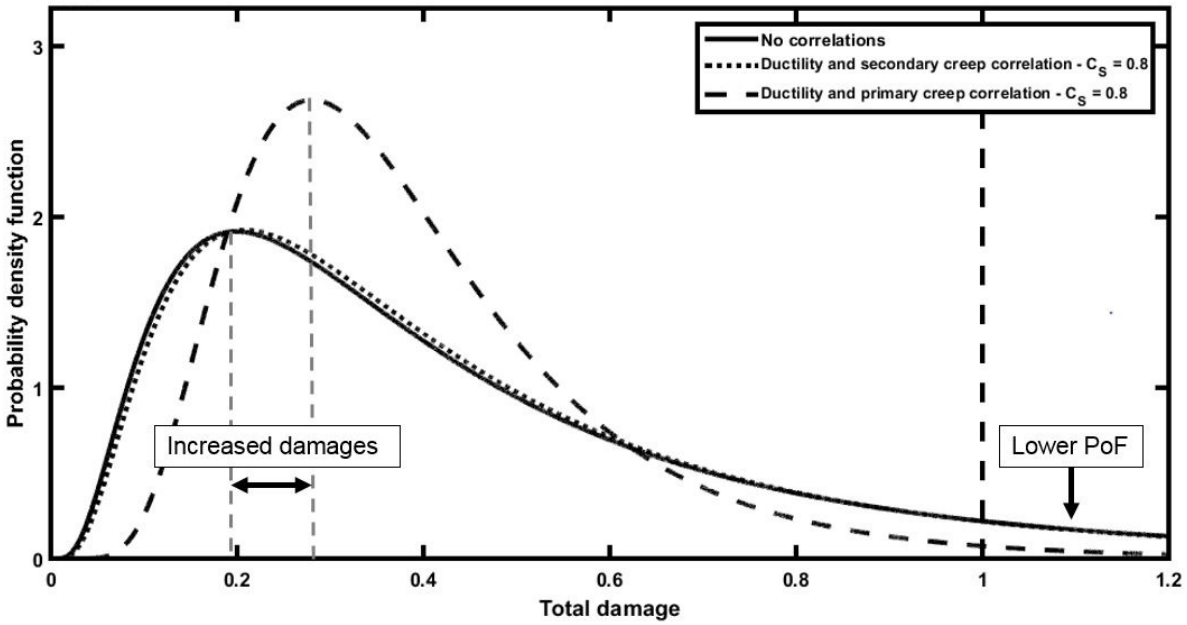

Figure 4.13: Probabilistic results for uniaxial test specimen under creep-fatigue conditions showing the effects of correlations between creep parameters.

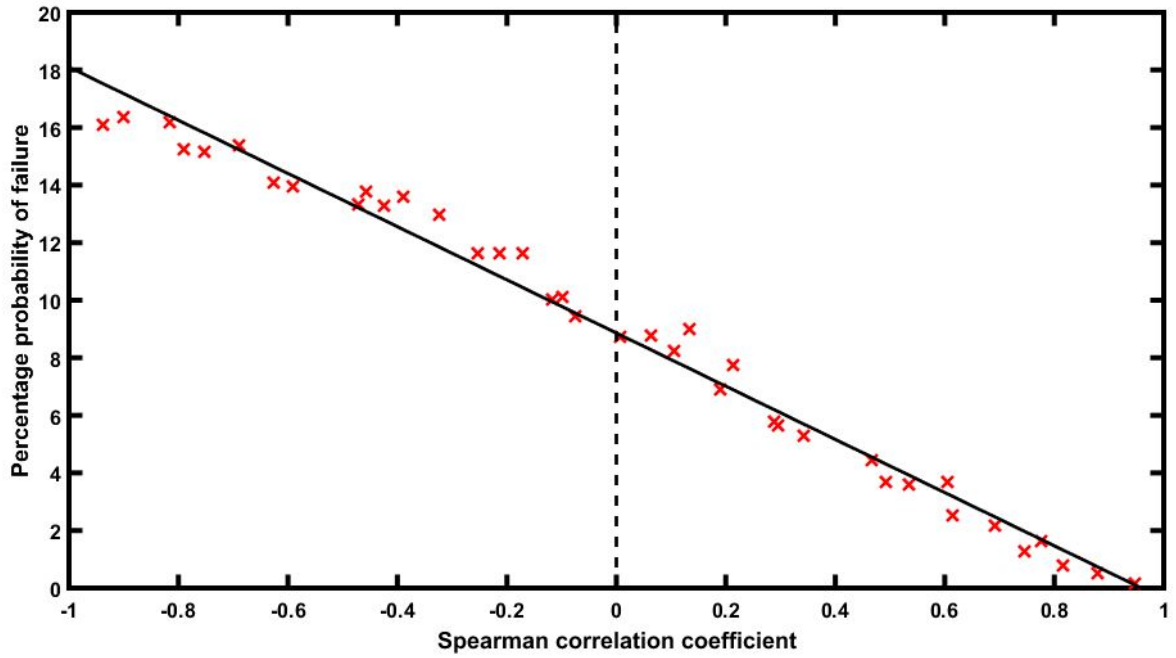

Figure 4.14: Probability of failure (Eq 4.6) calculated based on the results from probabilistic assessments incorporating the full range of correlation coefficients between K and ε_f.

4.4 Summary

This chapter examined issues of characterising and incorporating correlations between input parameters for implementation in probabilistic assessments. In line with the high temperature structural integrity focus of this project, a case-study considering the correlation between creep ductility and deformation was presented. The subject correlation was then included in the probabilistic assessment of the uniaxial creep-fatigue test (which was presented in Chapter 3) to demonstrate the effect that its inclusion can have on the assessment results. The most important conclusions from this chapter are summarised as follows:

1. Parameters involved in creep damage assessments can be correlated, with these correlations being additional uncertainties. These correlations can have major effects on probability estimates (e.g. the probability of failure).

2. However, due to limited data sets and large variability, there remain substantial uncertainties associated with important correlations. Nevertheless, uncertain knowledge of any possible correlations does not preclude conducting a probabilistic assessment. Rather a probabilistic assessment using uncorrelated parameters in conjunction with post-assessment sensitivity analyses can provide valuable insights into which inter-parameter correlations could potentially have marked effects.

3. Sensitivity analysis is therefore advised as a precursor to any investigation into possible correlations, thus providing focus for prioritising potentially influential and important correlations.

4. Even in the complete absence of any relevant data, trialling the full range of possible correlations between dominant parameters and examining their effects on a probabilistic output (say the PoF) can aid judgement as to how to address these issues.

5. With regards to the case-study, significant positive correlations were found between the scatter in creep ductility and creep deformation parameters. These represent cast-to-cast correlations, which typically dominate the variabilities in creep properties.

6. For a creep crack initiation probabilistic assessment, the inclusion of a positive correlation between creep deformation and ductility will lead to reduced probabilities of failure being predicted, as compared with ignoring such correlation.

For structural integrity applications at large, it is suggested that the methodology followed in this chapter can be adopted to identify and incorporate important correlations between dominant input parameters by following the general procedure proposed in Figure 4.3.

CHAPTER 5

LOADING UNCERTAINTIES

This chapter discusses methodologies for the examination of uncertainties in loading conditions for incorporation in prospective probabilistic assessments. These approaches are based on the use of plant data for transient (TR) as well as steady-operating (SO) conditions, with both potentially having large contributions towards the assessment results. Conventionally, the stress-states in a boiler plant component are found using thermal and mechanical (elastic) finite element (FE) models. The inputs to these models are typically boiler steam temperatures and pressures, and the outputs are the six stress components (SCs) and the metal temperatures at the assessment location(s) of interest. The proposed methodologies were developed based on experience gained from examining a tubeplate (TP) plant component, for which historical data was available. The ultimate aim of these approaches is to replace time intensive FE runs with probabilistic alternatives which incorporate the variabilities in the loading conditions of interest. The value of these approaches lies in the avoidance of running FE models for every probabilistic (i.e. MCS) trial (of which there typically may be more than 10^5), which would be computationally prohibitive.

5.1 Introduction

An important part of assessing the lifetime of a plant component operating at high temperatures is predicting the amount of creep and fatigue damages that will have been accumulated by the end of service. These assessment procedures are predominantly conservative, and therefore they commonly use bounding values (deterministic) for material properties and loading conditions (temperatures and stresses). However, various uncertainties exist when assessing a plant component and incorporating a wide array of probabilistic techniques provides a systematic

approach for addressing these uncertainties. As a result, and as part of a wider probabilistic framework, the ultimate interest is in the full utilisation of the available data for the purposes of quantifying the uncertainties which are simplified in deterministic approaches. The treatment of assessment stresses and temperatures is a key part of this probabilistic methodology. In this chapter methodologies for probabilistically treating transient (TR) and steady-operation (SO) loading conditions experienced by plant components are presented. Their chief aim is to replace bounding stresses and temperatures with stochastic equivalents which are informed by plant measurements.

The presented methodologies in this chapter are contextualised by frequently referring to a plant component which has been chosen (see Section 3.9) to prove the utilities of the proposed methodologies. This component is a tubeplate (TP) for which some TR and SO plant temperature measurements were available. Section 5.2 provides a brief description of the TP component, whilst Sections 5.3 and 5.4 are devoted to presenting the proposed approaches for dealing with TR and SO conditions respectively. Section 5.5 discusses some important considerations when incorporating the results from the proposed methodologies in a probabilistic assessment. It is worth nothing that this work is only concerned with the probabilistic treatment of elastic stresses, as these can be later translated to their elastic-plastic equivalents through a Neuber approximation [23]. Basing assessment stresses on simple elastic FE models comes with some limitations which should be considered, and is the topic explored in Section 5.5.1. This chapter concludes with Section 5.6 which summarises the key outcomes of this work.

5.2 Component Description

The tubeplate (TP) is a cylindrical component which has 37 tubeholes and is made of type 316H stainless steel forging. The failure mechanisms are driven by creep-fatigue, large thermal transients and over-heating due to tube restrictions. Due to legacy work that has been done on this component, two separate FE geometries have been used: a sixth model (Figure 5.1a) for transient instances and a full model (Figure 5.1b) for steady-operation events. Material properties used in all FE analyses were obtained from [46] and are reproduced in Table 5.1

Figure 5.2 shows the location of the start-of-dwell stress (σ_B, point B in Figure 5.2) at an intermediate position in the hysteresis cycle, which is typical for a point near the surface of a tube bore. During a start-up (SU) transient, the surface of a tubehole is heated up while the surrounding metal remains colder, thus the difference in thermal expansion produces a compressive stress (point A) near the surface of the tubehole. The reverse effect occurs during a reactor-trip (RT) transient where a tensile stress (point C) is induced on the surface. Point B in Figure 5.2 can include periods of boiler instability (IN) which are caused by large gradients

Table 5.1: Material properties for AISI Type 316 stainless steel used for the FE analysis [46]. T is the temperature in $^{\circ}C$, k is the thermal conductivity in W/mK, C_p is the specific heat in kJ/kgK, α is the thermal expansion coefficient in $1/^{\circ}C \times 10^{-6}$, E is Young's modulus in GPa, ν is Poisson's ratio and ρ is the density in kg/m^3.

T	k	C_p	α	E	ν	ρ
20	13.9	0.47	15.5	198.3	0.29	7966
100	15.1	0.49	15.8	192.3		
200	16.5	0.51	16.2	184.8		
300	18	0.53	16.7	177.3		
400	19.4	0.55	17.1	169.8		
500	20.8	0.57	17.6	162.3		
600	22.3	0.59	18.0	154.7		
700	23.7	0.61	18.4	147.2		

between the boiler tube temperatures (see Table 5.3) and can induce large thermal stresses in the tubeplate. For both TR and SO conditions, it is worth noting that the analyses in this work focused on the surface (bore) nodes of all tubeholes. For that reason, it is believed that the principal stress states will be close to biaxial (or uniaxial for edge nodes/elements). However, this biaxial effect might not be directly observed in the stress results shown in this chapter because the *global* coordinate system was kept fixed and as such it cannot be expected to be aligned with the *local* principal directions of individual surface or edge elements.

5.3 Transient Loading Conditions

5.3.1 Background

Plant components operating at high temperature cyclic conditions are susceptible to creep-fatigue damage, and for predicting such damage, approximations of the loading conditions are required. Loading conditions can be broadly considered to be either transient (TR) or steady-operation (SO). Both conditions can have large contributions towards the total creep-fatigue damage. Transients form a key part of constructing idealised hysteresis cycles; specifically the extremities of these cycles which directly affect fatigue damage via the total cycle stress and strain ranges, and the creep damage through the process of calculating the start-of-dwell stress (σ_B). To evaluate the stress range between the cycle extremities, all six stress components (SCs) at the hot and cold ends are required. The SCs are needed because the R5 Volume 2/3 procedures requires that Von Mises stress ranges are calculated from the ranges of individual SCs. Typically, the stress states for these extremities are obtained from transient thermal and mechanical (elastic) FE models. Key inputs for these analyses are the steam temperatures and pressures, steam flow rates and heat transfer coefficients. The outputs are the six SCs and metal temperatures at a predefined

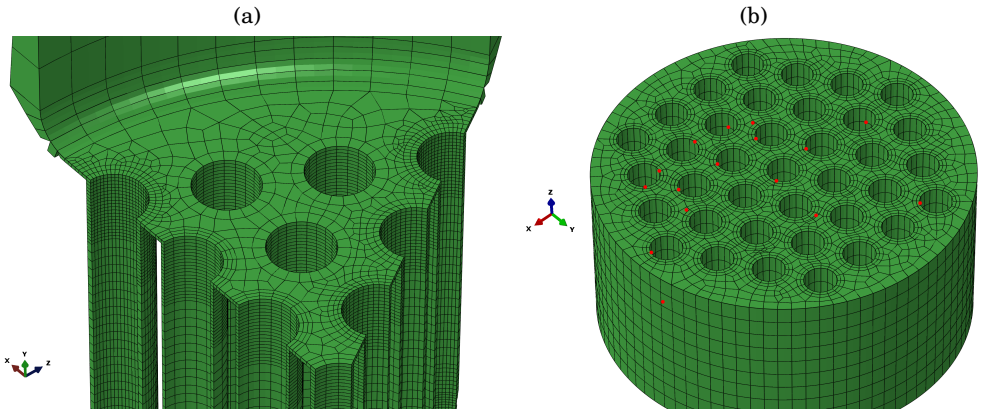

Figure 5.1: Finite element geometries used for thermal and mechanical modelling: (a) the one-sixth model used for transient modelling, and (b) the full model used for modelling steady-operation instances. Some of 37 assessment nodes (one per tubehole) which are stress hot-spots are denoted by the red dots in the right figure, most of which are concentrated towards the top surface of their respective tubeholes with some laying on the top edges.

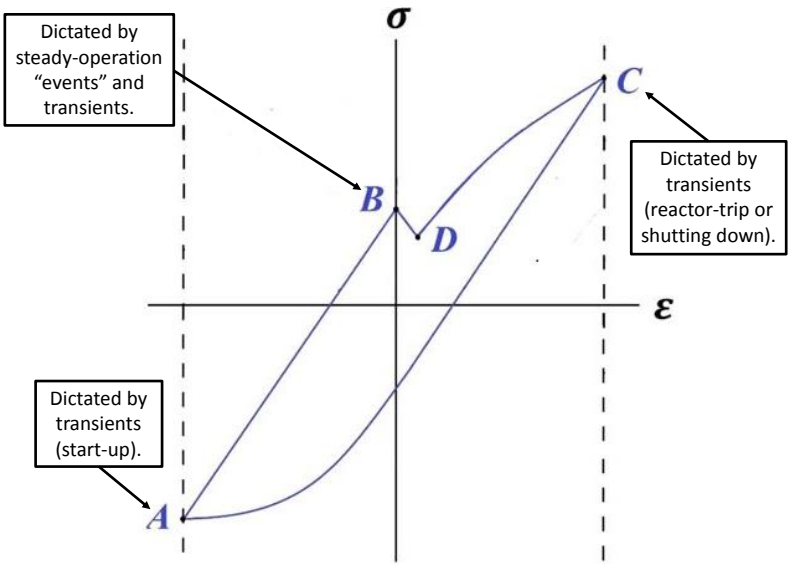

Figure 5.2: Schematic of a typical stress-strain (σ-ε) hysteresis cycle for a point located on the surface of a tubehole going through a reactor-trip to start-up (RT-SU) cycle. Points A and C are associated with SU and RT transients respectively [93].

assessment location. If a conventional deterministic assessment is being conducted, the most severe conditions for either extremities would be used. However, with the existence of variabilities in transient conditions across the lifetime of a component, assuming fixed conditions for all TR instances (typically based on a rather severe instance) can introduce substantial conservatism in the assessment results.

This section presents an approach for the preparation of transient stresses and metal temperatures for use in probabilistic creep-fatigue damage assessments. The proposed approach was based on experience gained from assessing the TP component for which historic plant data related to transient instances were available. The aim was to characterise the variabilities in TR conditions by examining numerous instances of the same type. Two types of transient conditions were considered in this work: start-up (SU) and reactor-trip (RT) instances, which are characterised by rapid increases and decreases of loading temperatures respectively. A procedure was followed to treat these TR instances which starts with the treatment of raw plant data related to a component of interest (the TP in this case). For the two types of TR conditions, 20 SU and 18 RT instances were examined (i.e. $N_{SU} = 20$ and $N_{RT} = 18$), with each having one characteristic stress state (e.g. σ_{SU} and σ_{RT} are the dominant stress components) and one metal temperature (e.g. T_{SU} and T_{RT}), which are the loading conditions used in the assessment. All six elastic stress components were examined to assess their variabilities. The characteristic metal temperature, which is important because material properties are heavily temperature dependent, was also examined.

5.3.2 Methodology

5.3.2.1 Treatment of transient plant data

Plant data were available for some start-up and reactor-trip instances: $N_{SU} = 20$ and $N_{RT} = 18$ instances. For each transient instance, the data consisted of the following parameters:

1. The boiler mass flow rate (in kg/s).
2. The boiler outlet temperature (in $^{\circ}C$).
3. The boiler outlet pressure (in MPa).

However, a few assumptions had to be made in order to use this data for modelling transients, which are listed below.

1. The parameters were measured at the boiler outlet which is downstream from the TP, but were the only available measurements which could be used to model the transient conditions. Therefore, it was assumed that these measurements are representative of the transient conditions at the tubeholes.

2. Measurements per tubehole were not available and, and as a result, all tubeholes were assumed to experience the same transient conditions defined by data for the parameters listed above. Therefore, any differences in stresses that will be observed between tubeholes can mainly be attributed to geometric constraints.

3. All available transient data relate to the upper part if the TP, as no data related to the lower surface of the TP were available. Therefore, it was assumed that the two sides experience the same transient conditions. This effectively reduces the problem to a 2D geometry, where the loading conditions mainly vary radially through the TP.

4. The two inputs to the thermal FE model which were treated as transient (i.e. changing with time) were:

    a) The temperature of each tubehole (in $^{\circ}C$), which were all taken to be equal the boiler outlet temperature. In effect, the boiler temperature was effectively taken to be an average temperature.

    b) The heat transfer coefficients (HTCs, in $W/m^2.K$) between the steam and the tubehole surfaces.

The approach for calculating the latter transient quantities is detailed in Appendix A. After the HTCs were calculated, the transient data was sampled to include key periods of rapid temperature changes. Thereafter the data was ready to be incorporated into the thermal FE model.

5.3.2.2 Transient FE Modelling

Transient stresses are inferred using thermal and mechanical (elastic) FE models. Concerning a creep-fatigue damage assessment, a single transient instance must be characterised by a single stress state (i.e. six SCs) and a characteristic metal temperature. For a single transient instance, and with the plant data as the starting point, the process for inferring the desired transient conditions is outlined in Figure 5.3. Examples of the FE results obtained from a single RT instance are shown in Figure 5.4. Over the time period during which a transient instance persists, the point in time at which transient stresses and temperatures are of concern (i.e. the characteristic conditions) is the one associated with the largest thermal stresses. The largest thermal stresses (see Figure 5.4b) usually occur at or within close succession of the point in time with the largest thermal gradient on the surface of a tubehole (see Figure 5.4a). In order to capture the transient behaviour of temperatures and stresses, a sufficient level of temporal step refinement is required, which was achieved in the example FE results shown in Figure 5.4. For a single point in time, this thermal gradient is defined as the difference between the maximum and minimum metal temperatures on the surface of each tubehole. As a result, in terms of chronology, the FE frame (i.e. time point) of interest is the one with the largest thermal stresses. This frame

consists of stress and temperature profiles for the entire TP. Therefore, if a single stress state is required, then a degree of rationalisation is needed to justify which point(s) over the entire FE domain from which stresses and temperatures should be extracted. As a starting point, only the nodes lying on the surfaces of the tubeholes were considered, and what follows is a rationalisation to provide a justifiable choice of the desired nodes.

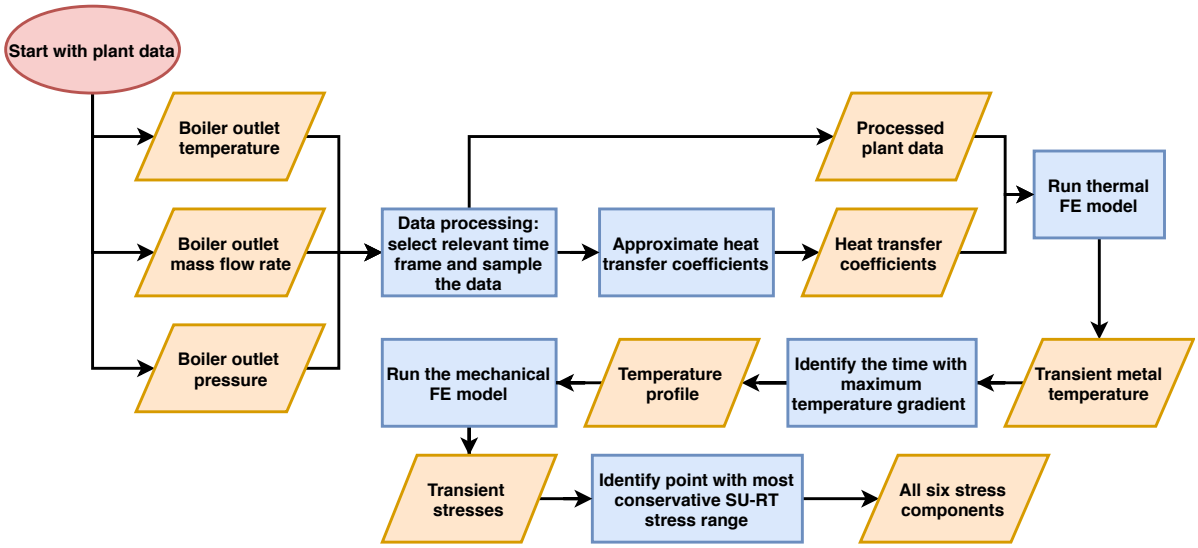

Figure 5.3: Flowchart showing the various stages involved in identifying the characteristic (peak) stress state during a single transient instance.

The overall elastic stress range for the creep-fatigue cycle ($\Delta\sigma_{el}^{CA}$ in Figure 5.2) is calculated based on the stress ranges of individual stress components:

$$\Delta\sigma_{el}^{CA} = \sigma_{el}^{RT} - \sigma_{el}^{SU} \tag{5.1}$$

where σ_{el}^{RT} and σ_{el}^{SU} represent the stress states at reactor-trip and start-up transients for a single plant loading cycle respectively. Although the notation suggests as much, this must not be interpreted as the algebraic difference between the peak Von Mises stresses for SU and RT. It must rather be understood as the Von Mises stress range formed from the component ranges between SU and RT:

$$(\Delta\sigma_{el}^{CA})^2 = \frac{1}{2}\Big[(\Delta\sigma_{11}-\Delta\sigma_{22})^2 + (\Delta\sigma_{22}-\Delta\sigma_{33})^2 + (\Delta\sigma_{33}-\Delta\sigma_{11})^2 + 6(\Delta\sigma_{12}^2 + \Delta\sigma_{13}^2 + \Delta\sigma_{23}^2)\Big] \tag{5.2}$$

where $\Delta\sigma_{ij}$ represents the stress range between the direct and shear stress components for $i = j$ and $i \neq j$ respectively. In the R5 Vol 2/3 assessment procedure, $\Delta\sigma_{el}^{CA}$ has a direct effect on the total damage. However, due to the procedure for constructing the hysteresis cycle, this stress range affects creep and fatigue damages in different ways. To examine the effect of the magnitude

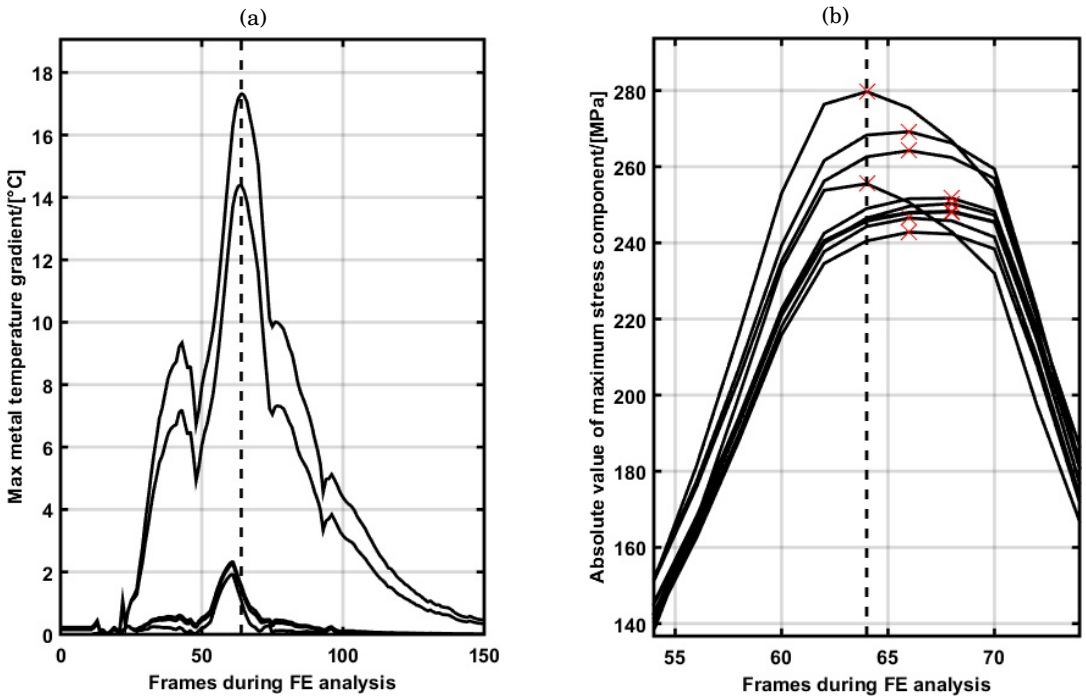

Figure 5.4: Examples of FE results for 10 tubeholes and for a single reactor-trip (RT) transient instance. The dashed lines in both plots highlight the frame with the highest temperature gradient across all 10 tubeholes. The maximum transient stresses for all 10 tubeholes (denoted by crosses) and the maximum transient temperature gradients typically occur within brief succession of each other. For RTs the stresses are positively signed.

of $\Delta\sigma_{el}^{CA}$ induced by the SU and RT transients, a deterministic assessment of the TP was used. For this purpose, a typical (fixed) stress state in steady-operation was assumed to evaluate point B shown in Figure 5.2. Figure 5.5 shows the effect of varying the magnitude of one transient type (say the SU) whilst keeping the other transient fixed. The key two conclusions that can be drawn are:

1. The most severe SU transient (i.e. producing the largest creep-fatigue damage) is associated with the stress state that would produce the largest $\Delta\sigma_{el}^{CA}$, and is characterised by the largest (negatively signed) stress component.

2. The most severe RT transient is associated with the stress state that would produce the smallest $\Delta\sigma_{el}^{CA}$, and is characterised by the smallest (positively signed) stress components.

However, it must be noted that the above conclusions are strictly applicable when creep damage dominates over fatigue damage, which is the case for the TP. Furthermore, these are direct manifestations of the *symmetrisation* rule in the R5 Volume 2/3 procedure (see Eq 6.14) and are valid reflections of material cyclic behaviour.

Solely following the above rationalisation poses an issue: $\Delta\sigma_{el}^{CA}$ is used to establish the point of most severe stress state for a given transient type (say RT), assuming the other (SU) is kept fixed. However, the latter can be variable and this can change the choice of location having the most severe RT transients. Therefore, in a probabilistic sense, the uncertainty in RT transients has two constituents:

1. One associated with the variability between RT transient instances themselves and;
2. A further uncertainty introduced by the modelling approach which effectively propagates the variability due to SU instances to the RT instances.

To address this issue, it was proposed that when examining RT instances, all possible SU stress states (20 in this case) would be trialled for each nodal location. As a result, for each RT instance, multiple *severe* (i.e. conservative) stress states are possible. Consequently, the stress state (single for SU and possibly multiple for RT) which characterises a single transient instance are extracted from the thermal and mechanical FE results at the frame with the highest thermal stresses, and at the surface location corresponding to the largest or smallest $\Delta\sigma_{el}^{CA}$ for SU and RT instances respectively. The metal temperature should be extracted from the thermal FE results at the same nodal location from which stresses are taken, but when this is not trivial a conservative assumption can be made, which will be discussed later in this section.

The processes outlined in Sections 5.3.2.2 and 5.3.2.1 effectively characterise a single transient instance (within a single plant loading cycle) by a single stress state (6 SCs) and one metal temperature. For the purposes of this work, the resulting data-sets for SU and RT will be termed the *processed transient FE data*.

5.3.2.3 Treatment of the processed transient FE data

For the available number of SU and RT instances, 38 instances in total, the processes detailed in Sections 5.3.2.2 and 5.3.2.1 were followed for all available transients, and for each instance the resulting processed data was kept as tubehole specific. Therefore, for a single instance the outputs were the six SCs and one metal temperature for all 10 tubeholes. As a result, the processed transient FE data constitutes $7 \times 10 \times 20$ SU transient data items and and a minimum of $7 \times 10 \times 18$ RT equivalents, though the latter data-set can be larger as previously explained.

The final stage is to establish whether stresses and metal temperatures vary significantly between tubeholes. This will inform the decision of whether each tubehole should be treated separately, or whether all tubeholes can be considered to experience the same transient conditions for a single instance. Inevitably, this will influence how these transients are incorporated into a probabilistic assessment. The proposed approach was to use the χ^2 test to compare between tubehole specific data-sets. If the data-sets for different tubeholes were found to be similar then

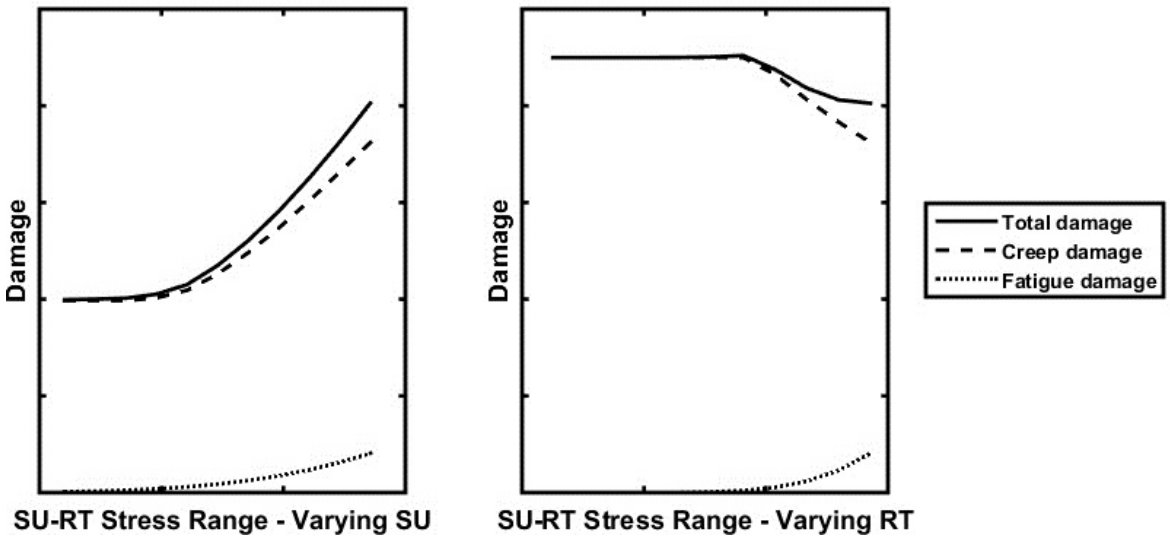

Figure 5.5: The effect of varying transient stress magnitudes on total, creep and fatigue damages obtained using a R5 Volume 2/3 deterministic assessment of the tubeplate. The x-axis on the left plot is increasing magnitude of *compressive* SU stress, whilst the one on the right plot is increasing magnitude of *tensile* RT stress.

that would suggest that each stress component could be sampled from a combined data-set which comprises *all tubeholes*. That would be an alternative to sampling from tubehole specific data-sets. To quantitatively test the validity of such assumptions the χ^2 test was used with the null hypothesis formulated as:

> *For each stress component, the data for a single tubehole (20 data points) is significantly different from the combined data for all tubeholes (200 data points) within a significance level of* α.

The χ^2 test is typically used to compare discrete data, and therefore, the processed FE data was converted into histograms first. For each transient type, six histograms per tubehole (one per stress component) were constructed to examine the variability across all modelled instances. Therefore, for each tubehole a histogram was based on 20 and 18 data points for SU and RT respectively. Examples of these histograms are shown in Figure 5.6 for direct components and Figure 5.7 for shear components. A further set of six histograms per transient type was produced, which looked at the variability of each stress component across the instances for *all tubeholes*. Therefore, each of these histograms was based on 200 data points and 180 data points for SU and RT respectively. Thereafter, and for each stress component, the χ^2 test statistic can be calculated to compare histograms for individual tubeholes with the histogram for all tubeholes:

$$\chi^2 = \sum_{n=1}^{N_b} \frac{(O-E)^2}{E} = D_T \sum_{n=1}^{N_b} \frac{(O_f - E_f)^2}{E_f} \tag{5.3}$$

where N_b is the number of bins used to construct the histograms, O and E are the observed and expected number of data points, O_f and E_f are the observed and expected frequencies (e.g. $O = O_f D_T$) and D_T is the total number of data points used to construct the histograms. The null hypothesis is rejected with an α level of confidence, if the calculated χ^2 test statistic is less than the critical value, or upheld otherwise. A 95% confidence interval was used in this case. The χ^2 critical value is obtained from tables (e.g. see [62]) depending on α and the degrees of freedom $\upsilon = N_b - 1$.

5.3.2.4 Correlations

Correlations Between Stress Components Because the SCs are required for calculating the cycle stress range (see Eq 5.2), in a probabilistic assessment it is important to account for correlations between SCs when sampling. The Spearman (rank order) correlation coefficient was judged to be appropriate for this application because it does not impose any restrictions on the type of distributions followed by the correlated parameters. This makes it viable for the application considered here which looks at discrete data. Correlation matrices linking the 6 stress components (each sized 6×6) can be computed. Depending on the outcome of the analysis proposed in Section 5.3.2.3 a case can be made for using tubehole specific matrices, or calculating a single correlation matrix based on the combined stress data for all tubeholes.

Correlations Between Tubeholes For a single stress component, a further investigation would examine stress correlations across tubeholes. This effectively attempts to introduce geometric effects on the TP level i.e. the link between a stress component for one tubehole and the same component for all remaining tubeholes. These correlations are quantified by six Spearman correlation matrices each sized according to the number of tubeholes being examined, for example 10×10 in the case of a one-sixth FE model of the TP. Furthermore, it must be noted that strong correlations between tubeholes are expected and likely attributed to the second assumption listed in Section 5.3.2.1. Therefore, this correlation may well be an artefact of the modelling approach rather than a correlation attributed to geometric effects. Nevertheless, no tubehole specific plant data was available for the TP and, as a result, investigating the interactions between tubeholes was not possible.

Correlations between temperature and stresses With temperatures and stresses being the two key loading conditions, it is deemed important to consider any possible correlations between the two. If this correlation is not taken into account, non-conservative effects maybe introduced, for example the high-stress and low-temperature combinations for SU could potentially produce larger damages. To incorporate these correlations, it is convenient to add the metal temperature correlations to the correlation matrix linking the stress components. Thus

correlation matrices linking the 6 stress components and the metal temperature (sized 7×7) can be computed at the same time and later incorporated simultaneously at the sampling stage.

Incorporation of correlations Incorporating the correlations discussed in Section 5.3.2.4 simultaneously is not trivial. For probabilistically modelling a single transient instance in a Monte-Carlo Simulation, a simple approach for producing correlated data samples of the inputs (6 SCs and 1 metal temperature) is proposed as follows:

1. For each tubehole produce N samples for each input based on the associated histogram. At this point these sampled inputs are completely independent and non-correlated. For a single transient instance, these data samples can be visualised by the following data array which includes all the samples for all tubeholes:

$$D = \begin{bmatrix} D_{1,11} & D_{1,22} & D_{1,33} & D_{1,12} & D_{1,13} & D_{1,23} \\ D_{2,11} & D_{2,22} & D_{2,33} & D_{1,12} & D_{1,13} & D_{1,23} \\ \vdots & \vdots & \vdots & \vdots & \vdots & \vdots \\ D_{TN,11} & D_{TN,22} & D_{TN,33} & D_{TN,12} & D_{TN,13} & D_{TN,23} \end{bmatrix} \tag{5.4}$$

   where $D_{TN,11}$, for example, refers to a set of N samples corresponding to the TN^{th} tubehole and the σ_{11} stress.

2. Correlate the data samples on the vertical axis of the D array associated with the most dominant stress component. For a transient type the most dominant stress component is usually the largest, but this can be systematically proved using a simple sensitivity analysis to check which stress component dominates the stress range calculation. For example, if we consider σ_{22} to be the most dominant for SU transients, then the data samples of interest are $D_{1,22}, D_{2,22}, ..., D_{T,22}$. This is achieved by using the correlation matrix between tubeholes, which were discussed in Section 5.3.2.4. For this category of correlations only the most dominant stress is considered as this component is known to be the most important contribution to the cycle stress range (Eq 5.2). For this application this is believed to be acceptable, especially when the dominant stress component is substantially larger than the other components. Therefore, directly correlating the other five stress components across tubeholes is judged to be of minimal importance.

3. Correlate the data samples on the horizontal axis in the above matrix ($D_{1,11}, D_{1,22}, ..., D_{1,23}$), whilst retaining the order of the data sample associated with the dominant stress (to follow the example above, this would be $D_{1,22}$) data-set to preserve the correlation incorporated in the previous step. The correlation matrix of interest in this case is the one discussed in Section 5.3.2.4, whilst considering that metal temperatures are also included at this stage.

In the full probabilistic assessment of the TP (presented in Chapter 6), it has been judged that each tubehole should be considered as an *independent* assessment location. This approach

essentially limits the importance of incorporating the correlations between tubeholes, as they are unlikely to affect the probability of failures of individual tubeholes. If interactions between tubeholes are to be considered, then these correlations might be important. However, as discussed in Section 5.3.2.4, in the absence of tubehole specific plant data, it is not possible to formally examine these correlations. In which case, the procedure in this section still applies, but the second step above would be omitted.

5.3.3 Results and Discussion

5.3.3.1 Transient stress results

Figures 5.6 and 5.7 show examples of the processed transient FE data for a single tubehole ($TN = 2$ in this case). Across the instances examined, the SU and RT which had the most severe stress states for Tubehole 2 are summarised in Table 5.2. For each stress component, the χ^2 tests revealed that data from individual tubeholes deviated significantly from the combined data for all tubeholes. This was indicated by the critical chi-squared values taken from appropriate tables (which depend on the desired α and ν) being consistently smaller than the χ^2 test statistics calculated using Eq 5.3. Consequently, this indicated that the null hypothesis (see Section 5.3.2.3) must be accepted. In physical terms, this essentially suggests that local geometries contributed significantly to the magnitudes of the stress components of each tubehole. Therefore, when probabilistically modelling the magnitude of each stress component, each tubehole should be treated separately according to the appropriate tubehole specific histogram.

It is worth noting at this point that due to the use of a one-sixth geometry for FE modelling the transient instances for the TP, there was a need to translate the results for the modelled 10 tubeholes to all of 37 tubeholes.

Table 5.2: Most severe transients out of the examined SU and RT instances for Tubehole 2 ($TN = 2$). These results were obtained using the FE model shown in Figure 5.1a which shows the orientation of the stress directions relative to the tubeplate geometry.

	Stress components/[MPa]						**Metal temp./[$^{\circ}C$]**
	σ_{11} (σ_{xx})	σ_{22} (σ_{yy})	σ_{33} (σ_{zz})	σ_{12} (σ_{xy})	σ_{13} (σ_{xz})	σ_{23} (σ_{yz})	
SU	12.58	-271.60	5.68	0.08	-0.11	-1.04	439.6
RT	22.30	-3.99	0.81	-1.60	5.63	2.13	337.9

5.3.3.2 Transient metal temperature results

In addition to stresses, metal temperature data taken at the location of maximum transient stress (e.g. see Figure 5.4b) was also extracted from the FE results. Metal temperatures are important in creep-fatigue assessments as they may influence the material properties used for

characterising the cycle extremities. For the application considered here, it was not possible to extract the metal temperatures from the same nodes as those used for stresses, because different mesh configurations were used in the thermal and mechanical FE models to aid computational efforts. Only the maximum and minimum metal temperatures per tubehole per instance were easily identifiable. Therefore conservative assumptions were adopted which entailed using the maximum and minimum temperatures on the surface of a tubehole as the characteristic metal temperatures for RT and SU transients respectively. These assumptions were tested using a probabilistic creep-fatigue assessment for the TP, and were found to be the most conservative. Figure 5.8 shows histograms of metal temperature data for Tubehole 2 based on the all the available SU and RT instances. The same approach using χ^2 to the one presented for stresses in Section 5.3.2.3 was followed for comparing tubehole specific data with the data collated from all tubeholes. The same conclusion as for stresses was drawn; it is more appropriate to use tubehole specific histograms when sampling metal temperatures.

5.3.3.3 Correlations

Correlations between stress components For each of the two considered transient types (SU and RT), 10 correlations matrices (each sized 6×6; one per tubehole) were computed. In Section 5.3.3.1, it was concluded that stress component magnitudes differed significantly between tubeholes. A similar conclusion was reached when correlations were examined, as no clear similarities between correlation matrices were found across tubeholes. For the SU instances, an example of such matrices, which in some cases had very strong (> 0.9) correlation coefficients, is:

$$\begin{bmatrix} 1.00 & 0.96 & 0.99 & -0.72 & 0.46 & -0.50 \\ 0.96 & 1.00 & 0.97 & -0.65 & 0.31 & -0.46 \\ 0.99 & 0.97 & 1.00 & -0.71 & 0.44 & -0.50 \\ -0.72 & -0.65 & -0.71 & 1.00 & -0.27 & 0.87 \\ 0.46 & 0.31 & 0.44 & -0.27 & 1.00 & 0.06 \\ -0.50 & -0.46 & -0.50 & 0.88 & 0.06 & 1.00 \end{bmatrix} \tag{5.5}$$

where this matrix relates the stress components in the order (from left to right and top to bottom in the matrix above): σ_{11}, σ_{22}, σ_{33}, σ_{12}, σ_{13} and σ_{23}. It worth highlighting that due to the approach taken for extracting stresses from the FE models, namely focusing on surface nodes, the stress states are likely to be biaxial or uniaxial if stresses are taken from an element located on a free surface or an edge. Therefore, the correlations between stress components are likely due the reorientation of stresses relative to the local principal axis. Similarly for stress magnitudes, inter-SCs correlations are to be treated on an individual tubehole basis. The alternative, which is to impose one correlation matrix for all tubeholes is judged to be inappropriate in this case as it will negate local dependencies between stress components.

Correlations between tubeholes Significantly strong correlations were found between tubeholes. For example, for the SU instances and for the maximum stress component (in this case σ_{22}, see Figure 5.6), the correlation matrix was:

$$
\begin{bmatrix}
1.00 & 0.98 & 0.99 & 0.99 & -0.11 & 1.00 & 0.99 & 0.99 & 1.00 & 0.97 \\
0.98 & 1.00 & 0.98 & 0.98 & -0.10 & 0.98 & 0.98 & 0.97 & 0.98 & 0.99 \\
0.99 & 0.98 & 1.00 & 0.99 & -0.11 & 0.99 & 0.99 & 0.99 & 0.99 & 0.97 \\
0.99 & 0.98 & 0.99 & 1.00 & -0.16 & 0.99 & 0.99 & 0.98 & 0.99 & 0.97 \\
-0.11 & -0.10 & -0.11 & -0.16 & 1.00 & -0.11 & -0.11 & -0.09 & -0.11 & -0.11 \\
1.00 & 0.98 & 0.99 & 0.99 & -0.11 & 1.00 & 0.99 & 0.99 & 1.00 & 0.97 \\
0.99 & 0.98 & 0.99 & 0.99 & -0.11 & 0.99 & 1.00 & 0.99 & 0.99 & 0.97 \\
0.99 & 0.97 & 0.99 & 0.98 & -0.09 & 0.99 & 0.99 & 1.00 & 0.99 & 0.96 \\
1.00 & 0.98 & 0.99 & 0.99 & -0.11 & 1.00 & 0.99 & 0.99 & 1.00 & 0.97 \\
0.97 & 0.99 & 0.97 & 0.97 & -0.11 & 0.97 & 0.97 & 0.96 & 0.97 & 1.00
\end{bmatrix}
\tag{5.6}
$$

where this matrix relates the σ_{22} components for the 10 tubeholes shown in the FE representation in Figure 5.1a. It must be acknowledged that these strong correlations between tubeholes are believed to be an artefact of the second assumption listed in Section 5.3.2.1, and therefore a non-physical effect caused by the modelling approach rather than a correlation attributed to geometric effects between tubeholes. In other words, the loading is defined essentially by just one parameter - the steam temperature. Since one parameter controls all stresses, the stresses at different tubeholes are bound to be correlated. Moreover, due to the lack of tubehole specific plant data, it is not possible to formally examine these correlations. If these corrections can be justifiably identified, then the procedure in Section 5.3.2.4 can still be implemented. However, for this current application it is judged that these correlations should be omitted from a prospective probabilistic assessment of the TP at this stage.

Correlations between metal temperature and stresses For SU and RT, Figure 5.9 shows histograms of the Spearman correlation between metal temperatures and the most dominant stress component. For both transient types, often a strong negative correlation was observed. These correlations are deemed to be important as they effectively link the two key transient loading conditions. Strategies for incorporating various correlation types was discussed in Section 5.3.2.4 and Section 5.3.2.4.

To clarify, for SU instances the stresses were kept compressive (i.e. negative) when calculating these corrections. Therefore, the correlations in Figure 5.9(a) indicate that a low temperature correlates with a smaller compressive stress, or the higher the temperature the more compressive the stress. A physical explanation for these correlations is that a point that has a high temperature relative to its surroundings will try to expand but will see a compressive stress due to the constraint from its colder surrounding points, which is the case for a SU transient. For RT the

reverse is correct; the point in question tries to contract but is stretched by its hotter surrounding points, therefore producing a high tensile stress.

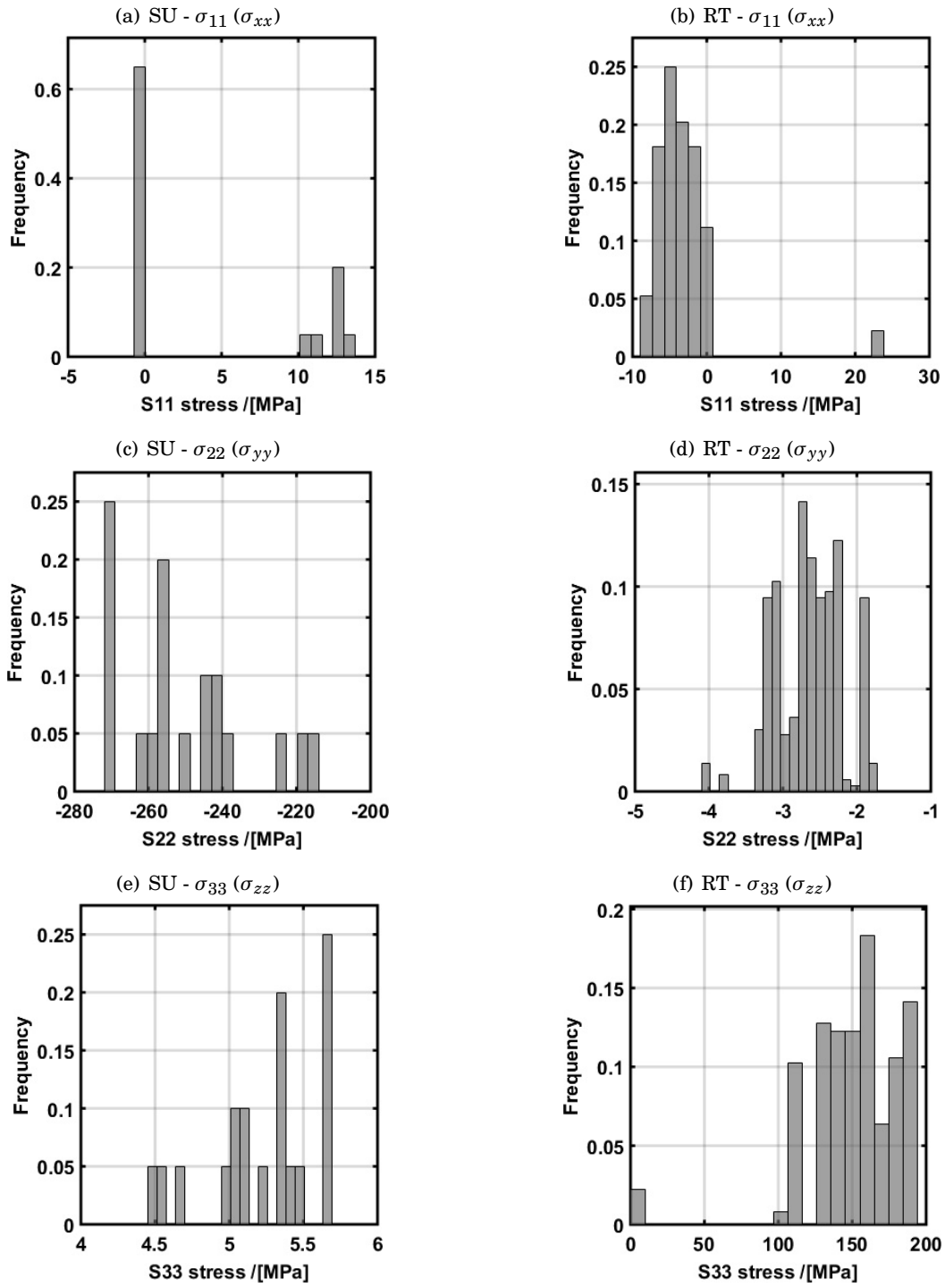

Figure 5.6: For Tubehole 2 ($TN = 2$) and for the examined start-up (SU) and reactor-trip (RT) transient instances (20 and 18 instances respectively), this figure shows histograms of the processed FE data for direct stress components. From these components, the dominant stresses for SU and RT are $\sigma_{SU} = \sigma_{22}$ and $\sigma_{RT} = \sigma_{33}$ respectively. These results were obtained using the FE model shown in Figure 5.1a which shows the orientation of the stress directions relative to the tubeplate geometry.

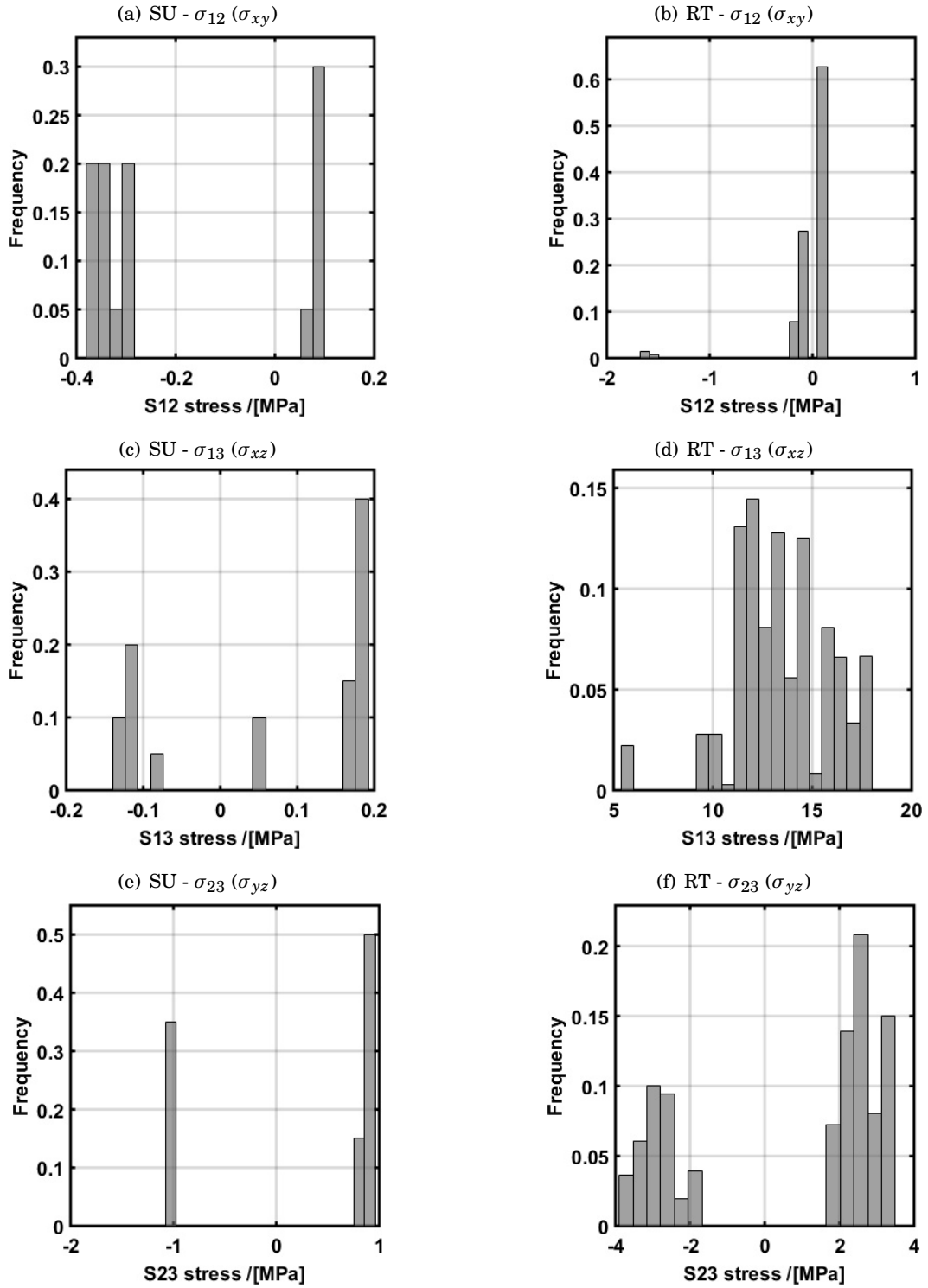

Figure 5.7: For Tubehole 2 ($TN = 2$) and for the examined start-up (SU) and reactor-trip (RT) transient instances (20 and 18 instances respectively), this figure shows histograms of the shear stress components. These results were obtained using the FE model shown in Figure 5.1a which shows the orientation of the stress directions relative to the tubeplate geometry.

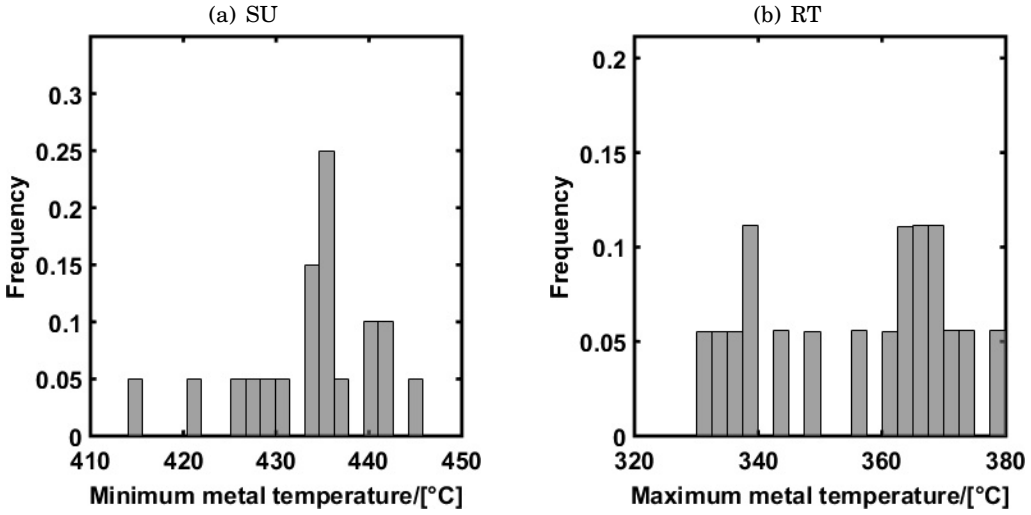

Figure 5.8: Histograms of metal temperatures (the temperatures used for the assessment: T_{SU} and T_{RT}) based on data for Tube 2 across all 20 SU and 18 RT instances. Medians were 435.60°$C$and 362.76°C for SU and RT instances respectively.

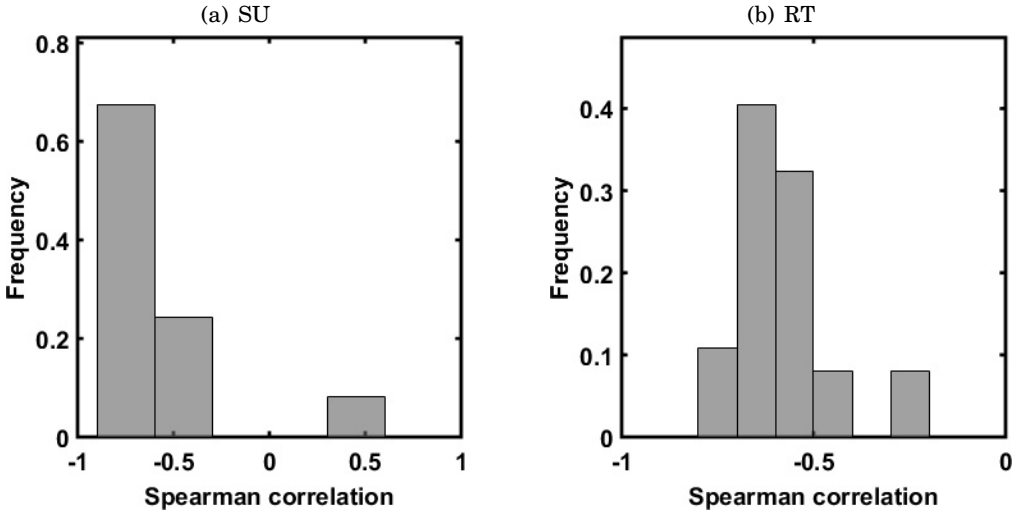

Figure 5.9: Across all 37 tubes, histograms of Spearman correlations coefficients between the assessment metal temperature (see Figure 5.8) and the most dominant stress component which is $\sigma_{SU} = \sigma_{22}$ for SU (see Figure 5.6c) and $\sigma_{RT} = \sigma_{33}$ for RT (see Figure 5.6f).

5.4 Steady-Operation Loading Conditions

5.4.1 Background

When assessing a plant component for creep-fatigue damage, a key requirement is the approximation of the stresses during nominal operating conditions. In this case nominal refers to periods of power production. Due to variabilities in the plant operating temperatures, the stress state that a component might experience is ever-changing. As a result, the common practice of assuming a fixed (bounding) stress state which persists during long periods of the component's life can be overly conservative.

In the R5 Volume 2/3 assessment procedure, a key stage is the approximation of various stress ranges experienced during a loading cycle, which for nominal operating conditions require the knowledge of the complete stress state (i.e. 6 SCs) at the assessment location of interest. The procedure for calculating the creep-fatigue damage which was adopted for the TP is presented later in Section 6.3.2. In general, stress states are modelled using thermal and mechanical (elastic) FE models which can be computationally intensive, and therefore pose a limitation on their use in probabilistic calculations. This issue is explored in [12, 17] and the adoption of the Response Surface Method (RSM, which is effectively a multivariate regression approach [12, 54, 57]) was suggested for reducing computational efforts.

This section presents a methodology for analysing plant data for inferring the uncertainties in stress components. This has been developed based on experience gained from examining the TP plant component for which some historical temperature data was available. The chief purpose of the proposed methodology is to provide a systematic approach for constructing a statistical predictive model for stresses. This model aims to act as a surrogate to replace computationally intensive FE models in probabilistic assessments. The surrogate model attempts to predict the evolution of the stress state as a function of plant operating conditions (e.g. the steam temperatures). The proposed approach begins by processing the raw temperature data obtained from plant measurements. This processed data is then used to train the predictive model which provides the stress state (as an uncertainty output) for a given set of input conditions.

5.4.2 Methodology

5.4.2.1 Treatment of raw historic temperature data

The available steady-operation plant data was in the form of hourly recorded thermocouple (TC) measurements. These TCs were situated above the upper surface of the tubeplate so as to sample the steam exiting from *some* of the tubeholes. This data spanned approximately 30 years of operation. The main challenge was associated with the shear size of this data-set, which

Table 5.3: Limits used for dividing the hourly temperature history for the TP into discrete events: either Normal (NX) or instability (IX) events [93].

Event type	**Normal**			**Instability**				
Mode	N0	N1	N2	I0	I1	I2	I3	I4
Max. temp./[$^{\circ}C$]	400-525	525-540	540-550	400-525	525-540	540-550	550-565	565-575
Tilt/[$^{\circ}C$]	< 60			> 60				

precluded its direct use in any damage assessment. The following is a general approach which was implemented to process this large data-set of hourly data spanning decades of component history. A sensible approach is to discretise the temperature history into *events* which are predefined coordinating to:

1. the maximum steam temperature of any tubehole, and

2. the maximum difference between the highest and lowest steam temperatures across the tubeplate, which is termed the *tilt*.

For this component, the limits used to define the temperature ranges for each type of event was obtained from previous work which proposed eight types of steady-operation events [93]. A distinction was made between *Normal* and *instability* events, with the latter typically producing larger thermal stresses. The limits used to discretise the temperature history are outlined in Table 5.3.

A MATLAB script was produced to process the raw data into an array comprising of event types, their durations and the steam temperatures of the 37 tubeholes. For a single event, it was assumed that mean conditions (steam temperatures and tilt) persist for the duration of the event. In this section this new data-set will be referred to as the *processed history data*. It must be emphasised that this arrangement of the raw history data does not necessarily influence the following stages of the general approach proposed in this chapter. This was mainly adopted for continuity of work on this component from previous efforts; it is a simple and convenient approach for condensing the large original raw data. Thereafter, a set of 1300+ history events were run in two FE models, firstly a thermal and then a mechanical model both in ABAQUS CAE. The FE geometry used for this is shown in Figure 5.1b. Running a complete event in FE required less than 3 minutes, and as such this batch of runs required approximately three days, though these time-scales are dependent on the processing capabilities available (e.g. number of cores, available memory, FE software and operating system).

5.4.2.2 Processing of FE data results

For the steady-operation stress analysis, choosing an assessment point (i.e. point of most probable crack initiation) was required. Strictly speaking, and for creep dominated cases, the most likely point to initiate a crack first is the point (or node) which has a historic stress state which most frequently leads to the highest start-of-dwell stress, σ_B. This requires that the transient stresses on either ends of the cycles, as well as the stress state during steady-operation are considered. Identifying the point of maximum σ_B can be non trivial especially when the variabilities of SU and RT transients are considered. However, the point of highest σ_B invariably corresponds to the highest stress range leading up to the creep dwell:

$$\Delta\sigma_{el}^{AB} = \sigma_{el}^{SO} - \sigma_{el}^{SU} \tag{5.7}$$

where σ_{el}^{SU} and σ_{el}^{SO} represent the elastic stress states for a SU transient and a steady-operation (including instabilities) condition respectively. Therefore, to simplify this analysis, the assessment point(s) for a single tubehole was chosen as the node(s) which had the highest probability of producing the largest $\Delta\sigma_{el}^{AB}$ relative to all possible SU transients. The probabilistic treatment of transient conditions, including SU, for the TP is discussed in Section 5.3, where 20 possible SU transient events were considered. This process for identifying key assessment locations is described as follows:

1. For a single steady-operation (static) FE run which represents an event, $\Delta\sigma_{el}^{AB}$ is calculated for all nodes around the surface of a single tubehole. For this step all possible SU transients are considered in turn, which in this case total to 20 SU events.

2. For each of the 20 possibilities, record the node which had the highest stress range. For a SO event, this was usually found to be the same node across all SU possibilities, though a small number of exceptions existed.

3. Repeat the procedure for all FE runs (1300+ runs in total).

4. For all 1300+ runs and for all 20 SU possibilities, count the number of times each node on the surface of a single tubehole had the highest stress range. Eventually, only a select number of nodes were found to be reoccurring.

5. The process above is repeated for all tubeholes.

The results from this procedure can be visualised using a probability map, which lists all the reoccurring nodes on the surface of all tubeholes and highlights their probability of having the largest $\Delta\sigma_{el}^{AB}$ stress range across all of the considered 1300+ SO events. An example of such a map is presented in Figure 5.10. As a result, the main assessment point(s) for a single tubehole would be the node(s) which had the highest probability of having the maximum stress range, as this is the most likely to initiate a crack first. Furthermore, this also provides a rationale for

examining multiple assessment locations, and the priority of which points to assess would be identified according to the probability map.

5.4.2.3 Treatment of processed FE data results

Identification of key inputs through sensitivity analysis The following stage in constructing the predictive model for stresses is identifying the input parameters in the prospective statistical model. In order to establish this, a sensitivity study was required in order to assess which input parameters are the most dominant. A simple approach for examining the strength between the output-input data is to simply plot the outputs against each of the inputs and compute correlations. However, identifying the key input parameters which may strongly affect the output can be challenging and requires both judgement as well as trial and error. For the TP only one parameter was identified as strongly dominating all six SCs, which was the largest *tilt* across the tubeplate. This was defined as the difference between the maximum and the minimum of the 37 steam temperatures.

Data discrimination For the TP, when the various stress components were examined as functions of tilt alone, the processed FE data exhibited a multi-modal behaviour. When a single dataset exhibits such behaviours, data discrimination can be used to subdivide it into smaller subsets each exhibiting a self consistent behaviour. A discussion on the use of discrimination using *Bayesian discriminant rule* can be found in [94]. Based on the same principles, [95] provides various data analysis toolbox in MATLAB®, which includes the *rda* function for data discrimination. The latter tool was implemented in this work in order to subdivide the processed FE data into separate modes.

If some modes are consistently more prevalent at specific input ranges, then this can be taken into account. According to these ranges, and for a value of an input tilt, there would be two possible scenarios for producing a stress prediction:

1. If the input value lies within a range exclusive to a single subset (mode), then only this specific subset would be used to infer the output.

2. If the input lies within a cross-over range, where the collective dataset suggests that a multi-modal behaviour can occur, then an associated multi-modal prediction can be produced. The probability of occurrence of each mode within this crossover region (p_m where $m = 1, 2..., M$) is dictated by the number of data points that belonged to each mode within the same range. For instance, if D is the total number of data points, D_B is a portion of D which lies within the cross-over range, and D_m is the number of data points belonging to each mode, then the probabilities can be conveniently defined as:

$$p_m = \frac{D_m}{D_B} \tag{5.8}$$

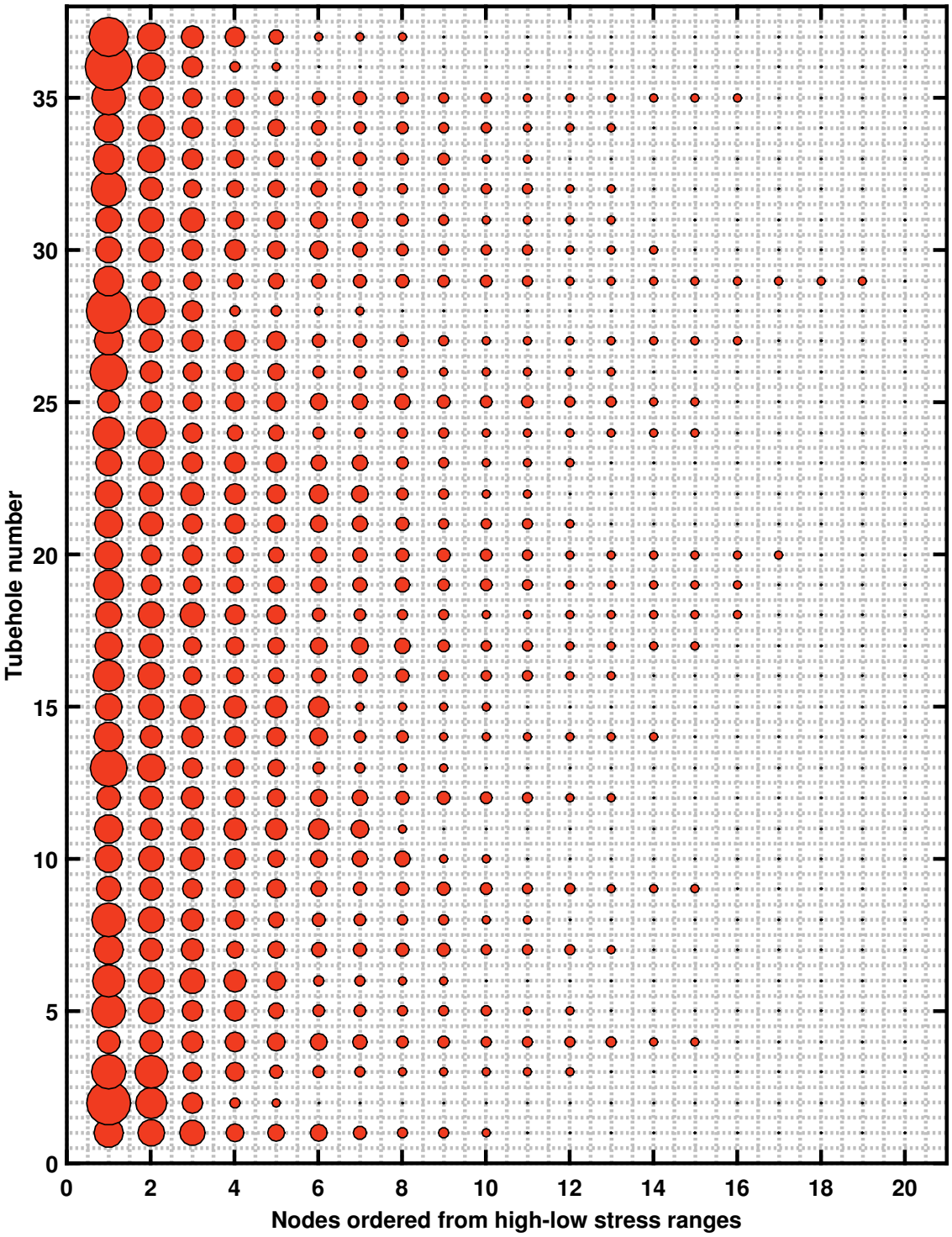

Figure 5.10: A probability map showing the relative frequency of 20 nodes on each tubehole ($1-20$ on the horizontal axis) having the largest stress range, for all tubes ($T = 1-37$ on the vertical axis). The size of each bubble is a measure of probability.

In a Monte-Carlo simulation the presence of these multiple modes and their respective ranges can be accounted for by subdividing the number of required trials (N) into appropriate subsets. For example, for a single input value, if the first scenario applies then all N trails would be sampled from the same mode. However, for the latter scenario, N would be divided into multiple subsets each of N_m trials according to the probability of each mode:

$$N_m = N \times p_m \tag{5.9}$$

The following stage of the proposed predictive model for steady-operation stresses is fitting each subset/mode with a linear regression (statistical) model, which is the subject of the following section.

Linear regression Following the segregation of the processed FE data into distinct modes, for each stress component and for each tubehole specific dataset, fits can be produced (using least-squares regression) based on the data in each group. For a linear model fit the following expression can be fitted to a system response or dataset [12, 57]:

$$Y = X\beta + \epsilon \tag{5.10}$$

where Y and X are the output and input matrices respectively. If the dataset is of size n, then Y and X are sized $n \times 1$ and $n \times p$, where p is the number of fitted parameters (e.g. $p = 2$ if a first order fit is used). β is the vector of fitted parameters (sized $p \times 1$) and ϵ is vector of residual terms (sized $n \times 1$). An estimate for β can be found using:

$$\hat{\beta} = (X^T X)^{-1} X^T Y \tag{5.11}$$

The approach is also referred to as the Response Surface Method, which for the case when considering only one input, it reverts back to a simple 2 dimensional linear regression problem. This approach assumes that all data points are of equal quality and weight. This would typically be the the case is the data-set being used is *balanced*, which assumed that the entire range of possible input values is covered. If that is not the case (i.e. the data-set is unbalanced) a weighted least-squares solution can be used to assign different weights to each data point, in which case the following solution applies [60, 61]:

$$\hat{\beta} = (X^T W X)^{-1} X^T W Y \tag{5.12}$$

where W is an $n \times n$ diagonal matrix of weights. In the balanced case, all diagonal elements in W are equal to 1. Setting the weights can be achieved by [60]:

1. Dividing the input range into bins of equal intervals.

2. Assigning each data point in the data-set to the appropriate bin.

3. All data points belonging to one bin will have equal weights.

4. All bins have equal total weights, and the total sum of all weights is equal to n.

For predicting stresses at a specific assessment location as functions of input tilt the following expression can be used:

$$(\sigma_i)_T = (\mu_i)_T + (\epsilon_i)_T \tag{5.13}$$

where $(\sigma_i)_T$ is the i^{th} stress component ($i = 1:6$) for a required tubehole ($T = 1:37$), $(\mu_i)_T$ is the predicted mean value (obtained from $X\hat{\beta}$) and $(\epsilon_i)_T$ is the residual (error) component which is sampled from the associated histogram.

Correlations If each stress component is considered an input parameter in a probabilistic damage assessment, then correlations between components must be considered as they have been proven to be important [93]. However, care must be taken in terms of identifying the correlations of interest and their interpretation. For a probabilistic calculation, what is needed is a correlation that links the sampled stress components for a single input tilt. That should not be confused with the correlation between the stress components coming from the processed FE results which in fact were for a wide range of tilts. Therefore, the required correlations can be interpreted as correlations between residuals (or errors) relative to the regression fit, rather than correlations between deterministically evaluated stress components. The latter correlation is indeed important, as the most dominant stress component are typically correlated for a range of tilts, and thus can have significant effects on stress range calculations. However, that correlation is accounted for by virtue of the regression fits i.e. the six components are linked (or correlated) since they are all functions of tilt. The residuals (which are treated as being independent of the input tilt) need to be correlated separately, and are advised not to be sampled independently. Therefore a 6×6 correlations matrix (linking the residuals of the stress components) can be calculated for each of mode of the original processed FE data. These correlations can have a significant effect on stress range calculations in probabilistic assessments. Even for correlations of modest strength, their effect can be important especially when there exists multiple dominant stress components, and the residual terms are large.

A physical explanation as to why stresses can be significantly correlated lies in the location of the assessment point. If the assessment point lies on a free surface or an edge, which is most commonly the case, then the stress state is biaxial or uniaxial. In which case the six stress components discussed in this work are just rotations of a biaxial or uniaxial principal stress state. For example, for a simple 2-dimensional case, the effect of rotating the stress axes is represented

by:

$$\begin{bmatrix} \sigma'_{11} \\ \sigma'_{22} \\ \sigma'_{12} \end{bmatrix} = \begin{bmatrix} c^2 & s^2 & 2sc \\ s^2 & c^2 & -2sc \\ -sc & sc & c^2 - s^2 \end{bmatrix} \begin{bmatrix} \sigma_{11} \\ \sigma_{22} \\ \sigma_{12} \end{bmatrix} \tag{5.14}$$

where c and s are the *cosine* an *sine* of the rotational angle.

This becomes apparent when the principal stresses are calculated from the processed FE data and one or two are insignificant relative to the more dominant components. Therefore, these correlations are, at least in part, attributed to fixing the stress axes for the entire FE model. This makes conducting the R5 V2/3 more straightforward because the orientation of each stress component is kept fixed. When this procedure is conducted for a fixed location, then what is of interest is the change in one stress component from one steady-operation event to the next. Therefore, these correlations essentially represent the relative orientation of the global axis with respect to the local principal axis. As a result, these correlations are location specific and must be inferred from stress results taken from the same node in the FE model.

For the application presented here, the Spearman correlation was deemed to be appropriate as it does not assume linearity (an assumption which may not apply for parameters of interest) and is a non-parametric statistic which does not impose any a priori assumptions on the distributions of the input parameters, which makes it more appropriate when dealing with discrete data-sets. More details on calculating and incorporating Spearman correlations can be found in Sections 4.2.1 and 4.2.2.

5.4.2.4 Uncertainty in metal temperature

The metal temperature is a key input parameter as it strongly affects the calculation results for both the creep and fatigue damages. For a single FE modelled SO event, the metal temperature is taken at the predefined assessment point which is the same nodal location from which stresses are extracted. The extracted data from the raw thermal FE results were the metal temperatures at the assessment location(s) for each tubehole. It was expected that the 37 metal temperatures would be strongly linked to the 37 input steam temperatures. Thus the proposed approach for predicting the metal temperature for a specific tubehole for a specific event uses the following expression:

$$(T_{SO})_T = (T_S)_T + \Delta T \tag{5.15}$$

where T refers to the tubehole number ($T = 1:37$), T_{SO} is the characteristic metal temperature and T_S is the stream temperature. The latter is taken as a deterministic input which is given by the processed history data (see Section 5.4.2.1). Furthermore, ΔT is sampled from a histogram

(e.g. see Figure 5.15), which is an appropriate approach if the dataset used to produce such histogram is large.

Correlations between ΔT and the stress component residuals can also be examined and incorporated. Perhaps a convenient way to accomplish this is by considering the ΔT term as an additional parameter in the stress correlations matrix. Thus the latter matrix becomes a 7×7 matrix which links not only stress component residuals, but also links these residuals and ΔT. With metal temperature and stresses being the main drivers for creep damage, it was deemed important to examine and incorporate these correlations in a prospective probabilistic assessment.

5.4.3 Results and Discussion

5.4.3.1 Stress results

After applying the processes discussed in Section 5.4.2.1 the TP historic data was processed and 1300+ steady-operation events were run in FE to produce metal temperature and stress results. Thereafter the approach proposed in Section 5.4.2.2 was conducted to identify the main assessment locations (nodes) for each tubehole. To reiterate, this was based on finding the locations which most frequently produced the largest $\Delta\sigma_{el}^{AB}$ across the 1300+ FE runs. The outcome was the probability map shown in Figure 5.10, which shows that only a select number of surface nodes would be expected to frequently have the largest stress ranges. For example, for Tubehole 2 ($T = 2$), one node had 50% chance to have the largest stress range. This map provided a rationale to select a limited number of nodes per tubehole on which to focus assessment efforts, as these are the most likely to creep crack initiate first.

The following stage was to extract the FE results from the chosen assessment locations, the outcome of which are frequently referred in this report as the processed FE data. The output of interest were the six SCs and the metal temperatures at the assessment locations. As discussed in Section 5.4.2.3, it was required to identify the key inputs which are later to be used to infer stresses. Various input parameters were postulated and trialed, but only one seemed to strongly dominate all 6 SCs, which was the tilt. The latter is defined as the steam temperature difference between the hottest and coldest tubeholes. A scatter plot showing the proposed input-output data (tilt *vs* $\Delta\sigma_{el}^{AB}$) is shown in Figure 5.11. The conclusion was that the tilt strongly dominated the output stress state, and thus only this input parameter was deemed to be worth considering at this stage.

Moving forward, the relationship between each SC and tilt exhibited a multi-modal behaviour, as shown in Figures 5.12 and 5.13. A possible explanation for this behaviour might be the existence of another input parameter which was not identified i.e. the scatter plot in Figure 5.11

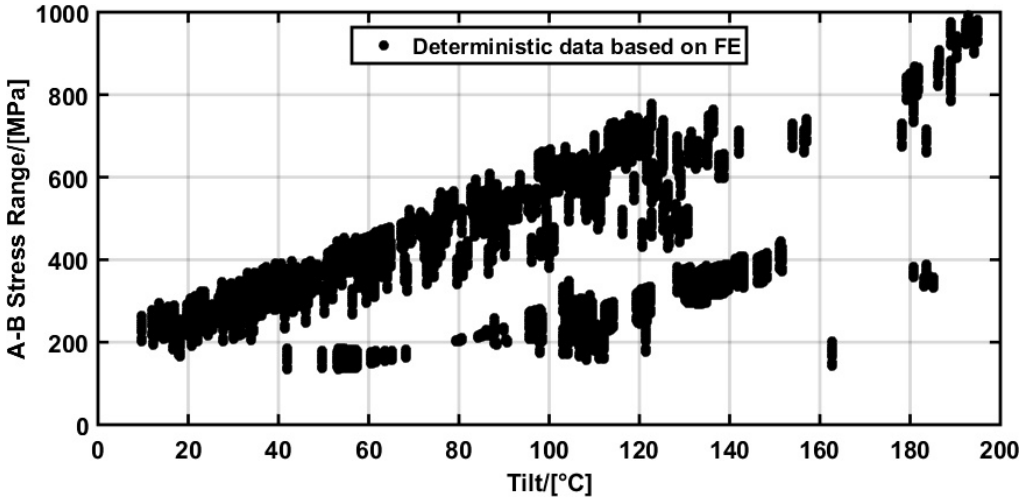

Figure 5.11: Scatter plot of a postulated input parameter (the tilt) against the output of interest ($\Delta\sigma_{el}^{AB}$). This data is for Tubehole 2 ($T = 2$) at the surface node most likely to have the highest stress range.

only shows a slice of a multidimensional surface. However, no such parameter was successfully identified for the TP. Modelling this behaviour required a separate treatment which was the subject of Section 5.4.2.3. For the purposes of the application at hand, it was deemed appropriate to segregate each stress component dataset into three distinct modes. The end results of this analysis for all stress components are given in Figures 5.12 and 5.13. For reference, these results were for Tubehole 2 ($T = 2$) taken at the nodal location that had 50% chance of having the largest stress range (see Figure 5.10). It was considered that accounting for the ranges over which each mode existed would be significant as previously discussed in Section 5.4.2.3. The modes across all stress components do (almost) perfectly correlate. That means if one point is part of Mode 1 for one stress component, it will (almost always) lie on the same mode for the other 5 components. This further supports a belief that these modes are most likely related to distinct modes of plant operating conditions, which are not easily incorporated.

After segregating the input-output datasets (6 sets, one per SC), least-squares regression (see Section 5.4.2.3) was used to fit linear models to the data. Figures 5.12 and 5.13 show datasets for the 6 SCs as functions of input tilt, each segregated into 3 modes and with the appropriate least-squares fits. It's worth noting that it was judged that Mode 3 subsets can be disaggregated, and this was believed to be conservative. Data points belonging to Mode 3 were consistently compressive and therefore would not increase creep damage. Therefore, only Modes 1 and 2 were considered in the proposed probabilistic predictive model for the TP. Note that this is a conservatism; some proportion of the operation will be under more benign conditions than assumed in the probabilistic model. Figures 5.12 and 5.13 also show the residuals relative to

the regression fits presented as histograms. These histograms were used to model the statistical model uncertainty for each stress component. This uncertainty is represented by the $(\epsilon_i)_T$ in Eq 5.13).

A Monte-Carlo simulation was implemented to produce probabilistic stress range predictions for the full range of possible input tilts, the outcome of which is shown in Figure 5.14. The inputs for this MCS were the stochastically modelled stress components using Eq 5.13, where the mean stress was obtained from the least-squares fit and the error term was produced by sampling the histograms shown in Figures 5.12 and 5.13. Correlations between stress component residuals (see Eq 5.16) were also incorporated and were found to be significant and strongly affected the sought probabilistic $\Delta\sigma_{el}^{AB}$ predictions. Figure 5.14 also shows the $\Delta\sigma_{el}^{AB}$ calculated from the original processed FE results (the deterministic data used to construct the predictive model), which is the same data shown in Figure 5.11. This data was superimposed on the $\Delta\sigma_{el}^{AB}$ predictions for verification purposes. The predictions were consistent with the deterministic data, and only a small number of data points lies outside the envelope (maximum-minimum and upper-lower confidence limits in Figure 5.14) produced by the probabilistic predictions. This was believed to be acceptable because the predictions were consistently higher than the points outside the envelope, and therefore was considered conservative. Table 5.4 presents some numerical measures which compare the probabilistic predictions with the deterministic results. It is worth noting that in an ideal case a judgement on whether the probabilistic predictions are appropriate can be made by counting the number of data points that lie outside the CIs and the maximum-minimum limits. Ideally no data should lie outside the latter, whilst a small number can be allowed to lie outside the former. For example if 98% confidence intervals are used, then around 2% of the data should lie outside the upper-lower CIs [93].

It must be acknowledged that some of the stress components were rather large, and these can be explained as follows:

1. The node lies on the upper edge of Tubehole 2 and, therefore, for this particular situation, this assessment location is a stress raiser.

2. The mesh used for the mechanical FE model was rather coarse, and thus extrapolation between nodes and integration points can produce large stresses.

3. Large metal temperature gradients were observed in the thermal FE results.

The above issues can be in part addressed by re-meshing the FE models with finer meshes. However, that was considered beyond the purposes of this work.

Table 5.4: For Tubehole 2 ($T = 2$), this table shows a summary of measures used for verification purposes.

Percentage of data within 98% CI	**Percentage of data within Max-Min limits**
96.2	99.3

5.4.3.2 Metal temperature results

Figure 5.15 shows a histogram of the differences between the metal and steam temperatures for all of the 1300+ SO events and all tubeholes. These results suggest that an underlying distribution does exist, and can be sampled to stochastically model the random variable ΔT in Eq 5.15.

5.4.3.3 Correlations

As previously discussed, correlations between stress components can have a strong effect on the quality of the probabilistic stress predictions. Therefore, it was judged that the correlations between ΔT and the stress component residuals should also be incorporated. With temperatures being as important as stresses for promoting creep damage, and with the stress component residuals being rather large, it was judged that this correlation is important in a prospective probabilistic assessment. To achieve this, it is suggested that ΔT should be considered as an extra term in the stress correlations matrix. This produces a 7×7 matrix which links not only stress component residuals, but also links these residuals and ΔT. For the same assessment location as the one considered in Figures 5.12 and 5.13, the correlations matrix was as follows:

$$\left[\begin{array}{cccccc|c} 1.00 & 0.05 & 0.04 & 0.52 & 0.05 & 0.09 & -0.02 \\ 0.05 & 1.00 & 0.62 & 0.35 & 0.62 & 0.71 & 0.70 \\ 0.04 & 0.62 & 1.00 & 0.58 & 1.00 & 0.52 & 0.57 \\ 0.52 & 0.35 & 0.58 & 1.00 & 0.59 & 0.30 & 0.18 \\ 0.05 & 0.62 & 1.00 & 0.59 & 1.00 & 0.52 & 0.56 \\ 0.09 & 0.71 & 0.52 & 0.30 & 0.52 & 1.00 & 0.88 \\ \hline -0.02 & 0.70 & 0.57 & 0.18 & 0.56 & 0.88 & 1.00 \end{array}\right] \tag{5.16}$$

with the bottom and far right elements of this matrix relating ΔT with the stress component residuals.

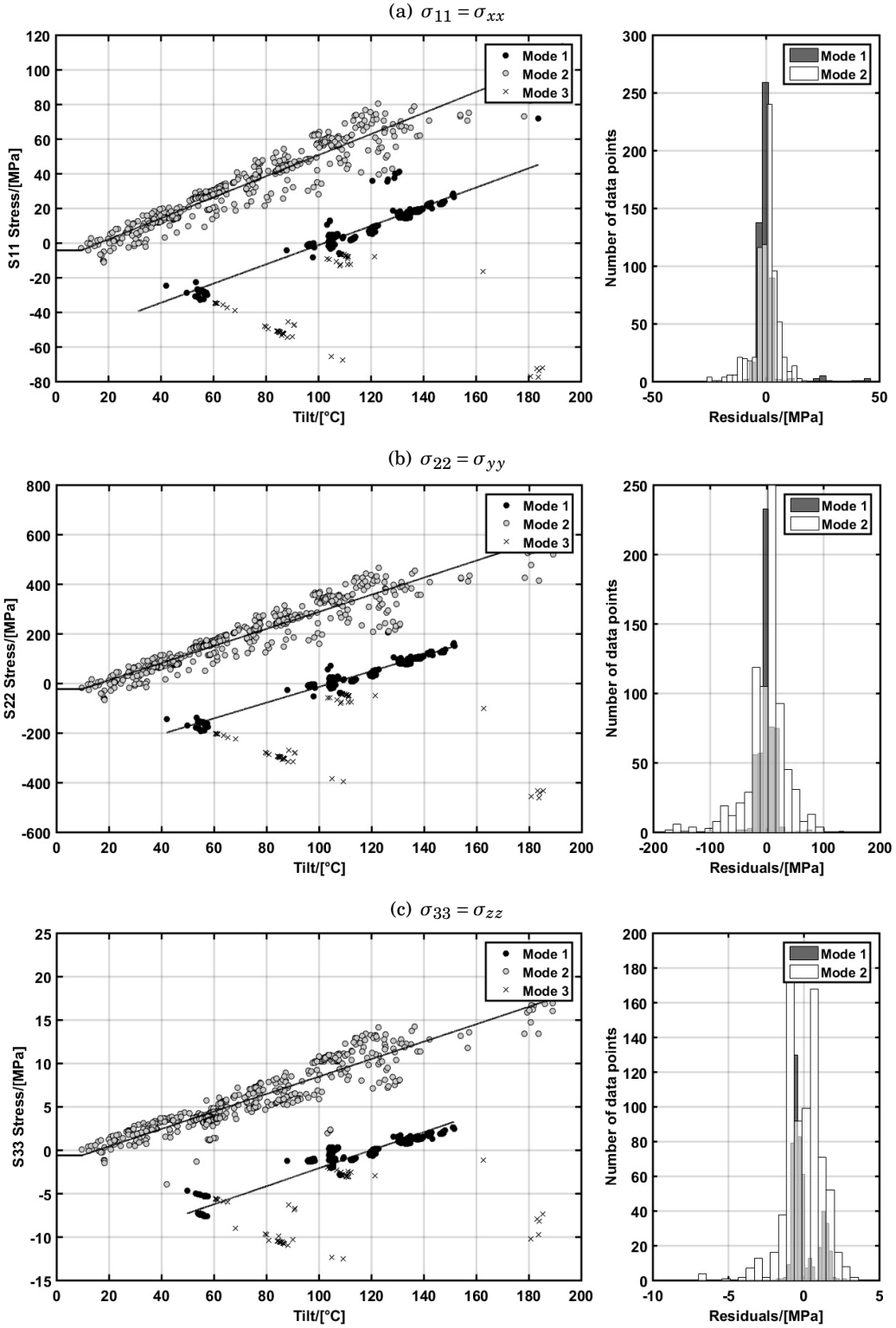

Figure 5.12: The processed FE data (the three direct stress components) segregated into three distinct subsets. These results are specific to Tubehole 2 (obtained using the FE model show in Figure 5.1b), at the location most probable to have the largest stress range (see Figure 5.10). The most dominant stress component is $\sigma_{SO} = \sigma_{22}$

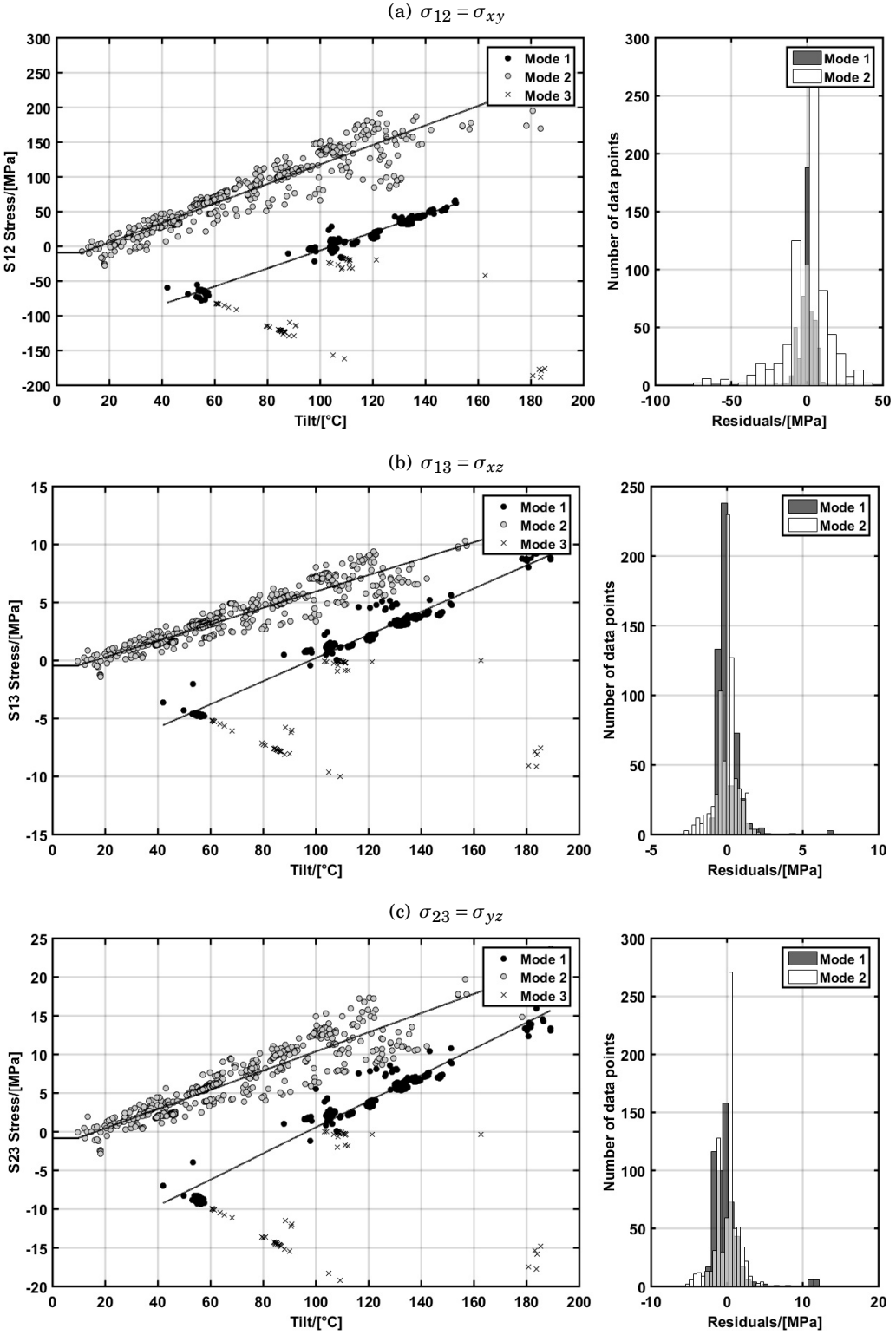

Figure 5.13: The processed FE data (the three shear stress components) segregated into three distinct subsets. These results are specific to Tubehole 2 (obtained using the FE model show in Figure 5.1b), at the location most probable to have the largest stress range (see Figure 5.10).

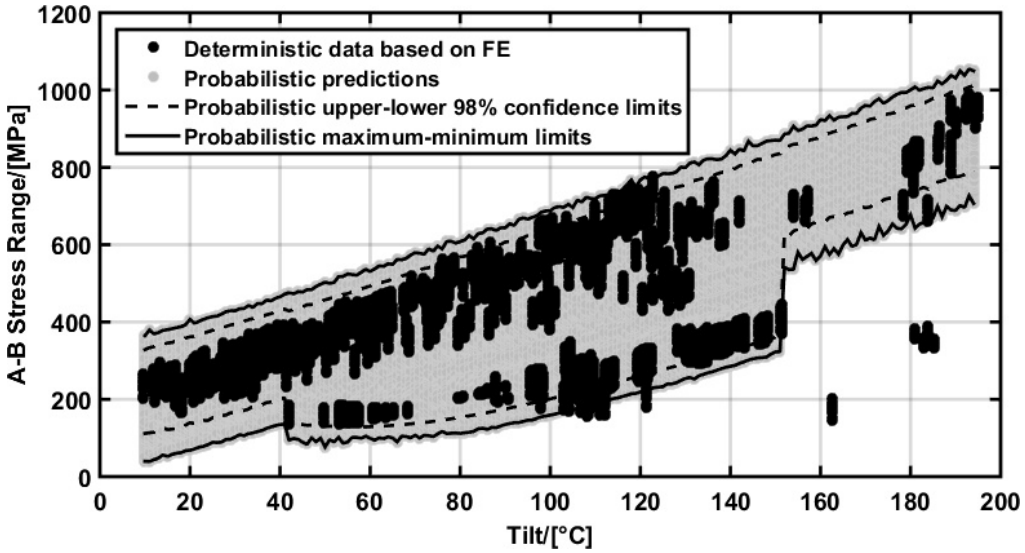

Figure 5.14: For tubehole 2 (i.e. T = 2) at the location most probable to have the $\Delta\sigma_{el}^{AB}$, this figure shows probabilistic stress predictions for a range of tilts superimposed onto the deterministic values of $\Delta\sigma_{el}^{AB}$ for verification purposes.

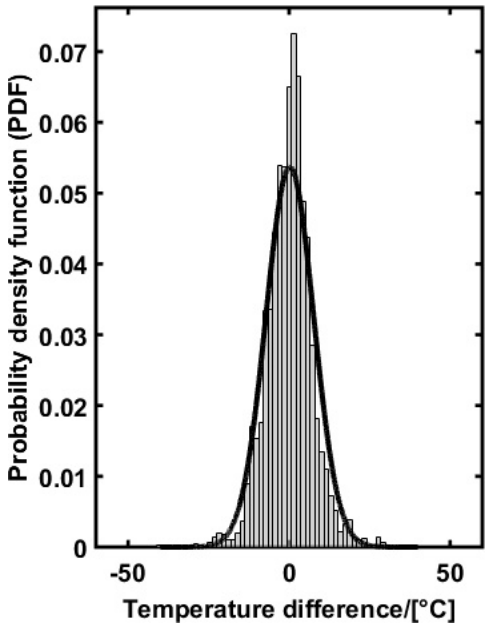

Figure 5.15: Histogram of the differences between steam and metal temperatures (ΔT) for all tubeholes across 1300+ events modelled using the thermal FE model. A fitted normal distribution is also shown superimposed on the data. Along with plant steam data for T_S, this ΔT is used in Eq 5.15 to model the characteristic metal temperature T_{SO} for a steady-operation event.

5.5 Important Considerations for Implementation in Probabilistic Assessments

5.5.1 Limitations of Stress Modelling Strategies

The approaches proposed in this chapter and their applicability do not in themselves depend on the nature of the failure mechanism being examined nor on the FE modelling conduced. The models constructed using these approaches do, however, depend on the quality and validity of the training data collated from the FE models used. In that sense, the limitations of the FE models (which must be acknowledged and understood in general) are a subset of the limitations of the models constructed using the approaches proposed in this chapter.

A key limitation in the work presented in this chapter is related to the probabilistic treatment of elastic stresses, which can be later translated to their elastic-plastic equivalents through a combination of a Neuber approximation and a Ramberg-Osgood model [23]. This is common practice in R5 Volume 2/3 applications as it is relativity simple and only requires an elastic FE model. The approach allows the evaluation of plasticity in a structure via a linear analysis and therefore avoids having to run a full-fledged nonlinear analysis, saving computational time. The Neuber rule states that the stress-strain product of the elastic solution is equal to the stress-strain product of the real elastic-plastic solution. Typically, this approach for estimating elastic-plastic stress and strain cycle ranges is considered conservative, an observation which is corroborated by the analysis presented in Section 3.7.4.3, which looked at the uncertainty introduced by using such approach when compared with experimental stress readings for a displacement controlled uniaxial specimen.

The Neuber approximation is intended for assessment locations which have high stress intensities (e.g. notches and inner surfaces of tubes) and applies when the yield zone is contained, i.e. it is surrounded by an elastic region. It is likely to be pretty good, therefore, for any local stress raiser around which cyclic yielding is contained. Where it becomes questionable is when yielding occurs across the whole section of a component and that constraint is lost as a result. In practice, however, when this requirement is not met, bigger problems such as ratcheting or failure to meet the primary stress limits are typically of more concern.

The limitations of any FE modelling strategy for investigating loading conditions must be understood to be inherited by the associated surrogate models. As such, if the stress FE modelling is conservative, then conservatism is also implicitly introduced in the surrogate model. Reducing conservatism would require constructing elastic-plastic FE models, run such models for a wide range of loading conditions, extracting the appropriate training data and then used this data to train a new surrogate models. This process is virtually the same as the one followed in this

chapter, with the exception being that elastic models were used, thus the resulting surrogate models are considered to be conservative. Nevertheless, basing the estimation of assessment stresses on elastic FE results may be too conservative, and a better representation of the cyclic stresses and strains may be needed. For probabilistic implementation it is advised that this approach be adopted for its simplicity in the first instance, and after a complete probabilistic assessment is constructed, a comparative sensitivity analysis can be conducted in order to assess the level of conservatism introduced. This could be done by comparing probabilistic damage results obtained using this approach as compared with the equivalent results but based on elastic-plastic FE stresses. This comparative analysis can be done over numerous test cases covering a range of loading conditions. However, attempting to use a full-fledged elastic-plastic FE model in the first instance may be too onerous, especially when it is not yet clear if such complex modelling is needed. It may be the case that even with the added conservatism, the required target reliability can be met, in which case there would be little incentive for further refining the stress modelling aspect of conducting a probabilistic assessment.

For cases where a full elastic-plastic model is needed (or just desirable), surrogate modelling strategies (the one presented in this chapter being an example) can still be used to capture and replicate the response of elastic-plastic FE models in prospective probabilistic applications. However, the FE model runs needed to provide the training data to prepare such surrogate models may inevitably be computationally taxing as compared with their elastic counterparts. The investment of computational time, analysis effort and added complexity in the probabilistic stress analysis can be justified depending on the judgement of the practitioner. Nevertheless, the surrogate modelling approaches are generally applicable to most cases involving replicating computationally intensive FE stress models. Furthermore, the uncertainty associated with the approach used for stress modelling (elastic with an approximation versus full-fledged elastic-plastic) is an epistemic uncertainty, the effect of which can be examined using sensitivity analysis as discussed in Chapter 3 (Section 3.4.6).

In the tubeplate case-study presented in Chapter 6, it was concluded that if the aim was to reduce the uncertainty in the probabilistic damage results (and hence obtaining a reduced probability of initiation estimate), then focusing on improving creep ductility modelling followed by creep deformation modelling would yield the most marked benefits. As such, the improvement of the stress modelling side of the probabilistic assessment was deemed less pertinent to demonstrating improved probability of initiation estimates.

5.5.2 Sampling of Transient Stresses and Metal Temperatures

Consider a component history that is divided into discrete cycles with each having peak transient stresses during the start and end of the cycle. The peak transient stresses for SU and RT events are denoted by points A and C respectively in Figure 5.2. When conducting a probabilistic assessment of a component (e.g. using a MCS with N trials), each cycle transient can have N possible stress states and metal temperatures. This requires a sampling strategy in order to ultimately translate the available plant data for the transient instances of interest into the samples required for a MCS. Given a transient type, it is deemed appropriate to assume that the samples assigned to different cycles should be treated as uncorrelated. This effectively means that there is no reason to believe that the transient for one cycle is affected by the same transient from the subsequent or preceding cycle(s), and therefore each transient within a given history is treated independently of:

- Transients of the same type but from other cycles.
- Transient of other types from any cycle.

For a single cycle, there are two proposed approaches which can be adopted for incorporating assessment metal temperatures (Figure 5.8) and stresses (Figures 5.6 and 5.7) in a prospective probabilistic assessment for a desired number of Monte-Carlo trials (N). For a given transient type these are:

1. Sampling metal temperature and stress components from tubehole specific histograms independently and then introduce correlations at a later stage. After quantifying the relevant correlations and exercise judgement as to which correlations to be included, various correlation types can be incorporated, a topic which was discussed in Section 5.3.2.4.

2. An approach which simply considers how may transient instances are available (N_{TR}, e.g. in this work $N_{SU} = 20$ and $N_{RT} = 18$ transient instances) and then assigns $1/N_{TR}$ of the N samples the metal temperature and stress state associated with one of the N_{TR} transient events. If this sampling strategy is adopted, then correlations need not be considered because each sample would be taken from a pool of coupled metal temperature and stress components data. This effectively means that correlations would be accounted for at the sampling stage.

The former approach is deemed more appropriate if a large number of transient events is available which provides an opportunity for rigorous statistical characterisation of the metal temperature and stress components. The latter approach, is more suited for situations where a limited number of events is considered, and is deemed to be the more appropriate approach for the application at hand. For a prospective probabilistic assessment, the rationalisation given in

this section ensures that every transient instance within any cycle during the entire history of the component will be assigned every possible condition according to the available plant data.

5.5.3 Sampling of Steady-Operation Stresses and Metal Temperatures

The steady-operation history for the TP consists of cycles which in turn are divided into discrete events (see Section 5.4.2.1) which are defined by: a tilt, a duration and 37 steam temperatures each corresponding to a specific tubehole. This data was termed the *processed history data* in this chapter. According to the predictive models for stresses and metal temperatures presented in Section 5.4.2, for each event 6 stress components and 1 metal temperature (and their respective uncertainties) can be obtained. Rerunning the predictive models for every event in the lifetime sequence can prove computationally intensive and, therefore, a better strategy is required. The proposed approach is as follows:

1. For stresses, examine the range of possible tilts across the entire component history according to the processed history data. Then for as many increments as required within this range (e.g. 10-200$^{\circ}C$ with a 1$^{\circ}C$ increment), produce probabilistic predictions for all 6 SCs. Each prediction constitutes a mean stress value (which is a function of tilt, tubehole, and nodal location) and an uncertainty (which is sampled from an appropriate histogram). Effectively, this constitutes a 'look-up' table approach to predict the evolution of the stress-operation stresses for the entire history of the component. Computational efforts are kept to a minimum on account of this process having to run only once at the start of the probabilistic code.

2. For predicting the metal temperature of a tubehole for a single event, given the Eq 5.15, T_S can be read directly from the processed history data, and the uncertainty ΔT can be sampled once from the histogram shown in Figure 5.15 at the start of the probabilistic code.

5.5.4 Stress and Temperature Permutations in MCS

One of the initial stages of setting up a MCS is the sampling of the uncertain input parameters according to their probability distributions, with the number of samples being equal to the number of desired trials, N. Sampling can be done either randomly or using a strategy such as Latin-hypercube sampling, the latter being more appropriate when a smaller number of samples are required. What follows is the arranging of the sampled input parameters to form the input sets for each of the MCS trials; for a single trial all input parameters are set to fixed values. After sampling, *random permutations* can be produced to rearrange all sampled inputs, with the number of permutations required being equal to the number of input parameters. This concept forms a key feature of the LHS approach, which ensures that each sample (or *bin*) of each input will be used at least once, though not all possible combinations of all input parameters can be

trialed of course [18].

Setting these permutations can require some judgement, a topic which is discussed in [18]. For a time *independent* material property, for example, a permutation is formed as part of a Latin-hypercube at the start of the probabilistic assessment, and this remains unchanged for this input parameter. The same concept is not applicable to time dependent input parameters such as thermal stresses and metal temperatures, which are in fact ever changing during the lifetime of the component. Given the discretisation of the loading history into events, each event is required to experience all possible stress and temperature samples over the course of the MCS. Therefore, ideally a set of permutations is required per event within the loading history. It is worth noting that if two parameters have been sampled and correlated, then the same permutation must be applied to both, to ensure that the correlation between their samples is retained. Given that a rather large number of events might exist, and if the loading conditions for each are treated as input parameters, then the size of the Latin-hypercube becomes too large to manage, and computational memory becomes an issue. Therefore, the permutations for time dependent loading parameters are left outside the Latin-hypercube, and a new permutation is produced at each event as the MCS progresses in time through the modelled loading history.

For the tubeplate, this loading history was discretised into cycles, which in turn are made of events. In a deterministic sense, a change from one event to the next warrants a change in metal temperatures and stresses. When considering how often the loading permutations need to be reproduced (e.g. whether at each event or cycle) judgement needs to be exercised. Nevertheless, there are commonly three possible options:

1. Using a fixed loading permutation for the entire history (as if stresses and temperatures were material properties). This implies that the loading for all cycles and all events are perfectly correlated, which is erroneous. So this option is easily discarded.
2. The loading permutation is reproduced at each event in time.
3. Each cycle will have its own independent permutation.

The first option is the most conservative of the three, and it is not physically justifiable. Therefore, this option is advised to never be used. The second and third options are closer to a physical situation, however, from one cycle to the next the distribution of temperatures over the tubeplate can change substantially, and as such using a new permutation at each cycle is not unrealistic. Therefore, the latter option is considered the most ideal, but it still is not physically perfect. As to which of the two options is more conservative, it depends on the component application of interest. Using a preliminary probabilistic assessment of the TP, it was found that the second option can be rather conservative, because if a small change in an input condition (in the case of the TP this would be the tilt) is considered, this would realistically translate to

proportional changes in the stress components. However, if a new permutation is used for every event, large changes in stresses can be observed purely because a different sample (or bin) is used from the stress and temperature distributions from one event to the following. This effect is believed to be especially conservative when the uncertainties in stresses and temperatures are relatively large. In essence, this option is not ideal, because if two consecutive events have similar input conditions, then a sudden change in the stress components should not be expected. Therefore, for the TP application it was judged that the third option should be implemented.

5.5.5 Incorporating Material Property Uncertainties

The FE models used in this work are purely elastic models, as the R5 Vol 2/3 assessment procedure converts elastic stresses and strains to their elastic-plastic equivalents using a Neuber approximation. In terms of material properties required as inputs to the FE models, Young's modulus (E) and the coefficient of linear thermal expansion (α) are the two key quantities. Given that in a probabilistic assessment these properties can be treated as uncertain variables, their scatter can affect the results of the FE models used. The scatter in E and α both independently result in a proportional variability in any strain controlled stresses, for example thermal stresses, whilst primary stresses should remain unaffected. Therefore, a scaling factors, U_E and U_α, can be defined according to the variabilities of E and α relative to their mean values (μ_E and μ_α, which are the fixed value used in the FE models). For instance, the scaling factor for E is defined as:

$$U_E = \frac{E}{\mu_E} \tag{5.17}$$

where E is treated stochastically. For 316H stainless steel at $550^{\circ}C$, E can be considered as following a normal distribution with a coefficient of variation (CoV_E) of approximately 0.064 [46]. In a probabilistic assessment, U_E is essentially a proxy for E, and therefore, must not be sampled independently from the latter. These scaling factors can be quite significant. For example, if the 95% upper and lower bounds are considered to be $1.6445 \times \sigma_E$ away from the mean, where σ_E is the standard deviation, then U_E can range between 0.89 and 1.11.

However, the stress results presented in this work include contributions from both mechanical (primary) and thermal (secondary) loads. So applying these factors to the stress results is not strictly correct, as only thermal stresses should be factored. Nevertheless, an exception can be made in situations where thermal stresses significantly dominate over primary stresses, which is the case for the TP. Therefore, an assumption can be made that such error is not significant and the approach discussed above can be adopted for its simplicity. This is also believed to be slightly conservative. Consequently, two independent factors (assuming E and α are not correlated) can be applied to the stress results to account for the variabilities of material properties they respectively represent.

5.5.6 Lessons Learned from FE Modelling

Building on previous work that has been done on the TP, two different FE model geometries (see Figure 5.1) were used to model TR and SO events separately. Furthermore, in some cases the mesh used for the mechanical FE models were finer than their thermal FE equivalents. Originally, using different geometries and mesh sizes for the TP was due to meet various computational requirements. When developing the approaches presented in this report, however, numerous challenges arose from these inconsistencies, chief of which are discussed below. Firstly, for either TR and SO events, using different mesh configurations for mechanical and thermal models provides a hindrance to extracting the required stresses and metal temperatures from the same nodal locations. Therefore, conservative assumptions had to be made. For example, after choosing and extracting stresses from an assessment location on a tubehole surface, instead of taking the metal temperature at the same point (which is desirable), the characteristic metal temperature had to be assumed to be either the maximum or minimum temperature on the entire surface. This can be avoided by using consistent mesh configurations.

Secondly, assumptions which had to be made to address the issues associated with using different geometries for TR and SO events are believed to be even more conservative. In this case, using the same nodal assessment location for extracting both TR and SO stresses and temperatures was not possible. Instead, an assumption had to be made that for a single tubehole the location of most severe transient also experienced the most severe SO stresses. This can be the case because both the most severe TR and SO stresses typically occurred at points near the upper surface. Moreover, this issue was partially mitigated in this work by keeping TR (both RT and SU types) and SO results as tubehole specific. This entire source of uncertainty and conservatism could have been eliminated by using consistent FE geometries for both TR and SO conditions. The degree of mesh refinement can be established through a convergence analysis (e.g. plotting average element size against stress at an assessment point), which is common practice in FE modelling and can automated through scripting.

5.6 Summary

A common approach when treating loading conditions for a plant component is the use of bounding values (deterministic) for temperatures and stresses. This approach is common practice, but can be over-conservative especially for plant assessments. Probabilistic techniques can provide systematic approaches for incorporating loading uncertainties given the availability of loading data. The methodologies outlined in this chapter were focused on probabilistically treating transient (TR) and steady-operation (SO) loading conditions experienced by plant components. As is often the desire when using a probabilistic framework, this attempts to replace bounding stresses and temperatures with stochastic equivalents which are informed by

plant measurements. Therefore, the proposed approaches allow for the examination of loading uncertainties and their incorporation in probabilistic creep-fatigue assessments, which is not achievable with a conventional deterministic approach. TR and SO loading conditions required separate and different treatments because the former is usually more constrained by data availability, while the latter may suffer less from this limitation. Therefore, two approaches for treating these uncertainties were considered separately, brief summaries of which are presented in the following two sections.

Transient Loading

For TR instances (for example start-up, SU, or reactor-trip, RT, transients), the approach was based on examining all recorded instances for each transient type. Firstly, the characteristic conditions for each instance are obtained, which consist of a single characteristic stress state (6 stress components, where σ_{SU} and σ_{RT} refer to the dominant components) and a characteristic metal temperature (i.e. T_{SU} and T_{RT}) per instance. Thereafter, and given the number of available historic instances (N_{TR}, e.g. N_{SU} which is the number of available instances for start-up transients), in a MCS trial each instance of the same type would be assigned one of the N_{TR} possible stress states and corresponding metal temperatures. This was the preferred approach when a limited number of recorded instances is available. When more data is available then an alternative process is possible and is summarised as follows:

1. The construction of histograms to examine the variability of the transient conditions (stress components and metal temperatures).

2. The examination of correlations between the stress components and the metal temperatures, which are characterised by a 7×7 correlations matrix, should also be considered as they are deemed important for producing representative predictions of these loading conditions.

3. Sampling the processed transient data in preparation for use in a probabilistic assessment. Considering that cycles within a component loading history are independent of each other was deemed appropriate, as discussed in Section 5.5.4. Consequentially, sampling for a single cycle is conducted such that every transient within any cycle during the entire history of the component will be assigned a range of possible transient conditions dictated by the available plant data.

Steady-Operation Loading

For steady-operation events, a different approach was proposed, which is only possible if a substantial amount of data is available. In essence, this approach aims to allow the prediction of the characteristic stresses and metal temperatures (e.g. σ_{SO} and T_{SO}, where the former

is the dominant component) during SO conditions (with associated uncertainties) based on some postulated input parameters. The process formalised on this subject is non-exhaustively summarised as follows:

1. Firstly raw plant data, which is typically in the form of steam temperatures, is discretised into SO events.

2. A large batch of these SO events are run in thermal/mechanical finite element (FE) models to infer the characteristic stresses and metal temperatures for each event. Ideally, these SO events would correspond to a wide range of possible operating situations.

3. The stresses and temperature data coming from the FE models are arranged in such a way to highlight any possible dependencies between the characteristic loading parameters and a number of possible predictive input parameters. This is comparable to a simple sensitivity study to identify which inputs can be used as the predictive parameters for inferring the loading conditions.

4. After identifying the key input parameters which seem to dominate the loading conditions, input(s)-output(s) relationships can be formulated to produce surrogate models. These are statistical models which are constructed using technique such as the Response Surface Method (RSM) [12, 54, 57]) or simple linear regression [61].

5. Investigations of important correlations between stresses and metal temperatures should also be conducted.

6. Finally a verification stage is needed to inspect the results produced by the predictive model for stresses to ensure the predictions are representative of the original processed FE stresses.

The limitations of the probabilistic modelling approaches for loading uncertainties are a collection of the limitations of the underlying assumptions used to construct the FE models and in the manner by which such uncertainties are incorporated in a prospective probabilistic assessment. Some of these issues and limitations where explored in Section 5.5 in light of the tubeplate case-study presented in this chapter. Invariably, when modelling a component with complex geometric features and susceptible to complex mechanisms of failure, some assumptions or simplifications are always needed, and the effect of such assumptions can be explored using comparative sensitivity analysis approaches (discussed in Chapter 3), as these are considered epistemic uncertainties. For example, the issue related to added conservatism introduced by relying on elastic FE models for stress analyses and the validity of the Neuber approximation were discussed in Section 5.5.1.

For a probabilistic assessment, the value of the outlined methodology is in providing stochastic predictions of loading conditions as functions of plant data, which can be incorporated with ease in an assessment. These are superior to the conventional approach of fixing the loading stresses and temperatures for long periods of the simulated component history, as unnecessary conservatism is avoided in favour of a more realistic representation of the historic loading conditions. The only other alternative to using statistical models would be to run FE models multiple times within each Monte-Carlo trial (of which there typically may be more than 10^5), which would be computationally prohibitive, especially if complex FE models are required.

CHAPTER 6

PROBABILISTIC METHODOLOGY FOR PLANT COMPONENTS

This chapter completes the methodology for conducting probabilistic assessments based on the Monte-Carlo method. This starts with the definition of the underlying procedure for assessing the failure mechanisms of interest, followed by the probabilistic modelling of the key input parameters, leading to the estimation of probabilities associated with individual assessment points, a whole component or a population of components. A case-study assessing a plant component (the tubeplate) for creep-fatigue crack initiation using the R5 Volume 2/3 procedure was conducted to provide context and demonstrate the utilities of implementing a probabilistic framework. Significant considerations have been devoted to four important issues: the correlations between dominant input parameters, conducting post-assessment sensitivity analyses, the extrapolation of assessment point probabilities to component-level and, thereafter, population-level estimates. Through presenting a case-study implementing the full probabilistic methodology, the aim is to promote wider application and acceptance within the structural integrity community, and further development of the methodology and constituent methods.

6.1 Overview

This chapter is intended to put previously discussed approaches into the context of the general probabilistic methodology, and introduce further approaches which allow for the extension of assessment location probabilities to population-level estimates. Firstly, for estimating probabilities related to individual assessment locations, Monte-Carlo simulations (MCS, see Section 3.4.1) were used to aggregate various sources of input uncertainty through a performance function (i.e. a procedural calculation e.g. see Section 6.3.2) to estimate the uncertainty in an output parameter and, thereafter, calculating probability estimates of interest. Statistical treatment of relevant

material properties was conducted in accordance with the discussions in Section 3.4.2.2, which for the tubeplate case-study entailed using normal and lognormal distributions. Furthermore, the latin-hypercube sampling approach (Section 3.4.3) was used to couple the input parameter samples, thus preparing the inputs to each MCS trial. Linked to the issue of sampling is the introduction of input parameter correlations which was the general topic of Chapter 4, where the approach for incorporating such correlations was specifically addressed in Section 4.2.2. Moreover, the treatment of loading uncertainties for plant components was considered in Chapter 5, which proposed the use of surrogate modelling (e.g. linear-regression statistical models) for estimating quantities related to loading stresses and metal temperatures, thus replacing computationally expensive FE models. The results obtained from the treatment of loading uncertainties for the tubeplate component (see Section 5.4.3) were included in the probabilistic assessments discussed later in the case-study. After conducting a probabilistic assessment for a single assessment location, various sensitivity analyses were conducted with reference to the concepts that were introduced in Section 3.4.6. The final components of the proposed probabilistic methodology are presented in Section 6.2, which expands the methodology to include approaches for estimating component-level probabilities which, in turn, can be translated to population-level estimates. The latter approaches are the subjects of Sections 6.2.3 and 6.2.2.

6.2 Methodology

6.2.1 Probability Estimates for Individual Assessment Locations

6.2.1.1 Estimating the PoI

For a creep-fatigue crack initiation assessment, the probability of initiation is calculated as the probability of incurring a total damage greater than unity:

$$PoI = P(D_T \geq 1) \tag{6.1}$$

The result of a probability creep-fatigue calculation is the total damage as an uncertain output, from which the PoI can be estimated using either of the following approaches:

1. Calculating the fraction of the MCS trials which lead to a total damage equal or greater than unity:

   $$PoI = \frac{m}{N} \tag{6.2}$$

   where m is the number of initiations. Ultimately this is the preferred approach but requires a suitably large number of trials to capture the PoI within a decent resolution. However, when estimating a PoI is not the main concern, the requirement for a large number of trials may not be as stringent. For example, when constructing a probabilistic assessment, a small number of trials might be used for developing and verifying the assessment iteratively.

2. The alternative is to fit an adequate PDF to the output damage results (e.g. normal or lognormal) and then integrate this function from unity to positive infinity. However, the validity of this method relies on whether the fitted distribution provides an adequate representation of the output distribution tail. The *Anderson–Darling* test [56] can be used in this case to aid judgement. If this criterion is not met, the estimates can still be used as crude indicators especially during the development and validation stages of the probabilistic assessments. However, when the output data does not include points near the failure criterion ($D > 1$), the tail is entirely defined by the assumed functional form of the PDF, which may not be representative of the *actual* tail of the data. In this case, a fitted distribution may miss important probabilistic results or data features near the failure criterion, rendering the associated PoI estimates questionable.

From the discussions above it becomes apparent that Eq 6.2 is the more rigorous approach for estimating the PoI, but poses some serious limitations when small probabilities need estimating. For instance, if a nuclear plant component is classified as an *'incredibility of failure'* component (IoF), then a failure frequency $\leq 10^{-7}$ per annum must be demonstrated [67, 72, 73], which would ideally require $10^7 - 10^9$ MCS trials [19]. This highlights an important consideration for high reliability applications, for which the only realistic strategy is to manage computational efforts through efficient code writing and the use of appropriate hardware as discussed in Section 3.6. For the application considered here, creep-fatigue crack initiation by itself is rarely considered gross component failure, as components may still be fully functional and safe to operate even when small cracks have formed. Therefore, there are further stages of failure following crack initiation (which were not considered in this work, e.g. creep-fatigue crack growth), and their incorporation into the probabilistic framework would eventually yield a failure probability that can be compared with a target frequency as the one prescribed for an IoF component.

6.2.1.2 Convergence of Monte-Carlo Results

Given that the MCS is attempting to estimate the PDF of a key output (creep-fatigue damage in this work), such an estimate can be affected by the number of trials used and therefore a check for convergence must be considered. There are two aspects of convergence which can be examined:

1. Convergence of the mean/median output and;

2. Convergence of the PoI estimate.

The Monte-Carlo estimate of a mean output ($\hat{\mu}$) is uncertain and can be represented by a normal distribution:

$$\hat{\mu} = \mu_{out} + \frac{\hat{\sigma}_{out}}{\sqrt{N}} Z \tag{6.3}$$

where μ_{out} is the real mean of the output (the quantity being estimated), $\hat{\sigma}_{out}$ is the standard deviation of the output, $\hat{\sigma}_{out}/\sqrt{N}$ represents the standard error of the estimate, and Z represents a standard normal distribution [96]. An appropriate number of trials can be chosen such that the estimated error is sufficiently small (within a confidence interval e.g. $Z = 1.96$ for 95%). Therefore, a percentage error can be estimated using:

$$E = 100 \times \frac{Z\hat{\sigma}_{out}}{\sqrt{N}\,\hat{\mu}} \tag{6.4}$$

However, this estimate applies to a MCS which uses random sampling. Therefore, if a latin-hypercube approach is used, a considerably smaller number of trails would be needed, although the magnitude of the error involved as a function of N is not trivially defined in such a case. To gauge convergence, the proposed approach is to estimate the number of trials needed based on a simple estimate for a generic Monte-Carlo simulation (Eq. 6.4). Then conducting that number of trials but using LHS, which is expected to need far fewer samples for convergence. Therefore, convergence should be attained, and progressively increasing the number of trials beyond that estimate can be done to verify that the convergence of the mean has indeed been achieved.

From a more practical perspective, the variability of the mean and, more importantly, the PoI can be examined by running the same MCS numerous times and computing means and standard deviations of the two quantities above. Convergence of the PoI is significantly slower because it relies on having as many output samples near the tail closer to the failure criterion. However, a limitation of this approach is apparent when the MCS has a large number of trials, as repeated runs become time consuming. Alternatively, the error associated with estimating the PoI can be produced by considering that the number of crack initiations (m) follows a binomial distribution [3]:

$$\epsilon = \frac{\sqrt{V(m)}}{E(m)} = \frac{\sqrt{NPoI(1-PoI)}}{NPoI} = \sqrt{\frac{1-PoI}{NPoI}} \tag{6.5}$$

where ϵ is an estimate of the error, while $V(m)$ and $E(m)$ are the variance and mean of m respectively.

6.2.2 Component-Level Probability Estimates

So far the discussion has been focused on estimating the initiation probabilities specific to points located on a component of interest. Determining which assessment points are most likely to initiate first is crucial, however, a further interest might be in the estimation of a component-level probability of initiation, PoI_C. The question of what specific probability is to be estimated needs some consideration, as some assumptions are inevitably required. It is assumed here that a PoI_C is interpreted as the probability of a shallow crack initiating *anywhere* within a component (i.e., at one or more locations) by the end of a predefined service history. Logically, this is greater than

its equivalent for individual assessment points. A simple, and conservative, assumption is to assume that all assessment locations are *completely* independent of each other, in which case PoI_C can be calculated using [3]:

$$PoI_C = 1 - \prod_{a=1}^{A_T} (1 - PoI_a) \tag{6.6}$$

where PoI_a is associated with an assessment point a and A_T is the total number of assessment locations. For high reliability components this will be quite conservative as, in reality, complete independence is not realistic. A situation where this consideration is especially important is when crack initiation is driven by material behaviour (e.g. creep ductility) which may be assumed to be the same for all assessment locations. The assumption of using homogeneous material properties can be challenged in situations where different assessment locations within a single component required different material properties, e.g. assessing a weldment may involve assessment locations in the weld, in the heat affected zone and in the parent material, each with separate creep properties. Another situation where complete independence between assessment locations may not be realistic is when considering that stresses endured by different locations can also be correlated, for example, if all stresses are related back to one or multiple plant parameters such as a boiler steam temperature. Because the steam temperatures related to different assessment locations are correlated, their stresses and metal temperatures will not be independent. As a result, it becomes obvious that the correlations between the assessment locations (arising from both loading conditions and material properties) are crucial in estimating the overall initiation probability of a whole component. A similar argument can be made when a population of components (made from the same material and/or part of the same plant) are considered, as the probability estimates of components will be correlated, and these correlations are important for estimating the population level probability.

Accordingly, a more realistic estimate, which is the one used in this work, can be obtained by tracking all assessment locations in parallel as the component history is simulated through time. As a result, PoI_C is simply calculated as the fraction of the MCS trials which have led to at least one crack initiation across the whole component. In essence, this is a *weak-link* argument, which implies that a single point of failure (crack initiation in this case) is considered to mean failure of the entire component [3]. What transpires from such analysis is that the PoI_C is dominated by the initiation of a small number of assessment points, which are usually the points with the highest $PoIs$. As a result a joint probability of initiation on the component-level (PoI_{JC}) can be estimated by tracking the dominant assessment locations. Furthermore, if a component is assumed to have homogeneous material properties, the assessment locations which dominate the PoI_C are dictated by the severity of loading. As a result, the main conclusion is that whether an initiation occurs is governed by material properties (chiefly creep ductility and secondly creep deformation), whilst the location of such initiation is linked to loading severity, which is location

dependent.

A further issue, however, needs to be considered when attempting to estimate a PoI_C. Following the approach above which attempts to account for the interdependence between assessment locations due to having the same material (specifically creep) properties, an inevitable issue is the fact that the non-dominant assessment locations (of which there might be a larger number then the dominant ones) need to be accounted for. These are the assessment locations which did not yield a quantifiable PoI given the resolution of the MCS. For example, if a MCS uses 1000 trials, non of which lead to initiation for a specific assessment location, the probability is not zero, but rather smaller than the minimum PoI of 10^{-3} that this example MCS would be able to estimate. This would indicate that this number of trials is not large enough for this example. In practice, however, there maybe situations where the number of trials is taken to the limit of computational power available, in which case being able to estimate such a small PoI becomes challenging. The following are the suggestions put forward to tackle this issue:

1. Firstly, if an assessment yields zero failures by the end of the simulation, then it would be sensible, and conservative, to assume that at least one MCS trial leads to initiation (even though the results suggest otherwise) and therefore the PoI would have a default minimum of $1/N$.

2. Secondly, to incorporate this assumption in the PoI_C estimate, Eq 6.6 can be rewritten to separate the terms associated with the dominant from the non-dominant assessment locations:

$$PoI_C = 1 - \prod_{b=1}^{B_T}(1 - PoI_b)\prod_{c=1}^{C_T}(1 - PoI_c) \tag{6.7}$$

   where B_T and C_T refer to the numbers of dominant and non-dominant assessment locations respectively, the sum of which is A_T. It is usually the case that $B_T < C_T$.

3. The product to the left (dominant terms) is estimated based on the weak-link argument put forward above, while the latter product is estimated based on assuming complete independence of the non-dominant terms:

$$PoI_C = 1 - (1 - PoI_{JC})\Big(1 - \frac{1}{N}\Big)^{C_T} \tag{6.8}$$

6.2.3 Population-Level Probability Estimates

After the component-level PoI is estimated, what might be of interest is the number of components predicted to have at least one crack initiation given a population of such components, N_{TC}. A possible assumption may be that all components have the same PoI_C, which would imply that they all have the same material properties and have experienced the same severity of loading.

In practice that is rarely the case, however, and if the PoI_C is estimated for a single component which is considered bounding, then the estimation of the number of components having at least one crack (N_{CC}) would be conservative. It must be clarified that this estimation is uncertain rather than exact, as it follows a binomial distribution:

$$PoI_P = \binom{N_{CC}}{N_{TC}} PoI_c^{N_{CC}} (1 - PoI_c)^{N_{TC} - N_{CC}} \tag{6.9}$$

where N_{TC} is the total number of components, N_{CC} is the expected number of components having at least one crack and PoI_P is the probability density of observing N_{CC} occurrences in the N_{TC} population. To reiterate, this approach is conservative and, depending on the target results to be demonstrated, maybe acceptable. Nevertheless, component specific assessments can be conducted (i.e. estimating PoI_C for a number of identical components separately), but is inevitably onerous. As a result, if the components have differences, then the discussion becomes the same as for a single component with multiple assessment locations (see Section 6.2.2). A consideration that must be addressed in such cases is whether the probability of at least one component developing a crack becomes dominated by the components with smaller individual $PoIs$, which would be the case if their numerical preponderance is sufficient. This is analogous to the discussion around Eq 6.7, as the product related to the non-dominant components becomes large due to their prevalence (i.e. $B_T << C_T$, but with reference to components rather than assessment locations).

6.3 Case-Study: The Tubeplate Plant Component

6.3.1 Background

This case-study is intended to demonstrate the implementation of the probabilistic methodology presented in Section 5.4.2. This examines the tubeplate (TP) boiler plant component (which was introduced in Section 5.2) which was assessed for creep-fatigue crack initiation. The underlying creep-fatigue assessment procedure is the R5 Volume 2/3 procedure which is summarised in Section 6.3.2. For the specific tubeplate under examination, the simulated history included 170 loading cycles ($C = 170$, and 3 of which were boiler reconnection cycles) spanning a period between 1984 and 2014. In total, this included approximately 19,000 steady-operation events (including instabilities), each of 100 hours or less.

The TP is manufactured from 316H stainless steel forging, the material behaviour of which is discussed in Section 6.3.3. This includes elastic, tensile, fatigue and creep properties and parameters, the variabilities (or data scatter) of which are considered. Normal and lognormal distributions were used to statistically represent these material properties and, therefore, the approach discussed towards the end of Section 3.4.2.2 was implemented. Loading uncertainties were also treated probabilistically, and a more detailed account of the methods and results involved in predicting stresses (σ_{SO}, σ_{SU} and σ_{RT}) and metal temperatures (T_{SO}, T_{SU} and

T_{RT}) based on plant data for the TP can be found in Chapter 5. Thereafter, key results obtained from the probabilistic creep-fatigue assessment are presented, including the $PoIs$ of individual tubeholes (which constitute the 37 assessment points located on the TP), and an estimate for a component-level probability PoI_C. The latter was then used to infer the numbers of tubeplates within a population which, according to the probabilistic assessment, are expected to have at least one instance of creep-fatigue initiation on any tubehole surface.

6.3.2 Procedure Definition

This section describes the main steps required to calculate the creep and fatigue damages for a single assessment point located on a component using the R5 Volume 2/3 procedure [23, 80]. This defines the performance function which maps the inputs onto the desired output, which in this case is the total creep-fatigue damage at the end of a simulated history. Broadly speaking, however, in reality the desired output variable is binary: “fail" or “not fail" by a stated time. Alternatively, this could be made a continuous variable by specifying the time at which failure occurs. Therefore, concentrating on damage is not central, nor necessary, for the probabilistic ideal. Accordingly, the probabilistic methodology presented in this work is divorced from this underlying procedure, and can be applied to a host of structural integrity methodologies. Nevertheless, the R5 procedure was chosen in order to demonstrate the proposed probabilistic approaches. A considerable portion of this procedure is devoted to constructing an idealised hysteresis cycle. An example of this is shown in Figure 5.2, which relates to the case-study.

For a generic plant component it is convenient to define two different types of load cycling. The first, which will be referred to as “cycles", relate to the reactor, or the boiler in question, starting up and subsequently shutting down. An example of such cycles is shown in Figure 5.2. However, during at-power operation of the reactor (or boiler), operating conditions can change from time to time. In Figure 5.2 this refers to the B-D portion of the total cycle. For the case-study considered in this work the most significant of these changes are substantial boiler tube temperature changes which occur due to boiler instabilities. The temperature changes lead to thermal stress changes, and hence also constitute stress cycling. These load cycles will be referred to as “events". Therefore, in general there are several “events" within each “cycle". Different cycles are labelled by the letter c ($c = 1 : C$, with C being the total number of modelled loading reactor or boiler cycles). By contrast, different events are labelled by the letter e ($e = 1 : E_C$, with E_C being the total number of events within a given cycle). The letter i ($i = 1 : I$) labels strain (or time) increments used to perform numerical integrations within each event. The presented procedure considers a single cycle as part of a loading history for a plant component and, therefore, all stresses and strains discussed in this section are loading cycle specific unless explicitly stated.

Cycle description

As shown in Figure 5.2, the hysteresis cycle was modelled as being divided into two portions:

1. Portion CA: Half-cycle without creep dwell (unloading). Point C represents the peak stress during a reactor-trip (RT) transient. Point A represents the peak stress caused by a start-up (SU) transient.

2. Portion ABDC: Half-cycle with creep dwell. This is divided into AB (loading) followed by BD (the creep dwell) and DC (the reactor-trip). B is the start of the steady (i.e. power producing) operation (SO), which may include periods of severe stresses and temperatures.

For the case-study all cycles within the simulated history were classified as RT-SU cycles (approximately 170 cycles in total), apart from three which were boiler cycles. The latter cycle type, which usually produces larger strain ranges, was treated deterministically by using conservative transient loading conditions.

Creep damage calculation

The R5 Volume 2/3 methodology includes a procedure for constructing the hysteresis loop (Figure 5.2) using only elastically calculated stresses, and is described as follows. The elastic stress range for portion CA (unloading) is the Von Mises stress based on the differences in stress components between the RT and SU transient stress states:

$$\Delta\sigma_{el}^{CA} = \sigma_{el}^{RT} - \sigma_{el}^{SU} \tag{6.10}$$

Although the notation suggests as much, this must not be interpreted as the algebraic difference between the peak Von Mises stresses for RT and SU. Instead, this must be understood as the Mises stress range formed from the component ranges, *not* the difference of Mises equivalents. The elastic-plastic stress and strain ranges are calculated using the *unmodified Ramberg-Osgood* expression:

$$\Delta\varepsilon_{ep}^{CA} = \frac{\Delta\sigma_{ep}^{CA}}{\bar{E}} + \left(\frac{\Delta\sigma_{ep}^{CA}}{A}\right)^{1/\beta} \tag{6.11a}$$

and the *Neuber* construction:

$$\Delta\sigma_{ep}^{CA}\,\Delta\varepsilon_{ep}^{CA} = \frac{(\Delta\sigma_{el}^{CA})^2}{\bar{E}} \tag{6.11b}$$

where $\bar{E}$, A and β were taken at maximum temperature for this half of the cycle, which is typically the characteristic metal temperature for the SU transient, T_{SU}. $\bar{E}$ is a modified Young's modulus, $\bar{E} = 3E/2(1+\nu)$. The amount of reverse plasticity, ε_p^{CA}, is also important as it later

dictates whether for the following cycle the creep strain is aggregated (i.e. continuous hardening) or re-primed:

$$\varepsilon_p^{CA} = \left(\frac{\Delta\sigma_{ep}^{CA}}{A}\right)^{1/\beta} \tag{6.12}$$

The volumetric strain and thereafter the total strain range are calculated using the following steps:

$$E_s = \frac{\Delta\sigma_{ep}^{CA}}{\Delta\varepsilon_{ep}^{CA}} \tag{6.13a}$$

$$\bar{\nu} = \nu\frac{E_s}{\bar{E}} + \frac{1}{2}\left[\frac{1-E_s}{\bar{E}}\right] \tag{6.13b}$$

$$K_v = \frac{(1+\bar{\nu})(1-\nu)}{(1+\nu)(1-\bar{\nu})} \tag{6.13c}$$

$$\varepsilon_{vol} = (K_v - 1)\frac{\Delta\sigma_{el}^{CA}}{\bar{E}} \tag{6.13d}$$

$$\Delta\varepsilon_T^{unload} = \varepsilon_{vol} + \Delta\varepsilon_{ep}^{CA} \tag{6.13e}$$

The procedure of *symmetrisation* and finding the *reverse stress datum* (σ_{RD}) depends on the magnitude of the elastic-plastic stress range:

$$\sigma_{RD} = \begin{cases} \frac{1}{2}\left[\Delta\sigma_{ep}^{CA} + (K_sS_y)_{cold} - (K_sS_y)_{hot}\right], & \text{if } \sigma_{ep}^{CA} \geq (K_sS_y)_{cold} + (K_sS_y)_{hot} \\ (K_sS_y)_{cold}, & \text{otherwise} \end{cases} \tag{6.14}$$

where *hot* and *cold* refer to the temperatures at the cycle extremities, which are the SU and RT metal temperatures, T_{SU} and T_{RT}, respectively. It worth noting that Eq 6.14 for the reverse stress datum is correct only when the top peak of the cycle (trip) is colder than the bottom (start-up) - which is particular to the situation being examined in the case-study. In general, when the temperature at the trip peak may exceed that at start-up, Eq6.14 should be re-written by replacing 'cold' with 'RT' and 'hot' with 'SU'.

Thereafter, portion AB which describes the loading before the creep dwell is considered. Each cycle within the component history can be considered to be comprising of E_C discrete events, with a change from one to the next constituting a significant change in the dwell stress. For any given cycle (c), the elastic stress range for the first event ($e = 1$) is calculated based on the individual ranges of each stress component between a SU transient and the elastic stress state for this first event ($\sigma_{el}^{SO}|_{e=1}$):

$$\Delta\sigma_{el}^{AB} = \sigma_{el}^{SO} - \sigma_{el}^{SU}|_{e=1} \tag{6.15}$$

The starting creep dwell stress for the first event, $\sigma_B|_{e=1}$, is found by solving the following *modified* Ramberg-Osgood expression:

$$\frac{(\Delta\sigma_{el}^{AB})^2}{\bar{E}} = \Big[\frac{\sigma_B|_{e=1}+\sigma_{RD}}{\bar{E}} + \Big(\frac{2\sigma_B|_{e=1}}{A}\Big)^{1/\beta}\Big](\sigma_B|_{e=1}+\sigma_{RD}) \tag{6.16}$$

where A, β, and $\bar{E}$ were taken at the characteristic metal temperature for the current event, $T_{SO}|_{e=1}$. Subsequently, the creep relaxation portion of the cycle (BD) is approximated by implementing a creep strain stepping scheme to calculate the stress drop and the creep damage for each SO event within a cycle. This is based on dividing each event into small strain increments. For a generic cycle (c) and for the first event only ($e = 1$), the starting creep strain (ε_{cr}) for the first increment ($i = 1$) is contingent on the plastic strain from the unloading section of the previous cycle:

$$\varepsilon_{cr}^{i=1}|_{c,e=1} = \begin{cases} 1\times10^{-6} & \text{if } \varepsilon_p^{CA}|_{c-1} \geq 0.01\% \\ \varepsilon_{cr}^{i=I}|_{c-1,e=E_C} & \text{if } \varepsilon_p^{CA}|_{c-1} < 0.01\% \end{cases} \tag{6.17}$$

where $\varepsilon_{cr}^{i=1}|_{c,e=1}$ is the starting creep strain for the c^{th} cycle, and $\varepsilon_{cr}^{i=I}|_{c-1,e=E_C}$ is the creep strain accumulated at the end of the last event ($i = I$ and $e = E_C$) of the previous cycle. The first of the two conditions in Eq 6.17 represents *primary reset* were the creep strain restarts from a small amount of strain close, but not equal to zero. Not setting the creep strain to zero is a practical requirement as some creep deformation models produce singular creep strain rates at zero creep strain. If the creep strain is accumulated from one cycle to the next, then this would represent *continuous hardening*, which is an alternative assumption but can only be used when the loading is known to be elastic. Thereafter a predefined creep strain increment ($\Delta\varepsilon_{cr}$) is aggregated:

$$\varepsilon_{cr}^{i+1} = \varepsilon_{cr}^{i} + \Delta\varepsilon_{cr}^{i} \tag{6.18}$$

The creep strain rate, $\dot{\varepsilon}_{cr}^{i}|_{N,e=1}$, is then calculated using an appropriate creep-deformation model (e.g. RCC-MR [37] or HTBASS [82]) as a function of the instantaneous creep strain ($\varepsilon_{cr}^{i}|_{N,e=1}$), the prevailing SO temperature ($T_{SO}|_{e=1}$) and the instantaneous (relaxing) dwell stress ($\sigma_{cr}^{i}|_{N,e=1}$). At the start of a cycle, the latter is equal to σ_B^1 for that cycle. Based on the creep strain rate and the chosen creep strain increment (e.g. $\leq 1\times10^{-6}$ was adequately small for this work), the time increment is:

$$\Delta t^i = \frac{\Delta\varepsilon_{cr}^{i}}{\dot{\varepsilon}_{cr}^{i}} \tag{6.19}$$

If this time increment is larger than the remaining duration of the creep dwell for that event, then a smaller $\Delta\varepsilon_{cr}^{i}$ is applied, until an appropriate time increment is achieved. The remaining dwell duration is calculated based on the original duration of this event and the summation of time increments thus far. The stress relaxation is then calculated using:

$$\frac{Z}{\bar{E}}\Big(\frac{d\sigma_{cr}}{dt}\Big)^i = -\Big[\dot{\varepsilon}_{cr}^{i}(\varepsilon_{cr},\sigma_{cr}) - \dot{\varepsilon}_{cr}^{i}(\varepsilon_{cr},\sigma_{ref})\Big] \tag{6.20a}$$

(6.20b) $$\sigma_{cr}^{i+1} = \sigma_{cr}^{i} + \Delta\sigma_{cr}^{i} = \sigma_{cr}^{i} - \frac{\bar{E}}{Z}\Delta t^{i}\left[\dot{\varepsilon}_{cr}^{i}(\varepsilon_{cr},\sigma_{cr}) - \dot{\varepsilon}_{cr}^{i}(\varepsilon_{cr},\sigma_{ref})\right]$$

where σ_{ref} is the *reference stress*, which includes the effect of primary stresses only. Depending on the assessment, a fixed (conservative) value for the follow-up factor (Z) can be used, but for the special case where a Neuber approximation applies (i.e. near a stress raiser or the inner bore of a tube), an explicit approximation for Z as a function of stress drop during relaxation (see Session 34 in [80]) can be used:

(6.21) $$Z = \frac{2-(\Delta\sigma_{cr}/\sigma_B)}{1-(\Delta\sigma_{cr}/\sigma_B)}$$

where σ_B is the start-of-dwell stress for a given event and the $\Delta\sigma_{cr}$ is the stress drop from the start of that event (i.e. $Z = 2$ at the start of an event when $\Delta\sigma_{cr} = 0$). The instantaneous creep damage (d_{cr}) is determined using a ductility exhaustion model:

(6.22) $$d_{cr}^{i+1} = d_{cr}^{i} + \frac{\dot{\varepsilon}_{cr}^{i}\Delta t^{i}}{S_F^{i}\varepsilon_f^{i}}$$

where S_F is the Spindler fraction which accounts for triaxiality [90]. The uniaxial ductility, ε_f, is determined using an appropriate model: either constant, strain rate dependent, or strain rate and stress dependent ductility, with the first option being the one used for the case-study. Eq 6.18-6.22 are repeated for $i = 1 : I$ for the duration of the first event. For the following event ($e = 2$) within the same (c^{th}) cycle, the stress at the beginning of the this new event needs to account for the amount of creep stress drop from the preceding event ($e = 1$):

(6.23) $$\Delta\sigma_{dwell}|_{e=1} = \sigma_{cr}^{1}|_{e=1} - \sigma_{cr}^{I}|_{e=1}$$

The start of dwell stress for the next event ($\sigma_B|_{e=2}$) is firstly calculated using Eqs 6.15-6.16 but using the elastic stress state for the new event ($\sigma_{el}^{SO}|_{e=2}$). This new start of dwell stress ($\sigma_B|_{e=2}$) is then corrected to account for the relaxation due to the previous event:

(6.24) $$\sigma_B\prime|_{e=2} = \sigma_B|_{e=2} - \Delta\sigma_{dwell}|_{e=1}$$

where $\sigma_B\prime|_{e=2}$ is the new start of dwell stress to be used in the relaxation calculations for the new event. This approach for accounting for consecutive events ensures that if two consecutive events have the same stress state then the relaxation is continued without any change in dwell stress, which must be realistically the case. Thereafter, Eqs 6.18-6.24 are applied to calculate the creep damage for all subsequent events within the the same cycle, with the assumption that creep strain hardening is continuous between events in the same cycle.

The total strain range for the half cycle with creep needs to be adjusted for creep and volumetric effects:

(6.25) $$\Delta\varepsilon_T^{load} = \varepsilon_{vol} + \Delta\varepsilon_{ep}^{AC} + \Big[\sum_{e=1}^{E_C}\sum_{i=1}^{I}\Delta\varepsilon_{cr}^{i}|_e - \frac{1}{\bar{E}}\sum_{e=1}^{E_C}\sum_{i=1}^{I}\Delta\sigma_{cr}^{i}|_e\Big]$$

The elastic stress range for this half cycle is reduced due to creep relaxation:

$$\Delta\sigma_{el}^{AC} = \Delta\sigma_{el}^{CA} - \sum_{e=1}^{E_C}\sum_{i=1}^{I}\Delta\sigma_{cr}^{i}|_e \tag{6.26}$$

Thus by solving the following modified Ramberg-Osgood expression for the *forward stress datum* (σ_F):

$$\frac{(\Delta\sigma_{el}^{AC})^2}{\bar{E}} = \Big[\frac{\sigma_{RD}+\sigma_F}{\bar{E}} + \Big(\frac{2\sigma_F}{A}\Big)^{1/\beta}\Big](\sigma_{RD}+\sigma_F) \tag{6.27}$$

This gives σ_F, and thereafter the elastic-plastic stress range is:

$$\Delta\sigma_{ep}^{AC} = \sigma_{RD} + \sigma_F \tag{6.28}$$

The total strain range used to calculate the fatigue endurance and damage is the greater of the strain ranges for the two half cycles:

$$\Delta\varepsilon_T = \boldsymbol{Max}\Big[\Delta\varepsilon_T^{load}, \Delta\varepsilon_T^{unload}\Big] \tag{6.29}$$

Finally the total creep damage for this cycle is

$$d_{cr,total} = \sum_{e=1}^{E_C}\sum_{i=1}^{I} d_{cr}^{i}|_e \tag{6.30}$$

Fatigue damage calculation

The fatigue damage per loading cycle ($d_f|_c$) is calculated based on the number of cycles to fatigue failure, N_f, which is determined from experimental data as a function of applied strain range and temperature:

$$N_f = f(\varepsilon_T, T) \tag{6.31a}$$

$$N_i = N_f \exp(-8.06N_f^{-0.28}) \tag{6.31b}$$

$$N_g = N_f - N_i \tag{6.31c}$$

$$N_g' = NgM \tag{6.31d}$$

$$N_0 = N_g' + N_i \tag{6.31e}$$

$$d_f|_c = \frac{1}{N_0} \tag{6.31f}$$

where the adjustment factor M was found to be 0.187 if the initiated crack depth is taken to be $0.2mm$ (see R5 Volume 2/3 [23] Appendix A10 for details).

Finally, the whole procedure in this section is then repeated for all loading cycles ($c = 1:C$), and the total creep-fatigue damage at the end of life is:

$$D_T = \sum_{c=1}^{C} d_T|_c = \sum_{c=1}^{C}\Big[d_f|_c + d_{cr,total}|_c\Big] \tag{6.32}$$

6.3.3 Material Behaviour of 316H Stainless Steel

This section is devoted to summarising the key material properties which were treated stochastically as part of the probabilistic assessment. Unless otherwise stated, these properties were mostly obtained from [46] and previous work by EDF Energy on deterministically assessing the TP component. The general approach when treating material properties has been to incorporate as much statistical information as available, with the understanding that the process of including input parameter distributions is an iterative process. After a complete probabilistic assessment is constructed, a sensitivity analysis can highlight the most dominant material parameters, hence providing feedback for targeting these parameters in following iterations of assessment development. In the initial stages of formulating a probabilistic assessment, lack of material data does not preclude the conducting of an assessment, as this must be understood to be an iterative process which can be improved in later stages. This mentality attempts to avoid the wasting of effort in time consuming data gathering for parameters which may not dominate the output, whilst focusing on those that do. For most of the parameters considered in this section, normal and lognormal distributions were used, as these two distribution types were found to provide good stochastic representations and, therefore, Eq 3.10 applied [21].

Mechanical and thermal

Some of the main material properties which were considered stochastically, as well as those which were assumed to have fixed values, are outlined in Table 6.1. Figure 6.1 shows the best estimate (mean) values and the lower-upper bounds for some of these quantities for 316H stainless steel. These plots describe the general trends of theses parameters and their scatter bands as function of temperature. For 316H a key source of material properties is the R66 handbook which does supply some information with regards to uncertainty [46].

Creep

Creep damage was defined using a ductility exhaustion approach, which requires the definition of creep ductility, ε_f. In [46] it is suggested that the uniaxial creep ductility of 316H can be modelled using a single lognormal distribution for all loading temperatures under and including $550^{\circ}C$. This essentially assumes the independence of creep ductility from loading stress and creep strain rate. The BE and LB values were taken to be 10.7% and 2.6% respectively [39]. With the ductility being a non-zero quantity, it was judged appropriate to model it using a three-parameter lognormal distribution which incorporates a minimum value (x_0) in its formulation. This describes a parameter x for which $\log_{10}(x - x_0)$ follows a normal distribution. A minimum value of is quoted in [39], which was used along with the mean and standard deviation shown in Table 6.2 to fit the desired three-parameter distribution. Figure 6.2 shows a comparison of two fitted distributions using the two and the three-parameter configurations of the lognormal distribution. Using a

three-parameter option provides more control over the shape of the tail of the distribution as shown in Figure 6.3.3.

For creep deformation a relatively new model has been developed by EDF Energy as part of the High Temperature Behaviour of Austenitic Stainless Steels (HTBASS) project. This is referred to as the HTBASS creep deformation model and is given by [82]:

$$\dot{\varepsilon_c} = \exp\Big(-\frac{Q_p}{RT}\Big)(\varepsilon_c + D\varepsilon_p)^{(x_0+x_1T)}\sigma^{T^\beta} + C_0\exp\Big(-\frac{Q_s}{RT}\Big)\sigma^{(T/T_n)^\gamma} \tag{6.33}$$

where the numerical values for the various parameters are outlined in Table 6.3. The strains are in absolute values, stresses in MPa and temperatures in Kelvin. The standard deviation of $log_{10}(\dot{\varepsilon_c})$ was taken as 0.3805 [82] and, therefore, a lognormal distribution was fitted to model the uncertainty in creep deformation.

Fatigue

A polynomial fit was used to find the mean number of cycles to fatigue failure, N_f [97]:

$$\begin{aligned} N = A + BS + CS^2 + DS^3 + ES^4 + FT + GT^2 + HT^3 \\ + JT^4 + KTS + LTS^2 + MTS^3 + PTS^4 \end{aligned} \tag{6.34}$$

where $S = \log_{10}(\Delta\varepsilon_T)$ with $\Delta\varepsilon_T$ in absolute (not %), $T = \text{Temp}(^\circ C)/100$ and $N_f = 10^{N^{-2}}$. The lower bound value for N_f was estimated by reducing $\Delta\varepsilon_T$ by 25% for a given endurance as advised in [97]. These are valid for values of N_f up to 10^5 cycles.

Table 6.1: Summary of the mechanical and thermal properties treated stochastically in the probabilistic R5 Volume 2/3 assessment of the TP component [46].

Description	Parameter	Units	Assumed distribution
Elastic properties: Young's modulus and Poisson's Ratio.	E	GPa	Normal
	ν	-	Deterministic
. Tensile properties: the 0.2% proof stress and the shakedown factor.	S_y	MPa	Normal
	K_S	-	Deterministic
Cyclic properties: constants in a *Ramberg-Osgood* expression.	A	MPa	Normal
	β	-	Deterministic
Coefficient of thermal expansion.	α	$\frac{1}{^\circ C} \times 10^{-6}$	Normal

(a) Young's Modulus

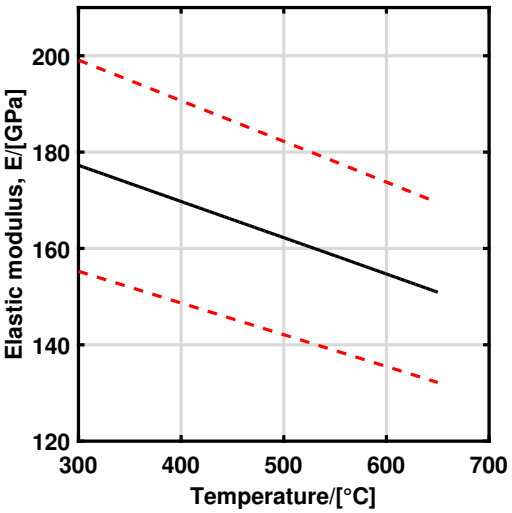

(b) Proof-stress

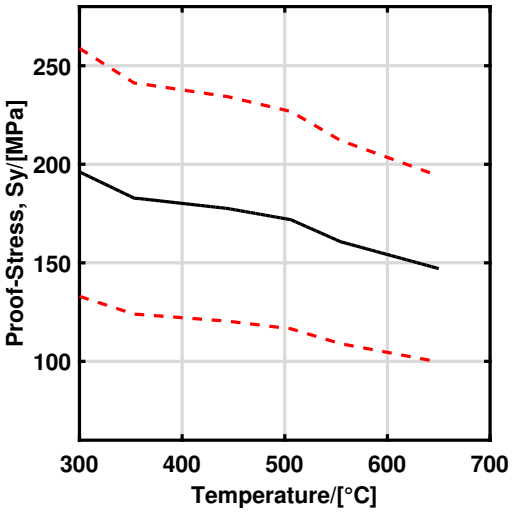

(c) Ramberg-Osgood coefficient (A)

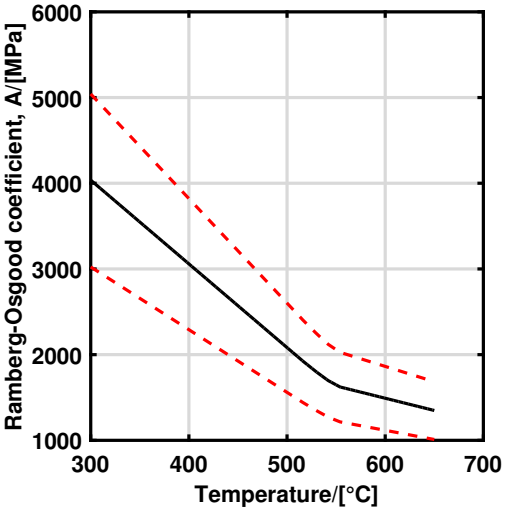

(d) Coefficient of thermal expansion (α)

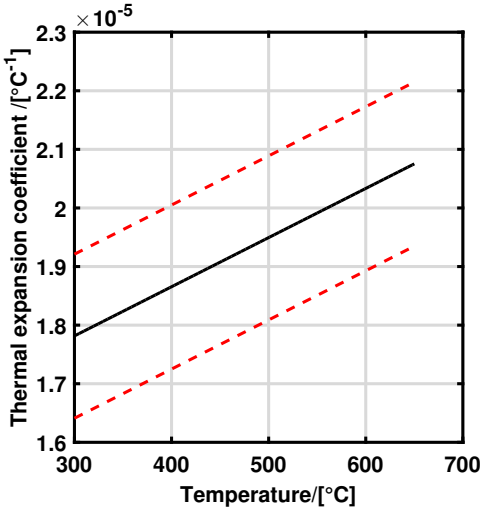

Figure 6.1: Plots of four parameters which were treated stochastically in the probabilistic assessment, with their best estimate values shown as functions of temperature (solid lines) along with their respective 95% confidence intervals (dashed lines).

Table 6.2: Statistical measures for the logarithm of creep ductility, $\log_{10}(\varepsilon_f)$, where ε_f is in percent. [46].

Mean	Standard deviation	Minimum value
1.029	0.299	0.231

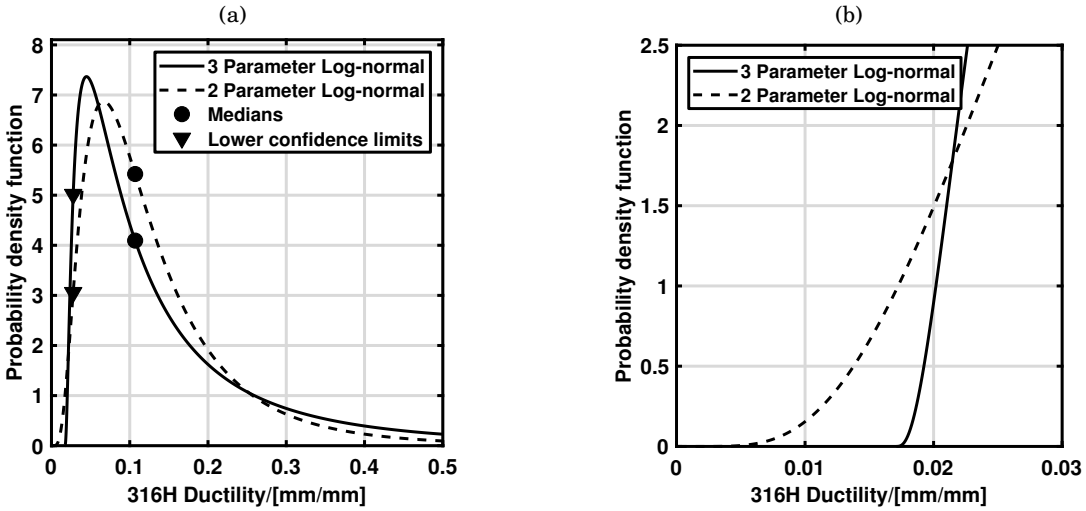

Figure 6.2: Shown in (a) is a comparison between using 2 and 3 parameter formulations of the lognormal distribution for modelling the uncertainty in creep ductility (ε_f). The two distributions have identical medians and lower-bounds. In (b) a zoomed-in view of the tails of the fitted distributions, highlighting that the 3 parameter lognormal provides more control over the location of the tail.

Table 6.3: Parameter values used in the HTBASS creep deformation model [82].

Q_p	R	D	x_0	x_1
474024	8.31446	9.19634×10^{-4}	-7.23794	5.08362×10^{-3}
β	C_0	Q_s	T_n	γ
0.261108	$10^{24.7512}$	773904	4194.56	-1.28005

6.3.4 Results and Discussion

6.3.4.1 Deterministic Results

Conducting a deterministic calculation is an initial stage of developing a probabilistic assessment. In this work, a deterministic assessment assumes all input parameters are set at their median values. All 37 TP tubeholes were examined and the deterministic damage results are shown in Figure 6.3. Whilst all tubeholes' damages were less than unity, it is apparent that a number of tubeholes incurred substantially larger damages than others; tubeholes 2 and 29 had the most severe damages. For clarity, all assessment results (deterministic and probabilistic) are associated with a specific point on the surface of each tubehole. Therefore, the damages shown in Figure 6.3 are associated with what are believed to be the most damaged points on each tubehole. In a traditional approach, such results could perpetuate a misleading belief that assessment locations which do not incur damages larger than unity will have zero PoI. However, a probabilistic mindset would reject such notion as the deterministic calculations do not account for the degree of scatter in the inputs as well as the damage output. Accordingly, a small damage does not always translate to a zero PoI. Nevertheless, it should be expected that the tubeholes which have larger damages would also be the most probable to initiate. Therefore, the deterministic damages give good insight as to which tubeholes to prioritise when conducting probabilistic assessments.

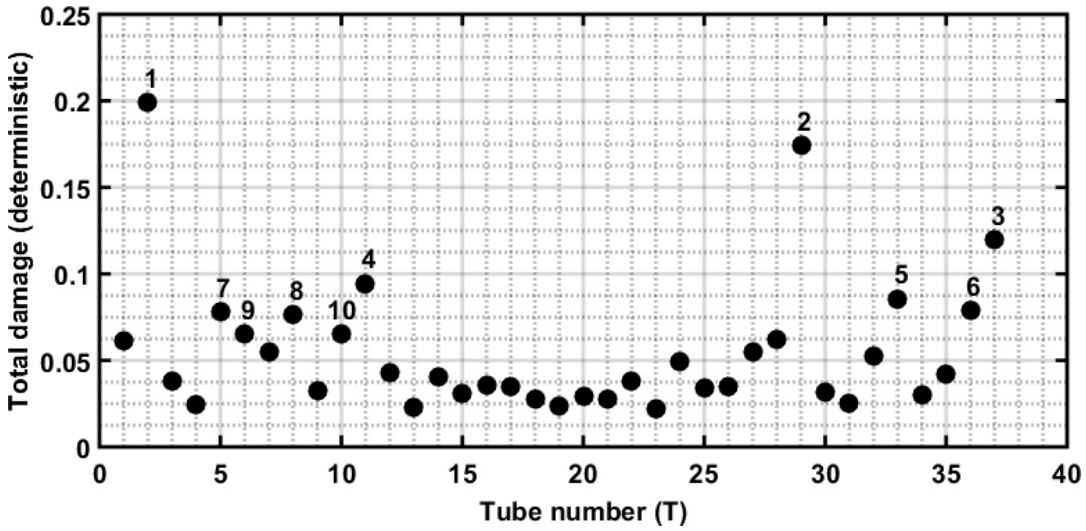

Figure 6.3: Total damage results of all 37 tubeholes using the deterministic (all parameters fixed at median values) assessment. The numbers indicate the order of the most damaged tubeholes from highest to lowest total damage.

6.3.4.2 Results for Individual Assessment Locations

For a single assessment point, one key probabilistic result is a histogram of the total creep-fatigue damage obtained from the N number of MCS trials conducted, an example of which is shown

in Figure 6.4. The constituents of the total damage are also presented separately to show that creep dominates the total damage, D_T, as indicated by the fatigue damage being relatively small. Thereafter, the PoI was calculated as the fraction of the total N trials that led to a damage greater than or equal to unity, as represented by Eq 6.2. The PoI of individual assessment locations can be tracked as the simulated history progresses, which is shown in Figure 6.5. Logically, for some initial period, no initiations would be expected, which was observed. Figure 6.5 also shows that once initiations start to occur, an initial jump is predicted. As will be discussed later, creep ductility and deformation are two dominant inputs. Therefore, the substantial jump at the start was attributed to trials which had fast creep rates and/or small ductilities, as these would be expected to initiate first. After these early groups of crack initiations, the subsequent increase in the PoI was gradual which mirrors the progressive accumulation of damage.

Convergence was also investigated, with Figure 6.6 showing an example of the convergence of the PoI and the median predicted damage for tubehole 29. For this tubehole it was judged that $N \geq 10^5$ gave adequate estimates. Figure 6.6(a) also highlights the fact that the estimated PoI is a random output, as it always has a degree of uncertainty which depends on the number of trials. For later calculations which involve component and population-level estimates (e.g. PoI_C and N_{CC}), an analysis can be conducted to assess their sensitivity towards the uncertainty in the PoI of individual assessment points. Such analysis was not conducted for this work. However, as later discussed, a small number of assessment points usually dominate the component-level probability and, therefore, it would be expected that estimating the uncertainties associated with these dominant points would suffice. Moreover, the validity of Eq 6.5 was examined by comparing its estimates for the coefficient of variance of PoI (i.e. ϵ) with its equivalent based on repeated runs. This comparison is presented in Figure 6.7, which shows good agreement between the two estimates, therefore suggesting Eq 6.5 can provide a significantly less time consuming alternative to executing repeated runs of the MCS.

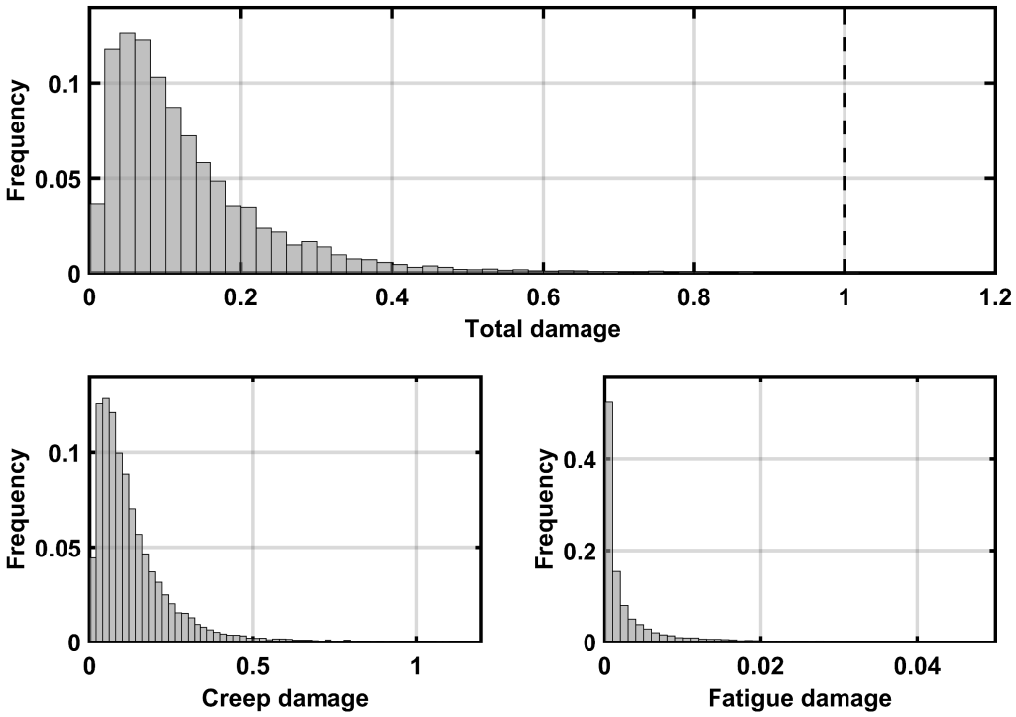

Figure 6.4: Example histograms of probabilistic damage results for a single assessment location. The criterion for creep-fatigue crack initiation is defined by $D_T \geq 1$ which also dictates the PoI (see Eq. 6.1). To clarify, there are some data at damages above 1, but too few to be visible on the histograms.

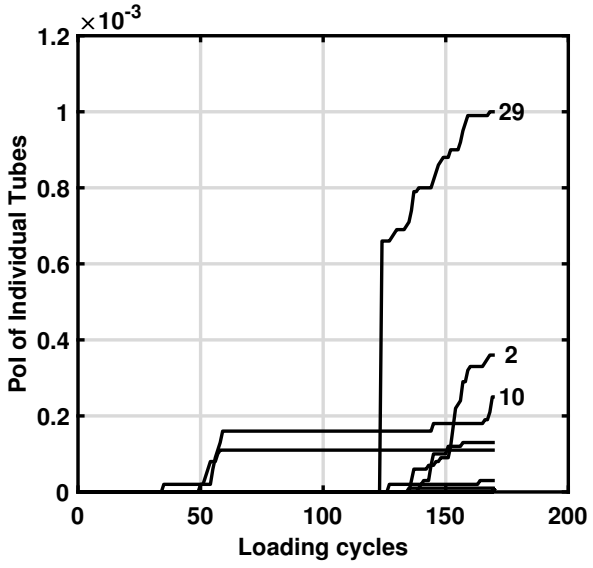

Figure 6.5: The evolution of the PoI for individual tubeholes during the simulated history ($\approx$ 170 loading cycles), with each line representing the results from a MCS per tubehole. The three most probable tubeholes to initiation a crack were 29, 2, and 10 as labelled.

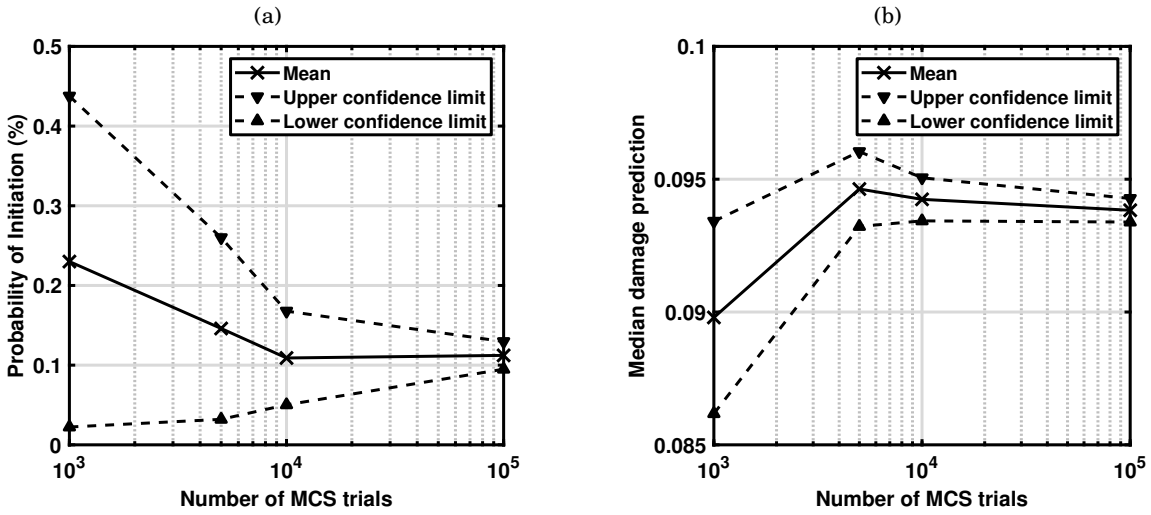

Figure 6.6: Convergence of (a) the PoI and (b) the median damage predictions for an individual assessment location (tubehole 29). The uncertainties (i.e. upper-lower limits associated with a 95% confidence interval) were estimated by examining the results obtained from repeated runs of the MCS and calculating standard deviations.

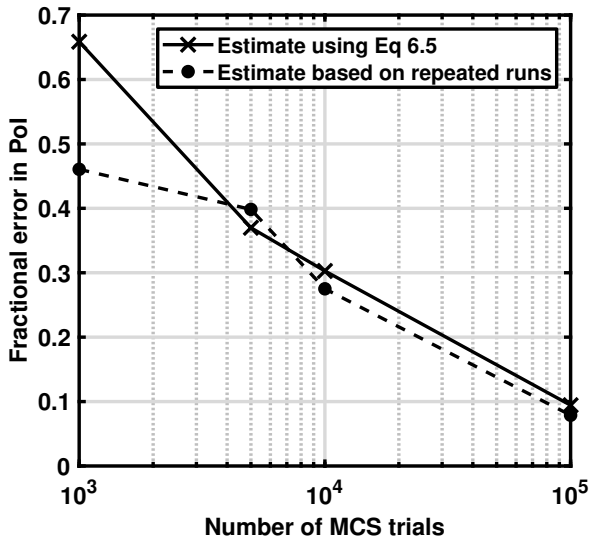

Figure 6.7: Comparison between two estimates of the error associated with the predicted PoI as a function N.

6.3.4.3 Sensitivity Analysis Results

Based on the concepts presented in Section 3.4.6, a number of calculations were conducted to assess the sensitivity of the output damage results towards various input conditions. Firstly, sensitivity measures were calculated using the four approaches detailed in [9] to assess the domi-

nance of all stochastic inputs. The easiest of the four approaches is the correlations based method, as it can be conducted with the results from a single MCS run and a Spearman correlations can be used. This is particularity useful in the development stage of a probabilistic assessment, but when using a small number of MCS trials (N) there is an inherent uncertainty with the SA results using this method. This stems from the fact that the smaller N is, the higher the chance of a Spearman correlation having arisen by complete chance, as shown in Figure 6.8 and detailed in Table 6.4. The complete set of SA results is shown in Figure 6.9, which indicate that creep ductility and deformation dominate the probabilistic damage results. This is consistent with the observations in [9] which looked at a similar but much simpler assessment.

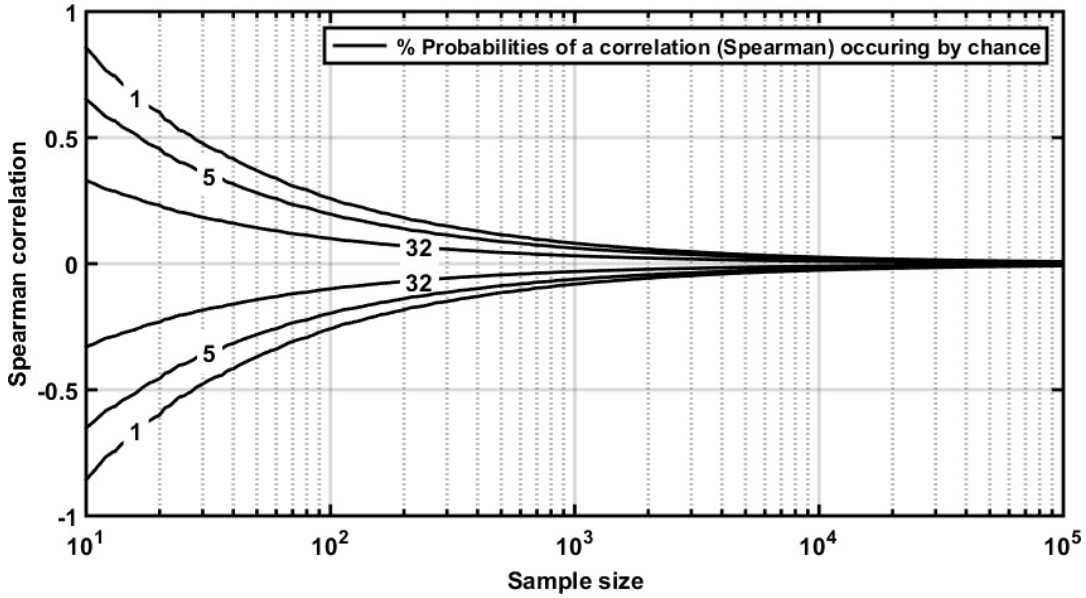

Figure 6.8: Uncertainty in correlation based SA results as a function of sample size (i.e. number of MCS trials, N) .

Table 6.4: Percentage confidence levels on calculated Spearman correlations (in %) as functions of sample size. For example, for a sample size of 10^3, there's a 95% change of a Spearman correlation $\leq$ 6.162% to have arisen by chance.

.

		Confidence level (%)		
		68	95	99
Sample size	10^1	33.07	65.18	85.66
	10^2	9.983	19.7	25.83
	10^3	3.128	6.162	8.097
	10^4	0.9935	1.955	2.57
	10^5	0.3142	0.619	0.8135

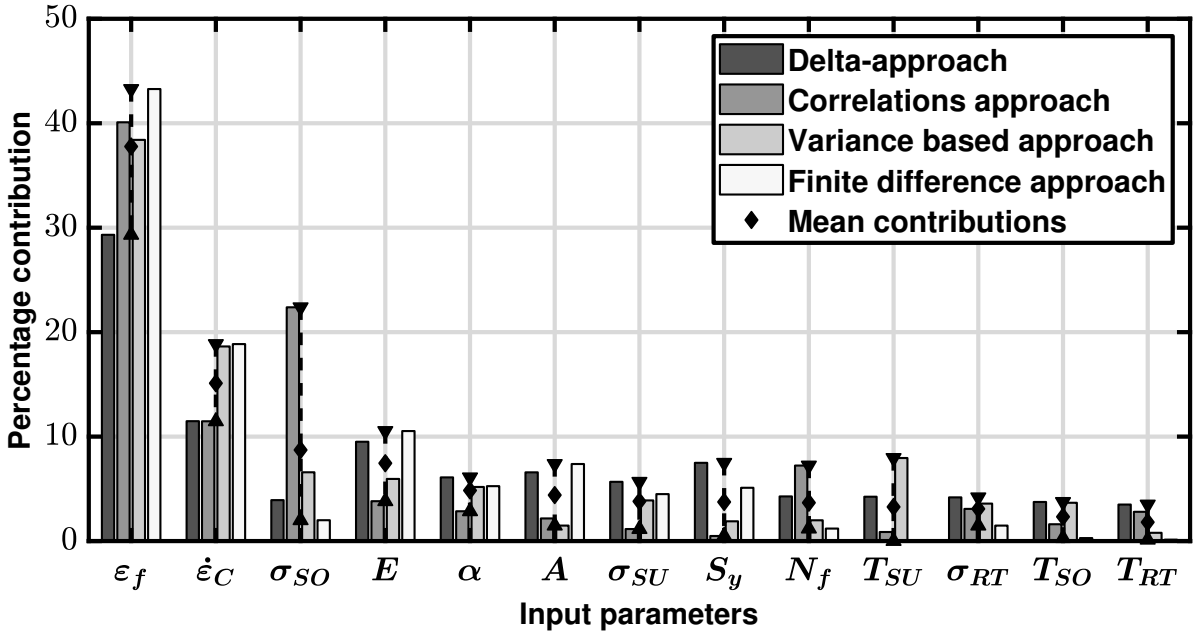

Figure 6.9: Sensitivity measures (contributions towards output uncertainty) based on four approaches, showing the comparative influence of 13 stochastic inputs towards the probabilistic damage results for a single assessment point.

In this work all input parameters were assumed to follow specific probability distribution types (mostly either normal or lognormal). However, the SA results presented in Figure 6.9 can provide focus for investigating whether better statistical representations of some input parameters are likely to yield significant changes in the results. With creep ductility (ε_f) being a crucial input, it was judged important to investigate the effect of using different parameter distributions. The following is a discussion of the benefit of using a three-parameter probability distribution which incorporates a minimum value (x_0) in its probability density equation. Figure 6.2 shows two PDFs for ductility, one of which uses a 3-parameter formulation. The overall effect on the output damage PDF was modest, however, using a 3-P lognormal resulted in a lower estimate for the PoI as highlighted in Table 6.5. Including a minimum value is logical within the context of ductility, as it is a positive non-zero number and the tail of the distribution is defined by a minimum value. Given the strong influence of ductility on the assessment results, it is compelling that including a minimum value can non-trivially reduce the estimated PoI. Furthermore, these observations corroborate the results in Figure 6.9 by indicating that creep ductility can significantly affect specifically the estimated PoI. Though this was not investigated, it is expected that the use of a more complex ductility model incorporating strain-dependency would produce substantial benefits, i.e. reduction in estimated damage, and is suggested as future work.

As discussed in Section 3.4.6, assessing sensitivity can also be done with respect to the various

Table 6.5: Comparisons between the $PoIs$ from two assessments using two-parameter (2-P) and three-parameter (3-P) configurations of the lognormal distribution for the input creep ductility (ε_f).

Assessment location	PoI (2-P)	PoI (3-P)
Tube 2	1.0×10^{-3}	0.6×10^{-3}
Tube 29	1.4×10^{-3}	1.3×10^{-3}

assumptions involved in the underlying assessment. When conducting a creep damage assessment a judgement needs to be made as to whether creep strain (though not creep damage) resets at the start of each loading cycle (full primary reset, PR) or whether it continuously aggregates throughout the loading history (full continuous hardening, CH). This assumption is represented by Eq 6.17 in the deterministic assessment. The former assumption produces larger damages because more time is spent in the primary creep stage (which is characterised by faster creep strain rates) as a fraction of the component lifetime. Typically PR is more appropriate when there is significant reverse plasticity at the end of each creep dwell. Most commonly though, a real situation is somewhere in between, as some cycles might lead to full primary reset due to large plasticity while others might unload elastically. A model has been recently developed to model the amount of creep strain re-priming as a function of plastic strain, which is termed the ζ_P model for creep hardening, though it is still under development [98].

The results can be sensitive to which assumption is used, and it is challenging to make a judgement without producing the results using both assumptions. Figure 6.10 shows the probabilistic damage results for a single tubehole, which shows the effect of using the three available options for creep hardening. As expected, there is a significant difference between using PR and CH, with the former producing larger damages, and by extension larger probabilities of initiation. Comparing the results for PR and the ζ_P model indicates that assuming PR is not excessively conservative and is closer to the ζ_P situation which is believed to be more realistic. This is a result of significant reverse plasticity being incurred which has been confirmed separately from the hysteresis cycle construction.

The main conclusions from this sensitivity study are that the assessment results are sensitive to the choice of hardening assumption and trialling with the ζ_P model provided valuable insight as to which assumption is more appropriate. The results indicate that PR is an acceptable assumption for assessing the TP, while incorporating the ζ_P model would be of limited benefit. Noteworthy is that the results presented in this work were all obtained using PR, unless stated.

The final aspect of sensitivity which was explored related to correlations between input parameters. A key correlation that was accounted for in this work was the correlation between

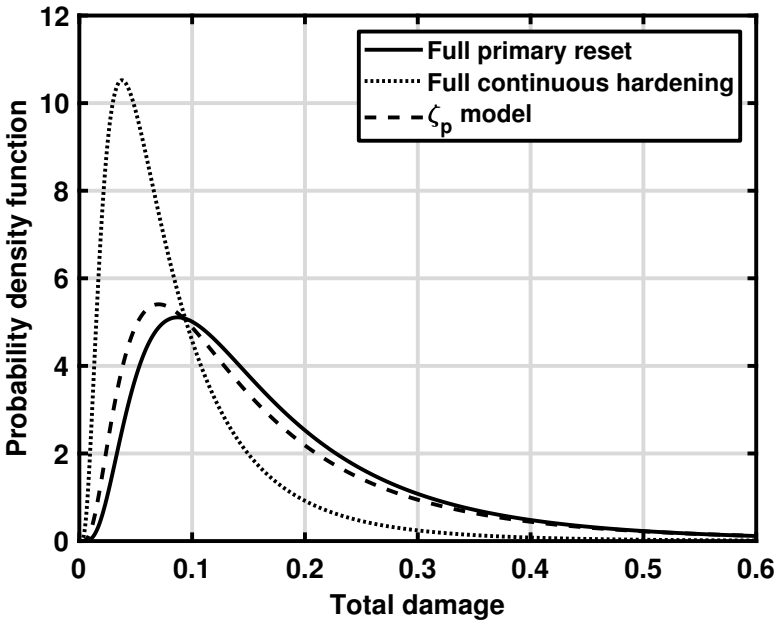

Figure 6.10: Comparison between probabilistic results for a single assessment point on the tubeplate, using three assumptions for creep hardening.

creep ductility and creep deformation. The importance of this correlation is corroborated by the results in Figure 6.9, as any correlations between dominant inputs are likely to have an effect on the out results. A single value correlation of 54% was used, which is the mean value found in [99] based on material data for 316H. Nevertheless, this correlation remains uncertain. A sensitivity study was conducted to examine the effect that varying this correlation has on the probabilistic assessment results. This was achieved by conducting a sequence of probabilistic assessments using the full range of possible (positive) correlations. The results of this study are shown in Figure 6.11, which show that this correlation does indeed have a significant effect on the PoI. This results from larger correlations reducing uncertainty and therefore scatter in the output damage results given by the MCS (see Figure 6.11(a)).

This case-study used a single value correlation in spite of the fact that this correlation was found to follow a normal distribution in [99]. However, an investigation was conducted to reveal the validity of such approach, which entailed trialing with a fully uncertain correlation as compared with using a single value. Implementing a fully stochastic correlation can be done as follows:

1. Sampling the correlation distribution, say N_c samples are drawn (all equally probable) where N_c has to be orders of magnitude smaller than the number of MCS trials, N.

2. Samples for each creep parameter are produced (N samples each), which are subsequently divided into N_c sub-samples.

3. Sub-samples from each parameter are paired and correlated according to each of the N_c sampled correlations.

Thereafter, the samples produced using stochastic and single value correlations were compared by virtue of scatter plots of ductility against creep rate, and by computing the *net* correlations for the two cases. This analysis revealed that the two approaches had virtually the same net correlation value which converged to the mean (54%) as larger samples were produced. This proves that using a single value correlation for a probabilistic assessment is not only simple, but also adequate and justifiable.

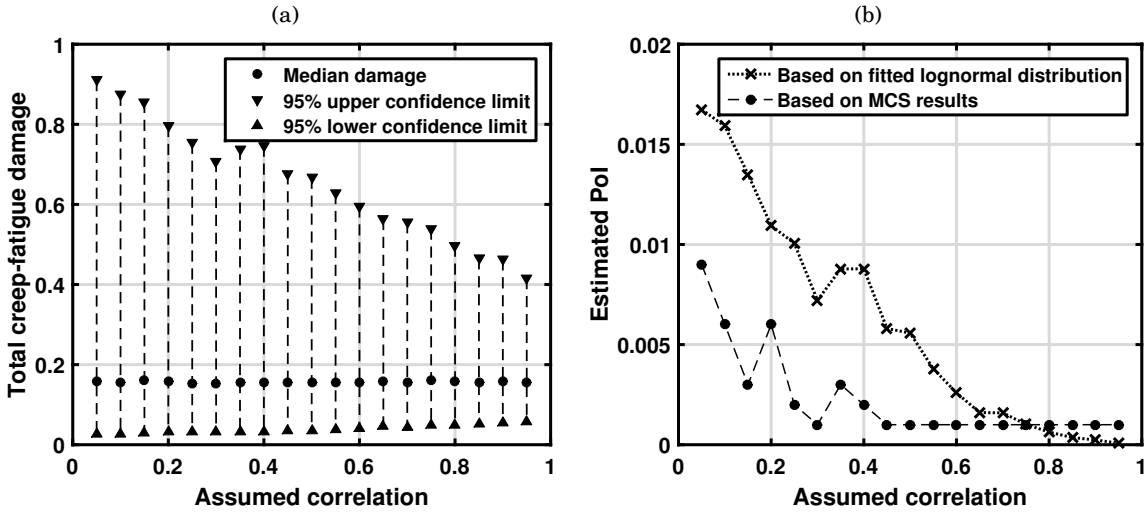

Figure 6.11: Plots showing the sensitivity of the probabilistic damage results towards the correlation between creep ductility and deformation. Larger correlations produce less scattered results and, as a result, lower $PoIs$.

6.3.4.4 Component-Level Results

Based on the methods discussed in Section 6.2.2, PoI_C which is the probability of having at least one crack initiation in the whole TP can be estimated from the $PoIs$ of individual tubeholes. The tubeholes which dominate PoI_C can be identified by counting the number of times each tubehole led to the first crack initiation. For the TP, the percentage number of times that each dominant tubehole led to cracking is shown in Figure 6.12, which provides a quantitative measure of dominance. Thereafter, PoI_C was calculated using Eq. 6.8, which assumes the independence of the non-dominant assessment locations but uses PoI_{JC} as the *joint* probability for the dominant ones. As a result, Eq. 6.8 assumes *partial* independence of the assessment locations. An estimate for PoI_C was also calculated using Eq. 6.6, which assumes *complete* independence of all tubeholes, and therefore is more conservative. A summary of these results is shown in Table 6.6. Furthermore, to assess the collective influence of the non-dominant tubeholes,

PoI_C was also calculated with and without their contribution as detailed in Table 6.6. These results suggest that such influence is rather subtle. Finally, the best estimate for PoI_C was 0.19 which accounts for all tubeholes and assumes partial independence.

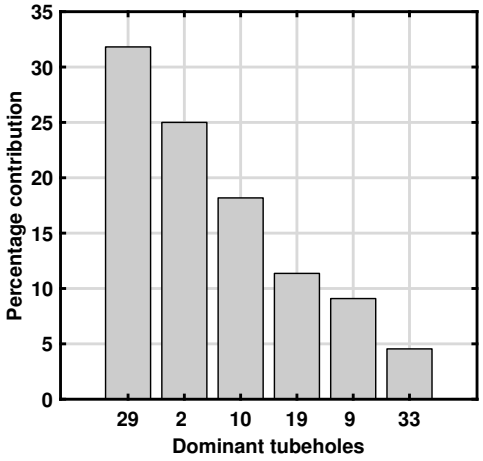

Figure 6.12: A breakdown of the percentage number of times each of the dominant tubeholes led to the first crack initiation across the whole tubeplate.

Table 6.6: Comparison of estimates of the component-level probability of initiation (PoI_C) based on assuming complete versus partial independence of the individual tubeholes, and based on considering the dominant tubeholes only (see Figure 6.12) versus all tubeholes.

Independence	PoI_C in %	
	Including dominant tubeholes only	Including all tubeholes
Complete	0.19	0.22
Partial	0.16	0.19

6.3.4.5 Population-Level Results

As discussed in Section 6.2.3, based on PoI_C a prediction can be made as to the number of components which have at least one crack initiation, N_{CC}, given a population of N_{TC} components. All components are assumed to be identical and have the same PoI_C and, therefore, N_{CC} follows a binomial distribution prescribed by Eq. 6.9. Note that this is not physically indicative for the real plant case, where some components will be less severely stressed or cycled than others. Therefore, the calculations herein are for illustration only, and will bound the real situation. Figure 6.13 shows the binomial PDF and CDF using the current estimate for PoI_C and $N_T = 128$ which is the total number of tubeplates in operation. One way to interpret these results is by examining an upper-bound value of N_{CC} (e.g. the 95% value), which in this case is 1. This means

that there is approximately a 95% probability of $N_{CC} \leq 1$.

What can also be of interest is the approximation of an acceptable PoI_C by the end of service given a target upper-bound N_{CC} (which can be demanded by safety regulations). An example of such acceptance limits on PoI_C as functions of the upper-bound N_{CC} is shown in Figure 6.14, where the ranges shown are those required to ensure a level of confidence $\geq 95\%$. This signifies that to ensure a probability of at least 95% that N_{CC} is zero, then $PoI_C < 0.04\%$ must be achieved, while for $N_{CC} = 1$ a range of $0.04 \leq PoI_C < 0.26\%$ must be demonstrated for the same minimum confidence level. These ranges follow from the binomial distribution being discreet in nature, which only provides probabilities for integer values of N_{CC} and, therefore, there exists a range of PoI_C that would yield the same upper-bound N_{CC}. Hence the ranges in Figure 6.14 ensure a confidence limit of 95% *or larger*.

6.3.5 Further Case-Study Development

For the tubeplate case-study a number of aspects that require further development have been identified:

1. **Ductility:** Adopting a rate dependent ductility (e.g. a SMDE model) would be expected to produce less conservative probability estimates in contrast with the currently used creep rate independent ductility approach. Furthermore, with reference to using a three-parameter distribution to statistically model ductility, reconsidering the ductility cutoff (currently at 1.7%) may be needed.

2. **Extend modelled operational history:** Currently the simulated history spans the period between 1984 and 2014, as plant measurements were available for that period. However, since this work has been concluded some further data up to 2018 have been issued, and it would be advisable to include that data in the probabilistic assessment. Moreover, a projection of future plant operation may be required to estimate the probabilities of initiation at 2024, which is the currently expected end-of-service for the tubeplate given the current accounting life of the power station in question.

3. **Modelling other identical tubeplates:** All results in this work are related to a specific tubeplate, as it was advised that the damage incurred in this tubeplate is likely to bound the damages of other identical tubeplates (there are 128 tubeplates in total). Accordingly, it might be of interest to model other tubeplates using their associated plant data.

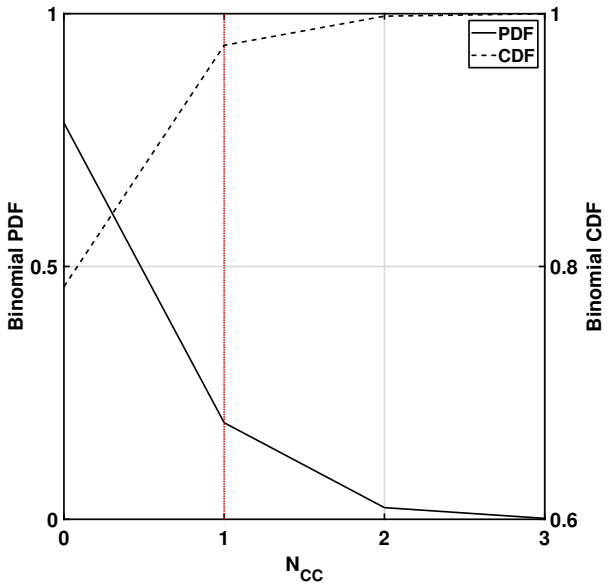

Figure 6.13: Binomial distribution (see Eq. 6.9) for a population of components of $N_{TC} = 128$ given that $PoI_C = 0.19\%$. The solid line (PDF) is the probability of having exactly the stated number of cracked tubeplates across the fleet of 128. The dashed line (CDF) represents the probability of having N_{CC} cracked tubeplates or fewer. The dotted vertical line denotes the 95% upper limit, highlighting the upper-bound value for N_{CC}, which in this case indicates that there is a 95% probability of there existing 1 cracked tubeplate or less.

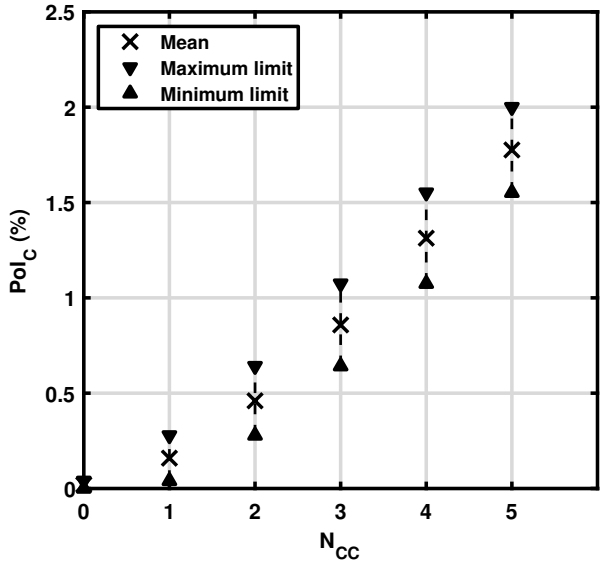

Figure 6.14: The required PoI_C corresponding to there being N_{CC} cracked tubeplates at a confidence level $\geq 95\%$. The maximum limits on PoI_C correspond to a confidence limit of roughly 95%; results are based on a population of $N_{TC} = 128$ components.

6.4 Summary

In general, a probabilistic framework integrates various sources of uncertain knowledge (some epistemic and other aleatory in nature) in order to infer the the state of a complex occurrence (e.g in this chapter the creep-fatigue crack initiation in a plant component was examined). The limitations and assumptions inherent in the input sources of information must be understood to be aggregated and inherited by the probabilistic framework and, therefore, the level of confidence in a given probabilistic estimate (e.g. the probability of failure) is invariably a reflection of the confidence held in each facet of the input knowledge. For instance, the results of a probabilistic structural integrity approach invariably depend on the validity of the underlying physics of failure models (often formalised by assessment procedures, codes and standards). However, if some elements of the required knowledge (e.g. the physics of failure models) are not perfect, this must not be taken to preclude the development of the probabilistic approach. On the contrary, a probabilistic approach must be viewed as the framework by which any given input uncertainty involved within an application can be examined and perpetually improved through focusing efforts on gaining and developing pertinent knowledge and data. The case-study in Chapter 3 provided an example of such endeavours, where a uniaxial specimen under controlled creep-fatigue testing conditions was assessed using a probabilistic model (noting that the failure probability was known because the specimen was taken to failure). The results from that case-study gave insight as to the performance of the underlying assessment procedure (R5 Volume 2/3). For example, by making use of the experimental stress data, examinations of the epistemic uncertainties introduced by important aspects of the procedure (the processes of hysteresis cycle construction and the estimation of creep relaxation) were possible. However, for the case-study examined in this chapter, such examinations were not possible because the probability of failure was unknown.

As a result, developing a probabilistic model must be understood to be an iterative process, where gaining confidence in the probabilistic estimates involves the improvement of the model constituents (e.g. improved characterisation of material properties, more complex stress modelling or more representative failure models). In essence, the process of validating a probabilistic model involves validating and improving its constituent elements. Verification exercises of prospective probabilistic methodologies can only be done for controlled case-study applications e.g. examining failed specimens that were subjected to controlled test conditions (similar to the case-study in Chapter 3) or assessing in-service components that have had histories of failures due to operation. Therefore, probabilistic approaches are likely to play a key part in the perpetual development of our general structural integrity understanding through verifiable case-studies, a topic which has been identified as an important area of further work. This will aid in gaining confidence in the probabilistic structural integrity methodologies and, consequently, more confidence in their implementation on more uncertain applications, for example in the context of plant components and systems.

This chapter built on the various topics introduced in Chapters 3 to 5, formulating a complete methodology which can potentially be applied to any structural integrity application, whilst giving a high-temperature creep-fatigue example for contextualisation and demonstrating its implementation. This methodology incorporates systematic methods for the management of uncertainties, from inputs to outputs. The most prominent of these probabilistic concepts included Monte-Carlo Simulations, latin-hypercube sampling, sensitivity analysis, correlations between creep properties, treatment of loading uncertainties and the extrapolation to component and population level estimates. The presented case-study demonstrated the proposed probabilistic methodology by showing how knowledge in the form of:

1. a creep-fatigue crack initiation procedure,
2. stochastically treated input parameters,
3. formulated and tested physics of failure models and assumptions,
4. a clearly defined probabilistic methodology, and
5. expertise in a high-level coding language

can aggregate into probability estimates of hierarchical elements: individual assessment points within a component, a component and a population of components. The effectiveness and utility of the methodology is especially pronounced for plant applications with their complexity lending itself well to statistical paradigms.

CHAPTER 7

CONCLUSION

This thesis concludes with the key arguments and ideas that have been explored in this PhD project. Also included is a reflection on the research methodology and suggested improvements for promoting wider implementation by interested practitioners. Finally, areas of further work are identified and suggested for the progression of this body of work.

7.1 General Conclusions

The Relevance of Probabilistic Techniques

Probabilistic techniques are unequivocally compatible and applicable to any structural integrity methodology that is prescriptively procedural in nature, whether it concerns aspects of design or fitness-for-service assessment. Furthermore, the case for probabilistic implementation is especially strong and compelling for applications where complexity and substantial uncertainty are inherent, thus requiring systematic approaches for examining and incorporating these aspects into structural integrity analyses. The techniques reviewed in this thesis have been applied to case-studies concerning creep-fatigue crack initiation. However, the application in itself is purely incidental, as these probabilistic techniques can be transferred to any structural integrity analysis by conceding that uncertainty is itself a form of knowledge that must be incorporated. As a result, probabilistic implementation is expected to have important implications for safety and decision making exercises.

The adoption of probabilistic approaches is intended to provide more confidence in structural integrity procedures and associated results. This is achieved firstly by examining and accounting for numerous sources of uncertainty, but also making full use of available data and state-of-the-

art understanding of the physics of failure. Probabilistic approaches must not be considered an alternative to conventional deterministic calculations, but rather a completely different, more realistic and often liberating mindset which embraces complexity and uncertainty rather than simplifying and often obfuscating them in favour of conservatism. Accordingly, they can be considered an evolution of traditional deterministic approaches, which have emerged from the reconciliation of statistical methods and physics of failure modelling, aided by advances in computational tools and hardware. The general case for adopting probabilistic approaches for structural integrity applications was detailed in Chapter 3, which included the main modes of application, the potential (and significant) benefits as well as the challenges involved. For implementing probabilistics within structural integrity there are various facets of knowledge required [10]:

1. Understanding of the underlying physics of failure.

2. A general appreciation of probabilistic approaches and statistical concepts, coupled with the ability to relate these to a physical issue of interest.

3. Knowledge related to component geometries, loading histories and material properties.

4. Computational experience to be able to produce efficient algorithms.

5. Predefined target reliabilities related to the levels of tolerable frequencies of failure for specific components of interest.

A key objective of this work was to supply a complete methodology which can potentially be applied to any structural integrity application, whilst giving a high-temperature creep-fatigue example for contextualisation and demonstrating implementation aspects. This methodology incorporates systematic methods for the management of uncertainties, from inputs to outputs. The effectiveness and utility of such methodologies become especially significant for plant applications, with their complexity lending itself well to statistical and probabilistic paradigms. Therefore, the purpose of current and future work is to promote a shift from over-conservative deterministic assessments towards a probabilistic framework, the aim of which is to identify, quantify and incorporate real-life uncertainties in structural integrity methodologies. The vision is to bridge the gap between the knowledge of statistical and probabilistic methods on one side, and the general structural integrity community on the other end. By promoting further implementation and engagement, the methodology will mature and emerge to be more extensive as well as coherent, which in turn will aid further acceptance within a wide range of structural integrity fields, thus promoting a unified probabilistic framework for structural integrity.

The Variety of Probabilistic Techniques

Numerous probabilistic techniques, approaches and methods can be introduced at various stages of a structural integrity methodology, which serve myriad purposes. However, there are often multiple alternatives that can be implemented at each stage. This thesis highlighted the main probabilistic approaches that would be needed to translate a procedure (i.e. a performance function) coupled with uncertain input parameters, models and assumptions into a desired stochastic output, from which probability estimates can be inferred. Nevertheless, this thesis was not intended to be an exhaustive review of everything probabilistic, but rather an attempt to demonstrate their integration. Still, an effort was made to review all the required tools and techniques that would be needed to conduct a full assessment using the Monte-Carlo method; these in essence being the building blocks of a general methodology. The key aim was to formulate an initial iteration of a prospective unified probabilistic methodology, which is intended to require further research and greater involvement of interested stakeholders.

Current Challenges to Probabilistic Implementation

When coupled with structural integrity methodologies, probabilistic methods produce more information (output data), valuable insight, measures of uncertainty (in inputs and outputs) and probability estimates when compared with their more traditionally employed deterministic counterparts. The main case for probabilistic implementation within structural integrity was presented in Chapter 3. It transpired that the added benefits come with significant challenges which require adequate consideration by practitioners and interested organisations. Associated with probabilistics, these are clear facets of utility, applicability, challenge and limitation, and it is imperative that these must be understood and appreciated in order to reap the potential benefits.

Probabilistic methodologies also produce results that need interpretation, a task which requires familiarly and experience in itself. Consequently, it has been acknowledged that probabilistics require significant time, effort, cost and knowledge. However, these requirements will become substantially less onerous as a result of consolidating the knowledge required. Most of the tools needed are already available in the public domain for little, or even no, cost and are being used in numerous industries. Nevertheless, substantial thought must be devoted to bringing practitioners up to a baseline level of understanding and awareness of probabilistic and statistical concepts through training and provision of verified supporting documentation. This will also have the benefit of continuously developing and evolving probabilistic structural integrity methodologies through feedback on use and verification, thus promoting the emergence of a unified approach. Investments in such developments will also be offset by the availability and use of probabilistic models aiding timely and informed decision making, whilst keeping safety

and reliability as paramount priorities.

There is a clear interest in the nuclear sector, as partially evidenced in the supporting and involvement of EDF Energy in this project, for formally incorporating probabilistics into structural integrity methodologies. The proposed implementation strategy is to start with the examination of component level probabilities, and linking these to populations of the same components and system comprising multitudes of components. Within nuclear structural integrity, the two most common areas of application are design of new assets and fitness-for-service assessments (including safety compliance and life-extension purposes) for in-service plants, while an interest for has also been expressed by decommissioning practitioners [100]. This sector wide interest provides an opportunity for the development of a unified probabilistic methodology for the life management of nuclear plant assets potentially throughout their life cycle.

A key challenge will be in demonstrating the validity of the probabilistic approaches to regulators, which in the UK have shown a degree of reluctance. It can be argued that if industry and academic stakeholders build a consensus on formalising a unified probabilistic structural integrity approach, that is transparent, accountable and undergoing perpetual development, in time the air of scepticism and perplexity surrounding this topic will be lifted, thus promoting wider acceptance, implementation and validation efforts. The current state of affairs in the UK is such that probabilistic implementation may be hindered by lack of sanction for their use in nuclear safety cases by the regulatory bodies, though there have been exceptions for graphite core applications in the past. Nevertheless, probabilistics still have clear benefits as they provide insight into major areas of uncertainty. In this thesis, a major example took the form of providing feedback for targeting research and development work on the reliable use of data (e.g. using cast specific data for assessing a specific component of interest) or highlighting and justifying the need for further data acquisition.

With regards to practitioners, extensive use, testing and verification of probabilistic methodologies are required, which can be done in the form of collating a host of case-studies ranging in complexity to provide contextual knowledge. Low risk case studies (typically less contentious than plant applications, such as the one disused in Chapter 3) can help trialling and disseminating probabilistic methodologies, as they serve to identify requirements, problem types, required resources and computational issues. On the other hand, there is a need (as demonstrated by the case-study in Chapter 6) for the scale-up of applications to higher risk case-studies, but their dissemination may be limited by their contentious nature (e.g. they may require the inclusion of sensitive information). Regardless of the level of sensitivity, case-studies will invariably form an important part of training practitioners and promoting further implementation; a notion that is backed by the experience gained from this project.

Like any analytical tool, probabilistic models are as good as the knowledge which they channel, but without an understanding of limitations, the results can be dubious and there is a clear danger that this might lead to disenchantment with their implementation. In any application, clearly stating assumptions is vital and caution is advised in terms of interpreting the results. One might ascertain that probability estimates (like any analytically quantifiable result) might be subject to misinterpretation if the underlying assumptions are not clearly understood. This thesis starts with the assertion that probabilistics are common sense put into calculations, but one does not require expertise in human psychology to know that common sense is anything but objective. Consequentially, clear reporting must not be overlooked and an acknowledgement that, equal to any analytical exercise, practitioners' bias can be a non-trivial factor that needs consideration. Historically, this bias has been addressed by virtue of independent verification (i.e. conducting the same probabilistic exercise completely and separately by a different practitioner), but with the amount of work required in developing a probabilistic assessment, the same approach might not be viable, thus prompting the need for more efficient and streamlined verification strategies. Nevertheless, in industries where independent verification is sacrosanct (e.g. the nuclear industry), the expense associated with dual working may be an inevitability for the application of probabilistics.

Further consideration that has been alluded to in this thesis is the need for appropriate computational tools (high-level programming languages such as Matlab, Python and R being considered appropriate), and it is advised that practitioners need to establish not only which tools are available to them, but also consider which ones require a degree of expertise for efficient implementation. The added benefit of the above mentioned high-level languages is that they provide effective visualisation tools, which can be essential for communicating and interrogating probabilistic results in a familiar form.

The formulation of clear methodologies, such as the ones discussed in this thesis, are part of the solutions to the issues discussed above, as they are needed for not just the preparation and implementation of probabilistic assessments, but also for the improvement, reporting, interrogation and acknowledgement of the limitations of the probabilistic methods and results.

7.2 Research Conclusions

As evidenced throughout this thesis, probabilistic structural integrity poses myriad technical challenges related to the integration of probabilistic approaches with currently employed structural integrity procedures. Invariably, some common themes do exist across the various structural integrity applications, and this thesis was limited to exploring five such important topics, whilst

keeping the research objectives in mind. The findings that have emerged from investigating these topics are presented in this section. The work conduced for this project focused on AGR high-temperature applications, with creep-fatigue failure being of major interest. However, the finding discussed in this section have parallel implications to other areas of structural integrity e.g. creep-fatigue crack growth, creep rupture, high/low cycle fatigue and fracture mechanics (e.g. Leak-Before-Break). However, it is recognised that the translation of these findings to other applications does require domain knowledge and expertise in these respective fields. This work did not attempt to exactly relate the various probabilistic approaches to every individual domain of structural integrity, as that would have been an exhaustive exercise and fairly in-depth knowledge of these areas would have been required. As such, creating these key links, which are crucial for the furthering of the general vision proposed by this work, has been highlighted as a major area of further work and collaboration with experts in the subject areas will be sought. The following subsections are devoted to summarising the specific conclusions that followed from the work presented in Chapters 3-6.

Improved Characterisation of Material Properties

In Chapter 3 an approach was discussed where two sources of uncertainty (or scatter) in a material property were identified and, where possible, quantified. These sources were attributed to case specific scatter and cast-to-cast variability, with the latter typically being more pronounced. Two key aspects were related to:

1. The identification of uncertainties in material data depending on their sources (i.e. those arising from cast-to-cast versus cast specific variations) with some being aleatory and other epistemic.

2. The importance of partitioning the available data (e.g. by applied stress) in order to obtain meaningful results with the best degree of confidence. The partitioning is key to isolating and subsequently characterising the aleatory and epistemic uncertainty components in material properties.

These issues are particularly relevant when considering populations of components which are manufactured from different (and perhaps unknown) casts, with the uncertainty associated with such problem being epistemic in nature. In such cases, taking these sources of uncertainty into account can be crucial for obtaining meaningful probabilistic results. Improved characterisation of material properties (of which the work discussed above is an example) can play important roles in probabilistic structural integrity in general, especially when such improvements can result in less conservative probability of failure estimates, and therefore can aid in meeting target reliabilities.

Sensitivity Analysis

Systematic sensitivity analysis approaches can be invaluable in the process of perpetually developing probabilistic models, as they highlight the areas of improvement that would yield the most significant and desirable alterations in the probabilistic results, and therefore they are tools which aid in focusing effort. For example, in Chapter 3 a case-study was presented, which examined the sensitivity of creep-fatigue damage toward variabilities in six key input parameters (all of which were quantities characterising material behaviour). This was intended to demonstrate the utility of sensitivity analysis techniques for guiding future work on reducing conservatism in the assessment procedure by better characterising the dominant input parameters. This idea was represented conceptually though a classic Stress-Strength interference problem depicted in Figure 3.1(c). The results shown in Figure 3.6 demonstrated that creep ductility (ε_f) and creep deformation (C_1) dominated the damage results for the case examined, an observation which was corroborated by similar results for the plant component case-study, which was discussed in Chapter 6 (see Figure 6.9). As a result, this indicates that better characterisation of creep parameters would yield the most significant improvements by reducing the uncertainty in the output results.

The concept of using sensitivity analyses can be understood within the wider context of structural integrity in general. This is by no means uniquely applicable to the presented creep-fatigue case-study, but rather can be applied to any structural integrity application provided sufficient domain expertise (e.g. physics of failure modelling and material data) and knowledge of such sensitivity analysis approaches is available. The sensitivity analysis methods and results from the case-study, along with a review of the key probabilistic approaches and method which are presented in Chapter 3, were published in [9].

Input Parameter Correlations

When developing a probabilistic assessment an important consideration is whether input parameters can be correlated, with these correlations being an additional form of input uncertainty. If incorporated, these correlations can have significant effects on the probabilistic output results and, by extension, a major effect on predicted probabilities. This issue poses a challenge when only limited data is available to measure inter-parameter correlations. Even with the availability of data, however, significant uncertainty can emerge in measured correlations, and thought is needed in terms of assessing ramifications of such uncertainty on the assessment results. Nevertheless, by treating these correlations as stochastic inputs, some pragmatic conclusions can be reached in terms of incorporating them into probabilistic assessments.

In Chapter 4, significant positive correlations were found between scatter in creep ductility and creep deformation parameters which, as previously discussed, are two of the main mate-

rial properties required for creep damage calculations in the R5 Volume 2/3 procedure. These represent cast-to-cast correlations, which dominate the variabilities in creep properties. The Spearman correlation was deemed appropriate for such applications, as it does not impose any restrictions on the distributions of the correlated parameters, and can be used for parameters following different distribution types. For a creep crack initiation probabilistic assessment, the inclusion of a positive correlation between creep deformation and ductility will lead to reduced probabilities of initiation being predicted, as compared with ignoring such correlation.

A main conclusion from the work presented in Chapter 4 is that uncertain knowledge of any possible correlations does not preclude conducting a probabilistic assessment. Rather a probabilistic assessment using uncorrelated parameters in conjunction with post-assessment sensitivity analyses can provide valuable insights into which inter-parameter correlations could have marked effects, thus providing focus for prioritising the investigation of such important correlations. Sensitivity analysis is therefore advised as a precursor to any investigation into possible correlations. In general, material properties are key sources of uncertainty that aggregate through the assessment procedure and contribute towards the output uncertainty. It is perhaps not surprising that correlations between dominant parameters can produce significant effects on the results, while correlations between non-dominant parameters would be virtually non-consequential. As demonstrated by the case-study examining the correlations between creep ductility and deformation and linking this back to sensitivity analysis, it was shown that correlations between dominant parameters can have significant effects on the probabilistic results of interest (e.g. the probability of initiation). This conclusion is believed to be general enough as to have implications to structural integrity probabilistic modelling in general, and is not just limited to creep-fatigue applications.

Loading Uncertainties

When there exists significant variability in loading conditions, as inherently the case for plant components, systematic approaches for examining and incorporating such uncertainties is required. Generally, setting assessment stresses and temperatures at fixed values for long periods of the simulated history is a simple approach, but it obscures the natural variability in the loading conditions and hence can produce significant conservatism. With some of the material properties being functions of loading stresses and temperatures (e.g. creep deformation through the HTBASS model), this effect can be influential in indirect ways that can significantly impact assessment results. Consequentially, using fixed (i.e. deterministic) loading values may be acceptable in some applications, but for situations where damage is driven by loading, it may be necessary to invest effort into systematically accounting for loading uncertainties to provide a better representation. Depending on the nature of the loading condition being examined, two approaches for the probabilistic treatment of in-service loads have been proposed:

- Surrogate modelling approaches for loading conditions that are contingent on ever changing operational quantities (e.g. steady-operation thermal stresses as functions of plant operating temperatures). This is especially applicable when assessment stresses are established using computationally intensive FE models.
- For loading conditions that can be considered as discrete occurrences, directly sampling from appropriate histograms (constructed using data obtained from suitable FE models) can be implemented.

An important conclusion from this work package is that the above approaches and their applicability do not in themselves depend on the nature of the failure mechanism being examined nor on the FE modelling conduced. The models constructed using these approaches do, however, depend on the quality and validity of the training data collated from the FE models used. In that sense, the limitations of the FE models (which must be acknowledged and understood in general) are a subset of the probabilistic models' limitations constructed using the proposed approaches above. For example, the FE models used in this work were elastic analyses, the results of which required converting to elastic-plastic stresses and strains. This approach is typically conservative, hence the associated surrogate models must be understood to have the same limitations as the underlying training data obtained from the elastic FE analyses. In such case, reducing conservatism would require constructing an elastic-plastic FE model, run such model for a wide range of loading conditions, extracting the appropriate training data and then used this data to train a new surrogate model. This process is virtually the same as the one followed in Chapter 5, with the exception being that elastic models were used, thus the resulting surrogate models are considered to be conservative.

Surrogate modelling was proposed for simulating the ever changing nature of plant loading conditions during nominal operation, thus providing a systematic approach for addressing rather then simplifying complex loading histories. In Chapter 3, the Response Surface Method (RSM) was presented as a viable option for surrogate modelling. In the case-study presented in Chapter 5, which looked at the tubeplate component, assessment stresses and temperatures were found to significantly vary across different assessment locations (i.e. tubeholes). This prompted the inclusion of individual response surfaces for each assessment location rather than assuming they all endured the same stresses and metal temperatures. This showed that some assessment locations were, naturally, more prone to severe stresses and temperatures and, therefore, would be expected to incur higher creep-fatigue damages. The value of surrogate modelling approaches is in the avoidance of running FE models in the Monte-Carlo simulation, which would, as an understatement, reduce its efficiency to the point of uselessness.

Transient loading was also considered, and was treated in a different way to steady-operation loading by assuming that transient instances are distinct occurrences (or instances) which have

a natural and inherent variability. Thus by examining batches of previously recorded transient instances (of the same type) related to the tubeplate, it was demonstrated that such variability can be introduced in a probabilistic assessment by sampling discrete data for the relevant stresses and metal temperatures. This discrete data originated from running the recorded plant data into transient FE models which were used to infer the characteristic transient conditions for individual transient instances. However, the FE modelling was only limited to the pre-assessment stage and, similarly to the treatment of steady-operating conditions, was not re-run multiple times in the Monte-Carlo simulation. Elements from Chapter 5 are under submission as part of a journal publication titled: *'Plant data analysis for incorporation of loading uncertainties in probabilistic damage assessments'*. A peer-reviewed conference publication [93] also included features of this work.

Probabilistic Implementation

This thesis culminated in Chapter 6, where key concepts introduced in Chapters 3 to 5 were built on to formulate a complete probabilistic methodology for the assessment of in-service plant components. Creep-fatigue failure notwithstanding (which was the focus of this work), the concepts introduced in this chapter are translatable to any application where the probability of failure for a component of interest is to be estimated. Though of course the nature of such failures may be different depending on the application of interest, and knowledge of the underlying physics of failure is indeed one of the prerequisites for conducting probabilistic failure analyses. The overall conclusion, therefore, was that a host of probabilistic approaches and techniques (examples of which were introduced throughout this thesis) can be aggregated to create probabilistic models (which incorporates myriad uncertainty sources) in order to estimate probabilities of failure of important components susceptible to any failure mechanism, as long as the physics of such mechanism are known and can be modelled. Furthermore, estimates of failure incidences for entire populations of components (collectively susceptible to in-service failures) can also be examined, and were also discussed in Chapter 6.

Generally, however, and based on the experience gained from this PhD project, it must be acknowledged that probabilistics require significant time, effort, cost and knowledge. However, these requirements will become substantially less onerous as a result of consolidating the knowledge required. Most of the tools needed are already available in the public domain for little, or even no, cost and are being used in numerous industries. Nevertheless, substantial thought must be devoted to bringing practitioners up to a baseline level of understanding and awareness of probabilistic and statistical concepts through training and provision of verified supporting documentation. This will also have the benefit of continuously developing probabilistic structural integrity methodologies through feedback on use and verification. The investment will also be offset by the availability and use of probabilistic models aiding timely and informed decision

making, whilst keeping safety and reliability as paramount priorities. The long-term vision proposed by this project is to bridge the gap between the knowledge of probabilistic methods and the general structural integrity community. By promoting further implementation and engagement, the methodologies will mature and emerge to be more extensive as well as coherent, which in turn will aid further acceptance within a wide range of structural integrity fields and, therefore, prospectively promoting a unified probabilistic framework for structural integrity.

7.3 Reflections on the Research Methodology

This work was conducted under the advisement of EDF Energy as the industry collaborator. This interaction has proved to be invaluable in establishing the key areas of work that required attention and the formulation of the various topics discussed in this thesis. Dissemination through conference presentations and the submission of papers to peer-reviewed journals has also played an important role. A main point of reflection is that case-studies were invaluable in terms of conveying and communicating the methodology and its constituent methods to interested audiences. As discussed in Section 7.4, it is suggested that collating a wide range of case-studies will be a beneficial future exercise.

From an early stage, a key intention for this project was formulating a probabilistic methodology that will be adopted by industry. The inclusion of some of the work on sensitivity analysis and correlations in the new R5 Volume 2/3 Appendix 15 (prepared by Prof R. Ainsworth on behalf of EDF Energy [41]) is evidence that the work is timely and topical. However, probabilistic methodologies aside, the underlying research methodology may have an effect on whether the outcomes of this project, and future related projects, will in fact result in industrial impact and meaningful implementation. Moving forward, a clearer focus is required in terms of formalising the research methodology in order to provide a framework for the perpetual development of the prospective unified probabilistic methodology. A relevant framework that can aid in this endeavour is the *Design for X (DFX) shell* [101, 102]. Within the current context, this would translate, depending on the desired focus, to frameworks tailored for *Design for Probabilistic Methodology* and/or *Design for Probabilistic Implementation*. The DFX shell is comprised of six stages for the development of a new process:

1. *Requirement analysis*: investigating the needs, requirements and objectives of a prospective unified probabilistic approach. This would be achieved through input solicitation from industry, academia and regulatory stakeholders. Due considerations towards aspects of *functionality* (i.e. what the methodology tries to achieve) and *operability* (i.e. the ease and clarity by which it can be implemented) would be essential.

2. *Modelling for product analysis*: this relates to the thinking behind the formulation of a probabilistic methodology which can be subdivided in term of:

   (a) Defining the constituent methods to a methodology (e.g. MCS, sampling, surrogate modelling, sensitively analysis, correlations, probability of failure estimates and binomial distribution estimates).

   (b) Assessing how the constituent methods interface with each other (i.e. how does information flow from one to the other).

   (c) Describing each constituent method, contrasting any that perform the same function (e.g. latin-hypercube sampling verses orthogonal sampling) and identifying their relationships.

3. *Modelling the process*: this is concerned with the representation of the methodology as a whole, including resource requirements (e.g. data) and outputs (e.g. performance parameters). This can take the form of a flow chart which schematically illustrates the skeleton of the methodology and can include as much sophistication and flexibility as needed. The illustration of how information flows through the methodology, from inputs to outputs, can also aid in this respect.

4. *Selecting performance measures*: identifying metrics that can be used to access the performance of the methodology. This can be somewhat subject and contentions, as it can clearly affect, in a feedback fashion, not only the perception of performance, but also further development.

5. *Compiling manuals and workbooks*: these can include various items of information: documented case-studies, technical articles related to specific methods, peer-reviewed publications, potential sources for input data, probabilistic and statistical methods, and guidance on computational deployment.

6. *Validation and verification*: assessing the strengths and limitations of the methodology, with the aim of identifying areas for further development and performance improvement. Furthermore, independent verification of the methodology and associated case-studies can increase confidence in probabilistic implementation in general. A more specific aim includes the validation and verification of the Design for Probabilistic Implementation framework itself (i.e. the process being presently discussed), thus assessing its impact on the success of the methodology.

Augmenting the above framework, in [103] a six-step process is proposed for formulating processes with the intention of maximising implementation. This is predominantly similar to the DFX shell, but places emphasis on one extra consideration: having novice practitioners (coincidentally a PhD researcher in this project) learn the methodology (or at least aspects of it)

and apply it to real-life problem. Given that a methodology may be at its very early formulation, the aim of this is to not only train junior practitioners, but also gain valuable feedback though direct implementation and verification. Furthermore, this has the additional benefit of creating more case-studies which, provided they are well documented and independently verified, can be helpful for future dissemination of the methodology.

This project constitutes the initial iterations of developing a unified probabilistic structural integrity approach, and it is expected that further iterations are inevitable. These will be driven by further involvement by interested practitioners (i.e. conducting a formal requirement analysis and seeking independent verification) to evolve the requirements, needs and the probabilistic methodology itself. This point feeds into the emphasis that such work cannot be considered a purely academic exercise, but rather a bridging-the-gap endeavour to bring practitioners to a common level of understanding in probabilistic implementation.

7.4 Future Work

During the course of this PhD project a number of work packages have emerged, and in this thesis the topics that were prioritised have been covered. Nevertheless, there are a number of further areas which are deemed worthy of future research, and this section provides brief descriptions of these topics.

Integration of Inspection Results

The creep-fatigue analyses conducted as part of this project have focused on the initiation aspect, with a damage of unity signifying the formation of a shallow crack. This could be extended into a creep-fatigue crack growth assessment which assesses whether the crack growth over the projected remaining lifetime of the component would still be considered acceptable. Coupled with assessment results, inspection results may be used for validation and proving a means for monitoring the crack. As a result, inspection results for plant components using non-destructive techniques (NDT) can provide key insights into whether a component that is cracked is still safe to operate under the stipulations of a safety case. It could be imagined that this applies if the original function of such cracked component is not compromised and the crack does not pose a safety concern. Currently, no methods are in place in order to systematically integrate inspection results (which are physical measurements, yet in themselves uncertain data) with the analytical results from a crack growth assessment. In a probabilistic paradigm, both inspection and assessment are forms of uncertain knowledge, which conceptually can be aggregated to augment the knowledge of the current state of the component. Potentially this could reduce the uncertainty in the knowledge of the state of a component, and by extension of systems of components, which could support and justify safety considerations.

Statistical Characterisation of Ductility

From the sensitivity analyses conducted in the case-studies in Chapters 3 and 6, creep ductility emerged as being significantly dominant and, therefore, improving the methods (statistical and phenomenological) used to model ductility could potentially produce significantly less conservative and representative results. For both case-studies, a strain independent (constant) lower-bound ductility model was implemented, which is a conservative approach. However, more complex models incorporating the effect of stress and creep strain rate on ductility (e.g. the Stress Modified Ductility Exhaustion model, SMDE) are expected to be more representative of the material behaviour; a point which was demonstrated in Chapter 3 by considering model uncertainty.

Correlations Between Components of a System

This refers to correlations between nominally similar components (e.g. boiler tubes or tubeplates) within an overall system (e.g. a boiler pod) in order to evaluate the probability of system failure. In Section 6.2.2 it was discussed how the failure (or initiation) probability of multiple points located on a component can be correlated, which in turn affects the component-level probability of failure. The same rationale can be applied when considering how the failure probability of a system may be affected by the correlations between the failures of its constituent components. An easy approach may be to just assume that failures of components are independent (i.e. there is no need to account for such correlations), however, this assumption has not been explored in this thesis. As a result, this topic is an area of further work, aiming to supply some justifiable advice and a systematic approach for assessing its impact.

Formalising Verification Strategies

Challenges related to independent verification have been acknowledged in this thesis. Specifically, there is a cost implication which may form a potential barrier for accepting probabilistics by industry. As a result, due consideration should be given to formalising clear and systematic strategies for independent verification of probabilistic assessments, thus streamlining and improving the efficiency of these processes. A further concern related to verification is due to a lack of statistically significant number of real failures for high reliability components (e.g. Incredibility of Failure, IoF, components). As a result, further work is needed for suggesting strategies tackling this issue, including conducting thorough verification exercises of prospective probabilistic methodologies on controlled case-study applications e.g. examining failed components that were subjected to controlled test conditions or assessing in-service components that have had histories of failures due to operation. Inevitably though, it is easy to conflate the verification of the probabilistic methods with the verification of the underlying physics of failure modelling. As it has been emphasised throughout this work, the results of a probabilistic approach invariably depend on the validity of the underlying physics of failure models (often formalised by assessment procedures,

codes and standards). Moving forward, a distinction between the two facets of verification must be clarified, as not only they are separate, but probabilistic approaches are likely to play a key part in the perpetual development and verification of our understanding of the physics of failure. The case-study in Chapter 3 is an example of such endeavours, where a creep-fatigue test under controlled testing conditions was examined through probabilistic approaches and the results gave insight as to the performance of the underlying assessment procedure.

Wider Structural Integrity Implementation

This project focused on creep-fatigue crack initiation, which poses challenges that can be specific to its application. Nevertheless, the probabilistic approaches and methods discussed in this thesis are generic enough to be applicable to other structural integrity applications which include: creep-fatigue crack growth, creep rupture, high/low cycle fatigue and fracture mechanics (e.g. Leak-Before-Break). If wider acceptance and practice of probabilistic methods and techniques is the aim, then it is imperative that extending its application to other areas of structural integrity will facilitate this endeavour. In part, this relates back to the issues discussed in Section 7.1, which discussed the need for a unified probabilistic structural integrity approach. Probabilistic creep-fatigue crack growth has already been the subject of research work, including: [11–17, 47]. Furthermore, some research in the above mentioned areas has been conducted at the University of Bristol, including a Masters project examining a case-study on probabilistic leak-before-break, and two fellow PhD projects on probabilistic fatigue for landing gear applications (with important conclusions already emerging as the project is still progressing) and probabilistic fracture mechanics (in its early days at the time of writing). As a result, an effort is needed for collating an assortment of case-studies spanning a wide range of applications and examining low to high risk components, in order to demonstrate the versatility and train future practitioners in probabilistic implementations. This discussion feeds into the important issue of convincing regulators to accept probabilistic analyses, for which industry-wide collaboration to facilitate wider acceptance will play a crucial role.

References

[1] D. S. Sivia, J. Skilling, Data Analysis: A Bayesian Tutorial, Oxford Univ. Press, Oxford, 2006.

[2] Hoole, J., Sartor, P., Booker, J., Cooper, J., Gogouvitis, X. V., Schmidt, R. K., Evaluating the Impact of Conservatism in Industrial Fatigue Analysis of Life-Limited Components, MATEC Web Conf. 165, 10017 (2018).

[3] P. Dillström, F. Nilsson, 7.11 - Probabilistic Fracture Mechanics, in: I. Milne, R. Ritchie, B. Karihaloo (Eds.), Comprehensive Structural Integrity, Pergamon, Oxford, 2003, pp. 465 – 489.

[4] Y. M. Goh, The Incorporation of Uncertainty into Engineering Knowledge Managment, Ph.D. thesis, University of Bristol, Bristol, United Kingdom (Jan 2005).

[5] Nuclear Structural Integrity Probabilistics Working Principles, Developed by the Nuclear Structural Integrity Probabilistics Working Group, Prepared by Rolls-Royce (Apr 2019).

[6] Probabilistic methods: Uses and abuses in structural integrity (2001).

[7] A. D. S. Carter, Mechanical Reliability, Second Edition, Macmillan, London, 1986.

[8] K. Nikbin, A Unified European Approach to High Temperature Defect Assessment Code and its Incorporation in a Knowledge Base System, International Journal of Pressure Vessels and Piping 78 (11) (2001) 929–935.

[9] N. A. Zentuti, J. D. Booker, R. A. W. Bradford, C. E. Truman, A Review of Probabilistic Techniques: Towards Developing a Probabilistic Lifetime Methodology in the Creep Regime, Materials at High Temperatures 34 (5-6) (2017) 333–341.

[10] N. A. Zentuti, J. D. Booker, J. Hoole, R. A. W. Bradford, D. Knowles, Probabilistic structural integrity, The UK Form for Engineering Structural Integrity (FESI) Bulletin: Vol. 12, Issue 2 (Winter 2018), pp. 16–23.

[11] B. Dogan, U. Ceyhan, J. Korous, F. Mueller, R. Ainsworth, Sources of Scatter in Creep-Fatigue Crack Growth Testing and Their Impact on Plant Assessment, Welding in the World 51 (7) (2007) 35–46.

[12] J. Wallace, R. Wang, D. Mavris, Creep Life Uncertainty Assessment of a Gas Turbine Airfoil, 44th AIAA/ASME/ASCE/AHS/ASC Structures, Structural Dynamics and Materials Conference. American Institute of Aeronautics and Astronautics, Apr 2003.

[13] P. Holt, R. Bradford, Application of Probabilistic Modelling to the Lifetime Management of Nuclear Boilers in the Creep Regime: Part 1, International Journal of Pressure Vessels and Piping 95 (2012) 48–55.

[14] K. Nikbin, M. Yatomi, K. Wasmer, G. Webster, Probabilistic Analysis of Creep Crack Initiation and Growth in Pipe Components, International Journal of Pressure Vessels and Piping 80 (7-8) (2003) 585 – 595.

[15] F. Ibisoglu, M. Modarres, Probabilistic Life Models for Steel Structures Subject to Creep-Fatigue Damage, International Journal of Prognostics and Health Management 6 (2015).

[16] T. J. Delph, D. L. Berger, D. G. Harlow, M. Ozturk, A Probabilistic Lifetime Prediction Technique for Piping Under Creep Conditions, Journal of Pressure Vessel Technology 132 (5) (2010) 051206–051206.

[17] Z. Liu, D. Mavris, A Methodology for Probabilistic Creep-Fatigue Life Assessment of Hot Gas Path Components, 45th AIAA/ASME/ASCE/AHS/ASC Structures, Structural Dynamics & Materials Conference. American Institute of Aeronautics and Astronautics, Apr 2004.

[18] R. A. W. Bradford, A Procedure for Probabilistic Creep-Fatigue Crack Initiation Assessment Consistent With R5 Volume 2/3, Tech. Rep. E/REP/BBAB/0028/GEN/13, EDF Energy Nuclear Generation Limited (Jan 2014).

[19] M. J. Chevalier, The Reliability of Degrading Structural Systems Operating at HighTemperature, Ph.D. thesis, University of Bristol, Bristol, United Kingdom (Mar 2013).

[20] R. A. W. Bradford, Application of Probabilistic Assessments to the Lifetime Management of Nuclear Boilers in the Creep Regime, transactions of the 23rd International Conference on Structural Mechanics in Reactor Technology, SMiRT-23, Manchester, Aug 2015.

[21] R. Bradford, P. Holt, Application of Probabilistic Modelling to the Lifetime Management of Nuclear Boilers in the Creep Regime: Part 2, International Journal of Pressure Vessels and Piping 111-112 (2013) 232–245.

[22] C. O'Neil, Weapons of Math Destruction, Penguin Books, 2017.

[23] EDF Energy Nuclear Generation Ltd, R5 Issue 3 Volume 2/3 (Rev.002): Creep-Fatigue Crack Initiation Procedure for Defect-Free Structures. Assessment Procedure for the High Temperature Response of Structures (Nov 2014).

[24] Y. Reich, The Study of Design Research Methodology, Journal of Mechanical Design 117 (2A) (1995) 211–214.

[25] W. D. Callister, D. G. Rethwisch, Materials Science and Engineering, 8th Edition, John Wiley & Sons Inc, 2011.

[26] R. W. Evans, B. Wilshire, Introduction to Creep, The Institute of Materials, 1993.

[27] M. E. Kassner, Fundamentals of Creep in Metals and Alloys, ELSEVIER, 2009.

[28] R. Viswanathan, J. Stringer, Failure Mechanisms of High Temperature Components in Power Plants, Journal of Engineering Materials and Technology 122 (3) (2000) 246–255.

[29] N. A. Zentuti, Multiaxial Stress Creep and Application to Austenitic Steels of the LICON Methodology for Accelerated Testing, Thesis for the degree of MSc in Advanced Mechanical Engineering, University of Bristol (2015).

[30] M. Saber, Experimental and Finite Element Studies of Creep and Creep Crack Growth in P91 and P92 Weldments, Ph.D. thesis, University of Nottingham (2011).

[31] D. J. Wulpi, Understanding How Components Fail, 2nd Edition, ASM International, 2000.

[32] G. Jackson, H. Chen, D. Tipping, Shakedown and Creep Rupture Assessment of a Header Branch Pipe Using the Linear Matching Method, Procedia Engineering 130 (2015) 1705–1718.

[33] A. Gotoh, Reheat Cracking - the Mechanism and Countermeasures, Welding International 7 (4) (1993) 266–268.

[34] P. M. James, J. K. Sharples, N. Underwood, UK Programme on Codes, Standard and Procedure Needs for SMR and Gen IV Reactors, Proceedings of the ASME 2018 Pressure Vessels & Piping Conference. Codes and Standards, PVP2018-85075, July 2018.

[35] American Society for Mechanical Engineers, BPVC Section III-Rules for Construction of Nuclear Facility Components-Division 1-Subsection NH-Class 1 Components in Elevated Temperature Service (2015).

[36] American Society for Mechanical Engineers, BPVC Section III-Rules for Construction of Nuclear Facility Components-Division 5-High Temperature Reactors (2019).

[37] AFCEN, RCC-MRx - Design and Construction Rules for Mechanical Components of Nuclear Installations (2015).

[38] British Standards Institution, BS 7910 - Guide to Methods for Assessing the Acceptability of Flaws in Metallic Structures (2013).

[39] EDF Energy Nuclear Generation Ltd, R6 Assessment of the Integrity of Structures Containing Defects, Revision IV, Issue 11 (2016).

[40] J. Sharples, P. Budden, Recent Developments Associated with the R6 Defect Assessment Methodology, Transactions of the 22rd International Conference on Structural Mechanics in Reactor Technology, SMiRT-22, San Francisco, California, USA, Aug 2013.

[41] M. Chevalier, EDF Energy Nuclear Generation Limited, Personal communication RE: R5 Volume 2/3 Appendix A15 (Advice on Probabilistic Assessments) for R5 Panel Endorsement on 20th-Nov-2018 (Oct, 2018).

[42] D. Cho, D. H. B. Mok, S. X. Xu, D. A. Scarth, Probabilistic Assessment of CANDU Reactor Core for Risk of Pressure Tube Failure due to Presence of In-Service Flaws, Proceedings of the ASME 2017 Pressure Vessels & Piping Conference. Codes and Standards, PVP2017-66101, 2017.

[43] D. Scarth, L. Gutkin, Acceptance Criteria for Probabilistic Fracture Protection Evaluations of CANDU Zr-Nb Pressure Tubes, Proceedings of the ASME 2018 Pressure Vessels & Piping Conference. Codes and Standards, PVP2018-85086, 2018.

[44] H. Conlin, P. G. Brabazon, K. Lee, Exploring the Role and Content of the Safety Case, Process Safety and Environmental Protection 82 (4) (2004) 283 – 290.

[45] M. Sheridan, D. Knowles, O. Montgomery, Comparison of R5 and ASME NH Creep-Fatigue Damage Assessment Methodologies, in: ASME 2013 Pressure Vessels and Piping Conference, American Society of Mechanical Engineers, 2013.

[46] EDF Energy Nuclear Generation Ltd, AGR Materials Data Handbook, R66, Issue 6, Rev.010 (Nov 2016).

[47] J. L. Huang, K. Y. Zhou, J. Q. Xu, X. H. Xu, Probabilistic Creep Rupture Life Evaluation of T91 Alloy Boiler Superheater Tubes Influenced by Steam-Side Oxidation, Materials and Corrosion 65 (8) (2014) 786–796.

[48] C. Bullough, A. Norman, The PD6605 Creep Rupture Data Assessment Procedure - An Appraisal of is Application 10 Years On, ECC Creep Conference, Zurich, Apr 2009.

[49] S. R. Holdsworth, Advances in the Assessment of Creep Data, Proceedings of the 9th Liege Conference: Materials for Advanced Power Engineering, pp. 946-947, Sep 2010.

[50] D. J. Smith, Reliability, Maintainability and Risk: Practical Methods for Engineers, 4th Edition, Butterworth-Heinemann, Oxford, 1993.

[51] E. B. Haugen, Probabilistic Mechanical Design, Wiley-Interscience, New York, 1980.

[52] Y. M. Goh, C. A. McMahon, J. D. Booker, Improved Utility and Application of Probabilistic Methods for Reliable Mechanical Design, Proceedings of the Institution of Mechanical Engineers, Part O: Journal of Risk and Reliability 223 (3) (Sep 2009) 199–214.

[53] M. Lemaire, A. Chateauneuf, J. Mitteau, Structural Reliability, ISTE Ltd and John Wiley Sons Inc., 2009.

[54] Y. M. Goh, J. Booker, C. McMahon, A Comparison of Methods in Probabilistic Design Based on Computational and Modelling Issues, Springer Netherlands, Dordrecht, 2005, pp. 109–122.

[55] J. D. Booker, M. Raines, K. G. Swift, Designing Capable and Reliable Products, Butterworth-Heinemann, 2001.

[56] K. Bury, Statistical Distributions in Engineering, Cambridge University Press, 1999.

[57] M. A. Bezerra, R. E. Santelli, E. P. Oliveira, L. S. Villar, L. A. Escaleira, Response Surface Methodology (RSM) as a Tool for Optimization in Analytical Chemistry, Talanta 76 (5) (2008) 965 – 977.

[58] K. L. Priddy, P. E. Keller, Artificial Neural Networks: An Introduction (SPIE Tutorial Texts in Optical Engineering, Vol. TT68), SPIE- International Society for Optical Engineering, 2005.

[59] J. Sacks, W. J. Welch, T. J. Mitchell, H. P. Wynn, Design and analysis of computer experiments, Statistical Science, Vol 4, No 4, pp 409-435, 1989.

[60] L. Gutkin, S. Datla, C. Manu, Pilot Study for Uncertainty Analysis in Probabilistic Fitness-for-Service Evaluations of Zr-2.5Nb Pressure Tubes: Uncertainty Characterisation, Proceedings of the ASME 2018 Pressure Vessels & Piping Conference. Codes and Standards, PVP2018-85011, 2018.

[61] M. Kutner, C. Nachtsheim, J. Neterand, W. Li, Applied Linear Statistical Models, 5th Edition, McGraw-Hill Irwin, London, 2005.

[62] D. C. Montgomery, G. C. Runger, Applied Statistics and Probability for Engineers, John Wiley and Sons, 2003.

[63] Matworks, Wilcoxon rank sum test: ranksum, URL: `https://uk.mathworks.com/help/stats/ranksum.html`, accessed 19th-Jun-2017 (2017).

[64] F. Pianosi, K. Beven, J. Freer, J. W. Hall, J. Rougier, D. B. Stephenson, T. Wagener, Sensitivity analysis of environmental models: A systematic review with practical workflow, Environmental Modelling & Software 79 (2016) 214–232.

[65] E. Borgonovo, A new uncertainty importance measure, Reliability Engineering & System Safety 92 (6) (2007) 771–784.

[66] O. Rakovec, M. C. Hill, M. P. Clark, A. H. Weerts, A. J. Teuling, R. Uijlenhoet, Distributed Evaluation of Local Sensitivity Analysis (DELSA), with Application to Hydrologic Models: Distributed Evaluation of Local Sensitivity Analysis, Water Resources Research 50 (1) (2014) 409–426.

[67] R. Bullough, F. M. Burdekin, O. J. V. Chapman, V. R. Green, D. P. G. Lidbury, J. N. Swingler, R. Wilson, The Demonstration of Incredibility of Failure in Structural Integrity Safety Cases, International Journal of Pressure Vessels and Piping 78 (2001) 539–552.

[68] Office for Nuclear Regulation (ONR), Civil Nuclear Reactor Build - Generic Design Assessment, Step 2 Assessment of the Structural Integrity of Hitachi GE's UK Advanced Boiling Water Reactor (UK ABWR), Assessment Report ONR-GDA-AR-14-012 (Revision 0) (Aug 2014).

[69] Health and Safety Executive (HSE) - HMSO, The tolerability of risk from nuclear power stations (1992).

[70] Health and Safety Executive (HSE) - HMSO, Advisory Committee on Major Hazards – Second Report (1979).

[71] Health and Safety Executive (HSE) - HMSO, Reducing Risks and Protecting People - HSE's decision making process (2001).

[72] A. Duddridge, Company Specification: Guidance on AGR Structural Integrity Related Safety Cases, EDF Energy (2009).

[73] M. W. Weightman, Safety Assessment Principles for Nuclear Facilities, Nuclear Installations Inspectorate part of the HSE (2006).

[74] K. Kurisaka, R. Nakai, T. Asayama, S. Takaya, Development of System Based Code (1) Reliability Target Derivation of Structures and Components, Journal of Power Energy Systems 5 (2011) 19–32.

[75] ISO 2394:2015, General principles on reliability for structures, Fourth Edition (Mar 2015).

[76] British Standards Institution, BS7910:2013+A1:2015, Guide to methods for assessing the acceptability of flaws in metallic structures (2016).

[77] EN 1993-1-1: EuroCode 3: Design of Steel Structures (1993).

[78] ASTM E2714-13 Standard Test Method for Creep-Fatigue Testing (2013).

[79] Z. Fan, D. J. Smith, X. Chen, M. W. Spindler, Creep-Fatigue Lives Prediction and Sensitivity Study of 316H at 550°C, Acta Metallurgica Sinica (English letters) 24 (2) (2011) 132–140.

[80] R. A. W. Bradford, T73S04 Creep-Fatigue Crack Initiation Tutorials, URL: http://rickbradford.co.uk/T73S04Tutorials.html, accessed 7th-Dec-2018 (2015).

[81] AFCEN, RCC-MR, Design and Construction Rules for Mechanical Components of FBR Nuclear Islands (1985).

[82] J. H. Maxted, HTBASS Creep-Fatigue Damage Model Analysis for Type 316h Stainless Steel, Tech. Rep. E/REP/BBGB/0187/GEN/16, EDF Energy Nuclear Generation Limited (Sep 2016).

[83] M. Spindler, W. Payten, Advanced Ductility Exhaustion Methods for the Calculation of Creep Damage During Creep-Fatigue Cycling, Journal of ASTM International 8.

[84] M. C. Cario, B. L. Nelson, Modelling and Generating Random Vectors with Arbitrary Marginal Distributions and Correlation Matrix, Delphi Packard Electric Systems (Warren, OH) and Department of Industrial Engineering and Management Science, Northwestern University, Evanston IL (1997).

[85] Matworks, Generate Correlated Data Using Rank Correlation, URL: https://uk.mathworks.com/help/stats/generate-correlated-data-using-rank-correlation.html, accessed 30th-Mar-2017 (2017).

[86] D. J. Smith, J. D. Booker, Statistical Analysis of the Effects of Prior Load on Fracture, Engineering Fracture Mechanics 14 (74) (2007) 2148–2167.

[87] M. B. Brown, A. B. Forsythe, Robust Tests for the Equality of Variances, Journal of the American Statistical Association 69 (346) (1974) 364–367.

[88] A. Trujillo-Ortiz, R. Hernandez-Walls, BFtest: Brown-Forsythe's Test for Homogeneity of Variances, URL: http://www.mathworks.com/matlabcentral/fileexchange/loadFile.do?objectId=3412&objectType=FILE, accessed 19th-Jun-2017 (2003).

[89] A. Mehmanparast, C. M. Davies, G. A. Webster, K. M. Nikbin, Creep Crack Growth Rate Predictions in 316H Steel Using Stress Dependent Creep Ductility, Materials at High Temperatures 31 (1) (2014) 84–94.

[90] M. W. Spindler, M. C. Smith, The Effect of Multiaxial States of Stress on Creep Failure of Type 316h Under Displacement Control, Proceedings of ASME 2009 Pressure Vessels & Piping Conference, Prague, Czech Republic, PVP2009-77963, July 2009.

[91] British Steelmakers Creep Committee, BSCC High Temperature Data: British Long Term Creep Rupture and Elevated Temperature Tensile Data on Steels for High Temperature Service, Iron and Steel Institute for the British Steelmakers Creep Committee, London, 1973.

[92] D. W. Dean, P. J. Budden, R. A. Ainsworth, R5 Procedures for Assessing the High Temperature Response of Structures: Current Status and Future Developments. Proceedings of ASME PVP2007, July 22-26, 2007, San Antonio, Texas, USA, paper PVP2007-26569.

[93] N. A. Zentuti, J. D. Booker, R. A. W. Bradford, C. E. Truman, Management of Complex Loading Histories for Use in Probabilistic Creep-Fatigue Damage Assessments, Proceedings of the ASME 2018 Pressure Vessels & Piping Conference. Codes and Standards, PVP2018-84400, 2018.

[94] M. Hubert, K. V. Driessen, Fast and Robust Discriminant Analysis, Computational Statistics and Data Analysis 45 (2) (2004) 301 – 320.

[95] S. Verboven, M. Hubert, LIBRA: a MATLAB Library for Robust Analysis, Chemometrics and Intelligent Laboratory Systems 75 (2) (2005) 127 – 136.

[96] J. Hammersley, D. Handscomb, Monte Carlo Methods, Chapman and Hall, 1964.

[97] R. P. Sore, Fatigue Endurance of Austenitic Stainless Steels and Weld Metals, Tech. Rep. E/REP/AGR/0161/00, British Energy Generation Ltd (Sep 2001).

[98] E. F. J. Shelton, HTBASS Creep Understanding: Re-Priming of Creep Deformation Behaviour During Cyclic Loading, Tech. Rep. 5147229/301/002: Issue 02, prepared by Atkins on behalf of EDF Energy Nuclear Generation Ltd (Oct 2016).

[99] N. A. Zentuti, J. D. Booker, R. A. W. Bradford, C. E. Truman, Correlations between Creep Parameters and Application to Probabilistic Damage Assessments, International Journal of Pressure Vessels and Piping 165 (2018) 295 – 305.

[100] J. D. Booker, Personal communication RE: Presentation on Probabilistic Structural Integrity Delivered at Sellafield Ltd on 6th-Mar-2019, and their involvement with the Centre for Doctoral Training at the University of Bristol (Feb, 2019).

[101] G. Q. Huang, K. L. Mak, The DFX shell: A Generic Framework for Developing Design for X Tools, Robotics and Computer-Integrated Manufacturing 13 (3) (1997) 271 – 280.

[102] J. Booker, A Survey-Based Methodology for Prioritising the Industrial Implementation Qualities of Design Tools, Journal of Engineering Design 23 (7) (2012) 507–525.

[103] E. K. Antonsson, Development and Testing of Hypotheses in Engineering Design Research, ASME Journal of Mechanisms, Transmissions and Automation in Design 109 (2) (1987) 153–154.

APPENDIX A - HEAT TRANSFER COEFFICIENT CALCULATIONS

The analysis presented in this appendix was taken from previous work conducted on deterministically assessing the tubeplate component by Frazer Nash on behalf of EDF Energy. The heat transfer coefficient between the steam and the inner surface of the tubes is calculated as:

$$h = \frac{kNu}{d} \tag{8.1}$$

where k is the thermal conductivity of steam (in $W/m.K$), d is the diameter of each tube and Nu is the Nusselt number which can be approximated (assuming a smooth tube) using the *Dittus-Boelter* correlation:

$$Nu = 0.023Re^{0.8}Pr^{n} \tag{8.2}$$

where Re is the Reynolds number, Pr is the Prandtl number and the exponent n is taken as 0.3 consistent with the case when the steam temperature is higher than the tubehole surface temperature. The Pr number is calculated as:

$$Pr = \frac{c_p \mu}{k} \tag{8.3}$$

where c_p (in J/kgK) is the specific heat and μ is the dynamic viscosity (in $Pa.s$). and the Re number as

$$Re = \frac{\rho v d}{\mu} \tag{8.4}$$

where ρ is the density of steam (in kg/m^3) and v is the flow velocity (in m/s). The flow velocity is calculated as:

$$v = \frac{\dot{Q}}{A} \tag{8.5}$$

where $\dot{Q}$ is the volume flow rate (in m^3/s) and A is the flow area (in m^2) which is taken to be the total area of the all tube (i.e. the flow area per header):

$$A = 37 \times \frac{\pi}{4} d^2 \tag{8.6}$$

$$\dot{Q} = \frac{\dot{m}}{\rho} \tag{8.7}$$

where $\dot{m}$ is the mass flow rate per header (in kg/s). However the available data is for the boiler mass flow which is fractured by a quarter to get the flow rate for a single header. Ultimately, the input parameters required to approximate the HTCs based on the above approach are:

1. The boiler mass flow rate (in kg/s).
2. The boiler outlet temperature (in $^{\circ}C$).
3. The boiler outlet pressure (in MPa).

For calculating the transient HTCs for the header, the same analysis applies, but the diameter and the flow area will be different.